BENZIMIDAZOLE-BASED FLUOROPHORES AND NONCOVALENT ORGANIC FRAMEWORKS

A Dissertation Presented to

the Faculty of the Department of Chemistry

University of Houston

In Partial Fulfillment

of the Requirements for the Degree

Doctor of Philosophy

By

Ha Tuyet Mai Le

December 2015

BENZIMIDAZOLE-BASED FLUOROPHORES AND NONCOVALENT ORGANIC FRAMEWORKS

Ha Tuyet Mai Le

APPROVED:

Dr. Ognjen Š. Miljanić, Chairman

Dr. Olafs Daugulis

Dr. Jeremy May

Dr. Shoujun Xu

Dr. Stanko R. Branković

Dean, College of Natural Sciences and Mathematics

In loving memory of my mother,

who had always encouraged me throughout my education,

and believed in me.

ACKNOWLEDGMENTS

I would like to think about choosing a research group like Hogwarts House-sorting because witches cast spells, mix potions, which is just a combination of chemicals, causing unnatural explosions, which was considered as magic back in those days. Hogwarts students graduate in their seventh year of magical education; just like that, after experiencing all "magical" courses, we are allowed to practice and perform "magic" with labmates, and hopefully we can graduate in fifth or sixth year after an exhausting test, namely defense. It will be truly enchanted if we have Sorting Hat of Hogwarts which is placed on the students' head, examining their mind then assigning them to their Houses based on abilities, personality, and preferences. Of course that hat doesn't exist; however, thanks to my friend's suggestion, I'm grateful to be accepted to Miljanić House which I have so far regarded as a perfect fit for me.

Five years of graduate student's life in that House was not too long, but enough for me to grow up and mature. The most influential person during that period is my advisor, Prof. Ognjen Miljanić. Remembering back five years ago, he was sufficiently courageous to say yes to an unknown student who applied from halfway around the earth. That's why I'm here in University of Houston now. I was personally afraid and tried to keep away from all professors; yet my advisor in some way is a good listener who encourages my confidence; since then we can have comfortable research discussions. Research wasn't always going well; luckily, he was ready to offer support and give guidance all the time. I must admit that in science, he was serious and disciplined, that, however, helps to train me become better and lead me to the completion of projects. In

his group, I was handed the freedom to think and create new ideas, so I had the chance to work with projects in two different fields. I was strongly inspired by his profile in the *Journal of Physical Organic Chemistry* to be enthusiastic, work harder and think bigger out of the box. I'm deeply thankful him for the chances to attend conferences in Dallas, San Francisco, and especially in Madrid, Spain. It was a great memory together with groupmates having a long road trip, sharing a nice house and learning new chemistries in ACS meetings. I'm pretty sure a lot of my friends envied my trip to Madrid for ISNA 16 conference; that was also my first time in Europe, and thanks my advisor as well as his family for sheltering and taking care of me during the trip in Barcelona.

I also want to express my appreciation to all professors of organic division for their devotion in teaching and willingness to answer my questions when I randomly stopped by their offices. They really transferred me from an engineer to a chemist and motivated me by new knowledge. Dr. Korp and Dr. Wang, I'm sorry for always bothering you with single crystal problems and I'm thankful for your patient instruction and thorough explanation. Dr. Wang, I still keep the memory back to the day we were in Argonne National Lab and collecting crystal data overnight; you are such a great partner. In the same vein, I would like to extend great thanks to Dr. Chen at Argonne National Lab for his support with synchrotron radiation. In addition, Prof. Jeffrey Rimer's group was generous enough to share the adsorption instrument with us, thank you very much.

I wish to thank all my big friends who have helped me along journey to conquer research projects. Dr. Lirag, my first project was with you, even though we carry on nonsense conversations all the time, but our cooperation was great, right? I also secretly

admired your surviving ability in any harsh condition. Dr. Saeed, you are more than a big brother, thanks for all fluorescence knowledge provided. Dr. Chen, you always make jokes out of me, but you are still my "crystal idol" with great expertise in porous material. I am forever indebted to Dr. Popov who mentored me in the CH activation chemistry to build up nCOFs and encouraged me to pursue new knowledge. Nadia, I'm joyful to have had you as my undergrad student, your excitement and enthusiasm led us to accomplish our cruciform project. Dr. Ji, your determination brought us a nice paper. I also had a memorable time with sweet groupmates: Dr. Osowska, Dr. Lim, Minyoung, Chia-Wei (with you, I am never late), Mohamed, Dr. Vujisić, thank all for suffering me for such a long time. I enjoyed being in gym team with companions: Jennifer (my best mommy), Johnathan, Po-An, Maria, Dr. Vujisić, Dr. Ji and our professional coach, Nadia.

I have received many supports from Vietnamese friends in UH, thanks to Dr. Truong, who introduced me to my advisor and helped me settle down during my first days in the USA. A special thanks to friends: Thien, Phong, Tung, Thao, who spent time having research discussion with me. Thanks to my housemates: Trang, Ky, Trieu, Diep for sharing the joys and sorrows in life. I would like to make a special mention to Minh, who always believes in me and maintains the long distance relationship with generosity.

Lastly, I would like to give thanks my family members for their moral support and encouragement in education. Mom, I lost the last chance meeting you on the way pursuing this degree, but I believe you always look after me from heaven, thus I dedicate this dissertation to you.

BENZIMIDAZOLE-BASED FLUOROPHORES AND NONCOVALENT ORGANIC FRAMEWORKS

An Abstract of Dissertation Presented to

the Faculty of the Department of Chemistry

University of Houston

In Partial Fulfillment

of the Requirements for the Degree

Doctor of Philosophy

By

Ha Tuyet Mai Le

December 2015

ABSTRACT

The previous studies of molecular cruciforms based on distyrylbis(arylethynyl)benzenes, tetrakis(arylethynyl)benzenes, tetrakis(alkynyl)ethenes, and benzobisoxazole cruciforms, and their use as chemical sensors will be introduced and summarized. We construct a simpler "half cruciform" architecture with benzimidazole core, namely L-shaped benzimidazole fluorophores. These fluorophores showed separate frontier molecular orbitals in donor–acceptor systems, similar to benzobisoxazole cruciforms. They display change in their fluorescent emission upon exposure to bases, acids and small anions. The preparation of other benzimidazole-based sensor precursors and initial study is also included. A new class of cruciform based on the benzobisimidazole central motif is introduced together with their synthesis and computational evaluation. These benzobisimidazole cruciforms exhibit strong optical responses to bases, albeit negligible to acids. A representative cruciform was examined and showed pronounced colorimetric response to anions.

Noncovalent organic frameworks are porous materials; their porosity results from noncovalent interactions. The series of perfluorinated precursors was synthesized and crystalized to obtain desired noncovalent organic frameworks. The porous framework was analyzed by porosity measurement, single, and powder X-ray diffractions.

TABLE OF CONTENTS

Chapter One Cross-conjugated Molecular Cruciforms as Chemical Sensors

1.1 Introduction....1

1.2 Distyrylbis(arylethynyl)benzenes....6

1.3 Tetrakis(arylethynyl)benzenes....13

1.4 Tetrakis(alkynyl)ethenes....18

1.5 Benzobisoxazole Cruciforms....22

1.6 Conclusion....28

Chapter Two L-shaped Benzimidazole Fluorophores—Synthesis, Characterization, Optical Response, and Sensing Properties

2.1 Introduction....30

2.2 Results and Discussion....34

2.2.1 L-Shaped Benzimidazole Fluorophores....34

2.2.2 Other Benzimidazole-based Sensor Precursors....41

2.2.3 X-Ray Crystal Structure Analysis of Other Benzimidazole-based Sensor Precursors....44

2.3 Conclusions and Outlook....49

2.4 Experimental Section....50

2.4.1 General Experimental Methods....50

2.4.2 Synthesis of Half-Cruciforms....51

2.4.3 UV/Vis absorption and fluorescence titrations of compounds **5**–**13** with acid—TFA and base—*n*-Bu_4OH 65

2.4.4 Synthesis of Other Benzimidazole-based Sensor Precursors.....71

2.4.5 Crystal Data for Extended Scope of Other Benzimidazole-based Sensor Precursors.....79

Chapter Three Benzobisimidazole Cruciform Fluorophores

3.1 Introduction.....84

3.2 Results and Discussion 87

3.2.1 Synthesis of Benzobisimidazole Cruciforms 87

3.2.2 Computational Studies.....90

3.2.3 Optical Properties.....91

3.2.4 Optical Response to Acids and Bases.....94

3.2.5 Optical Response of Cruciform **24m** toward Anions 97

3.3 Conclusions and Outlook.....103

3.4 Experimental Section.....104

3.4.1 General Experimental Methods 104

3.4.2 Synthesis of Benzobisimidazole Cruciforms 105

3.4.3 HOMOs and LUMOs of Cruciforms **24a**–**j**, **24l** and **24m**.....128

3.4.4 UV/Vis absorption and fluorescence titrations of cruciforms **24a**–**m** with acid—TFA and base—*n*-Bu_4NOH 129

3.4.5 Sensing of Anions in Organic Media with Cruciform **24m**.....136

3.4.6 Sensing of Anions in Aqueous Organic Media Using Cruciform **24m** 138

Chapter Four Synthesis, Characterization of Precursors for Noncovalent Organic Framework

4.1 Introduction 140

4.1.1 Intrinsically Porous Organic Crystals 142

4.1.2 Extrinsically Porous Organic Crystals 148

4.2 Results and Discussion 153

4.2.1 Synthesis of Precursors for Noncovalent Organic Framework 153

4.2.1.1 Synthesis of Bent Precursors 153

4.2.1.2 Trigonal Precursors with Alternate Components 155

4.2.1.3 Synthesis of Extended Trigonal Precursors 158

4.2.2 Crystal Structures of Precursors for Noncovalent Organic Framework 160

4.2.3 Gas Sorption for Noncovalent Organic Framework **52** 164

4.3 Conclusions and Outlook 166

4.4 Experimental Section 167

4.4.1 General Experimental Methods 167

4.4.2 Synthesis of Precursors for Noncovalent Organic Framework 168

4.4.3 Gas Sorption for Noncovalent Organic Framework **52** 189

4.4.4 Crystal Data of Crystalline Precursors and Noncovalent Organic Framework 192

References 195

*Note: Chapter 1 contains compounds labeled **1** through **75**. A separate numbering system is used for Chapters 2–5. The compounds are numbered **1** through **56**.*

ABBREVIATIONS AND ACRONYMS

ANN	artificial neural networks
APTRA	*o*-aminophenol-*N*,*N*,*O*-triacetic acid
BBO	benzobisoxazole
Boc	*tert*-butyl dicarbonate
Boc_2O	di-*tert*-butyl dicarbonate
BODIPY	4,4-difluoro-4-bora-3a,4a-diaza-s-indacene
BT	benzothiadiazole
CH	cyclohexane
CI	chemical ionization
COFs	covalent organic frameworks
CSI	cold spray ionization
DBAs	dehydrobenzoannuleno)benzenes
DCM	dichloromethane
DFT	density functional theory
DHA	dihydroazulene

DMA	*N*,*N*-dimethylacetamide
DMAP	4-dimethylaminopyridine
DMEDA	*N,N'*-dimethylethylenediamine
DMF	*N*,*N*-dimethylformamide
DMSO	dimethyl sulfoxide
DOSY	diffusion nuclear magnetic resonance spectroscopy
DSB	distyrylbenzene
EtOAc	ethyl acetate
EDTA	ethylenediaminetetraacetic acid
ESI	electrospray ionization
Et_3N	triethylamine
Et_2O	ether
EtOH	ethanol
FMOs	frontier molecular orbitals
HCA	hierarchical clustering analysis
H_2O	water
HOFs	hydrogen-bonded organic frameworks

HOMO	highest occupied molecular orbital
HRMS	high resolution mass spectrometry
ICT	photoinduced intramolecular charge transfer
i-Pr_2NH	diisopropylamine
IR	infrared
LDA	linear discriminant analysis
LUMO	lowest unoccupied molecular orbital
Me_2CO	acetone
MeCN	acetonitrile
MeOH	methanol
MOFs	metal-organic frameworks
nCOF	noncovalent organic framework
NMR	nuclear magnetic resonance
NMP	N-methyl-2-pyrrolidone
NBS	*N*-bromosuccinimide
OFETs	organic field effect transistors
OLEDs	organic light-emitting diodes

PET	photoinduced electron transfer
PCA	principal component analysis
PhMe	toluene
POPs	porous organic polymers
PPA	polyphosphoric acid
PXRD	powder X-ray diffraction
RET	resonance energy transfer
RGB	red/green/blue
TAEB	tetrakis(arylethynyl)benzene
TBA	tetrabutylammonium
TBACN	tetrabutylammonium cyanide
TBAF	tetrabutylammonium fluoride
TBAOH	tetrabutylammonium hydroxide
TEEs	tetramethynylethens
TFA	trifluoroacetic acid
THF	tetrahydrofuran
THP	tetrahydropyranyl

TIPS	triisopropylsilyl
TIPSA	triisopropylsilyl acetylene
TMS	trimethylsilyl
TMSA	trimethylsilyl acetylene
TPBTC	N^1,N^3,N^5-tris(pyridin-4-yl)benzene-1,3,5-tricarboxamide
TPEBs	tetrakis(arylethynyl)benzenes
TPP	*Tris*-*o*-phenylenedioxycyclotriphosphazene
*p*TSA	*para*-toluenesulfonic acid
UV/Vis	ultraviolet/visible
VHF	vinylheptafulvene
ZIFs	zeolitic imidazolate frameworks

Chapter One

Cross-conjugated Molecular Cruciforms as Chemical Sensors

1.1 Introduction

The field of chemosensing has been experiencing rapid growth during the last couple of decades. In contrast to biosensors, which involve the use of receptors based on a biological structure,[1] chemosensors are created from nonbiological entities, and are able to signal the presence of matter or energy.[2] There are generally three main approaches to designing a chemical sensor: (1) the "binding site-signaling subunit" protocol in which the analyte interacts with the binding site inducing the modulations in its covalent bonding partner–signaling subunit, (2) the "displacement" approach where the coordination of the analyte to binding site will displace the signaling subunit, and (3) the "chemodosimester" paradigm, which involves analyte-induced chemical reactions.[3,4] These devices transform chemical information into analytically useful signals such as: (1) change in physical properties (refractive index, conductivity, temperature, mass, or optical change), (2) chemical reaction, and (3) biochemical process.[5,6] In comparison with other detection techniques which necessitate advanced, complex instrumentation, optical detection (*via* fluorescence or colorimetric changes) has some dominant advantages due to the simplicity, speed, and low detection limits that can go down to a single molecule.[7,8]

A fluorescent chemosensor is a probe that forms complexes with an analyte reversibly with concomitant fluorescent-signal transduction.[9] Data can readily be obtained for a specific target by an operationally-simple detection scheme exploiting

binding-induced pertubations of photophysical processes such as photoinduced electron transfer (PET), photoinduced intramolecular charge transfer (ICT), and resonance energy transfer (RET).[10,11] Fluorescent organic molecules in general and fluorescent chemosensors in particular, typically are large conjugated π-electron systems.[11,12] For example, most polycyclic aromatic hydrocarbons are intensively fluorescent.[13]

A conjugated system is defined as a chain of alternating single and multiple bonds generating continuous *p*-orbitals with electrons delocalized throughout the molecule.[14, 15] As long as each contiguous atom in the chain has an available *p*-orbital—for example, unshared electrons in *p*-orbitals of a heteroatom, the molecule can be considered conjugated.[16] The delocalization of electrons among *p*-orbitals lowers the overall energy of the molecule and increases its stability.[17] Conjugation influences both the optical and electronic properties of these molecules. Conjugated systems find a wide range of applications, such as: organic semiconductors or semi-metals in the emerging field of plastic electronics. Polyacenes tend to form molecular crystals with high order allowing high charge mobilities rendering them useful in organic field effect transistor (OFETs) devices.[18] Two-dimensional conjugated systems such as graphite are considered semi-metallic that contain valence- and conduction-band overlap at the Fermi level.[19] Conjugated polymers have played an important role in organic optoelectronic devices which convert electrical signals into photon signals and vice versa, such as: photodiodes, light emitting diodes (LEDs),[20] solar cells,[21] photovoltaic cells,[22] and field-effect transitors.[23,24] The optical properties of conjugated molecules have many potential

applications including fluorescence sensing, colorimetric detection of biological targets, environmental analysis, and biological imaging.[25]

The characteristics of a conjugated π-system primarily can be regulated by the modulation of chain-length or the substituents along the backbone of the system, which in turn control the band gap of molecule.[26] As the number of *p*-orbitals increases in the conjugated system, the energy gap between highest occupied molecular orbital (HOMO) and lowest unoccupied molecular orbital (LUMO) becomes smaller. This is observed in bright colors of flowers and fruits as well as synthetic dyes and pigments generated by highly conjugated compounds.[27,28] However, adjustment of the HOMO-LUMO energy gap through changes in the chain length as well as substituent modification in a linear π-conjugated system requires significant effort in syntheses and brings about reactivity issues associated with long oligoenes. Additionally, in most, but not all conjugated systems, their frontier molecular orbitals (FMOs) are "congruent", delocalized and extensively superimposed throughout the entire π-conjugated system, thus making their independent-modification challenging.

An alternative strategy to predictable modulation of the HOMO–LUMO gap is the use of cross-conjugated cruciform π-systems. Because of their topography, cross-conjugated molecular cruciforms can easily separate their frontier molecular orbitals, and as a result, there is an ongoing interest in investigating these structures. A molecular cruciform is a cross-conjugated π-system characterized by rigid X-shaped geometry with two conjugation circuits intersecting at the central aromatic core. If a cruciform is carefully designed, the HOMO is located on the branch with electron-donating

substituents, while LUMO is situated on the axis with electron-withdrawing substituents. Upon the spatial separation of FMOs, analyte binding to such systems invariably alters the HOMO−LUMO gap and leads to a change in their optical properties. A cruciform structure consists of a conjugated core in the center with four conjugated pathways as well as four end-groups (Figure 1.1),[29] opening a wide range of possibilities for manipulation, and bodes well for other applications in molecular electronics[30] and crystal engineering.[31] Apart from cruciforms, other materials which possess spatially separated FMOs were exhaustively explored, including spiro compounds,[32] paracyclophanes,[33] swivel-type dimers,[34] and tetrasubstituted tolanes.[36]

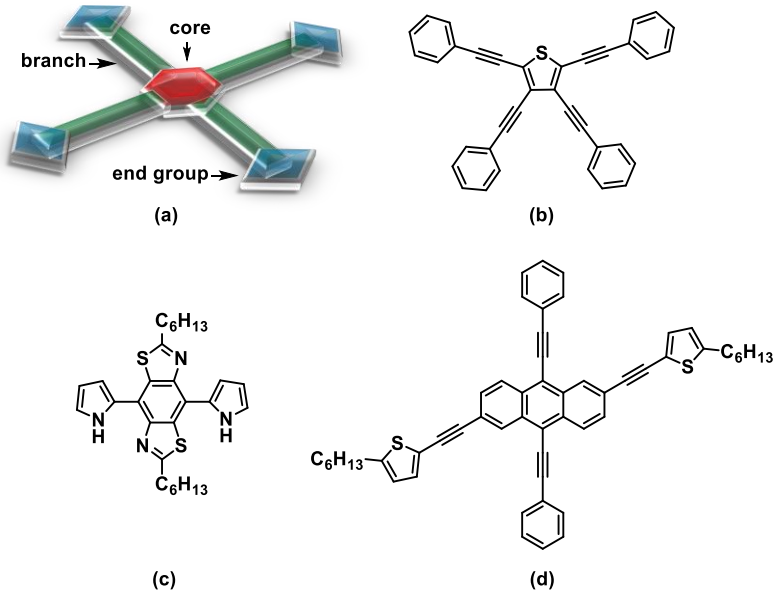

Figure 1.1 (a) Systematical view of a molecular cruciform, and three examples: (b) tetra(phenylethynyl)thiophene, (c) 2,6-didodecyl-4,8-dipyrrole-2-yl-benzo[1,2-*d*;4,5-*d*′]bisthiazole, and (d) 2,2′-[[9,10-bis(2-phenylethynyl)-2,6-anthracenediyl]di-1,2-ethynediyl]bis[5-hexylthiophene].

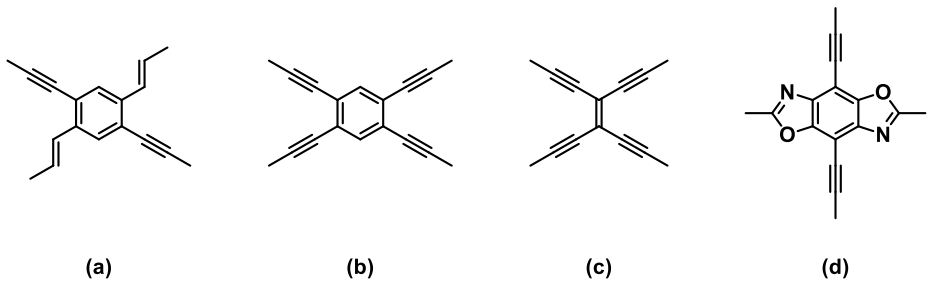

Figure 1.2 Selected core-branch combinations explored in molecular cruciforms.

Within the last two decades, several molecular cruciform platforms have been designed for these purposes, with spatially separated FMOs which can be autonomously addressed. The core positions in the center of cruciform structure are the connecting four intersection branches and the directing angle of the cross axes. For that reason, the core was studied in a variety of simple motifs, such asethylene, benzene ring, thiophene,[37] or biphenyl to more complicated scaffolds, such asheterocycle-fused aromatic rings like benzo[1,2-*d*:4,5-*d*′]bisthiazole,[38] indolo[3,2-*b*]carbazoles,[39] benzo[1,2-*b*:4,5-*b*′]dithiophenes,[40] and benzo[1,2-*d*:4,5-*d*′]bisoxazoles.[41] The core, together with the four branches, generates the rigid frame of the cruciform; the most commonly used arm in a cruciform is the ethynyl and *trans*-vinyl moiety (Figure 1.2). The last important part in the cruciform structure is the end groups, which typically are communication sites. Depending on the functional group and the geometry incorporated in the end group, the end groups can participate in molecular recognition events or secure the cruciform structure onto the metal surfaces. Being a supramolecular molecule, the cruciform has plentiful locations in its skeleton that can be modified in order to bind to an application target; Either structure or application field can be used to categorize cruciforms into small groups. Within the limit of this chapter, four representative cruciform families will be

discussed (Figure 1.2) concerning their synthetic strategy, characterization, and applications.

1.2 Distyrylbis(arylethynyl)benzenes

One of the most important families of cruciforms is the 1,4-distyryl-2,5-bis(arylethynyl)benzene studied by Bunz *et al.*[42] These cruciforms are constituted of two linear π-conjugated divisions, a perpendicular distyryl branch and an arylethynyl branch, intersected at a central benzene core. The exploration of this distyrylbis(arylethynyl)benzenes cruciform was initiated from Bunz's initial work on cross-conjugated polymers.[43] This group primarily focused on cruciform design, the use of cruciforms as building blocks in supramolecular assemblies[44,45] and as components of molecular electronics;[31,46] and their analyte-induced changes in fluorescence.[47,48,49] They also pioneered the development of simple, yet powerful differential sensor arrays using digital photography of emission colors, rather than exhaustive fluorescence spectroscopy.[50] The creation of sensor arrays allowed ratiometric sensing of two or more analytes at the same time with versatile system consisting of a sensor and solvent combination.

The general synthesis scheme that leads to cruciform synthesis starts from diiodide **1**, as seen in Scheme 1.1, whose photochemical bromination yields the tetrahalide **2**. An Arbuzov reaction converts **2** into the phosphonate **3**. The two last steps employ sequential Horner and Sonogashira couplings to incorporate styryl substituents (in **4**) and alkynyl groups (in **5**), respectively (Scheme 1.1).[42] Quantum chemical

calculations (B3LYP 6-31G**//6-31G**) also confirmed that the donor and acceptor substituents position the HOMO and LUMO on the respective styryl and arylethynyl branches. These donor-acceptor compounds typically show dramatic solvatochromicity, as exemplified by the emission spetrum in chloroform, which are substantially red-shifted from the emissions in hexane.[43b] This distinct solvent-dependent emission can be easily understood by stabilization of the charge-transfer excited state. In the solid state, different cruciform morphologies (thin film, crystalline phases, nanoparticles) display distinct emissive behavior.[31]

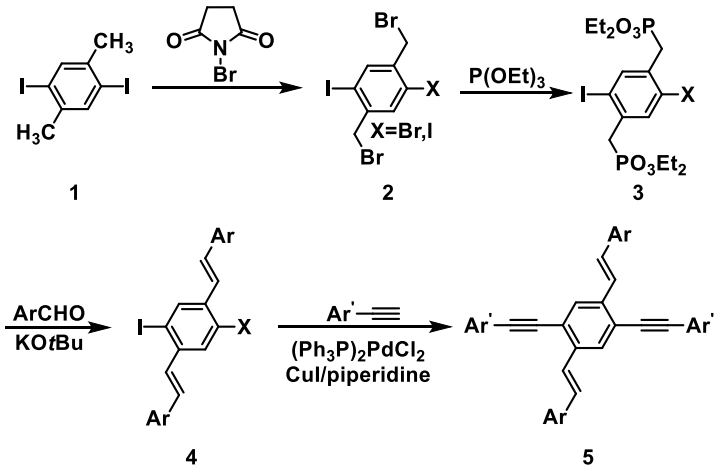

Scheme 1.1 General synthetic scheme for the synthesis of distyrylbis(arylethynyl)benzenes cruciforms.

These cruciforms were used as detectors for protons and metal ions.[47,48] A cruciform with a donor group on the styryl arm and the acceptor group on the ethynyl arm exhibits a two-step fluorescence response. When cruciform **6** possessing Lewis-basic nitrogens was exposed in a gradient to either trifluoroacetic acid (TFA) or $Zn(OTf)_2$, the

emission color changed from orange to blue to green. This rare phenomenon can be rationalized by the first binding of analyte to the anilines, lowering the HOMO and leaving the LUMO unperturbed. This binding caused a hypsochromic shift, while subsequent additions of analyte coordinates to the pyridine nitrogens, stabilizing the LUMO and generating a second bathochromic shift. The identification of Mg^{2+}, Ca^{2+}, Mn^{2+}, Zn^{2+} was performed with cruciform **6**, **7**, **8**, **9**, **10**. These +2 charged triflate metal salts were chosen as analytical targets because of their crucial biological activity. The size concomitant with the hardness of these ions are the main driving forces for varying their optical responses to different cruciforms, inducing the capability to discern all these metal ions in ideal conditions.[48] In order to increase the response toward protons or metal cations external stimuli, the phenothiazine-substitute, electron-rich tricyclic heterocycles was introduced into the cruciform structure. Metal cations coordinate with nitrogen in aniline and pyridine more preferably than the one in phenothiazine; consequently, the use of cruciforms **11**, **12**, **13**, **14**, **15** with different substitution pattern can enforce dissimilar emission color in the case of **6**. A small color array was built up to discern Ca^{2+}, Zn^{2+}, Mg^{2+}, in which zinc was distinguishable from magnesium ions without the interference of calcium ions. Their coordinative ability to phenothiazine–cruciform follows this trend: $Ca^{2+} < Zn^{2+} < Mg^{2+}$.[51] Together with **9**, two new cruciforms **16**, **17** were synthesized for the purpose of differentiation of ten different aromatic carboxylic acids which have closely spaced *p*Ka values.[52] These fluorophores generated various signature colors under ultraviolet (UV) light irradiation based on protonation-induced fluorescence shifts mechanism; the sensor array was constituted from recorded digital photography of three

fluorophores in each of six solvents containing excess amount each of 10 different carboxylic acids.

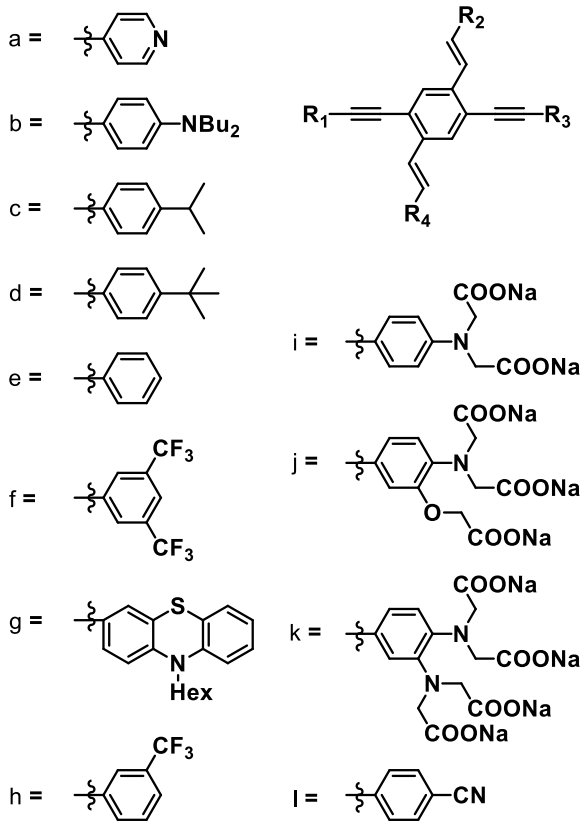

	R1	R2	R3	R4
6	a	b	a	b
7	a	c	a	c
8	d	a	d	a
9	e	b	e	b
10	f	b	f	b
11	b	g	b	g
12	d	g	d	g
13	a	g	a	g
14	h	g	h	g
15	f	g	f	g
16	l	b	l	b
17	e	a	e	a
18	e	i	e	i
19	e	j	e	j
20	e	k	e	k

Figure 1.3 Selected distyrylbis(arylethynyl)benzenes cruciform with specific optical properties.

By the combination of Horner reaction, Sonogashira coupling, and subsequent saponification, Bunz *et al*. created a series of water-soluble cruciforms **18**, **19**, and **20**.[53] In the presence of PIPES buffer, the expanded cruciforms functionalized with *o*-aminophenol-*N*,*N*,*O*-triacetic (APTRA) salts, or benzo-ethylenediaminetetraacetic acid (EDTA) receptor units featured metalloreactivity that was dependent on fluorophore concentration. The emission spectrum of **19** upon exposure to Zn^{2+} is tuned from red

shifting to blue shifting when the cruciform concentration was switched from 50 $\mu mol \cdot L^{-1}$ to 5 $\mu mol \cdot L^{-1}$. It was suggested that zincation exerted either the suppression or the breakup of excimeric species of **19**, which only occurred in the more concentrated solution. Surprisingly, the color change from metal ion addition was mostly rationalized by the breakup of aggregates, induced by a combination of electrostatic repulsion of the negatively charged carboxylate groups and the significant steric crowding of APTRA motif rather than metal binding to the lone pair of the aniline nitrogen.

To further explore the potential utility of this cruciform family as a sensor for amines, the terminal groups in distyrylbis(arylethynyl)benzenes were functionalized with a phenol group in **21** and **22**.[54] When the cruciform, carrying strategically placed phenolic functionalities, was exposed to an amine, the hydroxyl end group interacted with the amine, causing a photoinduced excited state proton transfer.[55] The difference in *p*Ka values of the hydroxyl group from the phenol and amines, as well as the structure of the amine, determined the emission color of the solution. As a result, after combining all the pictures of emission colors taken from the sensor array, twelve different amines were discernable upon exposure to **22** in eight solvents. The fluorophore's sensitive reaction to the added analytes inspired the Bunz group to immobilize cruciforms in or on surface-functionalized mesoporous SBA-15 silica.[56] The incorporated solid retained the highly fluorescent character of cruciforms in solution, displaying reactivity towards some volatile representative amines and organic acids. In order to sense various classes of amine analytes, such asprimary amines, primary diamines, and secondary amines, the cruciform possessing an aldehyde appendage **23** was achieved. A photography sensor

array utilizing a single cruciform **23** in seven different solvents can qualitatively identify thirteen different amines at a concentration of 10 μL amine in 2 mL of solvent, evaluated by the extracted red, green, blue (RGB) response patterns.[57] Compound **23** reacted with primary amines, primary diamines, and secondary amines to form imines, cyclic aminals, and hemiaminals, respectively; tertiary amines proved unreactive. In another aspect, the imine can also serve as a metallo-reactive motif; accordingly, post-functionalized aldehyde-substituted cruciforms were synthesized based on the simple imination between different primary amines and aldehyde-substituted cruciform **24**. Upon exposure to Cu^{2+} and Zn^{2+} salts, these imine-based cruciforms displayed ratiometric fluorescent-signal due to the coordination of the metal ions to the imine, thus acting as metal-reactive fluorophores.[58] Most recently, Bunz reported the construction of a water-soluble cruciform containing an aldehyde substituent and oligoethylene glycol side chain **25**. The arrangement between **25** and two other aldehyde-appended distyrylbenzene (DSB) into a sensor array produced an amine and amino acid reactive sensory tool in which analytes can selectively turn on fluorophores.[59]

To explore the construction of self-assembled probes capable of indirectly detecting simple inorganic anions, compound **26** appended by terpyridine moieties was produced, and was found to form a fluororphore-metal ion complex with Zn^{2+} ions. This complex could distinguish fluoride from other halides because of these anions' different affinity for zinc.[60]

Cruciforms containing basic nitrogen and phenol functionalities were shown to be successful in acid and base identification, respectively. Amphoteric cruciforms, whose

structures incorporated both dialkylaniline and hydroxyl substituents, were subsequently developed with the expectation to serve as a dual function sensor. [61] In both adsorption and emission spectra, cruciform **27** displays red-shifting from acid addition due to protonation and blue-shifting from base addition due of deprotonation, thus it is logical that **27** also expresses both cation-reactivity and amine-responsivity.

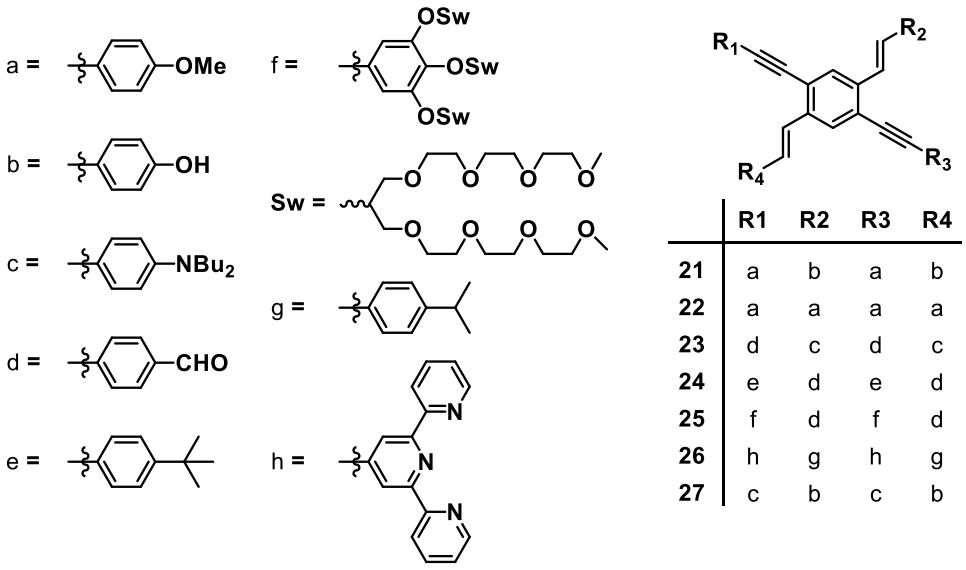

	R1	R2	R3	R4
21	a	b	a	b
22	a	a	a	a
23	d	c	d	c
24	e	d	e	d
25	f	d	f	d
26	h	g	h	g
27	c	b	c	b

Figure 1.4 Selected hydroxyl-distyrylbis(arylethynyl)benzene-based cruciforms.

An isocruciform, a small subset of distyrylbis(arylethynyl)benzenes, in which the substituent (either styryl or phenylethynyl) is of *ortho*- instead of the *para*-directionality in respect to its iso–substituent, as exemplified by compound **28** (Figure 1.5).[62] The isocruciforms have very similar optical and electrical properties to those of cruciforms, except their band gap is somewhat larger than in cruciforms because of the attenuated conjugated pathways in the *ortho*-connected isomers. They also have faster bleaching in dilute solution and in thin films compared to cruciforms, which makes them potentially

attractive as materials for photopatterning. On the other hand, stronger donor-acceptor substituents will display more localization of HOMO-LUMO in the isocruciform system, which is similar to normal distyrylbis(arylethynyl)benzenes. Unsymmetrical cruciforms, such as **29**, were also explored to gain a better understanding as could not be addressed with the symmetrical cruciforms.[63] For example, how the spectra of partially protonated symmetrical cruciforms look,the kinetic differences between protonation stepss, whether or not changing the topology of the donor and acceptor substituents affects the different conjugative pathways? It may also provide proof for decomplexation or enhanced complexation between metals and cruciform in the excited state.

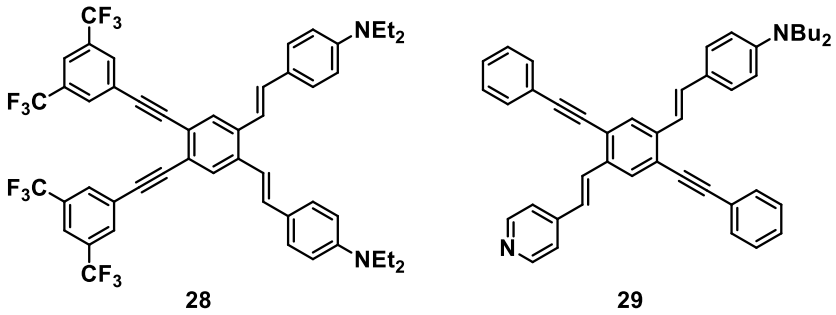

Figure 1.5 Selected representatives of isocruciform distyrylbis(arylethynyl)benzenes.

1.3 Tetrakis(arylethynyl)benzenes

Another significant cruciform molecule class is the 1,2,4,5-tetrakis(phenylethynyl)benzenes (TPEBs), synthesized, analyzed structurally and substitutionally by Haley and colleagues.[64] Furthermore, these molecular cruciforms were compared to those in the bis(dehydrobenzoannuleno)benzenes (bisDBAs) series.

BisDBAs possess the same basic carbon backbone as the TPEBs, but are secured into planarity by a diacetylene bridge (Figure 1.6).[65]

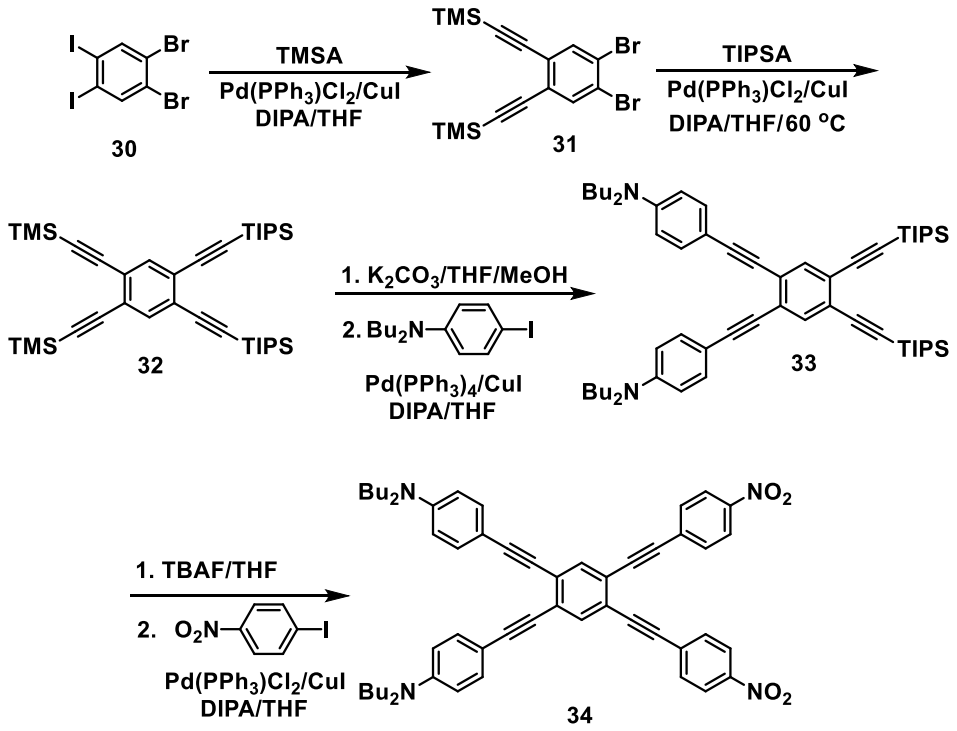

Scheme 1.2 An exemplary synthetic scheme for the synthesis of tetrakis(arylethynyl)benzenes cruciforms.

The general synthetic strategy for TPEBs mainly employed Sonogashira cross-coupling, starting from 1,2-dibromo-4,5-diiodobenzene **30**, and intended to incorporatel different donor or acceptor substitutes in the separate branches of the molecule. On account of the different activity between iodo- and bromo-substituents, Haley *et al.* . selectively cross-coupled the iodo-substituent with trimethylsilyl acetylene (TMSA), then bromo-substituent can undergo a second cross-coupling with triisopropylsilyl acetylene (TIPSA). These protecting groups were also removed in this sequence: TMS was initially

deprotected by K_2CO_3/ MeOH, and the resulting alkyne was cross-coupled with *N*,*N*-dibutyl-4-iodoaniline to give **33**, followed by the removal of TIPS with tetrabutylammonium fluoride (TBAF), and coupling of the resultant terminal alkyne with 4-iodo-1-nitrobenzene to give final product **34**. Changing the halogenated starting material with the appropriated isomer and following analogous synthetic schemes afforded other target TPEBs.

In order to explore the differences between the linear-conjugated (Figure 1.6, path a), cross-conjugated (path b), and "bent" conjugated (path c) pathways, cruciforms **34**–**38** were synthesized. Both **34** and **37** contained charge-transfer conduits in their linear-conjugated pathways; hence, they each have distinct low-energy bands compared to **35** and **36,** while **38** shows a much weakened low-energy band. This further implies thelinear-conjugated pathway is more efficient than the bent-conjugated or cross-conjugated donor to acceptor pathways. The larger net dipoles and linear-conjugated pathways in the donor-acceptor system provided the largest bathochromic shifts. The bisDBAs show bathochromic shift compared to the TPEPs due to the planarity in the bisDBA, which enhances the overall conjugation. Having similar highly polarized excited states like distyrylbis(arylethynyl)benzenes, the emission properties of these cruciforms display dramatic solvent dependency. Upon protonation, both absorption and emission signals were quenched because protonation at the donor site disrupted the donor-acceptor route. The molecular orbital plots are in agreement with experimental results, in which the HOMO and LUMO, respectively, were located in donor and acceptor substituted arms for both donor-acceptor system of TPEBs and bisDBAs.

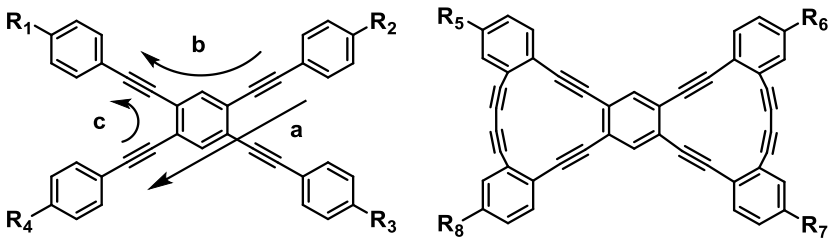

Figure 1.6 TPEBs (left) and bisDBAs (right).

Additional study of this cruciform family was constructed with a new donor-acceptor setup, for example, compounds **39**, **40**, **41**, in which the nitro group was replaced by a pyridine end group. This new design brought TPEBs closer to distyrylbis(arylethynyl)benzenes **6** in structure for easier comparison.[66] They also showed affinity to Zn^{2+}, but less so than **6**, suggesting probably less conjugation conferred by triple bonds relative to double bonds. However, these cruciforms have stronger solvatochromism and higher quantum yields than nitrophenyl acceptor-functionalized analogues; high quantum yields are reached even with spatially separated FMOs. A "sensing array" composed of fluorophores **39**, **40**, **41** and six metal ions shows the differential responses, implying the potential for a host of applications. In addition, the weaker acceptor groups benzotrifluoride and pentafluorophenyl were introduced into the TPEBs cruciform, as exemplified by **46**, **47**, in comparison to former analogues possessing nitrophenyl **37**, **38**, **42** or benzonitrile **43**, **44**, **45**.[67] This inductive acceptor-functionalized TPEBs exhibited strongly fluorescent intramolecular charge transfer and strong solvatochromism similar to resonance acceptor TPEBs **37**, **38**, **42**–**45**; however, they also showed high quantum yield, promising for nonlinear optical device materials. The pentafluorophenyl-acceptor TPEBs displayed more red-shifted absorption and

emission relative to benzotrifluoride-acceptor TPEB, approaching the benzonitrile and nitrophenyl systems in terms of optical band gap narrowing ability.[68]

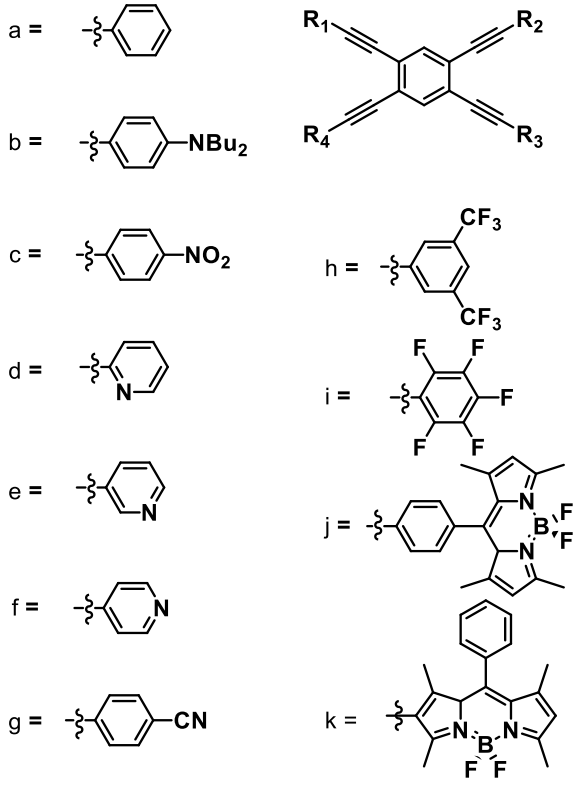

	R_1	R_2	R_3	R_4
35	a	a	a	a
36	b	b	b	b
37	b	b	c	c
38	b	c	b	c
39	b	d	d	b
40	b	b	e	e
41	b	f	b	f
42	c	b	b	c
43	g	b	b	g
44	b	b	g	g
45	b	g	b	g
46	b	b	h	h
47	b	b	i	i
48	b	b	j	j
49	b	b	k	k

Figure 1.7 Selected representatives of TPEBs.

Furthermore, the 4,4-difluoro-4-bora-3a,4a-diaza-s-indacene (BODIPY) core was also successfully incorporated into the tetrakis(arylethynyl)benzene (TAEB) structure, such as compounds **48**, **49**.[69] BODIPY caught attention and was chosen because they can act as stronger acceptors for increasing charge transfer, stronger net dipole, and exhibit larger bathochromic shifts. Hence, these cruciforms typically have the LUMO localized on axis with BODIPY-terminals and the HOMO on the donor-substituted branches. Experimental results revealed remarkable impacts of BODIPY upon properties of the

cruciform. For instance, it causes the impotence of solvatochromism and enhances the quantum yield to levels not yet seen with the TAEB molecules, but also tends to quench fluorescence in polar solvents.

Sun's research group shared a longstanding interest in donor-acceptor functionalized TPEBs. Their TPEBs were synthesized and also collated with benzoannulenes to explore two-photon absorption in combination with computational calculation.[70]

1.4 Tetrakis(alkynyl)ethenes

Tetrakis(phenylethynyl)ethene was first synthesized in 1969 by Hori *et al.* by the dimerization reaction of 1,5-diphenyl-3-bromo-1,4-pentadiyne in the presence of potassium t-butoxide in the mixture of tetrahydrofuran (THF) and N-methyl-2-pyrrolidone (NMP).[71] This conjugated system is of special interest for the generation of interesting macrocyclic and polymeric structures. In comparison to *cis*-stilbenes or 1,1,2,2-tetraphenylethylenes, tetraethynylethenes (TEEs) are more likely to facilitate π-conjugation due to their fewer steric interactions which can prevent coplanarity. Later on, Hauptmann, having the same fascination with the TEEs motif, had opened a new route for the synthesis of this structure, in which the starting material 1,1,2,2-tetraethynylethanes underwent dehydrogenation by *n*-BuLi and *t*-BuOCl and the persilylated and peralkylated derivatives **50**–**52** were reported.[72]

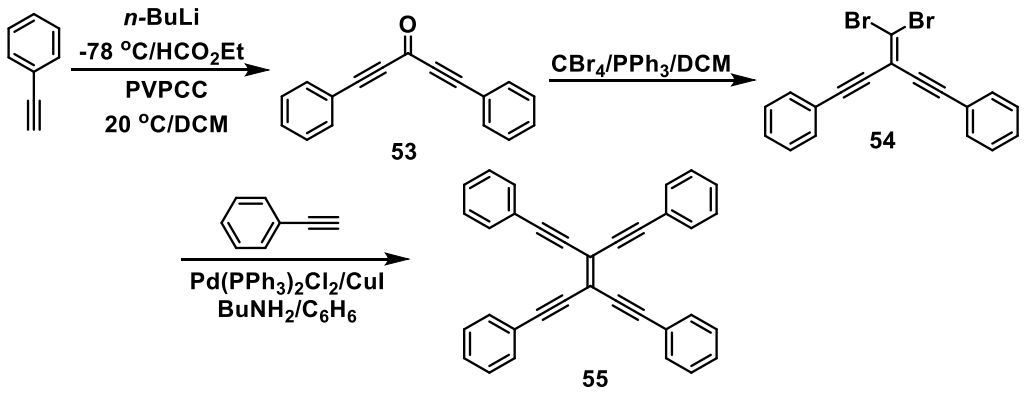

Scheme 1.3 Synthetic scheme for the synthesis of tetrakis(phenylethynyl)ethene cruciform.

Most recently, TEEs were primarily studied by Diederich's group with a new synthetic scheme, as exemplified by synthesis of tetrakis(phenylethynyl)ethene (Scheme 1.3)[76]. Starting from phenylacetylene deprotonation by *n*-BuLi, the following reduction of ethyl formate gives bis(phenylethynyl)-substituted secondary alcohol. Further oxidation by pyridinium chlorochromate furnishes the ketone **53**, which was transformed to bis(phenylethyny1)-dibromoolefin **54** in Wittig dihalomethylenation reaction. Finally, Sonogashira cross-coupling completed the target structure. TEEs with two or more free terminal alkyne **56**[77] were stabilized only in dilute solution and polymerized quickly in pure form, whereas tetra- and triprotected derivaties were more stable.[78]

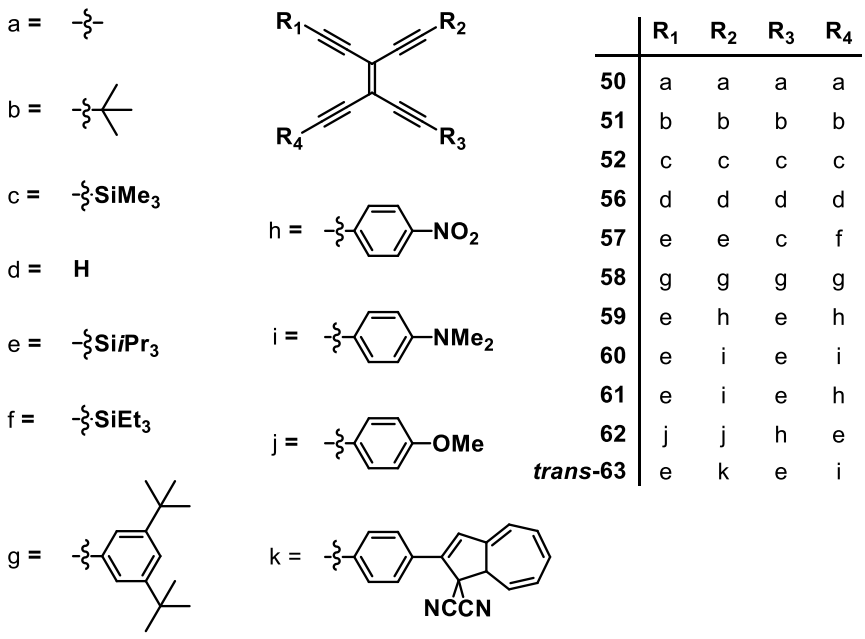

	R_1	R_2	R_3	R_4
50	a	a	a	a
51	b	b	b	b
52	c	c	c	c
56	d	d	d	d
57	e	e	c	f
58	g	g	g	g
59	e	h	e	h
60	e	i	e	i
61	e	i	e	h
62	j	j	h	e
***trans*-63**	e	k	e	i

Figure 1.7 Selected representative of tetraethynylethenes.

Tetrakis(phenylethynyl)ethene as a donor formed a π-complex with the n-electron acceptors 2,4,7-trinitrofluoren-9-one or (2,4,7-trinitro-9-fluorenylidene)malononitrile with 1:2 stoichiometry in the solid state and 1:1 complexes in solution. Complexation tuned the color of the solution immediately from yellow to orange-red, verified by the presence of the charge-transfer interaction. The strength of noncovalent complexation was affected by the spatial displacement of the phenyl rings in the donor molecules and the electrostatic point charge rather than the orbital interactions in the molecular complexation. The TEE-based systems herein are illustrated to be useful for rigid frameworks because their weak π-π interactions are needed for the goal of designer solid.[73] The synthetic versatility allowed for the formation of widely diversified rigid planar chromophores **52**, **55**, **57**, **58**; their redox properties were also reported. These chromophores can undertake successive reduction electron transfer on Hg electrodes in

THF + 0.1 M Bu_4NPF_6, producing chemically stable products on the time-scale of the electrochemical experiments. The substituents in TEEs can fine-tune the reduction potential of the molecule; however, the electrochemical analyses of donor-and/or acceptor-functionalized TEEs indicated that the conjugated core is inefficient at delocalizing charges between redox centers.[79,80] The structure-property relationship was further studied by more donor-acceptor TEEs **58**–**62**, providing insight into strategy, leading to desired optical nonlinearities and indicating their importance for third-order nonlinear optics. The TEE motif is also a promising solution for third-order nonlinear optical device's fabrication requirement due to their polymerization ability seen in **58**–**60,** as well as thermal stability with the melting point or decomposition above 200 °C.[81] The UV/VIS spectra of donor-acceptor molecules all show low-energy absorptions attributable to charge transfer from donor to acceptor in the excited state. Similar to TPEBs, the linear conjugation paths in *cis*- and *trans*-donor-acceptor-substituents is more effective than along cross-conjugation paths in the geminal substituents.[81b] TEEs were also shown to act as molecular switches for external stimuli, for example **63** which can be reversibly photoisomerized between its *cis*- and *trans*- forms, contains a dihydroazulene (DHA) unit, which can be transformed into a vinylheptafulvene (VHF) moiety upon specific irradiation and possesses a proton sensitive *N*,*N*-dimethylanilino group.[82] Under irradiation of λ_{max}=464 nm *trans*-**63** was converted to *cis*-**63**, while the reverse reaction requires λ_{max}=369 nm irradiation. With three possible switching processes, **63** can have eight interconvertible states, which can be very promising towards multifunctional molecular devices.

1.5 Benzobisoxazole Cruciforms[83]

Cruciforms with heterocyclic benzobisoxazole (BBO) central core have been studied by our group as well as the group of Nuckolls, who used these molecules as conjugated molecular wires that could be ornamented with solubilizing groups perpendicular to the conjugation circuit,[84] and the group of Jeffries-EL, who focused on the use of BBOs as electron-deficient building blocks for semiconducting polymers.[85]

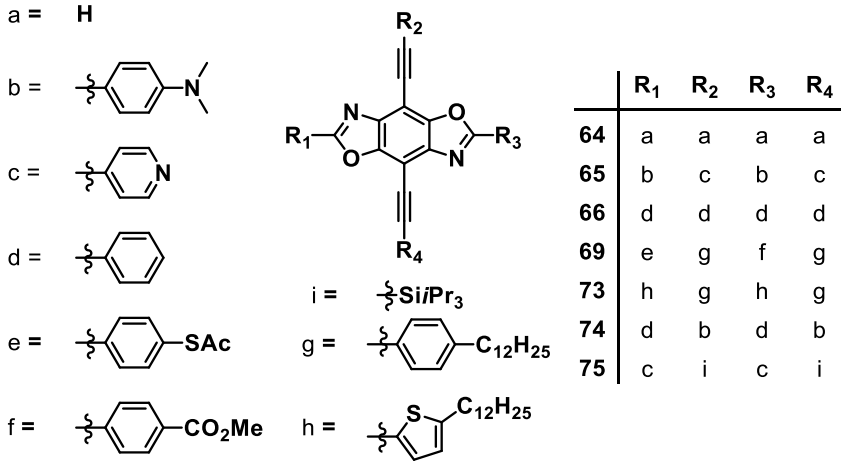

	R1	R2	R3	R4
64	a	a	a	a
65	b	c	b	c
66	d	d	d	d
69	e	g	f	g
73	h	g	h	g
74	d	b	d	b
75	c	i	c	i

Figure 1.8 Selected representative of BBO cruciforms.

Three general synthetic routes to cross-conjugated BBOs have been developed, allowing the incorporation of a wide variety of alkyl, aryl, heteroaryl, and arylethynyl groups in each of the four substitution positions available on the BBO nucleus. For clarity, Scheme 1.4 illustrates each route with just a single example; among them, these three routes have yielded close to 50 different cruciform systems. In 2003, Nuckolls and co-workers developed a versatile synthesis of aryl-substituted BBO cruciforms.[86] Starting

[83] Saeed, M. A.; Le, H. T. M.; Miljanić, O. Š. *Acc. Chem. Res.* **2014**, *47*, 2074–2083.

with azide-substituted benzoquinone **67** (Scheme 1.4A, accessible in five steps from 4-bromophenol), reduction with $Na_2S_2O_4$ and subsequent acylation produced diester **68**. By judicious choice of the reaction conditions, differentially substituted esters could be prepared, which was essential for the subsequent attachment of these cruciforms to metal surfaces. Final Staudinger cyclization produced cruciform **69**. This route was mild enough to allow incorporation of fragile functionalities such as acetate-protected thiols into BBO cruciforms. Our procedure for the preparation of donor-acceptor-substituted BBO cruciforms (Scheme 1.4B) started from 2,5-diamino-3,6-dibromobenzene-1,4-diol **70**.[87] The horizontal axis of the cruciforms was incorporated using microwave-assisted acyl condensation with the parent carboxylic acids in the presence of polyphosphoric acid (PPA).[88] Subsequent Sonogashira coupling was performed on **71** to introduce the vertical axis in the final cruciform **65**. While this protocol used harsher conditions than the one described by Nuckolls, the incorporated functional groups were not overly sensitive, and all of the reactions yielded the desired cruciform products. For other BBO cruciforms, the yields of the final Sonogashira coupling varied widely (9−96%). Occasional low yields could be attributed to the low solubility of the dibromo intermediate **71** (and analogues), possible coordination of metal catalysts with nitrogen-containing intermediates, and the electronic mismatch between terminal alkyne and aryl bromide coupling patterns. Jeffries-EL utilized orthoesters as condensation partners for **70** (Scheme 1C).[89] Subsequent Suzuki coupling of **72** with a phenylboronic acid yielded aryl/heteroaryl cruciform **73**.[86] Compound **72** and its analogues were also reacted with terminal alkynes through Sonogashira coupling[41a] and thiophenyltin reagents by Stille cross-coupling[86] to

deliver cruciforms substituted with alkynyl and heteroaryl groups along the vertical axis (not shown).

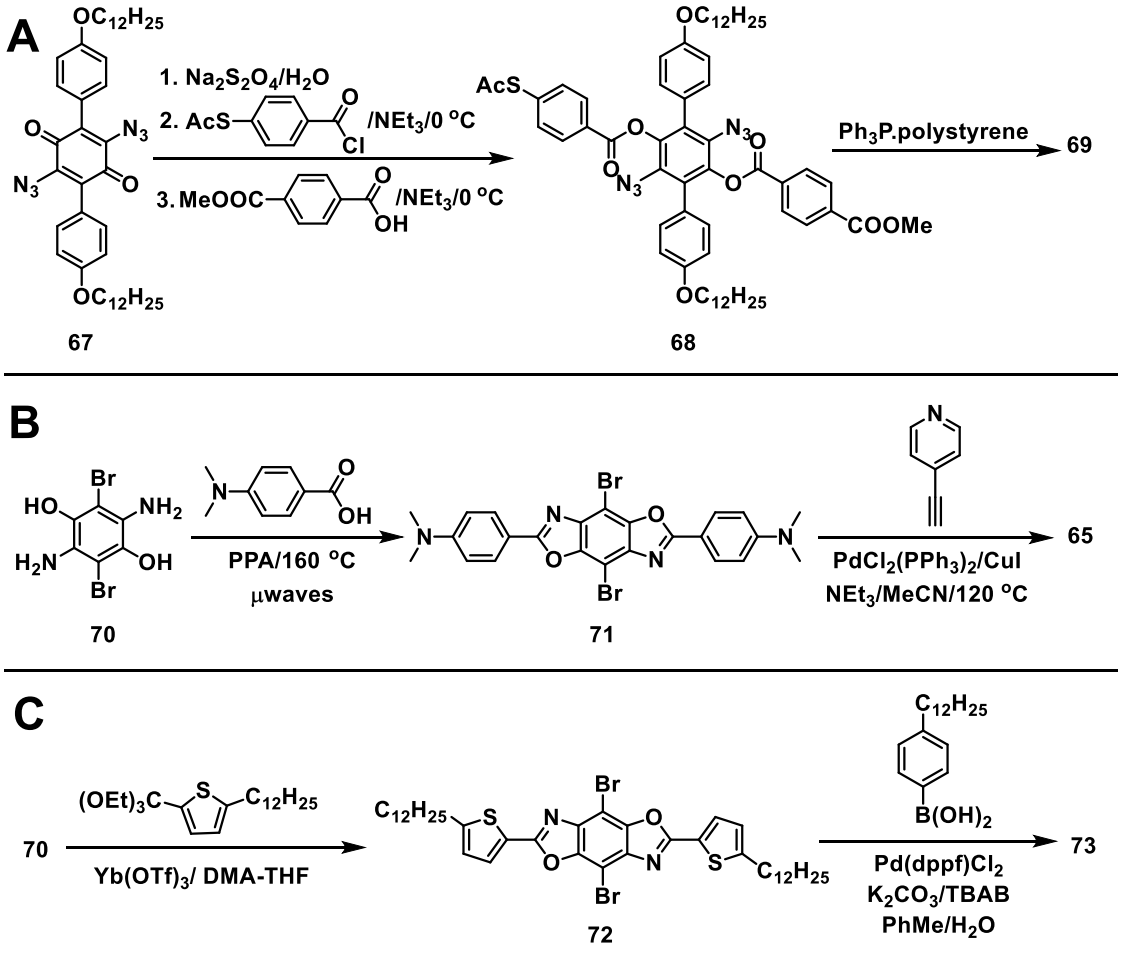

Scheme 1.4 Synthetic strategies used for the synthesis BBO cruciforms

Initial computational insight by density functional theory (DFT) at the B3LYP/3-21G level confirmed the FMOs of the donor-acceptor BBO cruciform **65** are spatially strictly localized: the HOMO is positioned along the electron-rich horizontal axis, while the vertical axis is electron-poor.[88] The localization of the FMOs is a consequence of both the donor-acceptor substitution and the properties of the [1,2-*d*;4,5-*d*′]-BBO parent

structure. In the parent BBO **64**, the LUMO communicates readily with both the horizontal and vertical axes; in the substituted system, the electron-withdrawing pyridines on the vertical axis steer this balance in favor of localizing the LUMO vertically. We have examined systems which are not donor-acceptor substituted both synthetically and computationally by preparing and calculating FMOs for a series of nine BBO cruciforms in which the substitution on both the vertical and horizontal axes was varied pairwise among the electron-rich 4-(*N*,*N*-dimethylamino)phenyl, electron-neutral phenyl, and electron-poor 4-pyridyl groups. As an illustration, the HOMO of the tetraphenyl-substituted parent cruciform **66** is very similar to the HOMO of **64** in that the HOMO has significantly more of its density localized along the vertical axis. In contrast, the LUMO of **66** is spread out over the entire molecule. Analyte binding to either of the two axes should still affect the two FMOs disproportionately. This phenomenon illustrates one important feature of the central BBO core: it can induce spatial separation of the FMOs without the explicit requirement of donor-acceptor substitution. Jeffries-EL and co-workers have performed analogous computational studies on aryl- and heteroaryl-substituted BBO cruciforms[90] with the aim of examining their HOMO−LUMO gaps for applications in the area of electronic materials. Using a combination of DFT calculations and ultraviolet photoelectron spectroscopy (which can measure absolute HOMO levels), they have shown that substitution can be used to modify the BBO cruciforms' HOMO−LUMO gaps across a 0.5 eV range.

All of the examined BBO systems are solvatochromic, with their emission shifting steadily toward the red with increasing solvent polarity. BBO cruciforms

reversibly respond to protonation by dramatic changes in their UV/Vis absorption and fluorescence emission properties. Cruciform **74** is substituted with electron donors along its vertical axis: its HOMO is localized along the vertical axis, while the more delocalized LUMO is still along the horizontal axis. Thus, protonation of the dimethylamino groups disproportionately stabilizes the HOMO, leading to blue shifts in the absorption and emission spectra. As is the case with **66**, high acid concentrations lead to some quenching in the emission spectrum, a phenomenon that we attribute to partial protonation of the BBO core under such conditions. The most complex case is presented by the donor-acceptor cruciform **65**. Here, initial protonation occurs on the more basic pyridines, stabilizing the LUMO and causing a red shift in absorption. The quenching of the emission suggests that this initial protonated species is nonfluorescent. With continued acidification, *N*,*N*-dimethylamino sites in **65** are also protonated, stabilizing the HOMO and resulting in a blue shift, which is observed in both the absorption and fluorescence emission spectra. Similar two-step optical responses were previously observed in distyrylbis(arylethynyl)benzenes **69** both upon protonation and upon exposure to Lewis acidic metal ions.

Cruciform **65** is highly solvatochromic: its solutions in five common solvents have widely different emission colors. Upon exposure to twelve aromatic carboxylic acids with closely related pH values and quite similar structures, the cruciform's emission colors changed, but no two carboxylic acids induced the same changes across all five solvents. This effect could therefore be used to qualitatively discriminate among structurally closely related carboxylic acid analytes without the need to perform rigorous

spectroscopic titrations. In addition to carboxylic acids, aryl- and alkylboronic acids are also capable of inducing substantial shifts in the emission colors of cruciform **65**. The distinguishability is much more vivid compared with the carboxylic acid example discussed above. The precise nature of the assembly formed between **65** and a boronic acid is still not clear. While hydrogen-bonded assemblies between pyridines and boronic acids have ample precedent,[91] direct N−B coordination bonds cannot be fully excluded. We hypothesized that self-assembled complexes of boronic acids with cruciform **65** could be used as hybrid sensors in which the chemical reaction is performed by the boronic acid, but reporting of that chemical reaction occurs using the cruciform fluorophore. We have demonstrated this approach in practice using phenols,[92] amines, and small organic and inorganic anions[93] as model analytes. Specifically, mixing cruciform **65** with two nonfluorescent boronic acids resulted in self-assembled complexes; subsequent exposure of each of these entities to analytes of interest resulted in another color change. These color changes again were never the same for two different analytes; these hybrid sensors are remarkably responsive to minute variations in analyte structure. With amine analytes, an interesting leveling effect was observed. Amines more basic than **65** would be expected to expel it out of its complex with a boronic acid, resulting in the recovery of the emission colors of the pure cruciform **65**. Another target was a fluoride anion, which can selectively and quickly deprotect bulky silyl groups on alkynes. With this aim in mind, we designed and synthesized BBO cruciform **75** decorated with two TIPS groups.[94] Fluoride addition caused rapid cleavage of the C−Si bond, resulting in the formation of a terminal alkyne and a corresponding shift of the

fluorescence emission maximum by −15 nm. With this dosimeter, fluoride can be detected at concentrations as low as 50 μM. As expected, cruciform **75** responded only to fluoride and not to other basic anions such as hydroxide and acetate, which would have deprotected smaller trialkylsilyl groups.

1.6 Conclusion

In the case of one-dimensional conjugated systems, properties can be tuned by elongation of the chain length or substitutions along the carbon backbone; while two-dimensional cross-conjugated cruciforms are more versatile, leaving more room for manipulation: at the core, along the branches and at the end group.

Changing any component in the cruciform skeleton resulted in a new material with new properties that can be employed in many applications. Chapter 1 primarily discussed,in chronological order, four cruciform families: distyrylbis(arylethynyl) benzenes, tetrakis(arylethynyl)benzenes, tetraethynylethenes, and BBO cruciform. For each type of cruciform, Bunz's, Haley's, Diederich's group, respectively, and our group have significantly contributed in synthetic development as well as explored their photonic and electronic properties in concurrent with computational calculation.

Haley's and Diederich's group concentrated on structure-property relationships of each cruciform family, introducing various aryl and silyl groups in tetrakis(arylethynyl)benzene and tetraethynylethene families, leaning toward the electronic device application and molecular switches. Bunz's and our group have investigated the effect of donor/acceptor substitutions on FMOs' distribution which

allows distyrylbis(arylethynyl)benzenes and BBO cruciforms to be attractive candidates for sensing application, as demonstrated in the responsive material for metal cations, carboxylic acids, aryl- and alkylboronic acids, amines, small organic and inorganic anions.

Chapter Two

L-shaped Benzimidazole Fluorophores—Synthesis, Characterization, Optical Response, and Sensing Properties[95]

2.1 Introduction

Molecular cruciforms,cross-conjugated molecules in which two conjugation circuits intersect at a central core, have been prominently used as fluorescent sensors for carboxylic and boronic acids, amines, metal ions, small organic and inorganic anions and phenols. With appropriate substitution, cruciforms localize their highest occupied moleucular orbital (HOMO) and lowest unoccupied molecular orbital (LUMO) on different "arms" of the molecule; this spatial separation of frontier molecular orbitals (FMOs) is essential to the use of cruciforms as sensors, since analyte binding to the cruciform invariably affects its HOMO–LUMO gap and the associated optical properties. Our group was particularly focused on the synthesis and study of cruciforms based on the benzobisoxazole nucleus.

[95] Lirag, R. C.; Le, H. T. M.; Miljanić, O. Š. *Chem. Commun.* **2013**, *49*, 4304−4306.

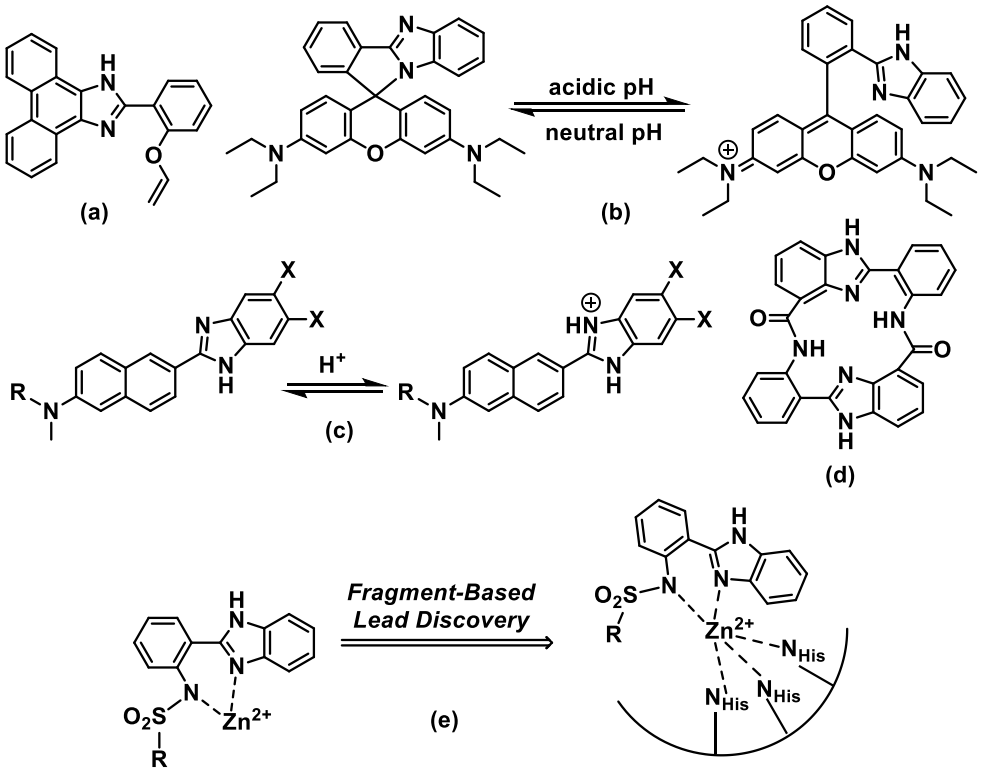

Figure 2.1 Select examples of benzimidazole-based sensors for different analytes: (a) Hg^{2+} cation,[97g] (b) acid,[98] (c) acid (under strong two-photon excited fluorescence),[99] (d) F^-, $H_2PO_4^-$, and benzoate.[100] (e) imidazole-based complex used for metalloenzyme inhibitors.[101]

Another heteroaromatic core, namely an imidazole, has amphoteric properties that allowed its extensive use in molecular recognition and sensing applications. In the imidazole structure, the pyridine-like nitrogen atom can be a binding site for metals and other cations while imidazole's N–H moiety can either participate in hydrogen bonding or be deprotonated by bases. The properties of sensors containing imidazole can be moderated by substitution as well as the length of the conjugated system.[96] Some select examples of imidazole-based applications in sensing and molecular recognition are

shown in Figure 2.1. Phenanthroimidazole-based fluorophores (Figure 2.1a) were used for recognition of Mg^{2+}, Cu^{2+}, ClO^{-}, Cd^{2+}, Hg^{2+} and H_2S.[97] Rhodamine B-benzimidazole diad (Figure 2.1b) was used for selective imaging of the pH of lysosomes and staining zebrafish intestines.[98] A family of small, two photon fluorophores derived from benzimidazole (Figure 2.1c) can monitor acidic pH values in live cells and mouse brain tissue via two-photon microscopy.[99] Cyclo[2]benzimidazole luminesces up to 150 fold upon anion binding, which cancels the excited-state intramolecular proton-transfer of the host.[100] Based on the high affinity of 2-(2'-benzene-sulfonamidophenyl) benzimidazole group toward Zn^{2+}, these scaffolds were employed to develop metalloenzyme inhibitors such as MNPi hits (Figure 2.1e).[101]

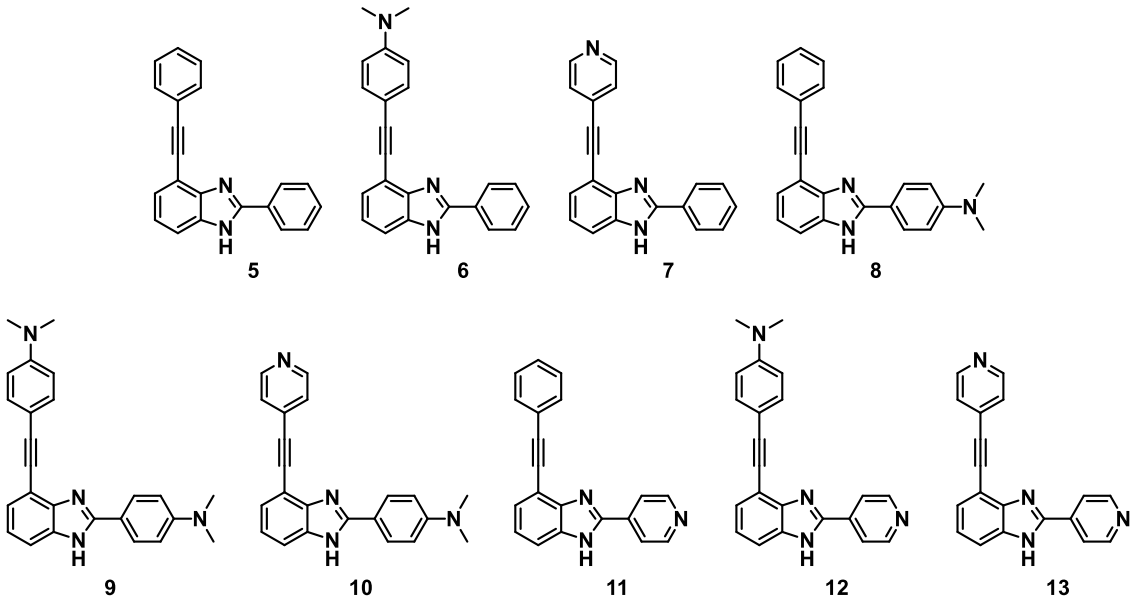

Figure 2.2 L-Shaped benzimidazole fluorophores **5**–**13**.

In this chapter, we introduce a new class of L-shaped fluorophores (Figure 2.2) based on the related benzimidazole nucleus. Formally, these systems represent

"cruciforms cut in half", and this structural simplification permits us to explore minimal systems which preserve spatially isolated FMOs. At the same time, the dual acidic–basic nature of the benzimidazole nucleus could potentially allow the use of this sensing motif in the direct identification and quantification of both acidic and basic analytes.

Inspired by these desirable characteristics of cruciforms, we sought other scaffolds possessing separated FMOs. Molecule 4-ethynyl-benzimidazole is an electron-rich conjugated system compared to benzothiadiazole (BT)[102] which was a common electron-deficient unit found in solar cell polymers.[103] Accordingly, the combination of benzimidazole and BT yielded a donor-acceptor system with localized FMOs referred to **14** and its deprotected product **15** (Scheme 2.2). Moreover, BT has strong affinity for metal cations attributed to its lone pair electrons;[104] 2-(pyridine-2-yl)-1H-benzo[*d*]imidazole **16** (Scheme 2.2) can work as a bidentate ligand for different metal ions. Therefore, metal ion analytes can interact with benzimidazole or BT core in different preference order; hence, they are predicted to give two-step optical responses.

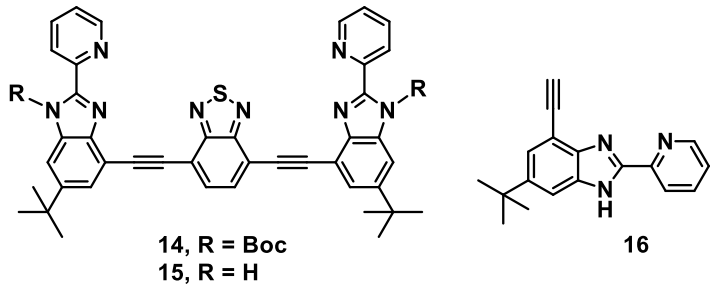

Figure 2.3 Benzimidazole-based conjugated systems **14**, **15** and **16**.

We also made progress toward the synthesis of a molecular switch based on benzimidazole core such as compounds **17** and **18** (Figure 2.4), which possibly occur in

two conformations: C-shaped (Figure 2.4, left) and Z-shaped one (Figure 2.4, right). We postulated that conformations of these molecules can be triggered by the presence of an anionic guest. Urea moieties are well-known hydrogen-bond donors to anions;[105] in the combination with imidazole possessing another hydrogen bond donor NH, this new structure could also act as the host for anion guest. We also expected that these receptors with rigid geometry may offer a specific cavity size and presumably bind to analytes selectively.

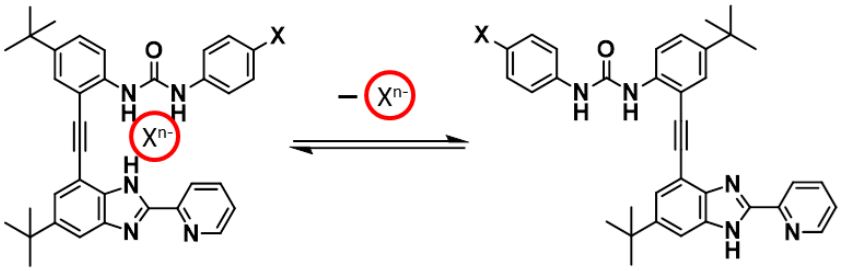

22, X = H
23, X = NO_2

Figure 2.4 Benzimidazole-based conjugated systems **17** and **18**.

In this chapter, the synthesis of these benzimidazole-based conjugated systems will be presented and the initial results toward these targets will also be discussed.

2.2 Results and Discussion

2.2.1 L-Shaped Benzimidazole Fluorophores

L-Shaped benzimidazole fluorophores **5**–**13** were synthesized (Scheme 2.1) in two steps starting from 3-bromo-*o*-phenylenediamine **1**.[106] Its oxidative condensation[107] with three commercially available aldehydes produced brominated imidazoles **2**–**4**, which

were subjected to Sonogashira couplings with either phenylacetylene, 4-ethynylpyridine, or 4-ethynyl-*N*,*N*-dimethylaniline, generated the final desired products in moderate yields. Fluorophores **5**–**13** were isolated as off-white, yellow or light green powders, following chromatography and/or recrystallization.

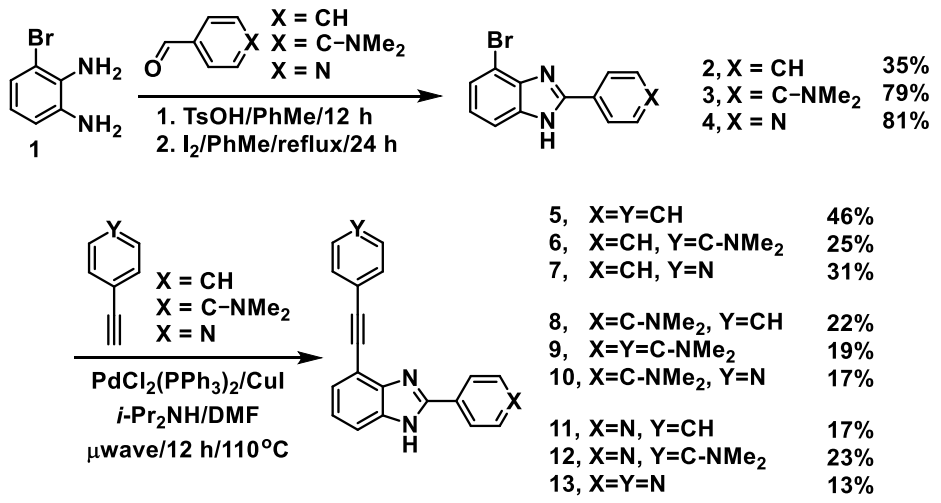

Scheme 2.1 Synthesis of half-cruciforms **5**–**13**.

In the case of donor-acceptor systems **10** (Figure 2.5, right) and **12** (not shown), their fluorescence emission was found to be highly solvent-dependent; on the other extreme, the very weak fluorescence of "neutral" diphenyl substituted compound **5** is independent of the solvent (Figure 2.5, left). It should also be noted that the NMR spectra of **5**–**13** are often more complex than structures in Scheme 1 would suggest, because of the N–H tautomerization between the imidazole's two nitrogen atoms.

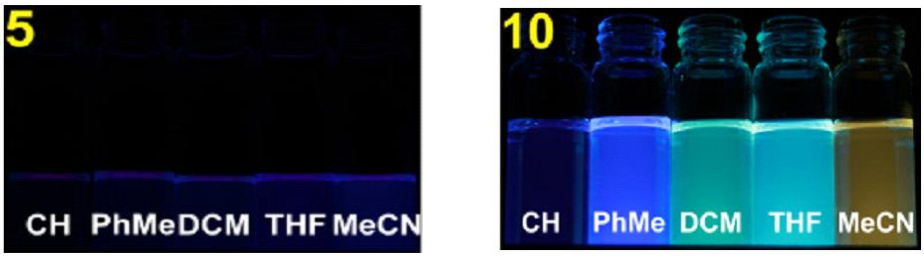

Figure 2.5 Emission colors of benzimidazoles **5** and **10** in five different solvents (CH = cyclohexane, PhMe = toluene, DCM = dichloromethane, THF = tetrahydrofuran, MeCN = acetonitrile, λ_{exc}= 365 nm).

Computational insight into the FMOs of **5**–**13** was obtained using Gaussian 09W[108] software package and its accompanying graphical interface program GaussView 5.0, at the B3LYP/6-31G^{++} level of theory. Figure 2.6 shows the HOMO and LUMO orbitals of all other L-shaped fluorophores. In two extreme cases, diphenyl substituted compound **5** and the donor–acceptor system **10**, trends previously observed for benzobisoxazole[88] (and other) cruciforms are again borne out. Both the HOMO and the LUMO of compound **5** are significantly delocalized across the molecule. In contrast, **10** shows considerably localized FMOs; most of the LUMO density is placed along the pyridine-bearing arm of the half-cruciform, while most of the HOMO density resides along the electron-rich dimethylaniline-group. In both compounds, the HOMO is the more localized of the two FMOs. Compounds **5** and **10** will be the chief subjects of discussion in this section, as they allowed us to separate the effects of the benzimidazole nucleus alone (in **5**) from those introduced by the donor-acceptor substitution and the resultant FMO spatial isolation (in **10**). In light of the spatially separated FMOs in **10**, its

solvatochromicity can be rationalized by the apparent charge separation in the excited state.

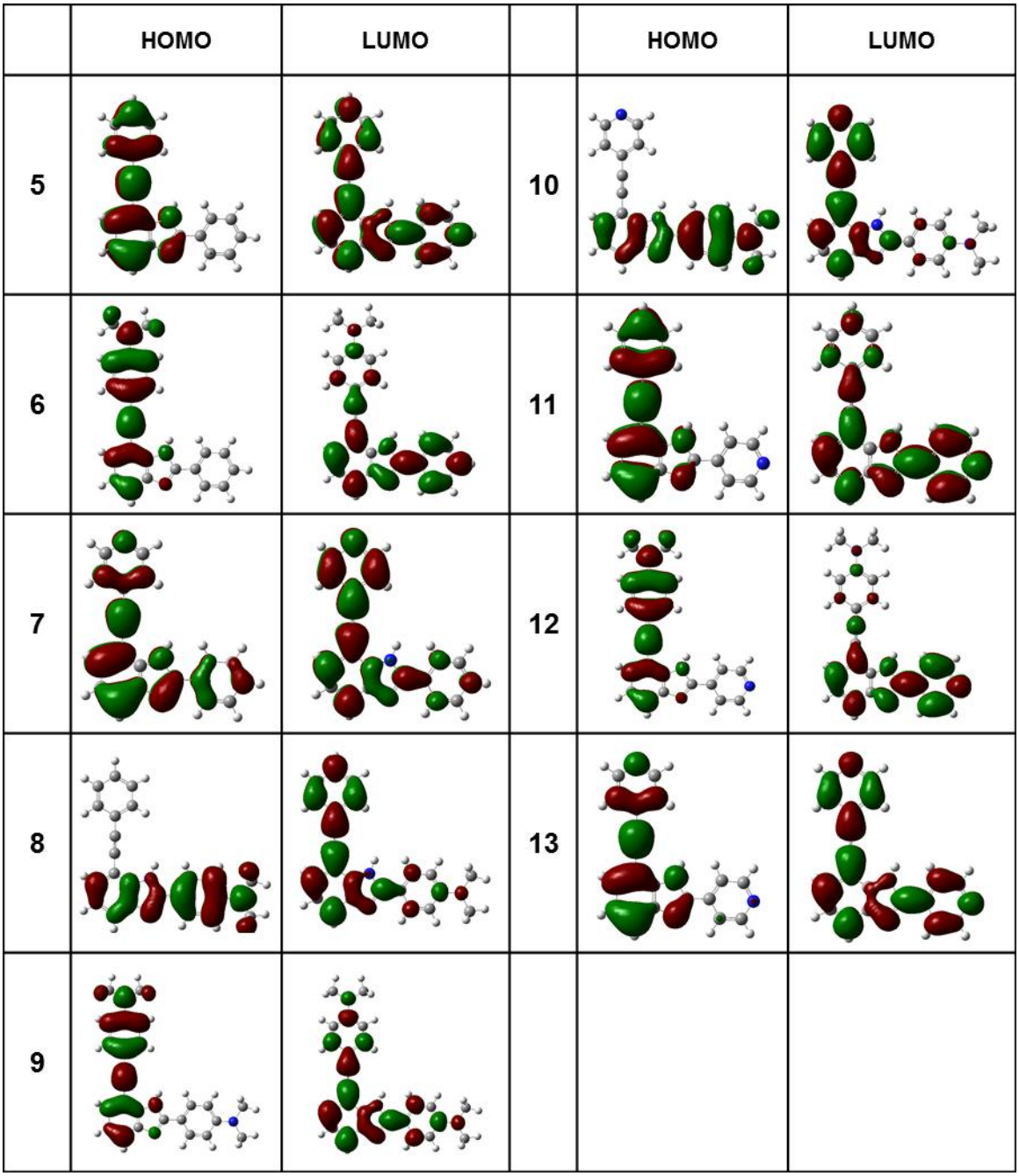

Figure 2.6 Frontier molecular orbitals of L-shaped benzimidazole molecules **5–13**.

Our next set of experiments focused on the titration of the solutions of the prepared benzimidazole fluorophores with a concentrated aqueous solution of tetrabutylammonium hydroxide (TBA^+OH^-).

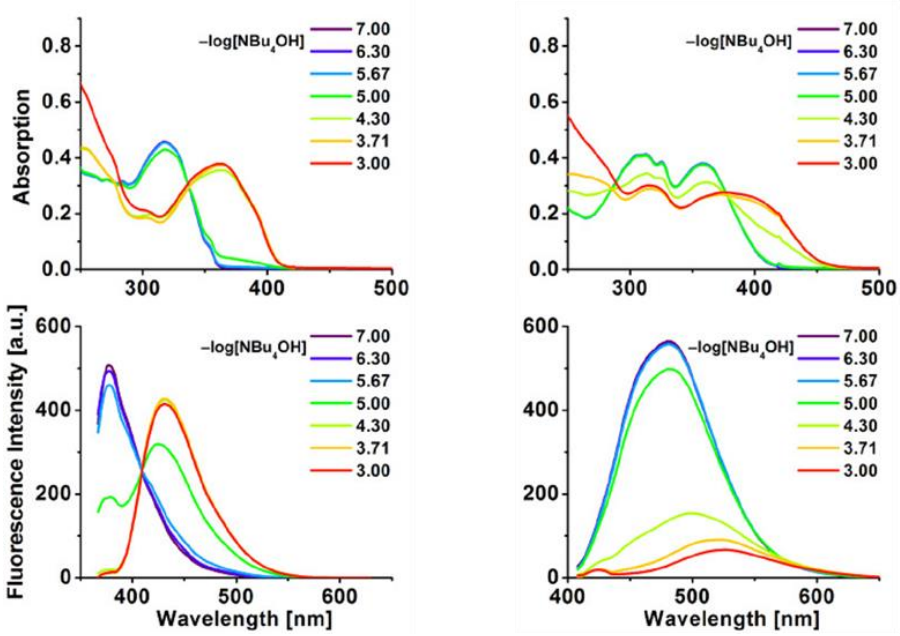

Figure 2.7 UV/Vis absorption (top) and emission (bottom) spectra for the titrations of THF solutions of fluorophores **5** (left two spectra, λ_{exc}=337 nm) and **10** (right two spectra, λ_{exc}=378 nm) with a concentrated aqueous solution of TBA^+OH^-.

In both fluorophores, red shifts in absorption (Figure 2.7, top; +45 nm for **5** and +18 nm for **10**) and emission spectra (Figure 2.7, bottom; +54 nm for **5** and +43 nm for **10**) were observed, with clear isosbestic points suggesting simple interconversion between just two species: compounds **5** and **10** and their conjugate bases deprotonated at the benzimidazole ($pK_a \approx 12.8$).[109] These red shifts indicate that deprotonation destabilizes the HOMO more than the LUMO; the largely analogous responses of **5** and

10 are a consequence of the fact that both FMOs in both compounds have significant densities along the imidazole N–H bond being cleaved.

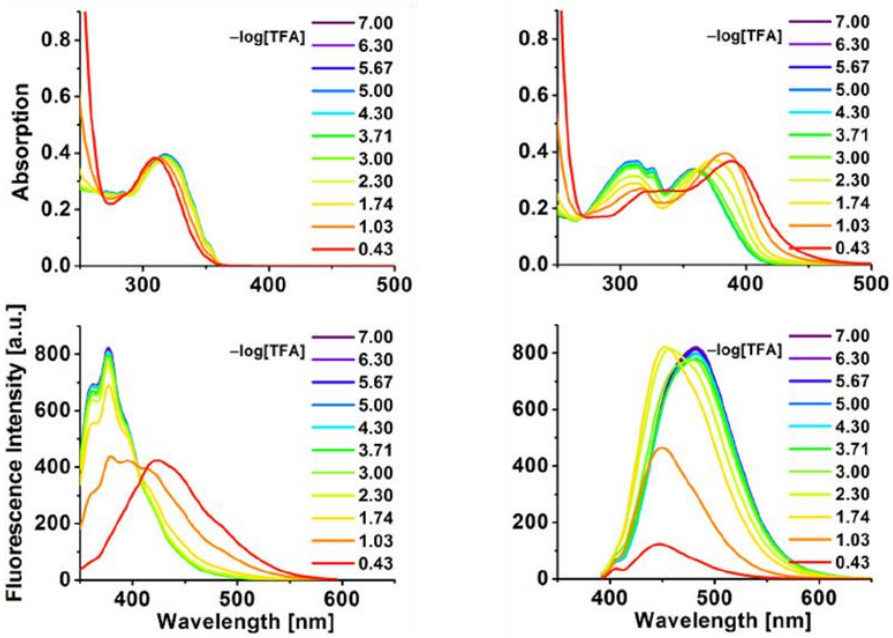

Figure 2.8 UV/Vis absorption (top) and emission (bottom) spectra for the titrations of THF solutions of fluorophores **5** (left two spectra, λ_{exc}= 313 nm) and **10** (right two spectra, λ_{exc}=362 nm) with a concentrated solution of TFA in THF.

Perhaps surprisingly, response of the prepared half-cruciform sensors to acids was more difficult to rationalize. Both **5** and **10** are largely unresponsive to trifluoroacetic acid (TFA) until −log[TFA] of approx. 2.30 is reached. At this point, **5** shows a minimal blue shift in absorption (Figure 2.8, top left; −7 nm) and a much larger red shift and slight attenuation of its emission (Figure 2.8, bottom left; +47 nm). Since this compound can be protonated only at the benzimidazole, it would follow that this protonation preferentially stabilizes the LUMO. Compound **10**, on the other hand, responds by a red shift in

absorption (Figure 2.8, top right; +29 nm) and a blue shift and significant attenuation of its emission (Figure 2.8, bottom right; −35 nm). In **10**, there are three possible protonation sites: dimethylaniline, pyridine and imidazole, with quite similar pK_a values for their conjugated acids of 5.15, 5.25 and 5.53, successively.[109,110] The observed blue shift in the emission is consistent with the stabilization of the HOMO, which would suggest that pyridine protonation is probably not operational, since the HOMO has essentially no density on the pyridine nucleus. It is still unclear, however, which of the other two sites is protonated first, and why absorption and emission maxima shift in the opposite directions. In order to obtain more predictable optical response to protonation, similar to those of our previously reported benzobisoxazole cruciforms,[88] it appears that a more basic pyridine nucleus (substituted e.g. with electron-donating methyl groups) would be a better choice.

Figure 2.9 Emission colors of compound **5** (left) and **10** (right) upon exposure to TBA salts of different anions (λ_{exc}= 365 nm).

Finally, we attempted to qualitatively assess whether half-cruciforms **5** and **10** can be used as fluorescent sensors for small inorganic and organic anions.[111] Dilute solutions of **5** and **10** in THF were exposed to excess of TBA^+ salts of several representative anions. Figure 2.9 summarizes the emission color changes resulting from these additions.

Both sensors minimally changed their fluorescence when exposed to the weakly basic Cl^-, NO_3^-, and ClO_4^- anions. However, more basic F^-, AcO^-, and $H_2PO_4^-$ anions turned on the fluorescence of **5** and also significantly modulated the emission color of **10**, particularly in the case of fluoride.

2.2.2 Other Benzimidazole-based Sensor Precursors

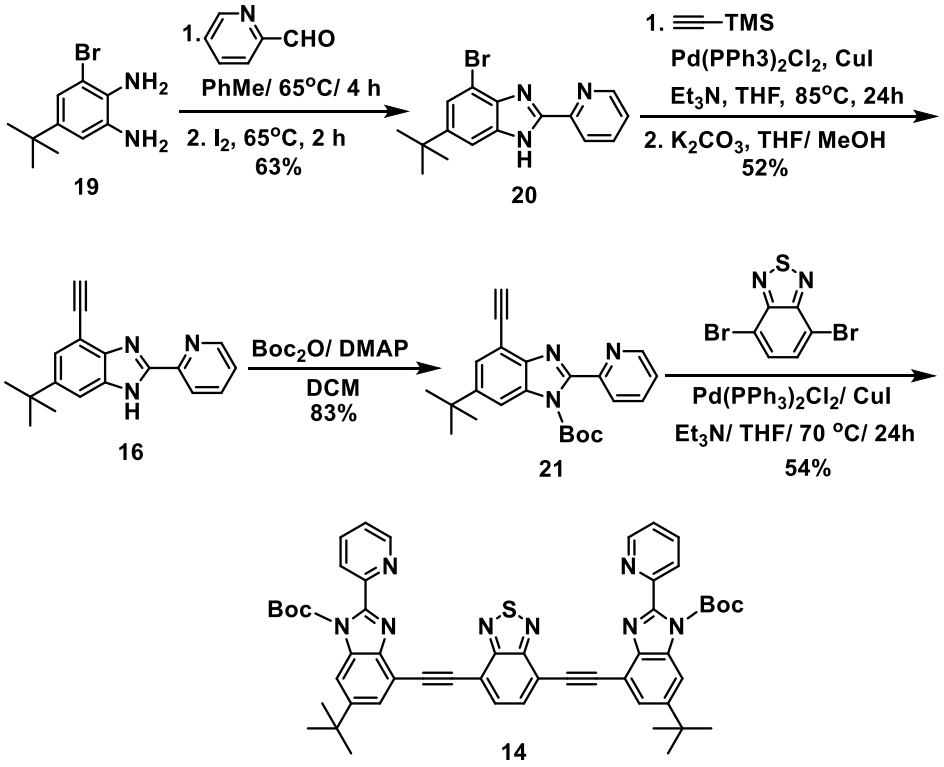

Scheme 2.2 Synthesis of a benzimidazole-based conjugated sensing system **14**.

Compound **14** was successfully synthesized following the procedure in Scheme 2.2. Starting from 3-bromo-5-*tert*-butylbenzene-1,2-diamine (**19**),[112] oxidative condensation with 2-pyridinecarboxaldehyde provided brominated imidazole **20**. Coupling of **20** with TMSA followed by deprotection of the TMS group delivered 4-

ethynylbenzimidazole **16**. *Tert*-butyl carbamate (Boc) protection upon treatment of **16** with di-*tert*-butyl dicarbonate (Boc_2O) in the presence of 4-dimethylaminopyridine (DMAP) generated **21**. Finally, **14** was obtained by the double Sonogashira coupling of **21** with 4,7-dibromo-2,1,3-benzothiadiazole.[113]

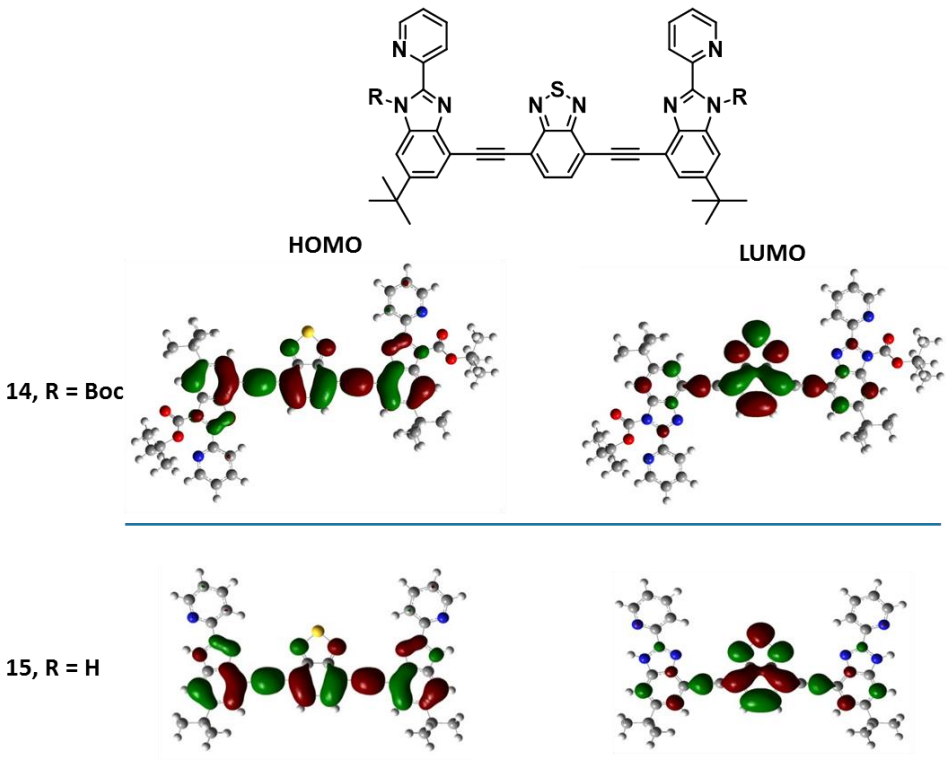

Figure 2.10 Frontier molecular orbitals of compounds **14** and **15**.

Using Gaussian 09W software package and its accompanying graphical interface program GaussView 5.0, at the B3LYP/3-21G level of theory, we examined the FMOs of the prepared molecules; the results show that both **14** and **15** have separated HOMO and LUMO (Figure 2.10): the LUMO is localized on BT, while HOMO mostly occupies the 4-ethynylbenzimidazole moiety. We succeeded in growing crystals of **16** with Zn^{2+} and Cd^{2+}, which proved that 4-ethynyl-6-(*tert*-butyl)-2-(pyridine-4-yl)-1H-benzo[*d*]imidazole

can serve as the bidentate ligand toward metal ions. Our preliminary investigation of optical responses of **14** toward metal cations shows the addition of Cd^{2+} and Hg^{2+} to solution of **14** will change its emission color respectively from green to orange and dark red under UV lamp excitation (λ_{exc} = 365 nm) (Figure 2.11). From the single crystal data of **14**, we observed that bulky Boc protecting group induced the pyridine ring to twist out of the conjugated plane of system; hence, metal ions prefer to bind to BT where the LUMO resides. The stabilization of the LUMO subsequently led to bathochromic shift as the result. Moreover, sulfur, considered a soft base in BT, can undergo soft-soft interaction with soft Lewis acids like Cd^{2+} and Hg^{2+}.[114]

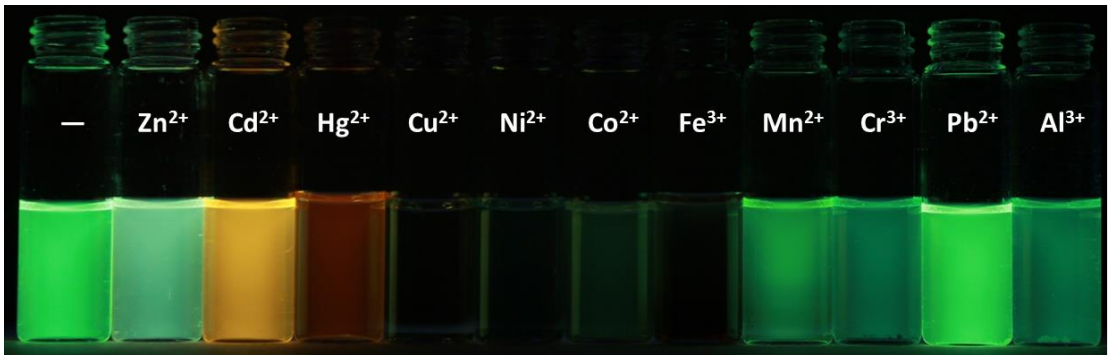

Figure 2.11 Emission color changes of a 10^{-5} M solution in MeCN **14** upon the addition of excess of eleven metal nitrate salts.

The synthesis of benzimidazole-based conjugated systems **17** and **18** is depicted in Scheme 2.3. In order to obtain urea derivatives **22** and **23**, 4-*tert*-butyl-2-iodoaniline was reacted with phenylisocyanate or 4-nitrophenyl isocyanate, respectively. Afterward, terminal alkyne **16** (synthesized via Scheme 2.2) undergoes Sonogashira coupling with either **22** or **23**, generating final targets: compound **17** or **18**, responsively.

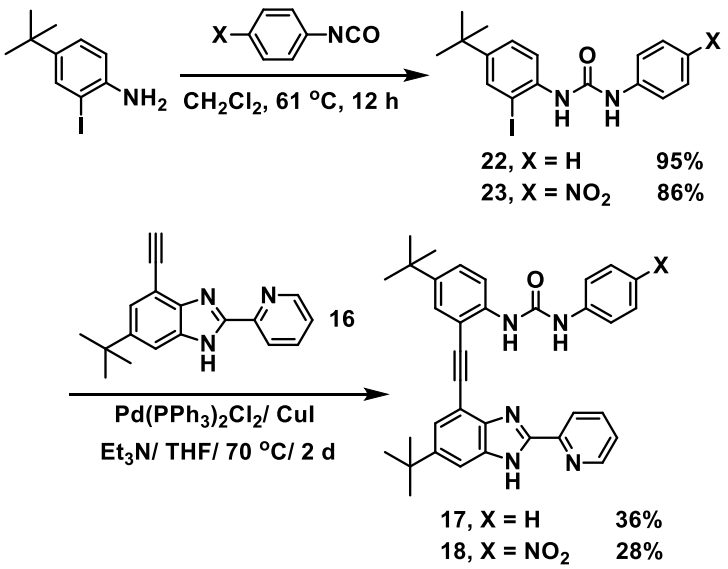

Scheme 2.3 Synthesis of benzimidazole-based conjugated systems **17** and **18**.

Recrystalization of **17** and **18** in MeCN by slow evaporation method afforded block-shaped crystals suitable for X-ray diffraction. This data will be further discussed in the next section.

2.2.3 X-Ray Crystal Structure Analysis of Other Benzimidazole-based Sensor Precursors

We were able to obtain the single crystal structures of complexes between compound **16** and both Zn^{2+} and Cd^{2+}. These present direct evidence of the metal cations binding to bidentate ligand **16**. Colorless block-shaped crystals of a complex of **16** with $Zn(OTf)_2$ was formed by slow evaporation of a MeCN/MeOH mixtrure. The complex crystalizes in space group $P2_12_12_1$, with four complexes per unit cell. As depicted in Figure 2.12a (only one of the four crystallographically independent molecules is presented), each Zn^{2+} cation is coordinated by three ligands; surrounded by six N atoms

from these ligands, the Zn^{2+} centered complex has a distorted octahedral coordination geometry. All the NHs of benzimidazoles point outward from the Zn^{2+} center, acting as the hydrogen-bond donors to either H_2O or OTf^-. All Zn–N bonds are between 2.10 and 2. 25 Å in length, which are typical values reported for Zn(II) complexes with imidazoles.[115] 2-Pyridyl groups are almost coplanar with ethynyl-benzimidazole system, and the largest torsion angle recorded is less than 11°.

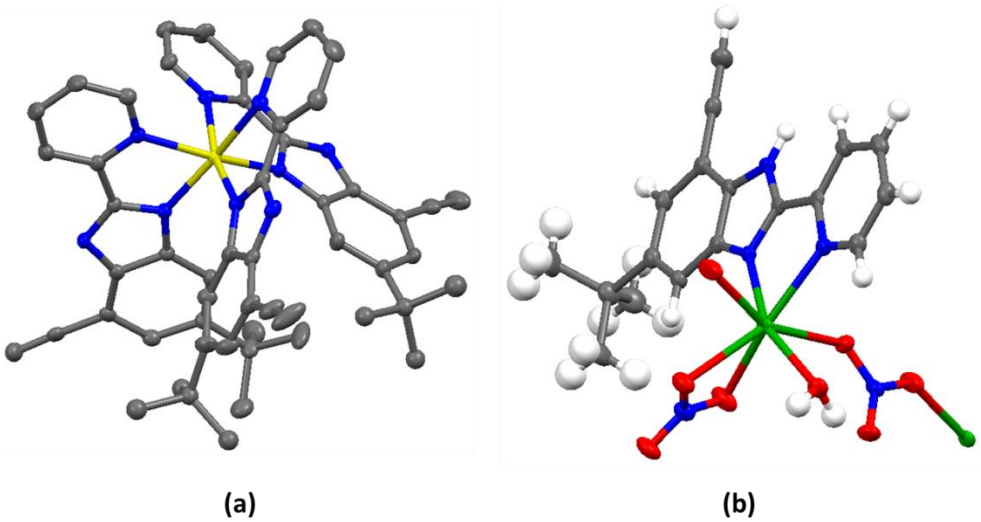

Figure 2.12 Crystal structures sketched in ellipsoid style describing coordination environment of (a) Zn^{2+} in the complex with ligand **16** (hydrogen atoms are omitted for clarity) (Zn, yellow; N, blue; C, grey). (b) Cd^{2+} in the complex with ligand **16** (Cd, green; N, blue; C, grey; O, red; H, white).

When $Cd(NO_3)_2.4H_2O$ was used as the starting material, colorless platelet crystals were obtained. The complex was found to crystallize in a triclinic space group *P*-1 with two complex units per unit cell. As illustrated in Figure 2.12b, each Cd^{2+} center coordinated by two N from one ligand **16** and five O atoms belonging to H_2O and three

different NO_3^-, giving rise to the distorted monocapped trigonal prism coordination geometry. Two Cd–N bonds are 2.27 and 2.37 Å and five Cd–O binds are between 2.25 and 2.46 Å, which falls well within the range reported in the literature.[116] The two pyridyl groups are almost coplanar with ethynyl-benzimidazole system, with a torsion angle of ~5°.

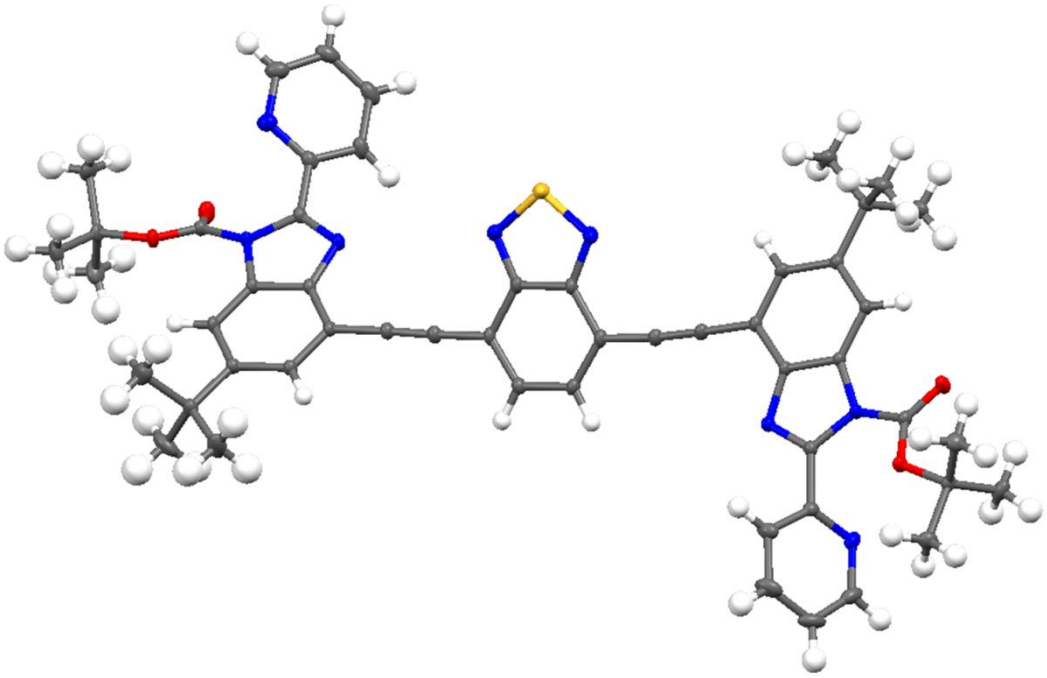

Figure 2.13 Crystal structure **14** (S, yellow; N, blue; C, grey; O, red; H, white). Ellipsoids shown at 50% probability.

Molecule **14** was recrystallized by slow evaporation of MeCN to afford yellow block-shape single crystals of sufficient quality for X-ray diffraction. Compound **14** crystalizes in space group *P*-1 with Z = 2. The crystal structure of **14** was depicted in Figure 2.13. Although benzimidazole can tautomerize between NH and N in solution to give the mixture of two isomers, the Boc-protected product **14** displays only one isomer

in which the Boc group is located on the side opposite of benzothiadiazole. Without metal coordination, the two pyridyl groups rotate about C–C bond instead of planarizing with benzimidazole to maintain conjugation of the system, with the torsion angles between pyridyl and imidazole units of the two sides being 33.7 and 57.2^{o}. Furthermore, the steric hindrance of the Boc-protecting group can also attribute to the non-planarization. This phenomenon rendered benzothiadiazole as an open, easily accessible site compared to the 2-(pyridine-4-yl)-benzo[*d*]imidazole sites. The whole molecule was asymmetric due to the opposite rotation of benzimidazole arms about the ethynyl bond corresponding to benzothiadiazole.

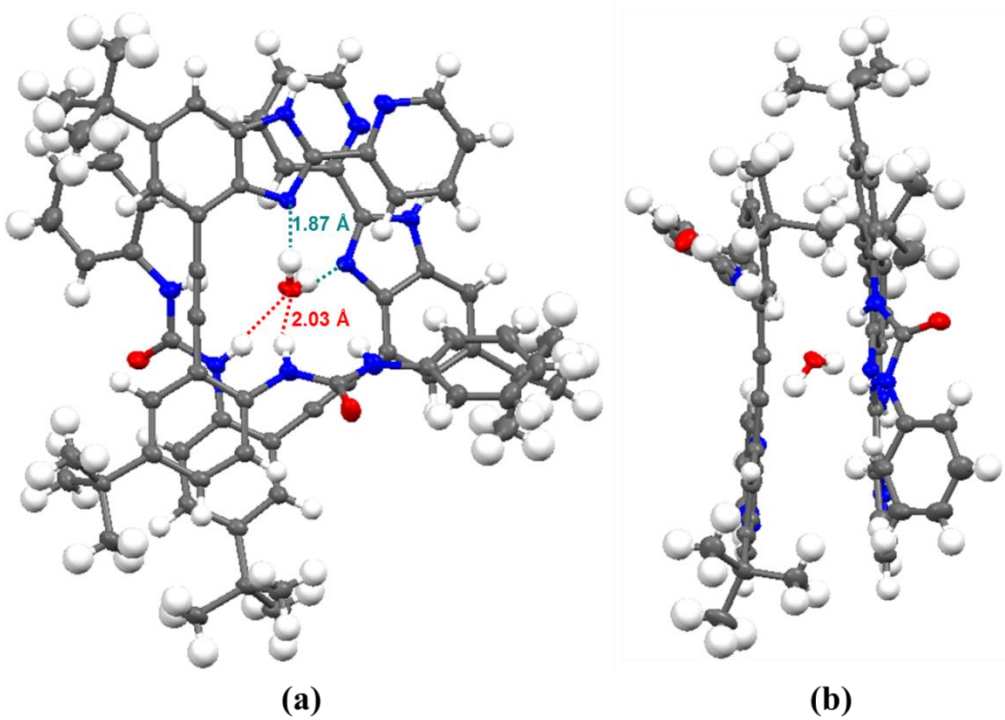

Figure 2.14 Crystal structures in ellipsoid style of molecule **17** in (a) perspective view, (b) side view (O, red; N, blue; C, grey; H, white).

Utilizing the slow evaporation method of the solution with MeCN, we obtained the block-shaped single crystals of compounds **17** and **18** suitable for X-ray diffraction. Even though **17** and **18** have different functional groups fabricated in urea part, they both crystallized in space group *C*2/c (monoclinic) with eight molecules occupied in one unit cell. As shown in Figures 2.14 and 2.15, both molecules form sandwich-type scaffolds, embracing a H_2O molecule in the middle, and each H_2O plays the role as a bridge to link two discrete molecules of **17** or **18**. In the case of **17**, the structure was secured only by four hydrogen bonds between two molecules and one water molecule. Hydrogen bonds [O···H–N] (water–urea) and [N···H–O] (imidazole–water) are 2.03 and 1.87 Å in length, respectively. On the other hand, the complex of molecule **18** was stabilized by six hydrogen bonds of two **18** and one water molecule. The withdrawing $–NO_2$ group in **18** induced both NHs in urea site to become good hydrogen bond donors toward the O of H_2O. Hydrogen bonds [O···H–N] (water–urea) and [N···H–O] (imidazole–water) are between 1.87 and 2.18 Å in length. All the hydrogen bonds observed are typical for hydrogen bond length.

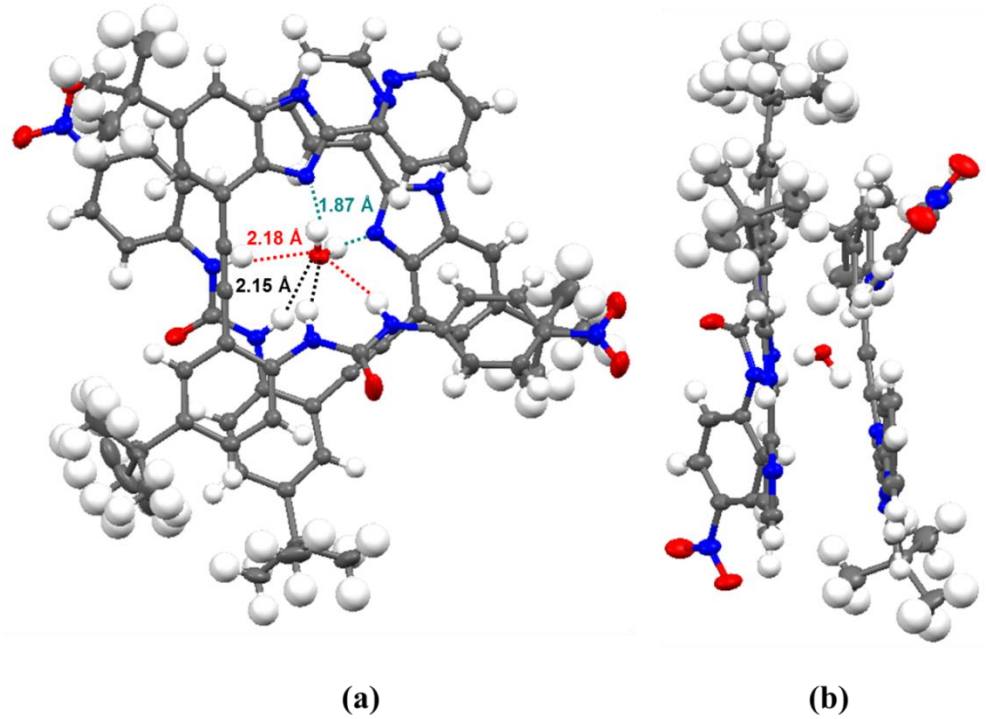

Figure 2.15 Crystal structure of **18** in (a) perspective view, (b) side view (O, red; N, blue; C, grey; H, white). Thermal ellipsoids are shown at 50% probability.

2.3 Conclusion and Outlook

In conclusion, L-shaped benzimidazole fluorophores described here can be easily synthesized in two steps. Their optical response to acids is moderate and somewhat difficult to rationalize, presumably on the account of (a) similar basicities of several possible protonation sites, and (b) incomplete spatial separation of FMOs within the molecules. On the other hand, their response to bases is much more dramatic, as all but two members of this class consistently shift their emission maxima toward the red region. The fact that these fluorophores preserve their fluorescence upon deprotonation is intriguing, as it suggests that benzimidazolate anions of **5**–**13** could potentially be used as

building blocks for the porous zeolitic imidazolate frameworks (ZIFs),[117] thus opening up routes to crystallographically ordered solid-state sensors.

We were also successful in synthesizing and obtaining single crystal data for the benzimidazole-based conjugated systems **14**, **17**, and **18**. Compound **14** exhibits a positive response toward Cd^{2+} and Hg^{2+}, which needs further investigation by careful titration of **14** with these salts. Boc-Deprotected derivative **15** will be prepared to compare its optical properties with **14**. Complexes of **17** and **18** with water have sandwich-mode structure, which infers the capacity of them having both hydrogen bond donor and acceptor sites in the same structure. Following steps for compound **17** and **18** will be the investigation of their recognition ability toward anions and probably cations.

2.4 Experimental Section

2.4.1 General Experimental Methods

All reactions were performed under nitrogen atmosphere in oven-dried glassware. Reagents were purchased from commercial suppliers and used without further purification. Solvents were used as received, except *N*,*N*-dimethylformamide, which was dried over activated alumina in an mBraun Solvent Purification System. Compounds 4-bromo-2,1,3-benzothiadiazole and 3-bromo-1,2-diaminobenzene were synthesized according to literature procedures.[118,119] Diisopropylamine was distilled over KOH pellets and degassed by a 15 min nitrogen purge prior to use. Microwave-assisted reactions were performed in a Biotage Initiator 2.0 microwave reactor, producing monochomatic microwave radiation with the frequency of 2.45 GHz. Mass spectral measurements were

performed by the Mass Spectrometry Facility of the Department of Chemistry and Biochemistry at the University of Texas at Austin. NMR spectra were obtained on JEOL ECX-400, JEOL ECA-500 and Bruker Avance-800 MHz spectrometers, with working frequencies (for ^{1}H nuclei) of 400, 500 and 800 MHz, respectively. All ^{13}C NMR spectra were recorded with simultaneous decoupling of ^{1}H nuclei. ^{1}H NMR chemical shifts are reported in ppm units relative to the residual signal of the solvent ($CDCl_3$: 7.25 ppm, DMSO-d_6: 2.50 ppm, acetone-d_6: 2.05 ppm). NMR spectra were recorded at 25 °C for samples analyzed in $CDCl_3$ and $(CD_3)_2CO$-d_6, while samples in DMSO-d_6 were analyzed at 90 °C with 1–3 drops of D_2O added to eliminate asymmetry induced by N–H tautomerization.[120] Infrared spectra were recorded on a Perkin-Elmer Spectrum 100 FT-IR spectrophotometer using Pike MIRacle Micrometer pressure clamp. Microanalyses were conducted by Intertek USA, Inc. Melting points were measured in open capillary tubes using Mel-Temp Thermo Scientific apparatus, and are uncorrected. Column chromatography was carried out on silica gel 60, 32–63 mesh. Analytical TLC was performed on Merck aluminum-backed silica gel plates.

2.4.2 Synthesis of Half-Cruciforms

Synthesis of 7-bromo-2-phenyl-1*H*-benzo[*d*]imidazole **2**

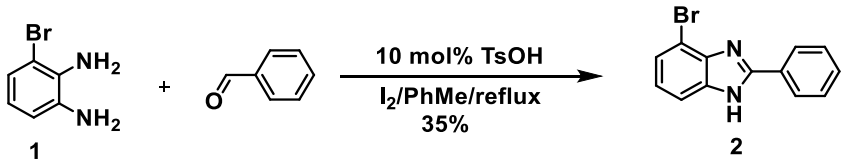

In a 250 mL round-bottom flask, compound **1** (2.12 g, 11.4 mmol) and benzaldehyde (1.16 mL, 11.4 mmol) were dissolved in PhMe (150 mL). *para*-

Toluenesulfonic acid (*p*TSA) (0.22 g, 1.17 mmol) was added and the solution was sonicated for 20 min. After sonication, the solution was heated at reflux with a Dean-Stark trap for 12 h. After that time, I_2 (2.90 g, 11.4 mmol) was added, and the solution was refluxed for 24 h. After cooling, the solvent was removed and the brown oily residue was sonicated with CH_2Cl_2 until it formed a solid precipitate. The solution was filtered and washed with hexane to give compound **2** as a yellow powder (1.11 g, 35%).

2: mp 225–227 °C. IR (neat): 3061, 1621, 1457, 1311, 1029, 931, 750, 690 cm^{-1}. UV-Vis (CH_3CN): λ_{max} (log ε) = 206 (4.71), 242 (4.36), 248 (4.30), 300 (4.46) nm. ^1H NMR (acetone-d_6, 500 MHz): δ 8.24 (dd, *J*=8.3, 1.5 Hz, 2H), 7.55 (d, *J*=8.0 Hz, 1H), 7.50 (m, 3H), 7.39 (dd, *J*=8.0, 1.2 Hz, 1H), 7.12 (dd, *J*=8.0, 7.5 Hz, 1H) ppm. ^{13}C NMR (acetone-d_6, 125 MHz): δ 152.7, 143.8, 136.3, 130.8, 130.4, 129.2, 125.5, 124.0, 113.2, 111.0 ppm. HRMS (ESI): Calcd for $C_{13}H_{10}BrN_2^+$: 273.0022. Found: 273.0020.

Synthesis of 4-(7-Bromo-1*H*-benzo[*d*]imidazol-2-yl)-*N*,*N*-dimethylbenzenamine **3**

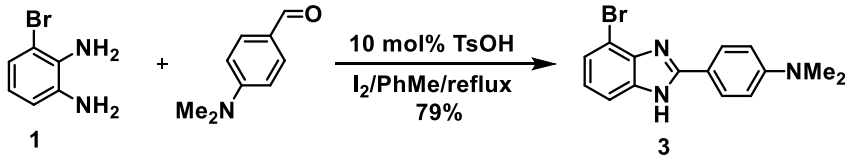

In a 250 mL round-bottom flask, compound **1** (1.12 g, 6.00 mmol) and 4-dimethylaminobenzaldehyde (895 mg, 6.00 mmol) were dissolved in PhMe (150 mL). *p*TSA (196 mg, 1.03 mmol) was added, and the solution was sonicated for 20 min, during which time a precipitate formed. After sonication, the solution was heated at reflux with a Dean-Stark trap for 12 h. After that time, I_2 (1.52 g, 6.00 mmol) was added and the solution was heated at reflux for 24 h. After cooling, the solution was filtered and the

residue washed with hexane and Me_2CO to give a reddish brown solid that was identified as **3** (1.50 g, 79%). Further purification can be achieved by recrystallization in Me_2CO or EtOH.

3: mp 161 °C, with decomposition. IR (neat): 3432, 1610, 1524, 1378, 1216, 816, 776, 641 cm^{-1}. UV-Vis (CH_3CN): λ_{max} (log ε) = 245 (4.46), 371 (4.64) nm. ^1H NMR (DMSO-d_6, 500 MHz): δ 8.08 (d, J=9.2 Hz, 2H), 7.65 (d, J=8.0 Hz, 1H), 7.63 (d, J=8.0 Hz, 1H), 7.32 (t, J=8.0 Hz, 1H), 6.89 (d, J=9.2 Hz, 2H), 3.05 (s, 6H) ppm. ^{13}C NMR (DMSO-d_6, 125 MHz): δ 153.8, 151.9, 133.4, 132.7, 130.4, 128.4, 126.9, 112.9, 112.2, 108.7, 105.7 ppm. HRMS (ESI): Calcd for $C_{15}H_{15}BrN_3^+$: 316.0444. Found: 316.0443.

Synthesis of 7-Bromo-2-(pyridine-4-yl)-1H-benzo[*d*]imidazole **4**

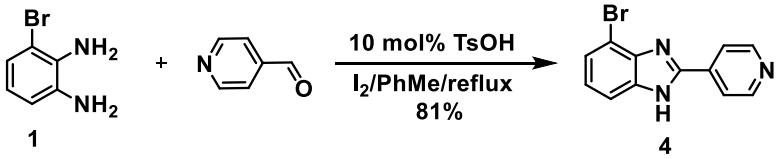

In a 250 mL round-bottom flask, compound **1** (2.51 g, 13.4 mmol) and 4-pyridinecarboxaldehyde (1.26 mL, 13.4 mmol) were dissolved in PhMe (150 mL). *p*TSA (255 mg, 1.34 mmol) was added and the solution was sonicated for 20 min. After sonication, the solution was heated at reflux with a Dean-Stark trap for 12 h. After that time, I_2 (3.40 g, 13.4 mmol) was added into the solution. Immediate formation of a yellow-brown precipitate was observed. The mixture was kept at reflux for additional 24 h. After cooling, the solution was filtered and the residue washed with hexane and Me_2CO and to give a pale yellow solid (2.98 g, 81%). Further purification can be achieved by recrystallization from Me_2CO or EtOH.

4: mp 243 °C, with decomposition. IR (neat): 3071, 1638, 1503, 1224, 1151, 1032, 808, 743, 683 cm^{-1}. UV-Vis (CH_3CN): λ_{max} (log ε) = 202 (4.59), 245 (4.20), 313 (3.95), 350 (3.95) nm. ^1H NMR (DMSO-d_6, 500 MHz): δ 8.96 (d, J=6.3 Hz, 2H), 8.50 (d, J=6.9 Hz, 2H), 7.68 (d, J=8.0 Hz, 1H), 7.54 (d, J=7.5 Hz, 1H), 7.26 (dd, J=8.0, 7.5 Hz, 1H) ppm. ^{13}C NMR (DMSO-d_6, 125 MHz): δ 147.4, 144.2, 141.2, 138.3, 127.0, 126.4, 123.6, 114.4, 111.5 ppm. HRMS (ESI): Calcd for $C_{12}H_9BrN_3^+$: 273.9974. Found: 273.9974.

Synthesis of Compound **5**

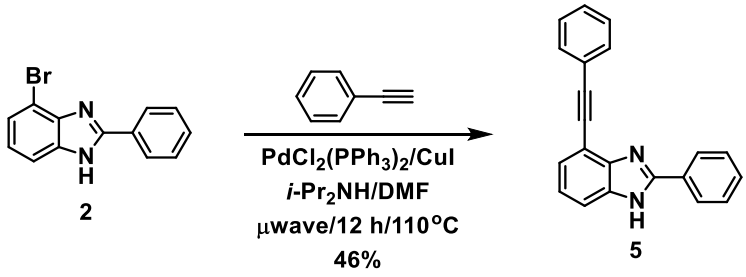

Phenylacetylene (450 mg, 4.40 mmol) was added to a thick-walled microwave pressure vial that contained a mixture of compound **2** (300 mg, 1.10 mmol), $PdCl_2(PPh_3)_2$ (60.0 mg, 0.09 mmol), CuI (20.0 mg, 0.11 mmol), *i*-Pr_2NH (5 mL), and DMF (5 mL). The vial was sealed and exposed to microwave irradiation for 12 h at 110 °C. After cooling, the reaction mixture was extracted with EtOAc, washed with brine, and then dried over anhydrous $MgSO_4$. The product was isolated by column chromatography, eluting with a hexane/EtOAc (7:3) mixture. The solvent was removed under reduced pressure, and the solid recrystallized from a mixture of THF and hexane to give pure compound **5** (150 mg, 46%).

5: white powder, mp 280 °C. IR (neat): 3052, 2324, 1473, 1459, 1418, 1395, 1253, 965, 973, 753, 707, 691 cm^{-1}. UV-Vis (THF): λ_{max} (log ε) = 213 (4.67), 233 (4.51), 247 (4.47), 261 (4.43), 272 (4.43), 283 (4.41), 318 (4.60) nm. ^{1}H NMR (DMSO-d_6 and 1 drop of D_2O, 500 MHz): δ 8.22 (br d, 2H), 7.64 (br d, 2H), 7.54 (m, 3H), 7.49 (m, 1H), 7.43 (m, 3H), 7.37 (d, J=7.5 Hz, 1H), 7.21 (dd, J=8.0 Hz, 7.5 Hz, 1H) ppm. ^{13}C NMR (DMSO-d_6 and 1 drop of D_2O, 200 MHz): δ 152.0, 144.4, 135.1, 131.6, 130.4, 129.8, 129.1, 128.9, 127.4, 126.8, 125.8, 122.9, 122.7, 112.9, 112.4, 109.6, 92.7, 87.7 ppm. HRMS (ESI/$[M+H]^+$): calcd for $C_{21}H_{15}N_2^+$ 295.1230, found 295.1230. Anal. Calcd. for $C_{21}H_{14}N_2 \cdot ¼THF$: C, 84.59; H, 5.16; N, 8.97. Found: C, 84.84; H, 3.95; N, 9.29.

Synthesis of Compound **6**

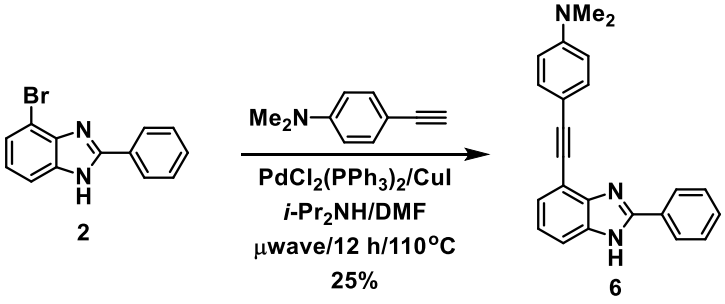

Anhydrous K_2CO_3 (831 mg, 6.01 mmol) was added to a solution of 2-(4-(*N*,*N*-dimethylamino)phenyl)trimethylsilylethyne (652 mg, 3.00 mmol) in a mixture of MeOH (5 mL) and THF (5 mL). After stirring for 30 min under nitrogen, the reaction mixture was filtered though Celite. The solvent was removed under reduced pressure to yield crude 4-ethynyl-*N*,*N*-dimethylaniline, which was used without purification in the next step. To minimize manipulations of this somewhat sensitive compound, we assumed a 95% yield for this reaction.[88]

The entire amount of 4-ethynyl-*N*,*N*-dimethylaniline (prepared as described above) was added to a thick-walled microwave pressure vial that contained a mixture of compound **2** (300 mg, 1.10 mmol), $PdCl_2(PPh_3)_2$ (60.0 mg, 0.09 mmol), CuI (20.0 mg, 0.11 mmol), *i*-Pr_2NH (5 mL), and DMF (5 mL). The vial was sealed and exposed to microwave irradiation for 12 h at 110 °C. After cooling, the reaction mixture was extracted with EtOAc, washed with brine, and dried over anhydrous $MgSO_4$. The product was isolated by column chromatography, eluting with hexane/EtOAc mixtures (60:40, 50:50, 20:80 and 0:100, successively). The solvent was removed under reduced pressure, and the solid was washed with EtOAc (5 mL) and THF (3 mL) to give pure compound **6** (90.5 mg, 25%).

6: mp 284 °C, with decomposition. IR (neat): 3091, 2206, 1607, 1588, 1524, 1457, 1386, 1363, 1186, 819, 747, 707 cm^{-1}. UV-Vis (THF): λ_{max} (log ε) = 253 (4.45), 293 (4.59), 317 (4.65), 351 (4.53) nm. ^1H NMR (DMSO-d_6 and 1 drop of D_2O, 500 MHz): δ 8.22 (br d, 2H), 7.51 (m, 5H), 7.41 (br s, 1H), 7.30 (d, *J*=7.5 Hz, 1H), 7.18 (dd, *J*=8.1 Hz, 7.4 Hz, 1H), 6.73 (d, *J*=9.2 Hz, 2H), 2.94 (s, 6H) ppm. ^{13}C NMR (DMSO-d_6 and 1 drop of D_2O, 200 MHz): δ 151.6, 150.1, 144.1, 135.1, 132.5, 130.1, 129.9, 128.9, 126.7, 125.2, 122.5, 113.9, 111.9, 111.4, 109.1, 94.2, 85.4, 39.5 ppm. HRMS (ESI/$[M+H]^+$): calcd for $C_{23}H_{20}N_3^+$ 338.1652, found 338.1650. Anal. Calcd. for $C_{23}H_{19}N_3 \cdot \frac{1}{3}$THF: C, 80.86; H, 6.04; N, 11.63. Found: C, 80.48; H, 5.46; N, 12.05.

Synthesis of Compound **7**

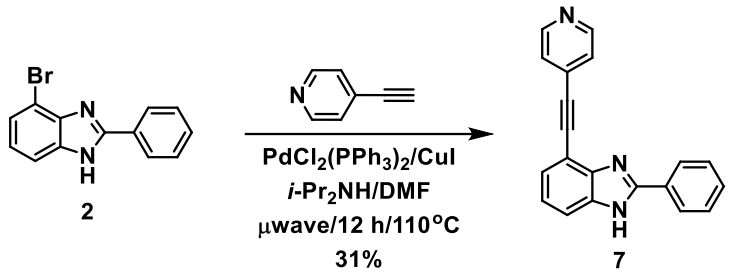

Anhydrous K_2CO_3 (1.00 g, 7.24 mmol) was added to a solution of 2-(4-(pyridyl)) trimethylsilylacetylene (630 mg, 3.59 mmol) in a mixture of MeOH (5 mL) and THF (5 mL). After being stirred for 30 min under nitrogen, the reaction mixture was filtered through Celite. The solvent was removed under reduced pressure to yield crude 4-ethynylpyridine, which was used without purification in the next step. To minimize manipulations of this somewhat sensitive compound, we assumed a 95% yield for this reaction.[88]

The entire amount of 4-ethynylpyridine (prepared as described above) was added to a thick-walled microwave pressure vial that contained a mixture of compound **2** (300 mg, 1.10 mmol), $PdCl_2(PPh_3)_2$ (60.0 mg, 0.09 mmol), CuI (20.0 mg, 0.11 mmol), *i*-Pr_2NH (5 mL), and DMF (5 mL). The vial was sealed and exposed to microwave irradiation for 12 h at 110 °C. After cooling, the reaction mixture was extracted with EtOAc, washed with brine, and dried over anhydrous $MgSO_4$. The product was isolated by column chromatography, eluting first with pure EtOAc, and then successively with EtOAc/MeOH mixtures in 95:5 and 90:10 ratios. The solvent was removed under

reduced pressure, and the resulting solid was recrystallized from a mixture of THF and hexane to give pure compound **7** (102 mg, 31%).

7: white powder, mp 251 °C, with decomposition. IR (neat): 3085, 2224, 1598, 1456, 1415, 1270, 831, 793, 735, 697, 685, 648 cm^{-1}. UV-Vis (THF): λ_{max} (log ε) = 210 (4.66), 235 (4.48), 242 (4.48), 247 (4.46), 259 (4.34), 274 (4.30), 287 (4.36), 322 (4.57) nm. ^{1}H NMR (DMSO-d_6, 500 MHz): δ 12.86 (s, 1H), 8.63 (d, J=6.3 Hz, 2H), 8.22 (d, J=7.5 Hz, 2H), 7.65 (d, J=7.5 Hz, 1H), 7.53 (m, 5H), 7.43 (dd, J=7.5 Hz, J=1.2 Hz, 1H), 7.24 (dd, J=8.1 Hz, 7.5 Hz, 1H) ppm. ^{13}C NMR (DMSO-d_6 and 1 drop of D_2O, 200 MHz): δ 152.5, 150.2, 144.5, 135.2, 131.0, 130.8, 129.7, 129.2, 127.1, 126.5, 125.7, 122.8, 113.4, 111.7, 109.6, 92.2, 90.2 ppm. HRMS (ESI/$[M+H]^+$): calcd for $C_{20}H_{14}N_3^+$ 296.1182, found 296.1183. Anal. Calcd for $C_{20}H_{13}N_3 \cdot {}^1/_6$ THF: C, 80.76; H, 4.70; N, 13.67. Found: C, 80.76; H, 4.31; N, 13.88.

Synthesis of Compound **8**

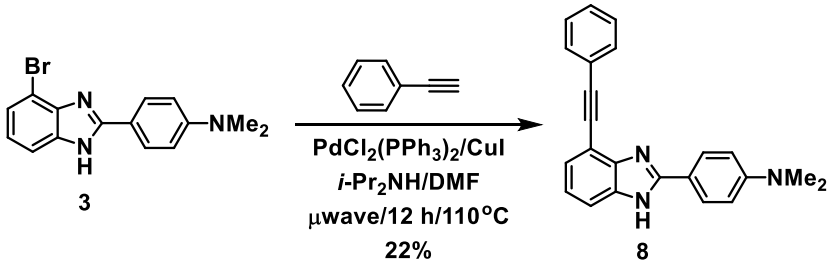

Phenylacetylene (387 mg, 3.79 mmol) was added to a thick-walled microwave pressure vial that contained a mixture of compound **3** (300 mg, 0.95 mmol), $PdCl_2(PPh_3)_2$ (60.0 mg, 0.09 mmol), CuI (20.0 mg, 0.11 mmol), *i*-Pr_2NH (5 mL), and DMF (5 mL). The vial was sealed and exposed to microwave irradiation for 12 h at 110 °C. After

cooling, the reaction mixture was extracted with EtOAc, washed with brine, and dried over anhydrous $MgSO_4$. The product was isolated by column chomatography, eluting with a hexane/EtOAc (70:30) mixture. The solvent was removed under reduced pressure, and the solid was recrystallized from a mixture of Et_2O, CH_2Cl_2, and hexane to give pure compound **8** (70 mg, 22%).

8: yellow powder, mp 247 °C. IR (neat): 3119, 2320, 1612, 1492, 1416, 1367, 1202, 956, 820, 753, 689, 668, 636, 601 cm^{-1}. UV-Vis (THF): λ_{max} (log ε) = 224 (4.59), 299 (4.48), 312 (4.45), 323 (4.46), 352 (4.57) nm. ^1H NMR ($CDCl_3$, 400 MHz): δ 7.96 (d, J=8.7 Hz, 2H), 7.68 (d, J=8.2 Hz, 1H), 7.58 (m, 2H), 7.40 (m, 4H), 7.20 (dd, J=8.2 Hz, 7.8 Hz, 1H), 6.74 (d, J=8.3 Hz, 2H), 3.03 (s, 6H) ppm. ^{13}C NMR ($CDCl_3$, 200 MHz): δ 162.2, 153.0, 151.8, 143.5, 131.8, 131.7, 128.5, 128.3, 126.2, 123.1, 122.5, 121.6, 116.0, 112.0, 93.5, 85.6, 40.2 ppm. HRMS (ESI): calcd for $C_{23}H_{20}N_3^+$ 338.1652, found 338.1654. Anal. Calcd for $C_{23}H_{19}N_3 \cdot ¼Et_2O$: C, 80.98; H, 6.09; N, 11.81. Found: C, 80.93; H, 5.48; N, 12.23.

Synthesis of Compound **9**

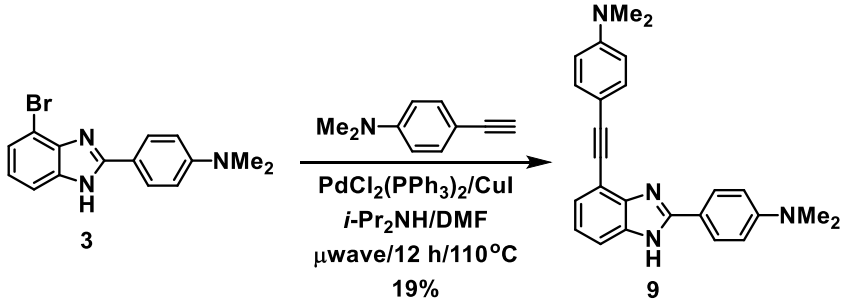

The entire amount of 4-ethynyl-*N*,*N*-dimethylaniline (prepared as in the synthesis of compound **6** described previously) was added to a thick-walled microwave pressure

vial that contained a mixture of compound **3** (300 mg, 0.95 mmol), $PdCl_2(PPh_3)_2$ (60.0 mg, 0.09 mmol), CuI (20.0 mg, 0.11 mmol), *i*-Pr_2NH (5 mL), and DMF (5 mL). The vial was sealed and exposed to microwave irradiation for 12 h at 110 °C. After cooling, the reaction mixture was extracted with EtOAc, washed with brine, and dried over anhydrous $MgSO_4$. The product was isolated by column chromatography, eluting with pure EtOAc. The solvent was removed under reduced pressure, and the solid was recrystallized from a mixture of THF and hexane to give pure compound **9 (**67 mg, 19%).

9: mp 276 °C, with decomposition. IR (neat): 3046, 2209, 1609, 1517, 1482, 1443, 1415, 1366, 1247, 1183, 920, 821, 755 cm^{-1}. UV-Vis (THF): λ_{max} (log ε) = 220 (4.60), 292 (4.46), 339 (4.66), 353 (4.62) nm. ^1H NMR (DMSO-d_6 and 3 drops of D_2O, 500 MHz): δ 8.00 (d, *J*=8.1 Hz, 2H), 7.42 (m, 3H), 7.20 (d, *J*=7.5 Hz, 1H), 7.09 (dd, *J*=8.1 Hz, 7.5 Hz, 1H), 6.79 (d, *J*=9.2 Hz, 2H), 6.71 (d, *J*=8.6 Hz, 2H), 2.96 (s, 6H), 2.92 (s, 6H) ppm. ^{13}C NMR (DMSO-d_6 and 1 drop of D_2O, 200 MHz): δ 152.6, 151.4, 150.1, 144.4, 135.0, 132.5, 127.9, 124.7, 121.5, 118.1, 117.0, 113.0, 111.8, 110.7, 109.4, 106.6, 93.8, 85.8, 39.5 ppm. HRMS (ESI/$[M+H]^+$): calcd for $C_{25}H_{25}N_4^+$ 381.2074, found 381.2073. Anal. Calcd for $C_{25}H_{24}N_4 \cdot ½THF$: C, 77.85; H, 6.78; N, 13.45. Found: C, 77.45; H, 6.00; N, 13.96.

Synthesis of Compound **10**

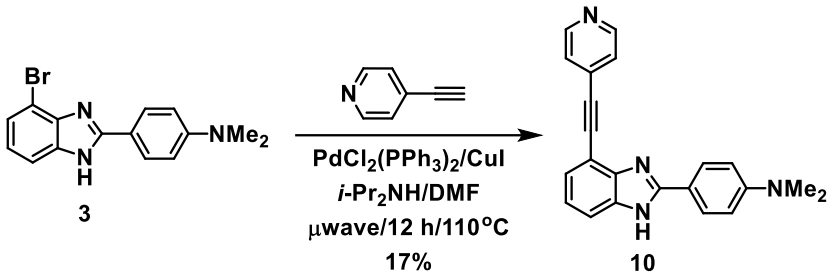

The entire amount of 4-ethynylpyridine (prepared as in the synthesis of compound **7** described previously) was added to a thick-walled microwave pressure vial that contained a mixture of compound **3** (300 mg, 0.95 mmol), $PdCl_2(PPh_3)_2$ (60.0 mg, 0.09 mmol), CuI (20.0 mg, 0.11 mmol), *i*-Pr_2NH (5 mL), and DMF (5 mL). The vial was sealed and exposed to microwave irradiation for 12 h at 110 °C. After cooling, the reaction mixture was extracted with EtOAc, washed with brine, and dried over anhydrous $MgSO_4$. The product was isolated by column chromatography, eluting with pure EtOAc. The solvent was removed under reduced pressure, and the solid was recrystallized from a mixture of THF and hexane to give pure compound **10** (55 mg, 17%).

10: mp 256 °C. IR (neat): 3419, 2227, 1609, 1500, 1413, 1365, 1352, 1205, 790, 739, 688, 608 cm^{-1}. UV-Vis (THF): λ_{max} (log ε) = 222 (4.65), 306 (4.56), 314 (4.56), 326 (4.53), 359 (4.53) nm. ^1H NMR (DMSO-d_6 and 1 drop of D_2O, 500 MHz): δ 8.62 (d, *J*=5.2 Hz, 2H), 8.02 (br s, 2H), 7.58 (br s, 3H), 7.35 (dd, *J*=8.0 Hz, 1.2 Hz, 1H), 7.16 (dd, *J*=8.1 Hz, 7.5 Hz, 1H), 6.81 (d, *J*=9.2 Hz, 2H), 2.97 (s, 6H) ppm. ^{13}C NMR (DMSO-d_6 and 1 drop of D_2O, 200 MHz): δ 153.5, 151.7, 150.0, 145.0, 135.1, 131.0, 128.2, 125.7, 125.5, 121.7, 116.6, 111.9, 111.5, 110.5, 92.5, 89.9, 39.5 ppm. HRMS (ESI/$[M+H]^+$):

calcd for $C_{22}H_{19}N_4^+$ 339.1604, found 339.1606. Anal. Calcd. for $C_{22}H_{18}N_4 \cdot {}^1/_6$ THF C, 77.69; H, 5.56; N, 15.99. Found: C, 77.24; H, 5.09; N, 13.34.

Synthesis of Compound **11**

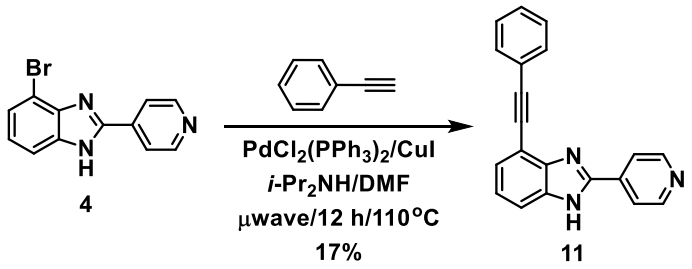

Phenylacetylene (418 mg, 4.09 mmol) was added to a thick-walled microwave pressure vial that contained a mixture of compound **4** (300 mg, 1.09 mmol), $PdCl_2(PPh_3)_2$ (60.0 mg, 0.09 mmol), CuI (20.0 mg, 0.11 mmol), *i*-Pr_2NH (5 mL), and DMF (5 mL). The vial was sealed and exposed to microwave irradiation for 12 h at 110 °C. After cooling, the reaction mixture was extracted with EtOAc, washed with brine, and dried over anhydrous $MgSO_4$. The product was isolated by column chromatography, eluting first with pure EtOAc, and then successively with EtOAc/MeOH mixtures in 95:5 and 90:10 ratios. The solvent was removed under reduced pressure, and the solid was recrystallized in the mixture of THF, CH_2Cl_2, and hexane to give pure compound **11 (**58 mg, 17%).

11: white powder, mp 226 °C. IR (neat): 3076, 1609, 1437, 1250, 999, 829, 756, 736, 696, 630 cm^{-1}. UV-Vis (THF): λ_{max} (log ε) = 227 (4.45), 264 (4.46), 281 (4.36), 288 (4.34), 323 (4.46) nm. ^{1}H NMR (DMSO-d_6, 500 MHz): δ 13.14 (br s, 1H), 8.74 (d, J=6.3 Hz, 2H), 8.13 (br s, 2H), 7.63 (br s, 3H), 7.43 (m, 4H), 7.28 (dd, J=8.0 Hz, 7.5 Hz, 1H)

ppm. ^{13}C NMR (DMSO-d_6 and 1 drop of D_2O, 200 MHz): δ 150.5, 149.6, 144.1, 136.9, 135.1, 131.7, 128.9, 127.4, 126.4, 123.7, 122.7, 120.8, 113.6, 112.9, 93.2, 87.2 ppm. HRMS (ESI/$[M+H]^+$): calcd for $C_{20}H_{14}N_3^+$ 296.1182, found 296.1185. Anal. Calcd for $C_{20}H_{13}N_3 \cdot {}^1/_5$THF: C, 80.65; H, 4.75; N, 13.57. Found: C, 80.41; H, 4.02; N, 13.97.

Synthesis of Compound **12**

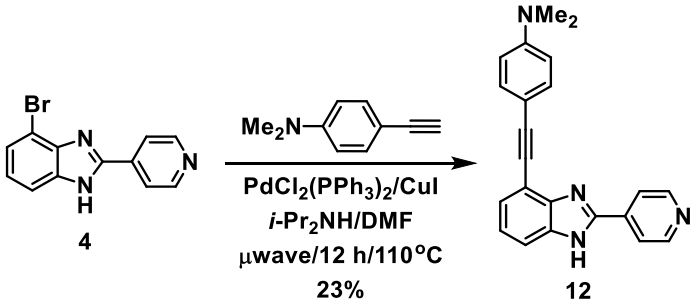

The entire amount of 4-ethynyl-*N*,*N*-dimethylaniline (prepared as in the synthesis of compound **6** described previously) was added to a thick-walled microwave pressure vial that contained a mixture of compound **4** (300 mg, 1.09 mmol), $PdCl_2(PPh_3)_2$ (60.0 mg, 0.09 mmol), CuI (20.0 mg, 0.11 mmol), *i*-Pr_2NH (5 mL), and DMF (5 mL). The vial was sealed and exposed to microwave irradiation for 12 h at 110 °C. After cooling, the reaction mixture was extracted with EtOAc, washed with brine, and dried over anhydrous $MgSO_4$. The product was isolated by column chromatography, eluting first with pure EtOAc, and then successively with EtOAc/MeOH mixtures in 95:5 and 90:10 ratios. The solvent was removed under reduced pressure, and the solid was recrystallized from a mixture of THF, MeOH and hexane to give pure compound **12** (85 mg, 23%).

12: yellow powder, mp 259 °C, with decomposition. IR (neat): 3098, 2215, 1608, 1524, 1445, 1363, 1186, 822, 795, 743, 701, 630 cm^{-1}. UV-Vis (THF): λ_{max} (log ε) = 265

(4.20), 294 (4.50), 315 (4.54), 357 (4.28) nm. ^{1}H NMR (DMSO-d_6 and 1 drop of D_2O, 500 MHz): δ 8.73 (d, J=6.3 Hz, 2H), 8.13 (br s, 2H), 7.60 (br s, 1H), 7.44 (d, J=8.6 Hz, 2H), 7.36 (d, J=8.0 Hz, 1H), 7.25 (dd, J=8.0 Hz, 7.5 Hz, 1H), 6.72 (d, J=9.2 Hz, 2H), 2.93 (s, 6H) ppm. ^{13}C NMR (DMSO-d_6 and 1 drop of D_2O, 200 MHz): δ 150.6, 150.4, 149.3, 143.9, 137.0, 135.2, 132.8, 125.9, 123.8, 120.8, 114.8, 112.1, 108.9, 95.1, 85.1, 39.5 ppm. HRMS (ESI/[M+H]$^+$): calcd for $C_{22}H_{19}N_4^+$ 339.1604, found 339.1605. Anal. Calcd for $C_{22}H_{18}N_4 \cdot$½THF: C, 76.98; H, 5.92; N, 14.96. Found: C, 75.33; H, 5.35; N, 15.33.

Synthesis of Compound **13**

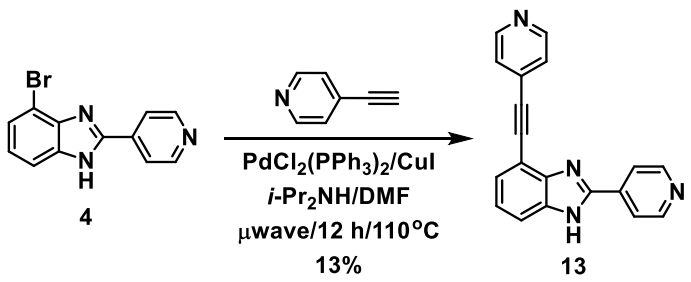

The entire amount of 4-ethynylpyridine (prepared as in the synthesis of compound **7** described previously) was added to a thick-walled microwave pressure vial that contained a mixture of compound **4** (300 mg, 1.09 mmol), $PdCl_2(PPh_3)_2$ (60.0 mg, 0.09 mmol), CuI (20.0 mg, 0.11 mmol), *i*-Pr_2NH (5 mL), and DMF (5 mL). The vial was sealed and exposed to microwave irradiation for 12 h at 110 °C. After cooling, the reaction mixture was extracted with EtOAc, washed with brine, and dried over anhydrous $MgSO_4$. The product was isolated by column chromatography, eluting first with pure EtOAc, and then successively with EtOAc/MeOH mixtures in 95:5 and 90:10 ratios. The

solvent was removed under reduced pressure, and the solid was recrystallized from a mixture of THF, MeOH, and hexane to give pure compound **13 (**41 mg, 13%).

13: mp 252 °C, with decomposition. IR (neat): 3067, 2227, 1601, 1438, 829, 792, 738, 698, 613 cm^{-1}. UV-Vis (THF): λ_{max} (log ε) = 262 (4.36), 277 (4.38), 289 (4.41), 327 (4.53) nm. ^{1}H NMR (DMSO-d_6, 500 MHz): δ 13.20 (br s, 1H), 8.75 (d, J=6.3 Hz, 2H), 8.64 (d, J=6.3 Hz, 2H), 8.13 (d, J=5.7 Hz, 2H), 7.72 (d, J=8.0 Hz, 1H), 7.56 (d, J=5.2 Hz, 2H), 7.49 (d, J=7.5 Hz, 1H), 7.31 (dd, J=8.0 Hz, 7.5 Hz, 1H) ppm. ^{13}C NMR (DMSO-d_6 and 1 drop of D_2O, 200 MHz): δ 150.7, 150.0, 149.8, 144.3, 136.8, 135.2, 130.7, 127.0, 125.7, 123.9, 120.8, 113.9, 112.3, 91.7, 90.4 ppm. HRMS (ESI/$[M+H]^+$): calcd for $C_{19}H_{13}N_4^+$ 297.1135, found 297.1136. Anal. Calcd for $C_{19}H_{12}N_4 \cdot \frac{1}{3}H_2O$: C, 75.48; H, 4.22; N, 18.53. Found: C, 75.19; H, 3.80; N, 18.22.

2.4.3 UV/Vis absorption and fluorescence titrations of compounds 5–13 with acid—TFA and base—*n*-Bu_4OH

UV-visible and fluorescence titrations were performed using Perkin-Elmer LAMBDA 25 UV/Vis Spectrometer and Perkin-Elmer Fluorescence Spectrometer LS-55, respectively. Five stock solutions of TFA—0.1 mM, 0.001 M, 0.01 M, 0.1 M, 1 M, and 10 M and four stock solutions of 40% aq. TBAOH—0.1 mM, 0.001 M, 0.01 M, and 0.1 M were prepared in THF. In a quartz cuvette, 3 mL of 1×10^{-5} M solution of a given fluorophore in THF were titrated using the stock solutions of TFA, or 40% aq. TBAOH to give the indicated range of acid and base concentrations. The excitation wavelength

used for fluorescence titration corresponded to the isosbestic points determined in the UV/Vis titration.

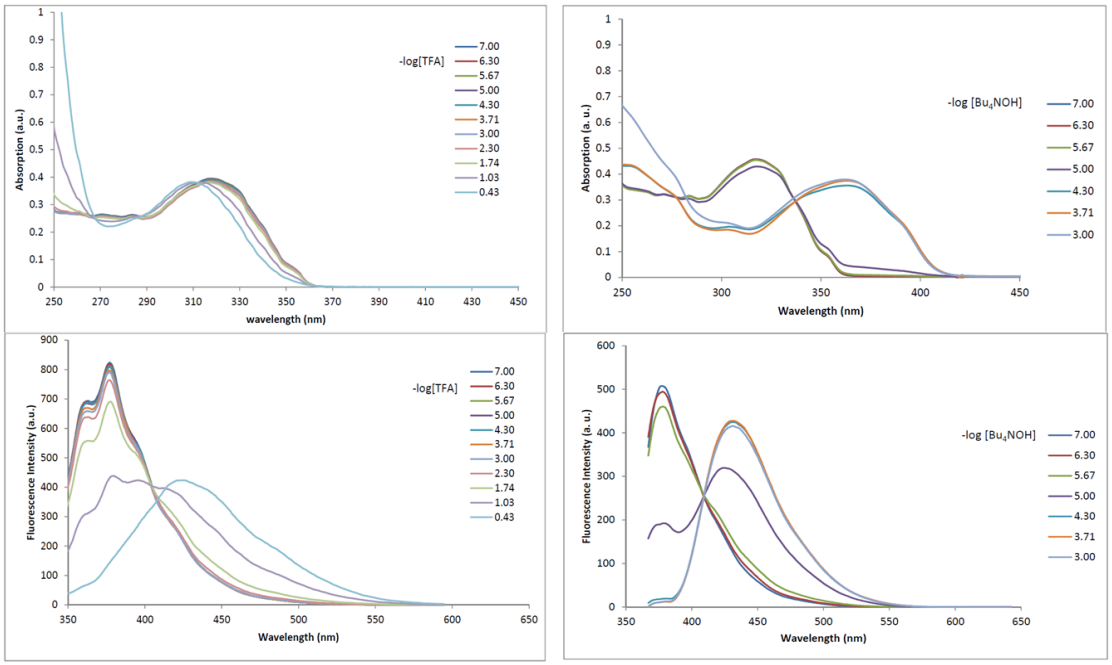

Figure 2.16 Absorption (top) and emission (bottom) spectra for the TFA titration (left, λ_{exc}=313 nm) and for TBAOH titration (right, λ_{exc}=337 nm) of **5**.

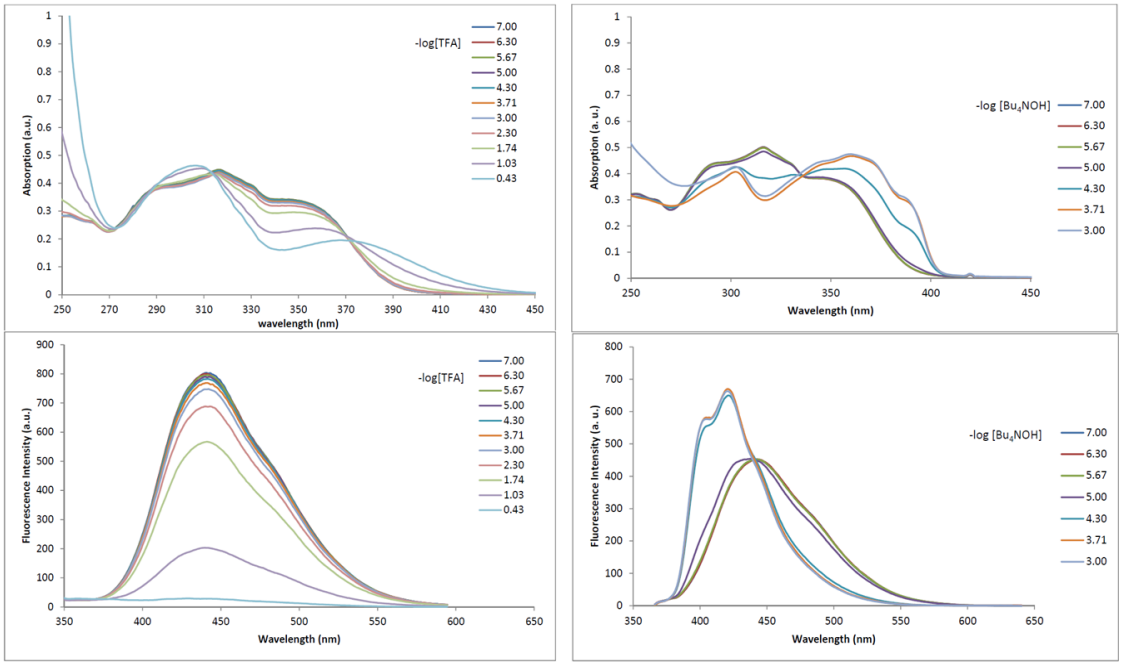

Figure 2.17 Absorption (top) and emission (bottom) spectra for the for TFA titration (left, λ_{exc}=313 nm) and for TBAOH titration (right, λ_{exc}=336 nm) of **6**.

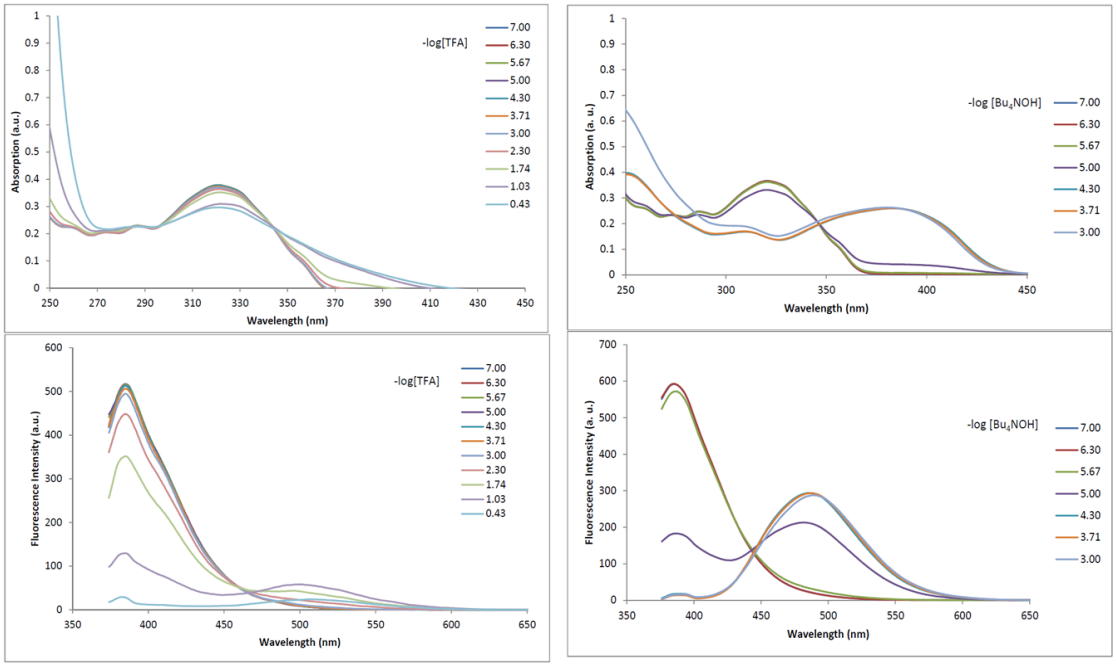

Figure 2.18 Absorption (top) and emission (bottom) spectra for the the TFA titration (left, λ_{exc}=344 nm) and for TBAOH titration (right, λ_{exc}=346 nm) of **7**.

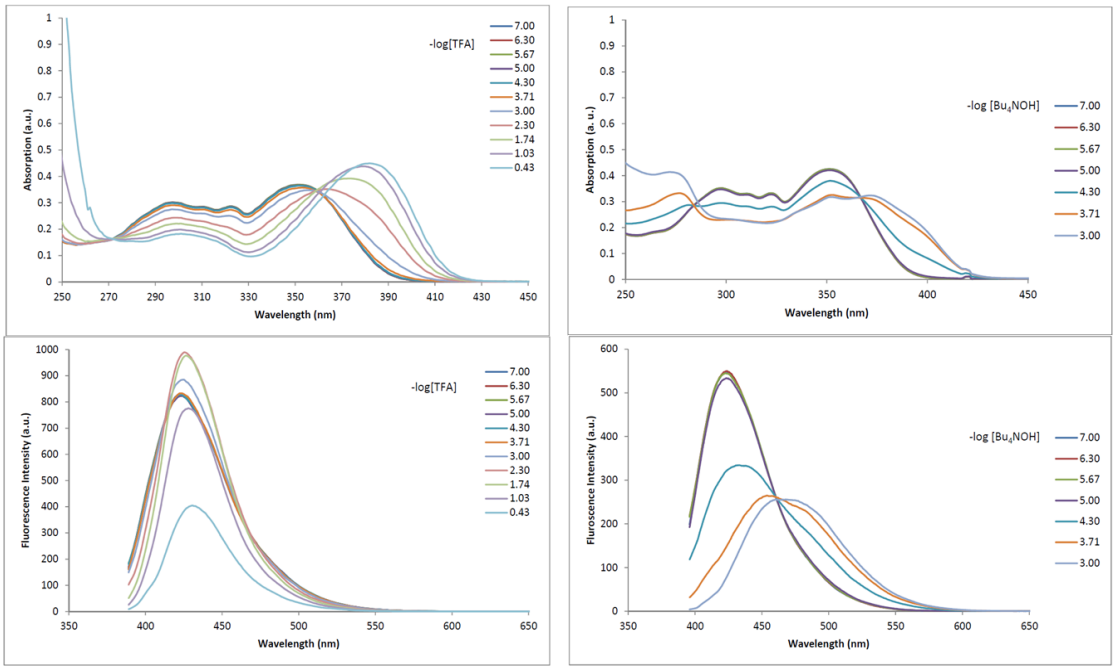

Figure 2.19 Absorption (top) and emission (bottom) spectra for the the TFA titration (left, λ_{exc}=359 nm) and for TBAOH titration (right, λ_{exc}=366 nm) of **8**.

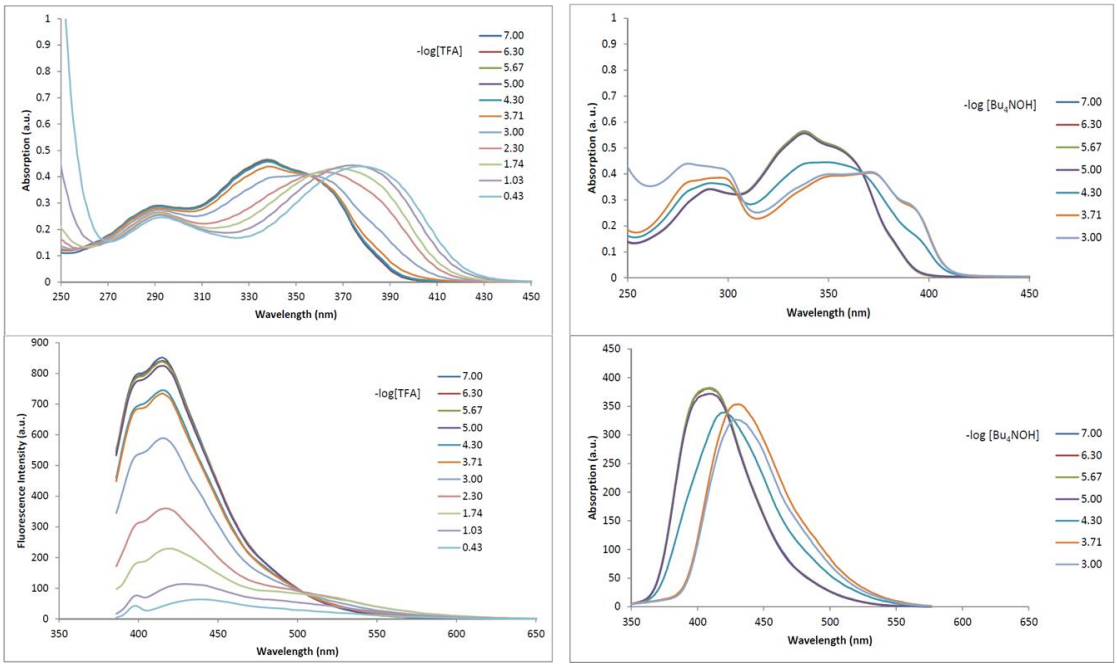

Figure 2.20 Absorption (top) and emission (bottom) spectra for the the TFA titration (left, λ_{exc}=356 nm) and for TBAOH titration (right, λ_{exc}=304 nm) of **9.**

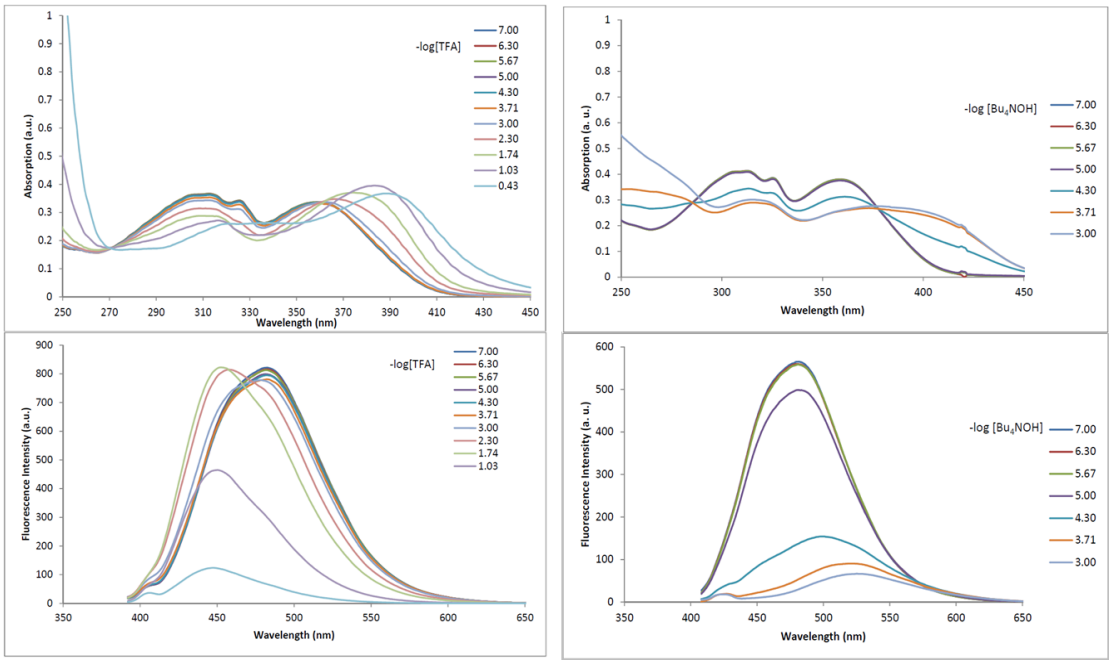

Figure 2.21 Absorption (top) and emission (bottom) spectra for the the TFA titration (left, λ_{exc}=362 nm) and for TBAOH titration (right, λ_{exc}=378 nm) of **10.**

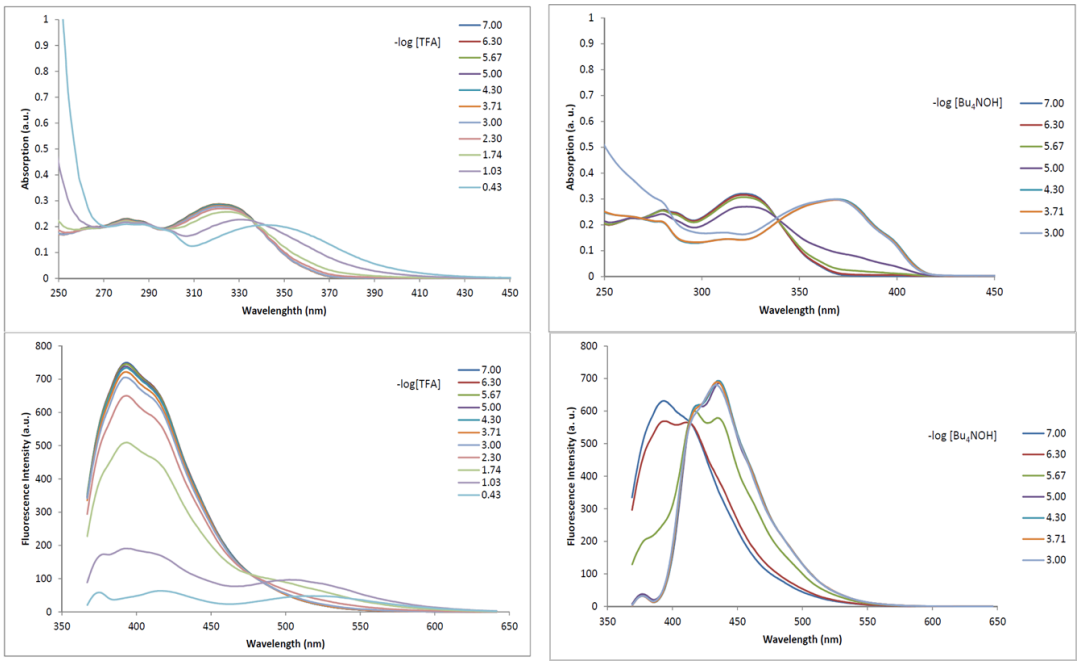

Figure 2.22 Absorption (top) and emission (bottom) spectra for the the TFA titration (left, λ_{exc}=337 nm) and for TBAOH titration (right, λ_{exc}=339 nm) of **11.**

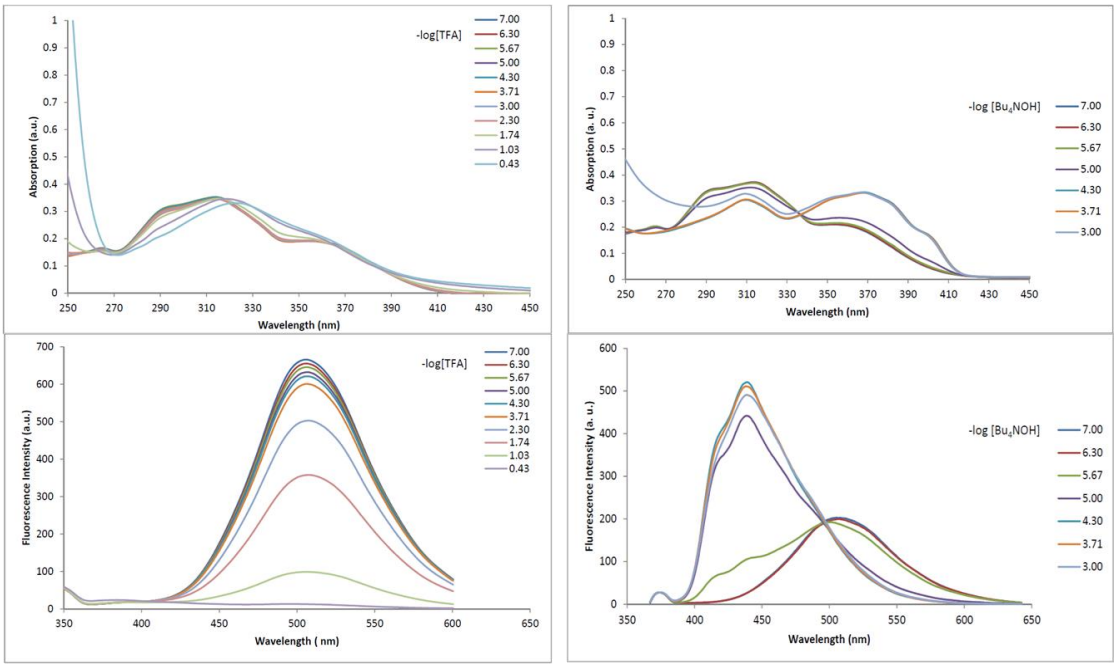

Figure 2.23 Absorption (top) and emission (bottom) spectra for the the TFA titration (left, λ_{exc}=317 nm) and for TBAOH titration (right, λ_{exc}=337 nm) of **12.**

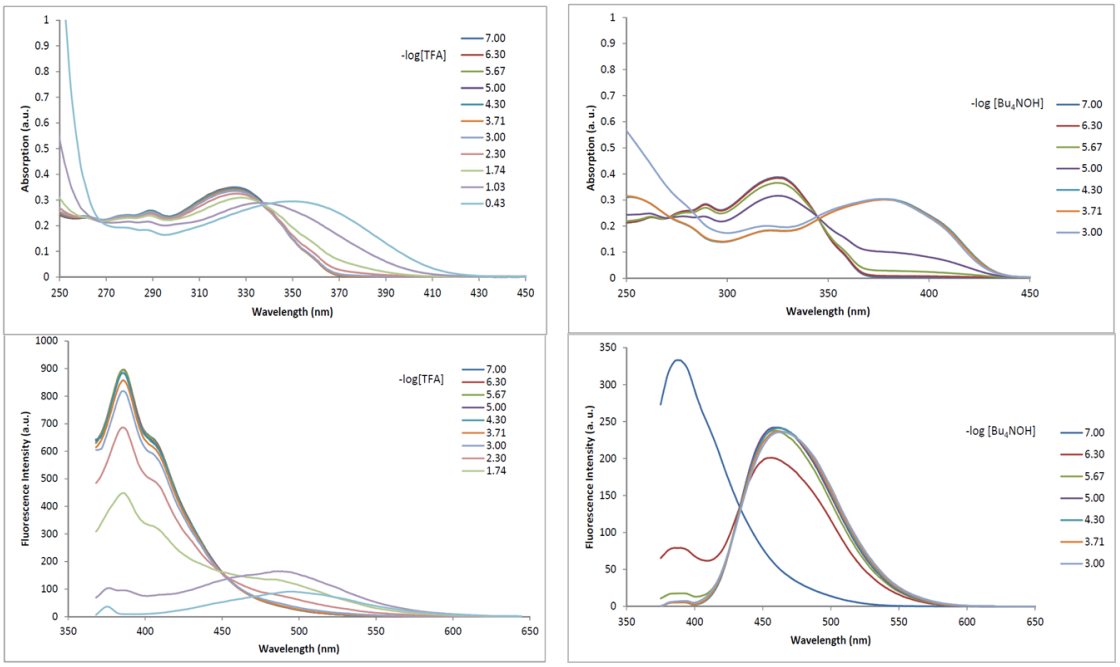

Figure 2.24 Absorption (top) and emission (bottom) spectra for the the TFA titration (left, λ_{exc}=338 nm) and for TBAOH titration (right, λ_{exc}=345 nm) of **13.**

2.4.4 Synthesis of Other Benzimidazole-based Sensor Precursors

Synthesis of 4-Bromo-6-(*tert*-butyl)-2-(pyridine-4-yl)-1H-benzo[*d*]imidazole **20**[121]

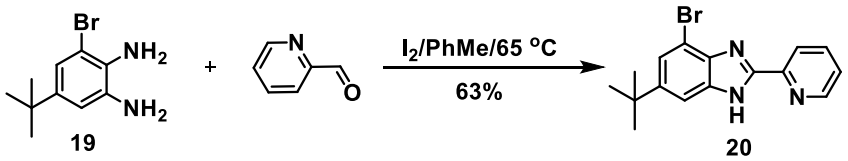

In a 1 L round-bottom flask, compound **19**[Error! Bookmark not defined.] (10.0 g, 41.1 mmol) and 2-pyridinecarboxaldehyde (4.2 mL, 44.2 mmol) were dissolved in PhMe (750 mL), the solution was heated up to 65 ^{o}C and gradually turned yellow. After 4 h, I_2 (10.5 g, 41.5 mmol) was added into the solution. Immediate formation of a brown precipitate was observed. The mixture was stirred at 65 °C for additional 2 h. After cooling, the solution was filtered and the residue washed with hexane and dried. The collected residue was mixed with Et_2O (300 mL), and triethylamine was slowly added to solution which was then sonicated, stirred and adjusted to the pH of 8. The whole mixture was subsequently extracted with Et_2O, washed with brine, and dried over anhydrous $MgSO_4$. The combined organic phase was concentrated giving a light yellow solid which was further purified by washing with Et_2O to afford white solid **20** (8.55 g, 63%).

20: ^{1}H NMR (DMSO-d_6, 400 MHz): δ 8.71 (m, 1H), 8.30 (m, 1H), 7.98 (m, 1H), 7.51 (m, 1H), 7.45 (m, 2H), 1.31 (s, 9H) ppm. ^{13}C NMR (DMSO-d_6, 500 MHz): δ 151.7, 150.0, 148.6, 148.3, 140.9, 138.2, 136.0, 125.5, 123.5, 122.1, 112.4, 108.2, 35.3, 31.9 ppm.

Synthesis of 4-Ethynyl-6-(*tert*-butyl)-2-(pyridine-4-yl)-1H-benzo[*d*]imidazole (**16**)

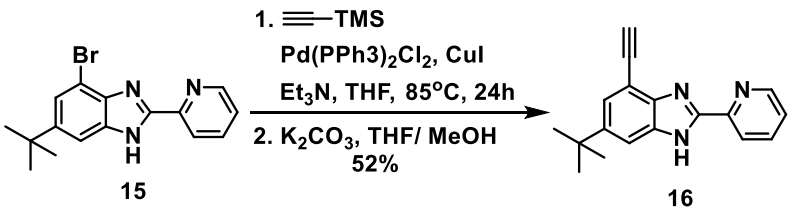

A 500 mL pear-shaped Schlenk flask was charged with compound **20** (7.0 g, 21.2 mmol), $PdCl_2(PPh_3)_2$ (1.50 g, 2.13 mmol), and CuI (654 mg, 3.43 mmol). The flask was sealed, then evacuated and backfilled with N_2 three times. In a separate flask, a mixture of Et_3N (60 mL), THF (60 mL), and TMSA (20 mL, 142 mmol) was degassed for 20 min and then slowly transferred, under positive N_2 pressure, via cannula to the reaction flask. The reaction mixture was stirred and heated at 80 °C for 2 d and then cooled to 20 °C. After that, EtOAc (300 mL) and THF (300 mL) were added to the reaction mixture which was then sonicated, dried over $MgSO_4$, filtered through a celite plug and washed with THF. The filtrate was concentrated under reduced pressure until a powder was formed. The collected solid was washed with Et_2O and cold EtOAc to afford a light green powder (4.8 g, 65% yield). This compound was used crude in the next step.

In a nitrogen-flushed 500 mL flask, trimethylsilyl-substituted alkyne produced in the previous step (4.80 g, 13.8 mmol) was dissolved in a mixture of THF (100 mL) and MeOH (100 mL), and treated with anhydrous K_2CO_3 (3.83 g, 27.7 mmol). The resulting solution was stirred at 25 °C for 2 h. The whole mixture was condensed *in vacuo* to give off-white solid which was mixed with MeOH (250 mL), and the solution was filtered through a plug of celite. The filtrate after concentration process was mixed with 200 mL

DCM and its pH was adjusted by addition of CH_3COOH to ~8. The solution was subsequently extracted with DCM, washed with brine, and dried over anhydrous $MgSO_4$. The combined organic phase was concentrated giving a light green solid which was further purified by short alumina column with DCM as eluent to generate **16** as a white solid (3.1 g, 52% over 2 steps).

16: ^{1}H NMR (DMSO-d_6, 400 MHz): δ 8.70 (m, 1H), 8.30 (m, 1H), 7.96 (m, 1H), 7.49 (m, 2H), 7.38 (m, 1H), 4.34 (s, 1H), 1.31 (s, 9H) ppm. ^{13}C NMR (DMSO-d_6, 500 MHz): δ 151.8, 150.0, 148.8, 146.5, 143.3, 138.1, 135.5, 125.4, 124.9, 122.2, 112.6, 109.8, 84.4, 82.3, 35.1, 31.9 ppm.

Synthesis of Compound **21**

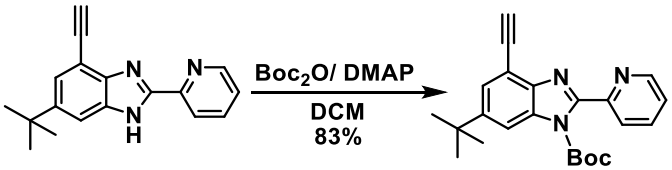

16 21

In a 500 mL round-bottom flask, compound **16** (1.50 g, 5.45 mmol) and DMAP (1.00 g, 8.18 mmol) were dissolved in DCM (100 mL). Then Boc_2O (2.40 g, 11.0 mmol) was added slowly into the solution. The mixture was kept stirring at 25 °C for 24 h. The product was isolated by silica column chromatography, eluting with EtOAc/hexane mixtures (from 1:4 to 3:10). The solvent was removed under reduced pressure to give pure compound **21** as a white solid **(**1.68 g, 83%).

21: ^{1}H NMR ($CDCl_3$, 400 MHz): δ 8.64 (m, 1H), 8.04 (m, 1H), 7.86 (m, 1H), 7.78 (m, 1H), 7.59 (m, 1H), 7.32 (m, 1H), 3.39 (s, 1H), 1.34 (d, 18H) ppm. ^{13}C NMR ($CDCl_3$, 400

MHz): δ 152.6, 151.0, 149.0, 148.9, 148.4, 141.6, 136.6, 134.0, 126.8, 124.5, 124.1, 113.2, 112.1, 85.2, 81.6, 80.5, 35.4, 31.7, 27.6 ppm.

Synthesis of Compound **14**

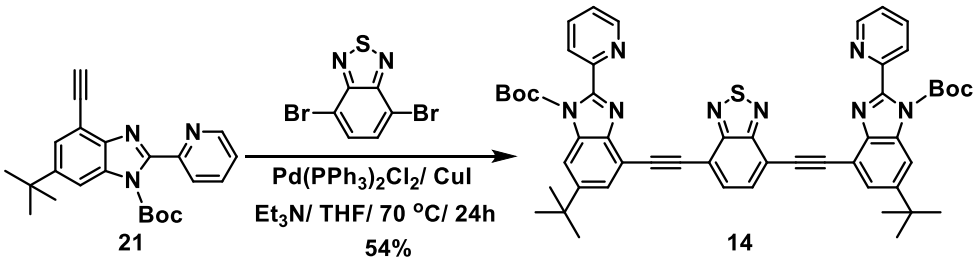

A 100 mL pear-shaped Schlenk flask was charged with compound **21** (1.00 g, 2.66 mmol), 4,7-dibromo-2,1,3-benzothiadiazole[113] (330 mg, 1.12 mmol), $PdCl_2(PPh_3)_2$ (160 mg, 0.23 mmol), and CuI (65 mg, 0.34 mmol). The flask was sealed, then evacuated and backfilled with N_2 three times. In a separate flask, a mixture of Et_3N (9 mL) and THF (9 mL) was degassed for 20 min and then slowly transferred, under positive N_2 pressure, via cannula to the reaction flask. The reaction mixture was stirred and heated at 70 °C for 24 h and then cooled to 20 °C. Upon completion, reaction mixture was dry-absorbed on silica gel. After purification by column chromatography on silica gel using eluting with EtOAc/hexane (from 1:4 to 3:2) as eluent and evaporation of the fractions containing the product, compound **14** was obtained as a yellow solid (534 mg, 54 % yield).

14: ^{1}H NMR ($CDCl_3$, 400 MHz): δ 8.69 (m, 2H), 8.09 (m, 2H), 7.98 (m, 2H), 7.93 (m, 2H), 7.84 (m, 2H), 7.79 (m, 2H), 7.38 (m, 2H), 1.43 (m, 36H) ppm. ^{13}C NMR ($CDCl_3$, 400 MHz): δ 154.5, 152.7, 151.0, 149.1, 148.9, 148.5, 141.3, 136.6, 134.2, 133.1, 126.9, 124.5, 124.2, 94.6, 89.3, 85.3, 35.5, 31.8, 27.6 ppm.

Synthesis of Compound **22**

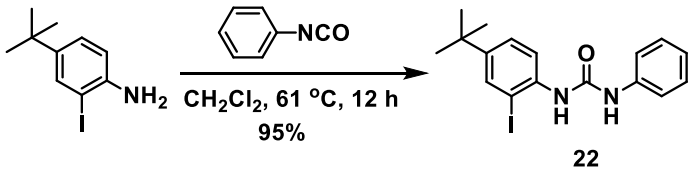

22

A 250 mL flask was charged with compound 4-*tert*-butyl-2-iodoaniline (2 g, 7.32 mmol), phenylisocyanate (0.81 mL, 7.45 mmol) and 100 mL of CH_2Cl_2. The flask was then heated at reflux for 12 h. Upon completion, reaction was cooled down to room temperature. The solvent was evacuated *in vacuo*. The collected oil starts to crystallize with addition of several drops of Et_2O. The crystal formed were filtered, washed with Et_2O and dried in air to afford compound **22** as a white solid (2.7 g, 95 % yield).

22: ^{1}H NMR (DMSO-d_6, 500 MHz): δ 9.30 (s, 1H), 7.79 (s, 1H), 7.73 (d, J=2.3 Hz, 1H), 7.66 (d, J=8.6 Hz, 1H), 7.42 (d, J=7.5 Hz, 2H), 7.35 (dd, J=8.6 Hz, 2.3 Hz, 1H), 7.25 (t, J=7.5 Hz, 2H), 6.94 (t, J=7.5 Hz, 1H), 1.22 (s, 9H) ppm. ^{13}C NMR (DMSO-d_6, 500 MHz): δ 153.0, 148.3, 140.2, 137.9, 135.8, 129.4, 126.2, 123.6, 122.4, 118.6, 92.5, 34.5, 31.5 ppm.

Synthesis of Compound **23**

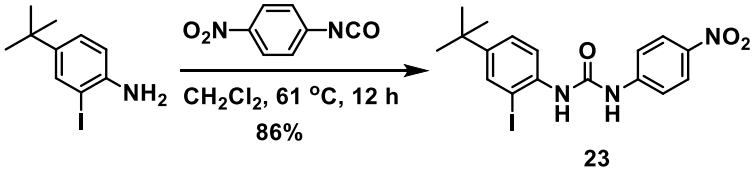

23

A 250 mL flask was charged with compound 4-*tert*-butyl-2-iodoaniline (2 g, 7.32 mmol), 4-nitrophenyl isocyanate (1.20 g, 7.32 mmol), and 100 mL of CH_2Cl_2. The

solution was heated at reflux for 12 h. Upon completion, reaction was cooled down to room temperature. The solvent was removed *in vacuo*, and the collected oil starts to crystallize with addition of several drops of Et_2O. The crystal formed were filtered, washed with Et_2O and dried in air to afford compound **23** as a white solid (2.8 g, 86 % yield).

23: ^{1}H NMR (DMSO-d_6, 500 MHz): δ 9.99 (s, 1H), 8.17 (d, J=9.2 Hz, 2H), 8.06 (s, 1H), 7.76 (d, J=2.3 Hz, 1H), 7.66 (d, J=9.2 Hz, 2H), 7.64 (d, J=8.6 Hz, 1H), 7.38 (dd, J=8.6 Hz, 2.3 Hz, 1H), 1.23 (s, 9H) ppm. ^{13}C NMR (DMSO-d_6, 500 MHz): δ 152.6, 149.2, 146.9, 141.6, 137.3, 135.9, 126.3, 125.8, 124.2, 118.0, 93.5, 34.5, 31.5 ppm.

Synthesis of Compound **17**

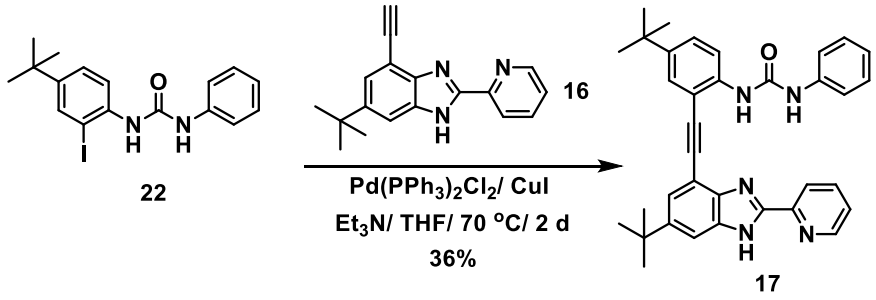

A 500 mL pear-shaped Schlenk flask was charged with compound **22** (1.12 g, 2.84 mmol), **16** (1.17 g, 4.25 mmol), $PdCl_2(PPh_3)_2$ (243 mg, 0.35 mmol), and CuI (119 mg, 0.62 mmol). The flask was sealed, then evacuated and backfilled with N_2 three times. In a separate flask, a mixture of Et_3N (40 mL), THF (40 mL) was degassed for 20 min and then slowly transferred, under positive N_2 pressure, via cannula to the reaction flask. The reaction mixture was stirred and heated at 70 °C for 2 d and then cooled to 20 °C. Upon completion, reaction mixture was dry-absorbed on alumina. After purification by

column chromatography on alumina, eluting with hexane followed by EtOAc/hexane (1:4), the fractions containing the product were evaporated. The collected solid was further purified by recrystallization in hexane/THF solution to obtain compound **17** as a white solid (555 mg, 36% yield).

17: white powder, ^{1}H NMR (DMSO-d_6, 500 MHz): δ 13.22 (m, 1H), 9.45 (m, 1H), 8.68 (m, 1H), 8.34 (m, 2H), 7.99 (m, 1H), 7.63 (m, 4H), 7.42 (m, 4H), 7.23 (m, 2H), 6.94 (m, 1H), 1.31 (d, 18H) ppm. ^{13}C NMR (DMSO-d_6, 500 MHz): δ 152.9, 151.9, 149.9, 148.6,146.6, 145.1, 143.0, 140.2, 138.3, 137.9, 135.6, 129.4, 128.9, 127.1, 125.3, 124.7, 122.5, 122.2, 120.4, 118.8, 113.1, 112.5, 109.8, 93.7, 89.3, 35.2, 34.5, 32.0, 31.6 ppm.

Synthesis of Compound **18**

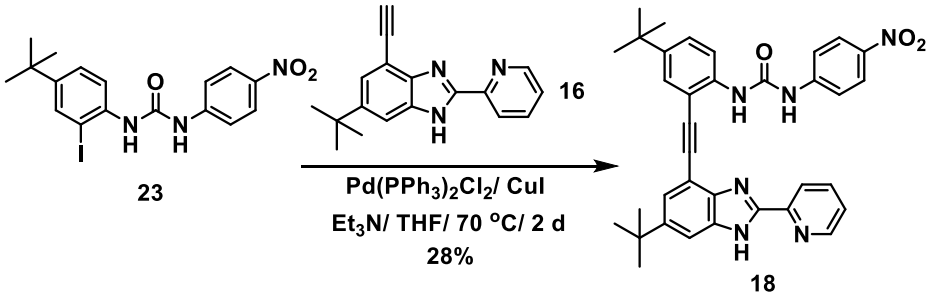

A 500 mL pear-shaped Schlenk flask was charged with compound **23** (1.60 g, 3.64 mmol), **16** (1.00 g, 3.64 mmol), $PdCl_2(PPh_3)_2$ (310 mg, 0.44 mmol), and CuI (152 mg, 0.8 mmol). The flask was sealed, then evacuated and backfilled with N_2 three times. In a separate flask, a mixture of Et_3N (40 mL), THF (40 mL) was degassed for 20 min and then slowly transferred, under positive N_2 pressure, via cannula to the reaction flask. The reaction mixture was stirred and heated at 70 °C for 2 d and then cooled to 20 °C. Upon completion, reaction mixture was filtered over celite plug and washed with THF.

The filtrate was concentrated *in vacuo*. The obtained residue after evaporation was mixed with 500 mL CH_2Cl_2; whole mixture was then sonicated and filtered through celite plug one more time, washed with CH_2Cl_2. The filtrate was concentrated to yield yellow solid which was further purified by recrystallization in CH_2Cl_2 to generate the final product **18** as a light yellow solid (598 mg, 28% yield).

18: ^{1}H NMR (DMSO-d_6, 500 MHz): δ 13.23 (m, 1H), 10.11 (m, 1H), 8.67 (d, J=4.0 Hz, 1H), 8.54 (m, 1H), 8.26 (m, 1H), 8.13 (d, J=8.6 Hz, 2H), 7.96 (m, 1H), 7.56 (m, 8H), 1.30 (d, 18H) ppm. ^{13}C NMR (DMSO-d_6, 500 MHz): δ 152.5, 151.9, 149.9, 148.6, 146.9, 146.6, 146.0, 143.1, 141.6, 137.9, 137.6, 135.6, 128.9, 127.2, 125.7, 125.3, 124.6, 122.1, 120.9, 118.0, 113.3, 113.0, 109.9, 93.9, 89.2, 35.2, 34.6, 32.0, 31.6 ppm.

2.4.5 Crystal Data for Other Benzimidazole-based Sensor Precursors

Table 2.1 Crystallographic Data of Complex of **16** and Zn^{2+}

Empirical formula	$C_{56}H_{55}F_6N_9O_8S_2Zn$	
Formula weight	1225.58	
Temperature	123(2) K	
Wavelength	1.54178 Å	
Crystal system	Orthorhombic	
Space group	$P2_12_12_1$	
Unit cell dimensions	a = 17.8064(6) Å	α = 90°
	b = 17.9019(6) Å	β = 90°
	c = 18.1657(10) Å	γ = 90°
Volume	5790.7(3) $Å^3$	
Z	4	
Density (calculated)	1.406 Mg/m^3	
Absorption coefficient	7.953 mm^{-1}	
F(000)	2536	
Crystal size	0.40×0.40×0.30 mm^3	
θ range for data collection	3.47° to 66.57°	
Index ranges	$-19 \le h \le 20$, $0 \le k \le 21$, $0 \le l \le 21$	
Reflections collected	38985	
Independent reflections	9934 [R(int) = 0.0217]	
Completeness to θ = 66.57°	98.2 %	
Absorption correction	Empirical	
Max. and min. transmission	0.7528 and 0.5992	
Refinement method	Full-matrix least-squares on F^2	
Data / restraints / parameters	9756 / 120 / 678	
Goodness-of-fit on F^2	1.022	
Final R indices [$I > 2\sigma(I)$]	R_1 = 0.0412, wR_2 = 0.1031	
R indices (all data)	R_1 = 0.0417, wR_2 = 0.1035	
Absolute structure parameter	0.037(17)	
Extinction coefficient	0.00030(4)	
Largest diff. peak and hole	0.717 and −0.808 e / $Å^3$	

Table 2.2 Crystallographic Data of Complex **16** and Cd^{2+}

Empirical formula	$C_{20}H_{22}CdN_6O_7$	
Formula weight	570.84	
Temperature	123(2) K	
Wavelength	1.54718 Å	
Crystal system	Triclinic	
Space group	*P*-1	
Unit cell dimensions	a = 6.8528(5) Å	α = 101.253(2)°
	b = 12.8069(9) Å	β = 95.586(2)°
	c = 13.8060(9) Å	γ = 97.484(2)°
Volume	1168.81(14) $Å^3$	
Z	2	
Density (calculated)	1.622 Mg/m^3	
Absorption coefficient	7.953 mm^{-1}	
F(000)	576	
Crystal size	0.4×0.2×0.06 mm^3	
θ range for data collection	3.56° to 66.67°	
Index ranges	$-7 \le h \le 7$, $-15 \le k \le 14$, $0 \le l \le 16$	
Reflections (collected)	7677	
Reflections (unique)	3820 [R(int) = 0.0381]	
Completeness to θ = 66.67	92.3 %	
Absorption correction	Empirical	
Max. and min. transmission	0.7528 and 0.3081	
Refinement method	Full-matrix least-squares on F^2	
Data / restraints / parameters	3677 / 1 / 311	
Goodness-of-fit on F^2	1.094	
Final R indices [$I > 2\sigma(I)$]	R_1 = 0.0309, wR_2 = 0.0829	
R indices (all data)	R_1 = 0.0317, wR_2 = 0.0844	
Extinction coefficient	0.00075(19)	
Largest diff. peak and hole	0.944 and −1.223 e/$Å^3$	

Table 2.3 Crystallographic Data of Compound **14**

Empirical formula	$C_{52}H_{50}N_8O_4S$	
Formula weight	883.06	
Temperature	100(2) K	
Wavelength	0.40651 Å	
Crystal system	Triclinic	
Space group	*P*-1	
Unit cell dimensions	a = 11.4698(4) Å	α = 95.8680(10)°
	b = 11.5247(4) Å	β = 100.7520(10)°
	c = 18.0194(6) Å	γ = 90.1580(10)°
Volume	2327.25(14) $Å^3$	
Z	2	
Density (calculated)	1.260 Mg/m^3	
Absorption coefficient	0.043 mm^{-1}	
F(000)	932	
Crystal size	0.08×0.05×0.04 mm^3	
θ range for data collection	1.118° to 19.325°	
Index ranges	$-18 \le h \le 18$, $-18 \le k \le 14$, $-26 \le l \le 29$	
Reflections collected	68422	
Independent reflections	19755 [R(int) = 0.0843]	
Completeness to θ = 14.117°	95.5 %	
Absorption correction	None	
Refinement method	Full-matrix least-squares on F^2	
Data / restraints / parameters	11935 / 0 / 598	
Goodness-of-fit on F^2	1.015	
Final R indices [$I > 2\sigma(I)$]	R_1 = 0.0574, wR_2 = 0.1281	
R indices (all data)	R_1 = 0.1124, wR_2 = 0.1475	
Extinction coefficient	N/A	
Largest diff. peak and hole	0.424 and −0.499 e/$Å^3$	

Table 2.4 Crystallographic Data of Compound **17**

Empirical formula	$C_{35}H_{36}N_5O_{1.5}$	
Formula weight	550.69	
Temperature	123(2) K	
Wavelength	1.54178 Å	
Crystal system	Monoclinic	
Space group	*C*2/c	
Unit cell dimensions	a = 14.2619(3) Å	α = 90°
	b = 16.4405(3) Å	β = 91.179(1)°
	c = 24.9304(5) Å	γ = 90°
Volume	5844.3(2) Å^3	
Z	8	
Density (calculated)	1.252 Mg/m^3	
Absorption coefficient	0.615 mm^{-1}	
F(000)	2344	
Crystal size	0.30×0.15×0.10 mm^3	
θ range for data collection	3.55° to 66.59°	
Index ranges	$-16 \le h \le 16$, $0 \le k \le 19$, $0 \le l \le 28$	
Reflections collected	19953	
Independent reflections	5129 [R(int) = 0.0169]	
Completeness to θ = 66.59°	96.1 %	
Absorption correction	Empirical	
Max. and min. transmission	0.7528 and 0.6799	
Refinement method	Full-matrix least-squares on F^2	
Data / restraints / parameters	4266 / 4 / 387	
Goodness-of-fit on F^2	0.996	
Final R indices [$I > 2\sigma(I)$]	R_1 = 0.0363, wR_2 = 0.0984	
R indices (all data)	R_1 = 0.0417, wR_2 = 0.1003	
Extinction coefficient	N/A	
Largest diff. peak and hole	0.249 and −0.319 e/Å^3	

Table 2.5 Crystallographic Data of Compound **18**

Empirical formula	$C_{35}H_{35}N_6O_{3.5}$	
Formula weight	595.69	
Temperature	123(2) K	
Wavelength	1.54178 Å	
Crystal system	Monoclinic	
Space group	*C*2/c	
Unit cell dimensions	a = 13.8284(3) Å	α = 90°
	b = 16.6575(3) Å	β = 93.3037(8)°
	c = 26.4125(5) Å	γ = 90°
Volume	6073.9(2) Å^3	
Z	8	
Density (calculated)	1.303 Mg/m^3	
Absorption coefficient	0.694 mm^{-1}	
F(000)	2520	
Crystal size	0.40×0.40×0.25 mm^3	
θ range for data collection	4.16° to 66.50°	
Index ranges	$-16 \le h \le 16$, $0 \le k \le 19$, $0 \le l \le 30$	
Reflections collected	20342	
Independent reflections	5430 [R(int) = 0.0176]	
Completeness to θ = 66.50°	97.8 %	
Absorption correction	Empirical	
Max. and min. transmission	0.7528 and 0.6856	
Refinement method	Full-matrix least-squares on F^2	
Data / restraints / parameters	5032/ 4 / 437	
Goodness-of-fit on F^2	1.077	
Final R indices [$I > 2\sigma(I)$]	R_1 = 0.0391, wR_2 = 0.1053	
R indices (all data)	R_1 = 0.0401, wR_2 = 0.1065	
Extinction coefficient	0.00024(6)	
Largest diff. peak and hole	0.291 and −0.210 e / Å^3	

Chapter Three

Benzobisimidazole Cruciform Fluorophores [122]

3.1 Introduction

Cross-conjugated molecular cruciforms have been the subject of much scrutiny in recent years, as their modular optoelectronic properties make them versatile elements in sensing and molecular electronics applications. As mentioned in Chapter One, Nuckolls, Jeffries-EL, and our group have extensively studied molecular cruciforms based on the central benzobisoxazole (BBO) motif, represented by structure (a) (Figure 3.1). We have demonstrated that BBO cruciforms represent a viable fluorescent sensor for a broad variety of analytes and are capable of detecting minute structural differences between those analytes.[93,123a] In a related effort, we have shown (Chapter Two) that cruciforms can be "cut in half" and the oxazole nucleus can be replaced by an imidazole to give L-shaped half-cruciforms of the general structure (b) (Figure 3.1). Bielawski et al. have studied fluorophores based on benzobisimidazolium salts represented by general structure (c) (Figure 3.1).[124]

[122] Le, H. T. M.; El-Hamdi, N. S.; Miljanić, O. Š. *J. Org. Chem.* **2015**, *80*, 5210–5217.

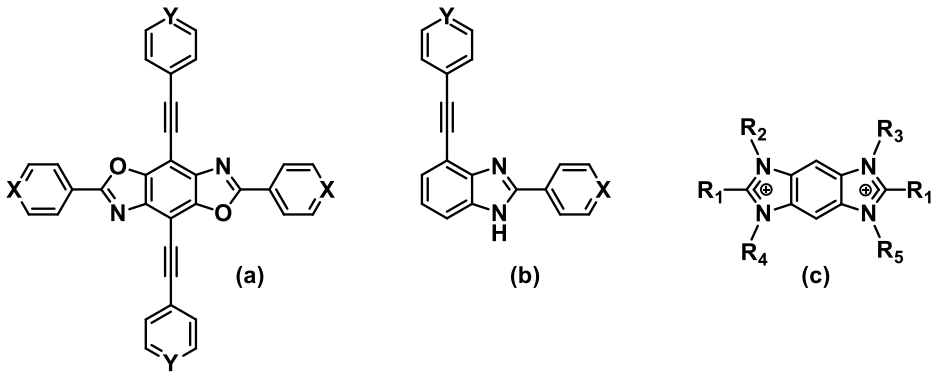

Figure 3.1 Previous examples of fluorophores based on cross-conjugated BBO (a) and benzimidazole (b) geometries and benzobisimidazole (BBI) motif (c).

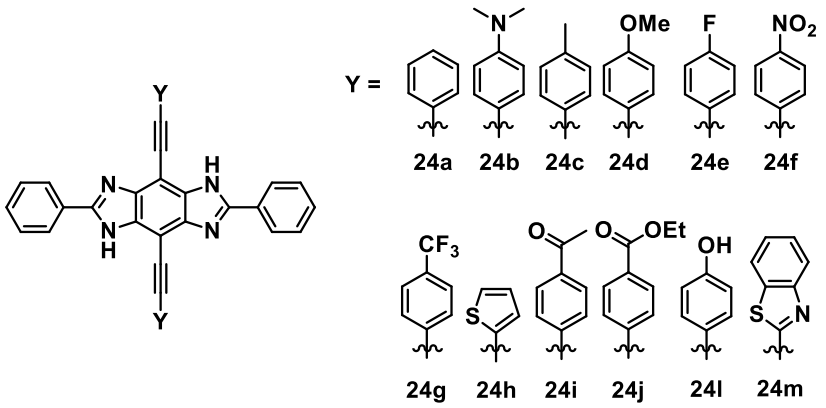

Figure 3.2 BBI cruciforms **24a**–**m**.

In this chapter, we present "the missing link" in this series of fluorophores: the synthesis and characterization of X-shaped BBI-based cruciforms **24a**–**m** (Figure 3.2). These new fluorophores are direct analogues of structure (a) (Figure 3.1) in which the two oxazole nuclei have been replaced with imidazoles. Like their previously reported BBO counterparts, the highest occupied molecular orbibals (HOMOs) of these new fluorophores are localized along the vertical bisethynylbenzene axes, while their lowest

unoccupied molecular orbitals (LUMOs) remain relatively delocalized across the molecule, except in cruciforms substituted with electron-withdrawing groups along the vertical axis. BBI cruciforms exhibit a pronounced response to deprotonation in their UV/Vis absorption and emission spectra, but their response to protonation is significantly attenuated.

While most of the examined cruciforms were highly fluorescent—and useful as sensors,[123] few showed useful colorimetric response. In this chapter, we also report benzothiazole-ornamented BBI cruciform **24m**, which is not just fluorescent, but also brightly colored when observed under visible light. We further show how this compound responds to anions in organic medium and in aqueous solutions observed by the naked eye or under UV excitation.

Dynamic features in molecular recognition of supramolecular chemistry are normally elucidated by the use of diffusion-ordered nuclear magnetic resonance spectroscopy (DOSY)[125] and mass spectrometry[126] employing soft ionization techniques such as electrospray ionization (ESI) and cold spray ionization (CSI). Over the past few decades, within the field of molecular recognition aimed toward molecular sensing, a new technique emerged, utilizing a multicomponent sensor array.[127] The combination of differential synthetic receptors/sensors under varying testing conditions results in differential signal arrays, which can be used in analyte identification using pattern recognition protocols[128] such as principal component analysis (PCA), hierarchical clustering analysis (HCA),[129] linear discriminant analysis (LDA),[130] or the use of artificial neural networks (ANN).[131] Literature reflects successful studies applying

differential sensing arrays.[129,132] Recently, pioneering work by Bunz[50,52] resulted in the development of cruciform-based sensor arrays have also been developed to identify structurally related analytes. The array was constructed from several cruciforms dissolved in solvents of varying polarity, which were then exposed to analyte sets. Emission changes upon analyte binding were recorded by a semi-professional digital camera in a dark room. Representative cut-outs of emission color photographs were then organized into panels which allowed quick naked-eye distinction among analytes. In the case that quantification of response was needed, Red/Green/Blue (RGB) values could be extracted from these photographs using freely downloadable software such as Color Contrast Analyser,[133] and the obtained numerical data can be statistically processed. Using this approach, Bunz and our groups employed 1,4-distyryl-2,5-bis(arylethynyl)benzene and BBI cruciforms, respectively, to distinguish different sets of analyte, such as metal cations, carboxylic acids, and boronic acid.[123b,50 ,134] A hybrid benzobisoxazole–boronic acid sensing ensemble from our group expanded the sensing capability of this cruciform to vicariously detect nucleophilic analytes—amines and ureas.[93,123] The anion identification in this chapter was also carried following this established protocol.

3.2 Results and Discussion

3.2.1 Synthesis of Benzobisimidazole Cruciforms

Despite the structural similarity between BBO and BBI cruciforms, their respective synthesis approach were quite different. BBO cruciforms could be easily elaborated from the readily available 2,5-diamino-3,6-dibromobenzene-1,4-diol,[135] whose

o-aminophenol functionalities engaged in acyl condensation to generate the horizontal axis, while the two bromine substituents reacted via Sonogashira coupling to establish the vertical axis. As the corresponding 1,2,4,5-tetraamino-3,6-dibromobenzene[136] proved difficult to prepare and handle, we chose to begin the synthesis of BBI cruciforms with a hydrochloride salt of 1,2,4,5-tetraaminobenzene[137] (**25**, Scheme 3.1). Its condensation with benzoic acid in the presence of polyphosphoric acid (PPA) yielded intermediate **26**,[88] which was then doubly brominated on the central benzene ring with *N*-bromosuccinimide (NBS) to produce compound **27**. The vertical axis was established by the subsequent Sonogashira coupling with a terminal alkyne bearing functionalities of interest, yielding cruciforms **24a** and **24b** (route A, highlighted in dark red in Scheme 3.1). In an alternative and more general approach (route B, highlighted in blue), the roles of coupling partners were switched: compound **27** was first reacted with triisopropylsilyl acetylene (TIPSA), then desilylated to reveal two terminal alkyne functionalities in precursor **28**. Compound **28** was subsequently functionalized through a second Sonogashira coupling to produce cruciforms **24c**−**m**. Cruciform **24l** was obtained after acidic hydrolysis of the tetrahydropyranyl (THP) protecting group in **24k**.

It should be noted that this synthetic route was plagued with difficulties. First, compound **25** was very difficult to handle on account of its sensitivity to oxidation and high polarity. Second, analogues of the highly insoluble intermediate **26** bearing other functional groups along the horizontal axis proved difficult to prepare and impossible to purify, and their subsequent bromination yielded mixtures of products. Thus, we were not able to effectively vary the substitution along the horizontal axis of these cruciforms.

Finally, the closing Sonogashira couplings proceeded in moderate yields (27−60%), which was likely a consequence of the low solubility of the precursors.

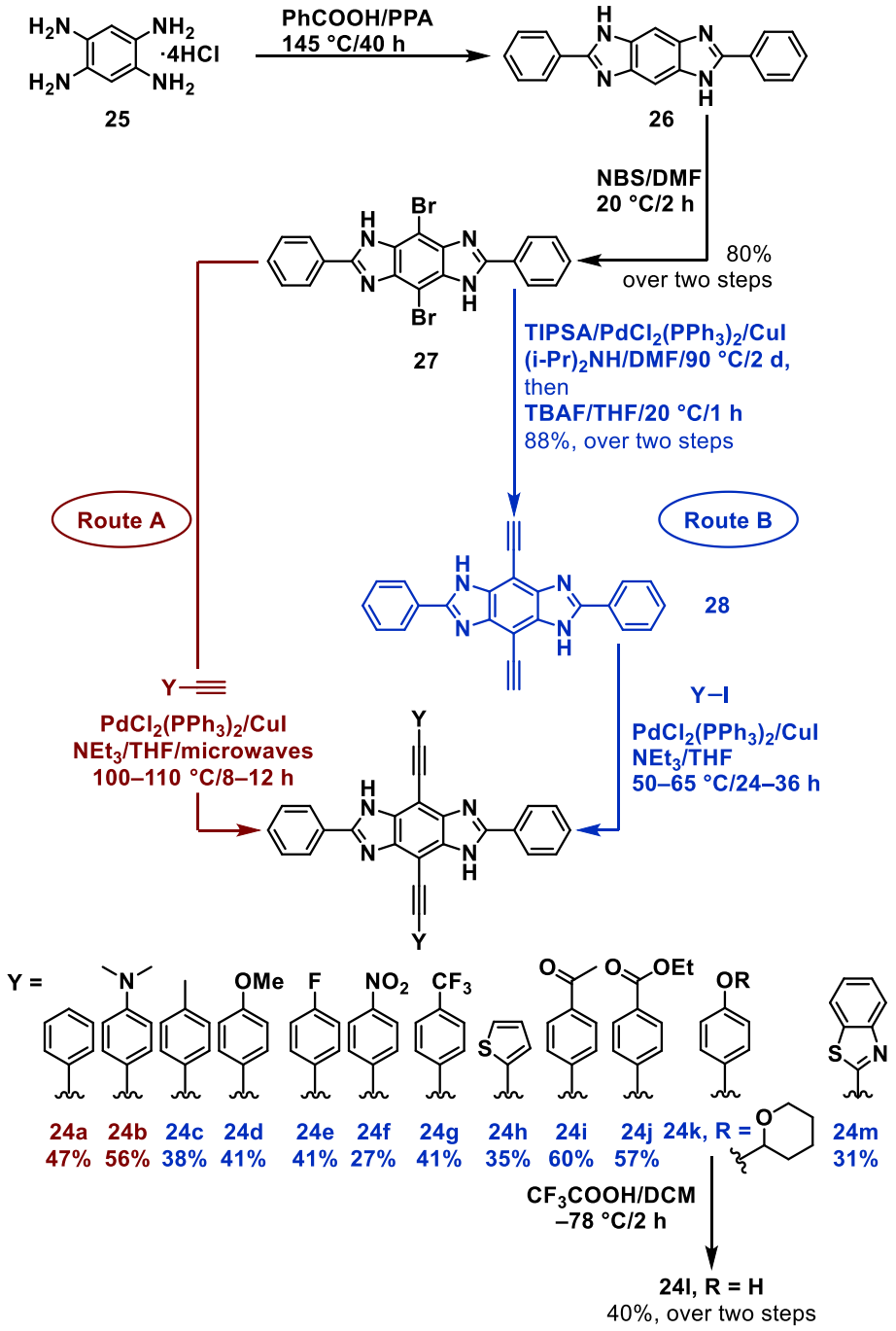

Scheme 3.1 Synthesis of BBI cruciforms **24a**–**m**.

3.2.2 Computational Studies

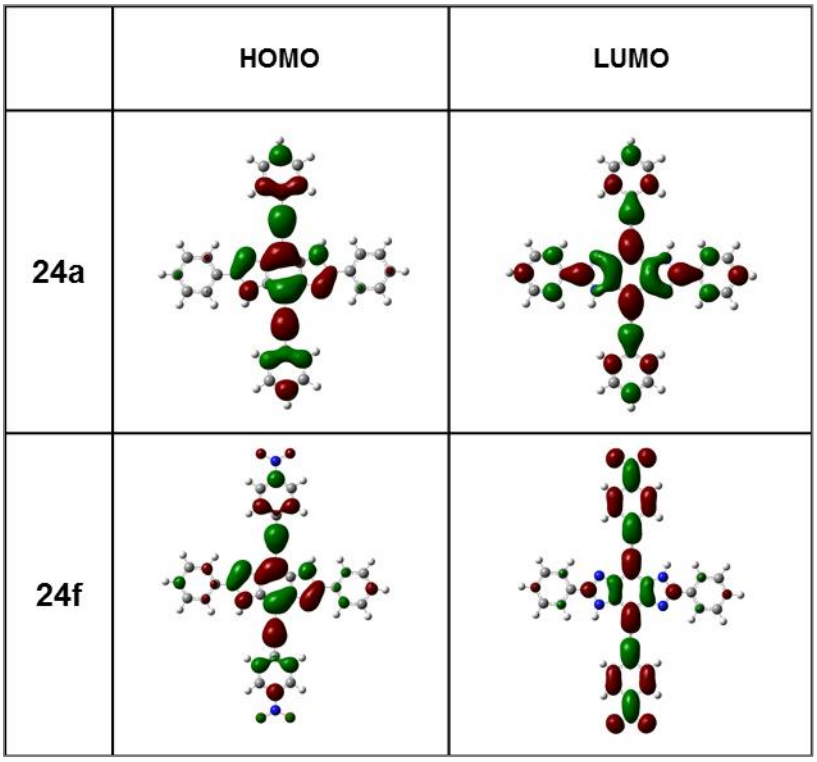

Figure 3.3 HOMOs and LUMOs of cruciforms **24a** and **24f** (calculated with Gaussian using B3LYP hybrid density functional and 3-21G basis set).

Frontier molecular orbitals (FMOs) of cruciform **24a**−**m** have been calculated using Gaussian 09W[108] software, and the B3LYP hybrid density functional and 3-21G as the basis set. FMOs of two exemplary cruciforms **24a** and **24f** are shown in Figure 3.3. In both systems, the HOMO resides dominantly along the vertical axis. As observed previously for the related BBO-based cruciforms,[88] this vertical localization of the HOMOs is a consequence of orbital properties of the BBI core and is largely independent of the substitution. The LUMO of **24a** is, in contrast, delocalized across the molecule. In the case of a cruciform substituted with electron-withdrawing groups along the vertical

axis, such as **24f** (Figure 3.3, bottom), the LUMO also resides along the electron-poor vertical axis of the molecule. As synthetic access to cruciform variants with different substitution on the horizontal axis was restricted, we were unable to probe the effects of placing strongly electron-withdrawing or electron-donating groups along the horizontal axis. HOMOs and LUMOs of other cruciforms will be presented in experimental section.

3.2.3 Optical Properties

Compounds **24a**−**m** are yellow to red powders with moderate solubility in most common organic solvents. Their ^{1}H NMR spectra are complicated by facile tautomerization of both imidazoles but are otherwise consistent with their structures. They are highly fluorescent[138] in solution and mildly in the solid state when irradiated with a hand-held UV lamp (λ_{exc} = 365 nm). UV/Vis absorption and fluorescence emission spectra of **24a**−**m** are shown in Figure 3.4 and summarized in Table 3.1. UV/Vis absorption spectra (Figure 3.4, top) of all cruciforms are essentially superimposable with a single broad absorption band centered between 380 and 395 nm. The only exception is **24b**, whose absorption spectrum shows an additional band at 425 nm and **24m** with λ_{max} of absorption at 420 nm. In their fluorescence emission spectra (Figure 3.4, bottom), a somewhat greater level of distinction can be noticed. Compound **24b** is a clear outlier, with a relatively featureless emission band at 487 nm. All other cruciforms' emission spectra show two distinct maxima: a more intense one, centered between 428 (for **24e**) and 470 (for **24m**) nm, and a lower intensity band, centered between 452 (for **24e**) and 500 (for **24m**) nm. Most of these trends are visible by the naked eye (Figure 3.5) in that colors of all cruciforms except **24b** look similar under both UV and visible light.

Table 3.1 Optical Properties and Calculated HOMO−LUMO Gaps for Cruciforms **24a−m**.

compound	absorption λ_{max} (nm)	emission λ_{max} (nm)	Stokes shift (cm^{-1})	calcd HOMO-LUMO gap (eV, nm)
24a	386	430	2651	3.02, 411
24b	386	487	5373	3.00, 414
24c	386	432	2759	2.99, 415
24d	385	438	3143	2.91, 426
24e	383	428	2745	3.01, 412
24f	388	451	3600	2.61, 475
24g	392	438	2679	2.99, 415
24h	391	443	3002	2.83, 438
24i	382	458	4344	2.86, 434
24j	395	451	3144	2.90, 428
24l	383	439	3330	2.93, 423
24m	420	470	2533	2.73, 454

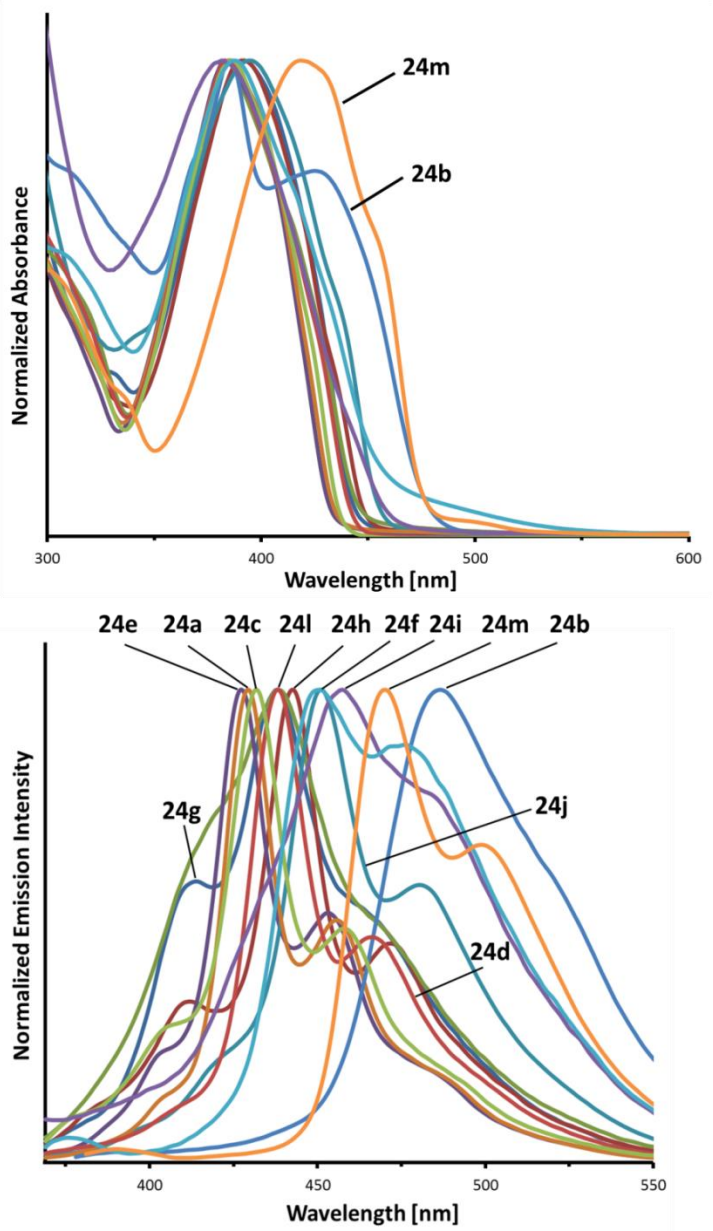

Figure 3.4 Normalized UV/Vis absorption (top) and emission (bottom) spectra of cruciforms **24a**−**m** in THF. Excitation wavelengths for emission spectra: 335 (**24a**), 348 (**24b**), 336 (**24c**), 337 (**24d**), 333 (**24e**), 339 (**24f**−**24h**), 330 (**24i**−**24j**), 337 (**24l**), 351 (**24m**) nm.

3.2.4 Optical Response to Acids and Bases

In contrast to BBO-based cruciforms, these new BBI-based systems are amphoteric and were expected to show significant changes in their UV/Vis absorptions and emissions upon both protonation and deprotonation. To experimentally confirm this hypothesis, we performed titrations of **24a**−**m** with both an acid (trifluoroacetic acid, TFA) and a base (tetrabutylammonium hydroxide, TBAOH) in THF. Full experimental details of these titrations are given in the experimental section. In general, BBI cruciforms show a rather moderate response to acids: with excess acid (−log[TFA] < 1.0), a blue shift in absorption of up to $\Delta\lambda = -18$ nm was observed. This set of observations could be rationalized by protonation of BBI nitrogen atoms (pK_a = 5.55 for benzimidazolium cation)[109] at high acid concentration. The only cruciform with a different response was **24b** (Figure 3.5, left), whose significantly more basic $-NMe_2$ groups became protonated at lower concentrations of TFA. In the emission spectra of **24a**−**m** small but less consistent changes were observed: for some cruciforms, emission shifted minimally toward the red region, while for others it shifted toward the blue or was quenched.

Response of BBI cruciforms to bases is much more dramatic. Upon exposure to high concentrations of base (−log[TBAOH] < 2.5), red shifts in absorption of approximately $\Delta\lambda$ = 100 nm occurred for all studied cruciforms and were accompanied by equally significant shifts in the emission (as illustrated for **24a** in Figure 3.5, right); for more acidic **24f**, even lower concentrations of base induced similar shifts. As noticed

previously in L-shaped half-cruciforms,[139] deprotonation of BBI's N−H moieties (pK_a = 12.78)[109] causes these dramatic changes in fluorescence.

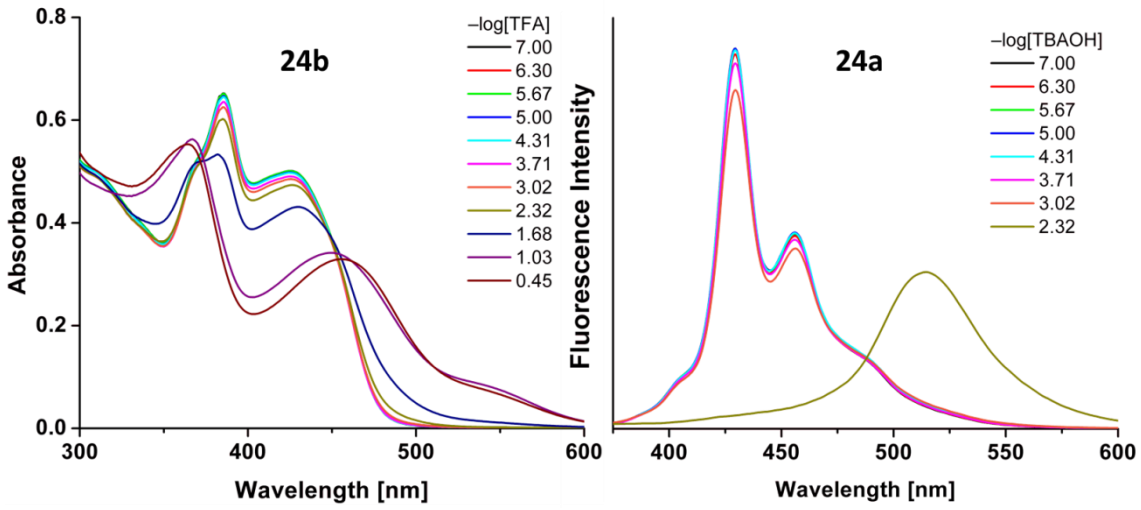

Figure 3.5 Exemplary titrations of BBI cruciforms with acid and base. Spectra on the left plot changes in UV/Vis absorption spectra of cruciform **24b** as a function of added TFA. Spectra on the right plot fluorescence response of cruciform **24a** to the addition of TBAOH (λ_{exc} = 335 nm). Both titrations were performed in THF.

Especially, titration of **24m** with TBAOH resulted in stepwise change in UV/Vis absorption (Figure 3.6, left), and a profound change in fluorescence emission (Figure 3.6, right) spectra. This behavior is ascribed to the two consecutive deprotonations of the BBI. As TBAOH is added to the solution of **24m**, a new absorption band centered at 504 nm appears, and a clear isosbestic point is observed at 459 nm. With further increases in the concentration of TBAOH, another red shift band appears with λ_{max} at 589 nm, but an isosbestic point is not observable here; this fact we interpret as a consequence of two

simultaneous deprotonations of **24m** (i.e. the first deprotonation is not completed before the second one starts).

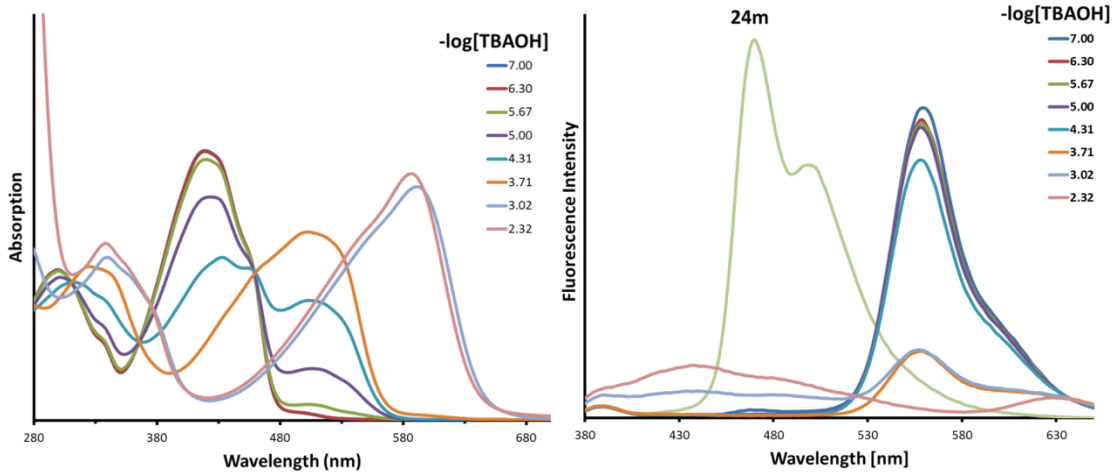

Figure 3.6 UV/Vis absorption (left) and fluorescence emission (right) titrations of THF solutions of cruciform **24m** with TBAOH.

Most of these changes were detectable by the naked eye as well. Digital photographs of vials containing 10^{-5} M solutions of **24a**–**m** under visible and UV light are shown in Figure 3.7, and the dramatic response of these cruciforms to a base is apparent.

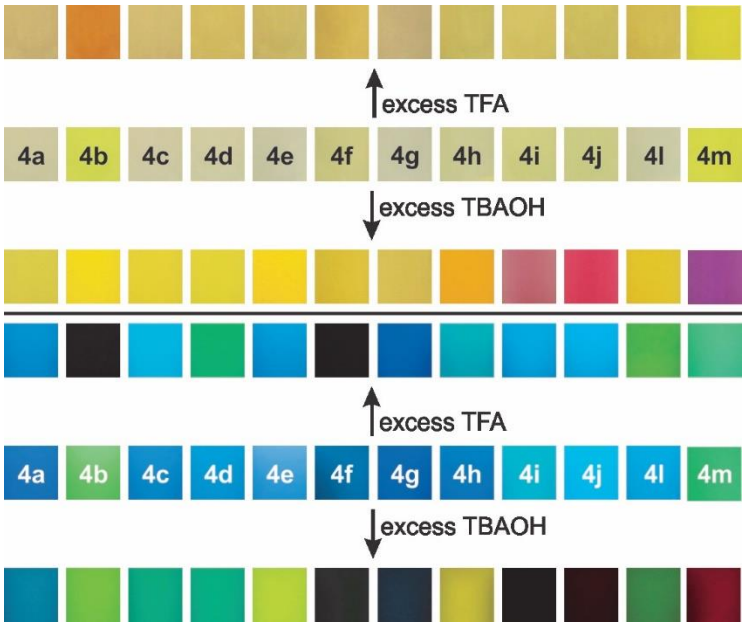

Figure 3.7 Acid- and base-induced changes in the colors of 10^{-5} M solutions of cruciforms **24a**–**m** in THF, as observed under visible (top) and UV (bottom) light. For emission color photographs, λ_{exc} = 365 nm, shutter speed 0.05 s.

3.2.5 Optical Response of Cruciform 24m toward Anions

We tested the response of cruciform **24m** to various anions in THF and DMSO. Anions were added *in excess* as their tetrabutylammonium salts, and photographs of each solutions' colors under visible and UV/Vis light are shown in Figure 3.8, left. Several trends were observed: weakly basic Cl^-, Br^-, ClO_4^- and NO_3^- resulted in negligible changes in both color and emission of **24m**'s solution in THF; in DMSO, these anions did not change the solution's color, but they did influence the emission, which shifted from green to yellow-orange. More basic anions such as F^-, AcO^-, CN^-, and $H_2PO_4^-$ produced marked changes in both the color and fluorescence emission in both solvents. Iodide caused no changes in DMSO; in THF, it darkened the color and caused emission

quenching. Finally, N_3^- showed a pretty minor change in colors under visible light, but more significant shifts in emission colors in both solvents.

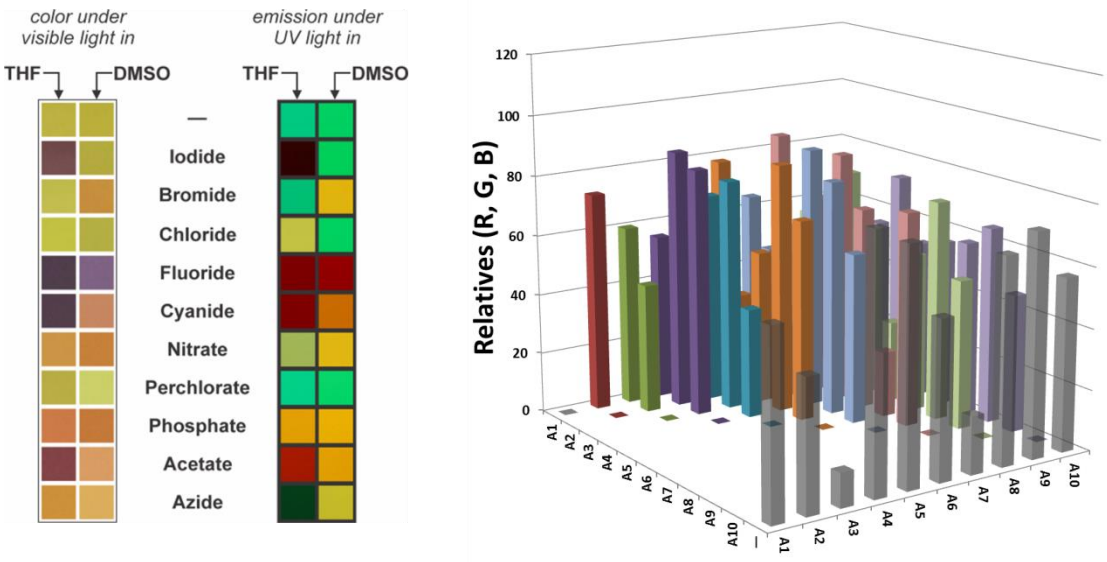

Figure 3.8 Left: response of 10^{-5} M solutions of cruciform **24m** to anions added as their tetrabutylammonium salts. Excitation wavelength for fluorescence photos 365 nm; shutter time: 1/10 s for fluorescence photos, 1/80 s for photos in visible light. Right: the correlation diagram shows standard deviations of RGB values for A1–A10 (corresponding to iodide–azide) (summed over 4 conditions: 2 solvents exposed to either visible light or UV light), relative to all other analytes. The semi-transparent bars in the row marked with ‘‘—’’ indicate standard deviations relative to the blank solution of **24m**, summed over all 4 conditions.

However, rapid recognition of ten anionic analytes was still accomplished utilizing digital photography method developed by Bunz, in which the relative standard deviation of extracted RGB values’ set of any two analytes was used for confirmation

(Figure 3.8, right; and see Experimental Section for more details). Overall, qualitative distinction among 10 analytes could be obtained exclusively by two solvents in UV excitation and, for the first time, visible light excitation.

^{1}H NMR titrations of **24m** in DMSO-d_6 were also carried on to investigate the optical response process. In the case of F^- (Figure 3.9), the addition of 1 equiv of F^- induced BBI NH signal to vanish, demonstrating strong interaction from hydrogen bonding between them. Furthermore, the addition of 5 equiv of F^-, the new triplet signal appeared at 16.1 ppm,[140] which was attributed to H_2F^- and confirmed the deprotonation of BBI NH by excessive amount of F^-. With the increasing amount of TBAF, the peaks at 7.6 ppm became more deconvoluted.

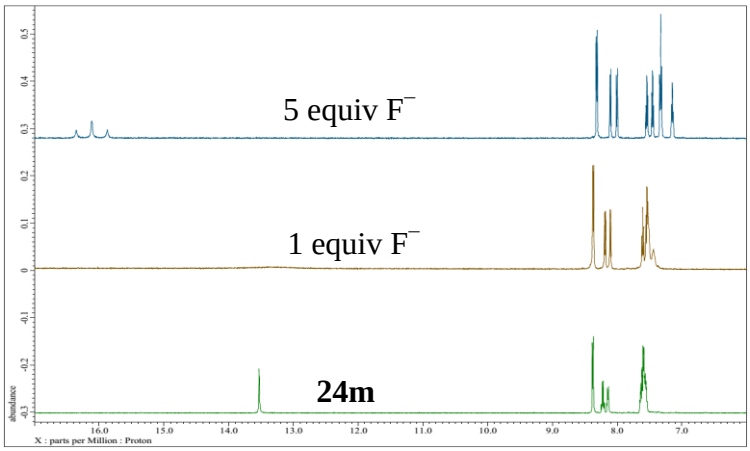

Figure 3.9 ^{1}H NMR spectra in titration experiment of **24m** with TBAF in DMSO-d_6.

Similarly, in the case of CN^-, the NH vanished after adding 0.5 equiv of CN^-, with deconvolution of the peaks at 7.6 ppm, but no new signal appeared (Figure 3.10, left). The mechanism of color change due to the addition of tetrabutylammonium cyanide

(TBACN) into **24m** fluorophore/THF solution was confirmed by neutralization (Figure 3.10, right). The addition of cyanide to the sensor solution changed the color of the solution from bright yellow to magenta, while further addition of TFA to that mixture returned the solution back to the original color. Cyanide, as a base, can deprotonate or form hydrogen bonding with BBI NHs. Afterward, the addition of TFA neutralizes cyanide and releases the BBI.

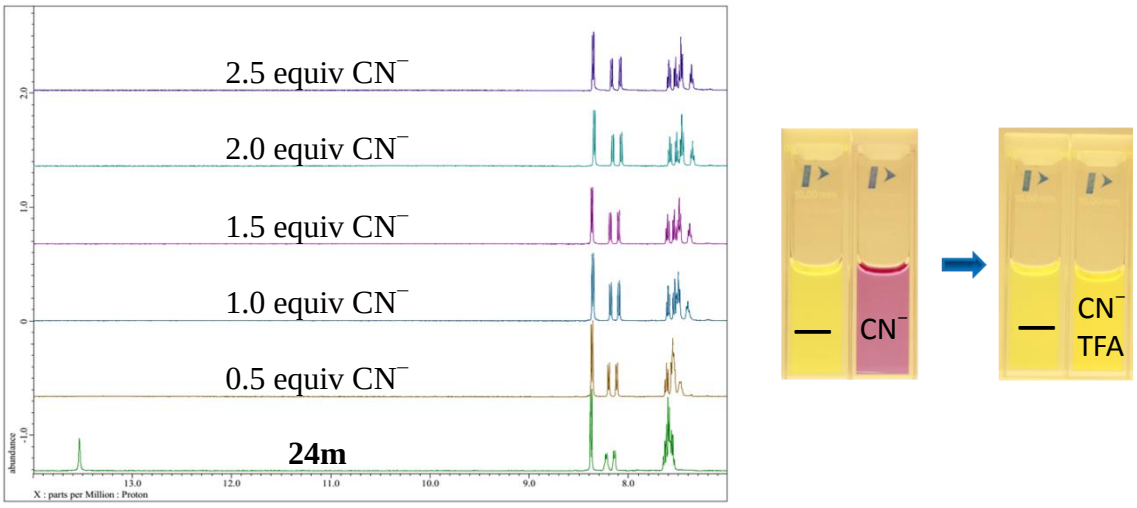

Figure 3.10 Left: ^{1}H NMR spectra in titration experiment of **24m** with TBACN in DMSO-d_6. Right: color change of **24m** by initial addition of TBACN followed by addition of TFA, cuvette marked with ‘‘—’’ is **24m** in THF.

Our final set of experiments targeted detection of anions in aqueous solutions. As cruciform **24m** is not soluble in pure H_2O, it was dissolved in 4:1 mixtures of THF, DMF and DMSO with H_2O. Similar anion response tests to those described above for purely organic solvents were performed, with the difference that in this case anions *in excess*

amounts were used as the Na^+ salt form. Optical response of solutions of cruciform **24m** to anions in aqueous solution is summarized in Figure 3.11.

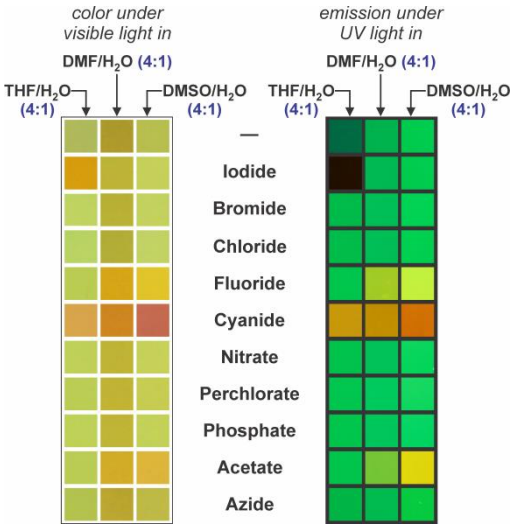

Figure 3.11 Response of 10^{-5} M solutions of cruciform **24m** to anions added as their Na^+ salts in aqueous solvents. Excitation wavelength for fluorescence photos 365 nm. Shutter time: 1/10 s for fluorescence photos, 1/80 s for photos in visible light.

Cruciform **24m** essentially does not respond to Br^-, Cl^-, NO_3^-, ClO_4^-, $H_2PO_4^-$, or N_3^- in any of the examined solvents. With I^-, a change is noticeable in THF/H_2O mixture, where its addition causes quenching of the fluorescence. More basic F^- and AcO^- ions cause slight shift in color and fluorescence toward orange in all solvents but THF/H_2O. However, with CN^-, pronounced shifts in both color and fluorescence are observed in all solvents, allowing its unambiguous identification through simple observation of color (in e.g. DMSO/H_2O mixture) and/or fluorescence (in e.g. THF/H_2O solution).

Why are we able to distinguish CN^- from F^- and AcO^- in aqueous solution, but not in organic solvents? Acidities of HCN, HF, and HOAc in DMSO are comparable

(pK_a values of 12.9,[141] 15.0[141] and 12.6,[142] respectively), but in H_2O they are very different. HCN is the weakest acid with pK_a of 9.40,[143] and both HF (pK_a = 3.17) and HOAc (pK_a = 4.76)[144] are more than 20,000 times more acidic. Conversely, CN^- is the strongest base in an aqueous solution, and **24m** is a weak enough acid not to be deprotonated by F^- and OAc^-, but only by CN^-. We confirmed that the mechanism of CN^- detection is a simple deprotonation, by treating the solutions containing **24m** and excess CN^- with TFA; upon neutralization, colors and emission returned to that of pure **24m**. On the other hand, specificity for CN^- was confirmed by an UV/Vis experimentation in which 10^{-5} M solution of **24m** in DMSO/H_2O (4:1) was treated with a 50-fold excess of Na^+ salts of the corresponding anions (Figure 3.12), whereonly CN^- caused a noticeable shift (red curve). Furthermore, UV/Vis titration of **24m** with CN^- exhibits λ_{max} shift starting with 10 equiv of CN^- (Figure 3.12, right).

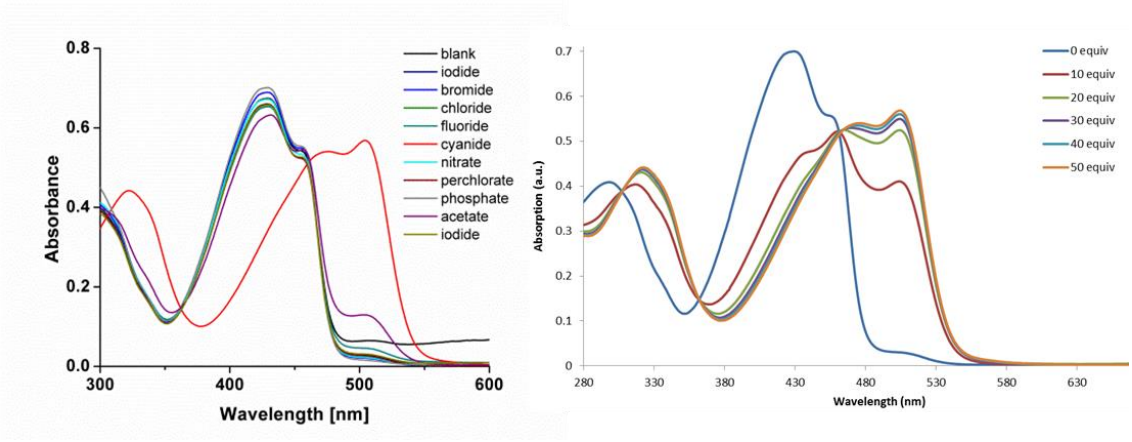

Figure 3.12 Response of UV/Vis absorption of a 10^{-5} M solution of cruciform **24m** in DMSO/H_2O (4:1) to an addition of: left—a 50-fold excess of various anions added as their sodium salts; right—incremental amount of TBACN.

3.3 Conclusion and Outlook

In summary, we have synthesized a series of twelve cross-conjugated cruciform fluorophores based on the BBI nucleus using a combination of acid-catalyzed condensation and Sonogashira coupling. These materials are fluorescent in the solid state and strongly so in dilute solutions. All of them also show a pronounced red shift upon deprotonation of their imidazole N−H functionalities, while in contrast, their response to acids is much more attenuated. This lack of response is partially a consequence of our inability to synthetically access diverse substitution patterns on the horizontal axis, which in turn meant that we could modulate the LUMO orbitals of **24a**−**m,** only to a limited extent. Thus, unlike in the BBO series,[88,123] systems with completely spatially separated FMOs could not be produced and studied. At the same time, it is highly encouraging that almost all of the BBI cruciforms maintain a certain level of fluorescence regardless of their protonation state. This feature could be explored in the preparation of, e.g., fluorescent and guest-responsive porous materials, such as zeolitic imidazolate frameworks (ZIFs),[117] utilizing these cross-conjugated BBIs.

We also have prepared and characterized the optical properties of a BBI-based cruciform **24m** which shows pronounced colorimetric response to anions.

3.4 Experimental Section

3.4.1 General Experimental Methods

All reactions were performed under nitrogen atmosphere in oven-dried glassware. Reagents were purchased from commercial suppliers and used without further purification. Solvents were used as received, except THF and *N*,*N*-dimethylformamide (DMF), which were degassed by a 30 min nitrogen purge prior to use in Sonogashira couplings. Compounds 1,5-dichloro-2,4-dinitrobenzene[145] and 1,3-diamino-4,6-dinitrobenzene[146] were synthesized according to literature procedures. Triethylamine (Et_3N) was degassed by a 30 min nitrogen purge prior to use. Microwave-assisted reactions were performed in a Biotage Initiator 2.0 microwave reactor, producing monochromatic microwave radiation with the frequency of 2.45 GHz. NMR spectra were obtained on spectrometers with working frequencies (for ^1H nuclei) of 400, 500, and 600 MHz. All ^{13}C NMR spectra were recorded with simultaneous decoupling of ^1H nuclei. ^1H NMR chemical shifts are reported in ppm units relative to the residual signal of the solvent ($CDCl_3$: 7.25 ppm, $(CD_3)_2SO$: 2.48 ppm, D_2O: 4.79 ppm, $(CD_3)_2CO$: 2. 05 ppm). All NMR spectra were recorded at 25 °C for samples in $CDCl_3$, D_2O, and $(CD_3)_2CO$, while samples in DMSO-d_6 were recorded at temperatures ranging from 25 to 90 °C. Mass spectra of compound **27** and 2,6-diphenyl-4,8-bis((triisopropylsilyl)ethynyl-1,5-dihydrobenzo[1,2-*d*:4,5-*d′*]diimidazole were obtained using magnetic sector CI mass analyzer, while cruciforms **24a**−**l,m** were analyzed using a QT of mass analyzer. Melting point measurements were performed in open capillary tubes, and the reported values are uncorrected. Column chromatography was carried out on silica gel 60, 32−63 mesh, and

basic aluminum oxide Act. 1, 50−200 μm. Analytical TLC was performed on plastic-backed silica gel IB-F plates and aluminum oxide IB-F plates.

3.4.2 Synthesis of Benzobisimidazole Cruciforms

Synthesis of 1,2,4,5-Benzenetetramine Tetrahydrochloride **25**[147]

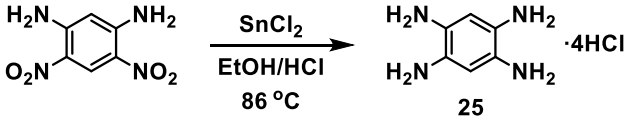

25

A 1 L Schlenk flask was flushed with nitrogen and charged with 1,3-diamino-4,6-dinitrobenzene[146] (6.00 g, 30.3 mmol), concentrated HCl (311 mL), and EtOH (155 mL). The reaction flask was attached to the condenser and heated at 50 °C with stirring for 10 min. After 10 min, a solution of anhydrous $SnCl_2$ (52.0 g, 274 mmol) in EtOH (80 mL) was added to the reaction mixture. The beaker containing the $SnCl_2$ solution was washed with an additional portion of EtOH (40 mL) and the washings were added to the reaction flask. The reaction was heated at 86 °C for 2 d, to ensure the reaction went to completion. The reaction resulted in a white precipitate forming in the flask. After cooling, the solution was filtered and the residue was washed with EtOH to give the product as a light pink solid (8.1 g). The crude product was used without further purification.

25: IR (neat): 2923 (s, $\tilde{\nu}_{N+-H}$), 2495 (s), 1601 (m, $\tilde{\nu}_{C-C}$), 1556 (s), 1511(s, $\tilde{\nu}_{N+-H}$), 1221 (s, $\tilde{\nu}_{C-N}$), 1127 (m), 1054 (w), 860 (m, $\tilde{\nu}_{C-H}$) cm^{-1}. ^1H NMR (D_2O, 400 MHz): δ 6.77 (s) ppm. ^{13}C NMR (D_2O, 100 MHz): δ 125.1, 113.5 ppm.

Synthesis of 2,6-Diphenyl-1,5-dihydrobenzo[1,2-*d*:4,5-*d'*]diimidazole **26**[88]

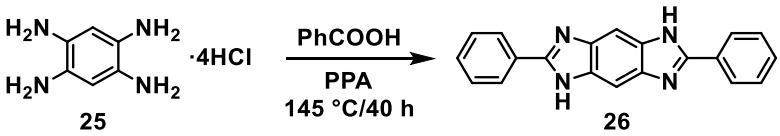

In a 500 mL round bottom flask equipped with a condenser, a mixture of **25** (10.3 g, 36.3 mmol), benzoic acid (17.7 g, 145 mmol), and polyphosphoric acid (PPA, 70 g) was heated up to 140 °C. The reaction temperature was slowly increased to 145 °C and maintained at that temperature for 40 h. After the reaction was finished, the mixture was allowed to cool down, and was then poured into ice water. Stirring was continued while the mixture was made very basic by the addition of NaOH pellets (pH=14). The precipitate was filtered, washed with H_2O, and dried in air overnight. The solid was further dried in a rotary evaporator whose bath was heated for 2 h at 80 °C, finally giving crude **26** (11.25 g). Because of its low solubility, this material was used for the next step without further purification.

Synthesis of 4,8-Dibromo-2,6-diphenyl-1,5-dihydrobenzo[1,2-*d*:4,5-*d'*]diimidazole **27**

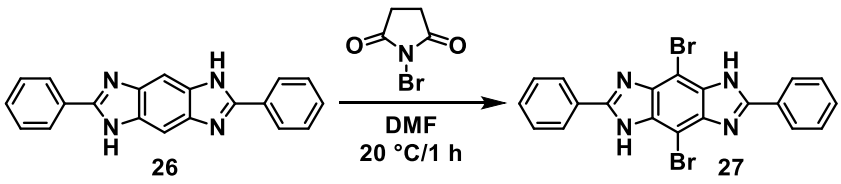

A 250 mL round bottom flask was charged with DMF (165 mL) and the solvent was stirred vigorously while the ground powder of compound **26** (10.8 g, 34.7 mmol) was added to it. *N*-Bromosuccinimide (NBS, 12.3 g, 69.3 mmol) was added next, and the reaction mixture was stirred at 20 °C for 1 h. The formed precipitate was filtered under

reduced pressure, washed with EtOH, and dried in air to obtain 13 g of a white powder, which was the identified as the target compound **27** (mp >350 ^{o}C). The overall yield for the synthesis of compound **27** from compound **25** in 2 steps is 80%.

27: IR (neat): 3160 (w, $\tilde{\nu}_{N-H}$), 1560 (m, $\tilde{\nu}_{C=N}$), 1480 (s), 1460 (s), 1330 (m, $\tilde{\nu}_{C-N}$), 1280 (s), 1230 (s), 867 (s), 772 (m), 725 (s), 685 (s, $\tilde{\nu}_{C-Br}$) cm^{-1}. ^{1}H NMR (DMSO-d_6, 400 MHz): δ 13.01 (s, 2H), 8.32 (m, 4H), 7.53 (m, 6H) ppm. ^{13}C NMR (DMSO-d_6, 100 MHz): δ 153.6, 153.3, 140.4, 139.9, 133.1, 132.6, 130.9, 130.0, 129.3, 127.9, 90.9 ppm. HRMS (CI/[M]$^{+}$): calcd for $C_{20}H_{12}Br_2N_4^{+}$: 465.9429, found: 465.9435.

Synthesis of 2,6-Diphenyl-4,8-bis((triisopropylsilyl) ethynyl-1,5-dihydrobenzo[1,2-*d*:4,5-*d'*]diimidazole

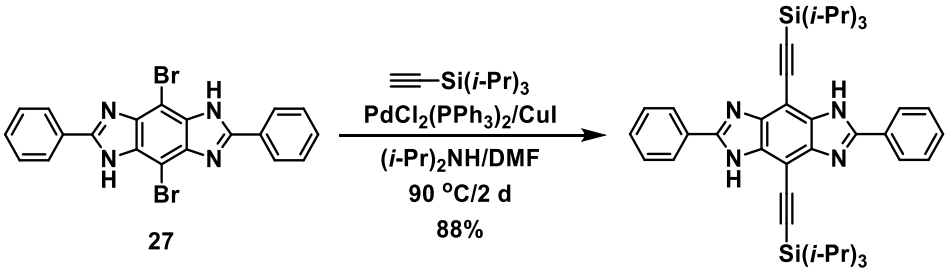

A 500 mL pear-shaped Schlenk flask was charged with compound **27** (13.0 g, 27.8 mmol), $PdCl_2(PPh_3)_2$ (1.95 g, 2.77 mmol), and CuI (1.06 g, 5.56 mmol). The flask was sealed, then evacuated and backfilled with N_2 three times. In a separate flask, a mixture of (*i*-Pr)$_2$NH (200 mL), DMF (100 mL), and TIPSA (25 mL, 111 mmol) was degassed for 20 min and then slowly transferred, under positive N_2 pressure, via cannula to the reaction flask. The reaction mixture was stirred and heated at 90 °C for 2 d and then cooled to 20 °C. Afterwards, silica gel (150 mL) was added to the reaction mixture,

and the solvent was removed under reduced pressure until a brown powder was formed. This powder was subjected to column chromatography on silica gel, using a mixture of CH_2Cl_2 and hexane as an eluent (starting with a 1:1 volume ratio, and proceeding until 7:3 ratio). The solvent was removed *in vacuo* to give a yellow crude product which was further purified by recrystallization from EtOH (150 mL), finally giving the desired product as a bright yellow powder (16.4 g, mp 310 ^{o}C).

IR (neat): 3460 (s, $\tilde{\nu}_{N–H}$), 2940 (s, $\tilde{\nu}_{C–H}$), 2860 (s), 2140 (m, $\tilde{\nu}_{C\equiv C}$), 1480 (m, $\tilde{\nu}_{Si–C}$), 1450 (s), 1330 (s, $\tilde{\nu}_{Si–C}$), 997 (w), 883 (w), 775 (w), 740 (s), 668 (s) cm^{-1}. ^{1}H NMR ($CDCl_3$, 500 MHz): δ 9.43 (s, 2H), 8.08 (d, $^{3}J_{H–H}$ = 6.9 Hz, 4H), 7.52 (m, 6H), 1.27 (m, 42H) ppm. ^{13}C NMR ($CDCl_3$, 125 MHz): δ 152.3, 151.8, 142.7, 141.9, 134.4, 133.7, 130.5, 130.3, 129.6, 129.2, 129.1, 126.7, 102.2, 99.8, 97.1, 19.0, 18.9, 11.7, 11.5, 11.3 ppm. HRMS (CI/$[M]^{+}$): calcd for $C_{42}H_{54}N_4Si_2^{+}$: 670.3887, found: 670.3871.

Synthesis of 4,8-Diethynyl-2,6-diphenyl-1,5-dihydrobenzo[1,2-*d*:4,5-*d'*]diimidazole **28**

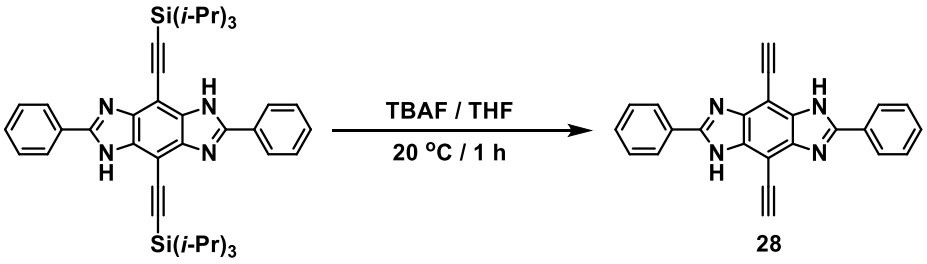

In a nitrogen-flushed 100 mL flask, tris(isopropyl)silyl-substituted alkyne produced in the previous step (2.00 g, 2.98 mmol) was dissolved in THF (20 mL), and treated with 1M solution of TBAF in THF (6.56 mL, 6.56 mmol). The resulting solution was stirred at 20 °C for 1 h, and a yellow precipitate was formed. The precipitate was

collected by filtration and washed with THF. The residue was mixed with H_2O (150 mL) and sonicated for 10 min to give fraction A. Meanwhile, the solvent in the filtrate was removed under reduced pressure. The remaining solid was mixed with EtOH (10 mL), followed by H_2O (40 mL), to give fraction B. Subsequently, fraction A was combined with fraction B. The mixture was sonicated for 10 min, filtered, washed with H_2O, and dried *in vacuo* to yield 1.06 g of crude **28** as a dark yellow powder, which was used in the next step without purification.

28: ^{1}H NMR (DMSO-d_6, 500 MHz): δ 13.03 (s, 2H), 8.32 (d, J=6.9 Hz, 4H), 7.52 (m, 6H), 4.88 (m, 2H) ppm. ^{13}C NMR (DMSO-d_6, 125 MHz): δ 153.5, 153.2, 143.0, 142.7, 134.8, 134.5, 130.6, 130.3, 129.3, 127.8, 95.8, 91.4, 90.6, 90.0, 78.3 ppm.

Synthesis of Cruciform **24a**

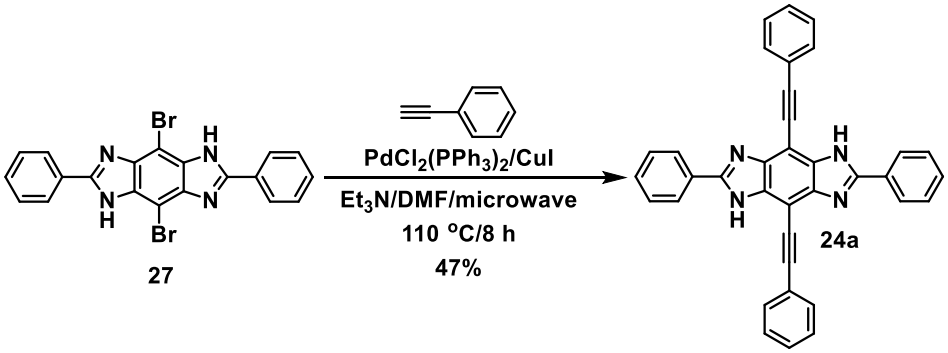

Phenylacetylene (781 mg, 7.65 mmol) was added to a thick-walled microwave pressure vial that contained a mixture of compound **27** (300 mg, 0.64 mmol), $PdCl_2(PPh_3)_2$ (90 mg, 0.13 mmol), CuI (45 mg, 0.24 mmol), Et_3N (5 mL), and DMF (5 mL). The vial was sealed under nitrogen and exposed to microwave irradiation for 12 h at 110 °C. After cooling, the reaction mixture was extracted with EtOAc, washed with

brine, and dried over anhydrous $MgSO_4$. Afterward, Al_2O_3 (80 g) was added to the combined organic layer and the solvent was removed under reduced pressure until a brown powder formed, which was purified by gradient elution column chromatography on alumina (300 g) using EtOAc and hexane as eluents (starting volume ratio 3:17, ending volume ratio 9:11). The solvent was removed *in vacuo* to yield the crude product which was further purified by recrystallization from THF to give **24a** as a yellow powder (153 mg, 47%, mp 309 °C with decomposition).

24a: UV/Vis (THF): λ_{max} (log ε) 386 (4.90) nm. IR (neat): 3056 (w, $\tilde{\nu}_{N–H}$), 2160 (w, $\tilde{\nu}_{C\equiv C}$), 1958 (w), 1596 (m, $\tilde{\nu}_{C=N}$), 1557 (w), 1526 (w), 1476 (s), 1454 (s), 1441 (w), 1402 (m), 1342 (s), 1280 (m), 1215 (w), 1177 (w), 1156 (w), 1115 (w), 1069 (m), 1028 (m), 999 (w), 943 (m), 913 (w), 775 (m), 752 (s), 728 (m), 686 (s), 624 (s), 565 (w) cm^{-1}. ^1H NMR (DMSO-d_6, 600 MHz): δ 12.96 (s, 2H), 8.34 (d, $^3J_{H–H}$ = 7.6 Hz, 4H), 7.78 (m, 4H), 7.56 (t, $^3J_{H–H}$ = 7.6 Hz, 4H), 7.51 (m, 8H) ppm. ^{13}C NMR (DMSO-d_6, 150 MHz, 40 °C): δ 153.5, 142.6, 134.0, 130.5, 129.3, 127.9, 123.7, 103.7, 98.7, 96.6, 89.9, 86.4, 84.6, 82.9 ppm. HRMS (ESI/$[M]^+$): calcd for $C_{36}H_{22}N_4^+$: 510.1844, found: 510.1849.

Synthesis of Cruciform **24b**

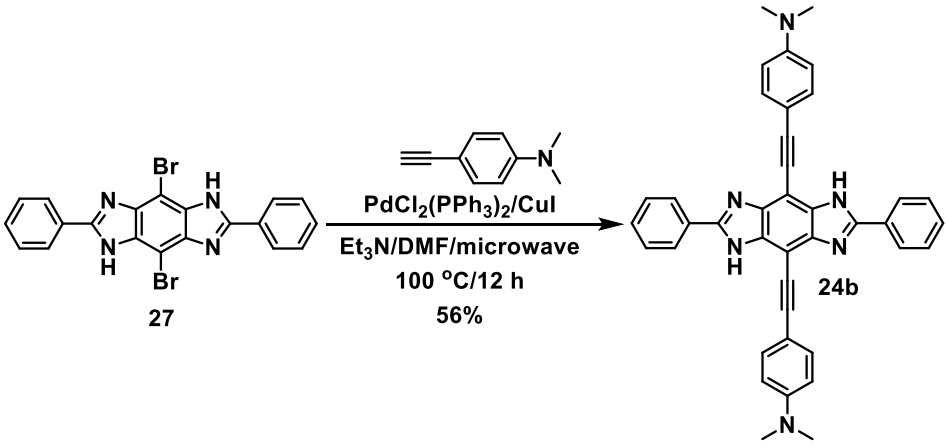

Anhydrous K_2CO_3 (1.11 g, 8.00 mmol) was added to a solution of 2-(4-(*N*,*N*-dimethylamino)phenyl)trimethylsilylethyne (875 mg, 4.00 mmol) in a mixture of MeOH (5 mL) and THF (5 mL). After stirring for 30 min under nitrogen, the reaction mixture was filtered through Celite. The solvent was removed under reduced pressure to yield crude 4-ethynyl-*N*,*N*-dimethylaniline, which was used without purification in the next step. To minimize manipulations of this compound, we assumed a 95% yield for this reaction.[88]

The entire amount of 4-ethynyl-*N*,*N*-dimethylaniline (prepared as described above) was added to a thick-walled microwave pressure vial that contained a mixture of compound **27** (300 mg, 0.64 mmol), $PdCl_2$ $(PPh_3)_2$ (90 mg, 0.13 mmol), CuI (45 mg, 0.24 mmol), Et_3N (5 mL), and DMF (5 mL). The vial was sealed under nitrogen and exposed to microwave irradiation for 12 h at 100 °C. After cooling, the reaction mixture was extracted with EtOAc, washed with brine, and dried over anhydrous $MgSO_4$. Afterward, 80 g of aluminum oxide was added to the combined organic layer and the solvent was

removed under reduced pressure until a brown powder was formed, which was purified by gradient elution column chromatography on alumina, using EtOAc/hexane eluent system (solvent ratios ranging from 4:16 to 9:11). The solvent was removed *in vacuo* to give the crude product, which was further purified by recrystallization from THF to afford 214 mg (56%, 0.36 mmol) of a tangelo-colored powder (**24b,** mp 220 ^{o}C, with decomposition).

24b: UV/Vis (THF): λ_{max} (log ε) 386 (4.81), 425 (4.70) nm. IR (neat): 3086 (w, $\tilde{\nu}_{N-H}$), 2190 (s, $\tilde{\nu}_{C\equiv C}$), 1604 (s, $\tilde{\nu}_{C=N}$), 1530 (m), 1514 (m), 1479 (m), 1457 (m), 1402 (w), 1345 (s), 1290 (m), 1232 (m), 1183 (s), 1065 (m), 1029 (m), 999 (w), 945 (m), 920 (w), 843 (w), 810 (s), 777 (m),725 (m), 690 (s), 634 (w), 580 (w) cm^{-1}. ^{1}H NMR (DMSO-d_6, 500 MHz): δ 12.90 (d, $^{3}J_{H-H}$=5.2 Hz, 2H), 8.34 (m, 4H), 8.57 (m, 10H), 6.79 (d, $^{3}J_{H-H}$=8.6 Hz, 4H), 2.98 (s, 12H) ppm. ^{13}C NMR (DMSO-d_6, with 20 mg of TBAF trihydrate added, 150 MHz): δ 159.5, 149.3, 146.5, 139.9, 132.1, 127.9, 126.6, 125.3, 114.0, 112.8, 96.1, 94.0, 91.8, 51.9 ppm. HRMS (ESI/[M]$^{+}$): calcd for $C_{40}H_{32}N_6^{+}$ 596.2688, found 596.2692.

Synthesis of Cruciform **24c**

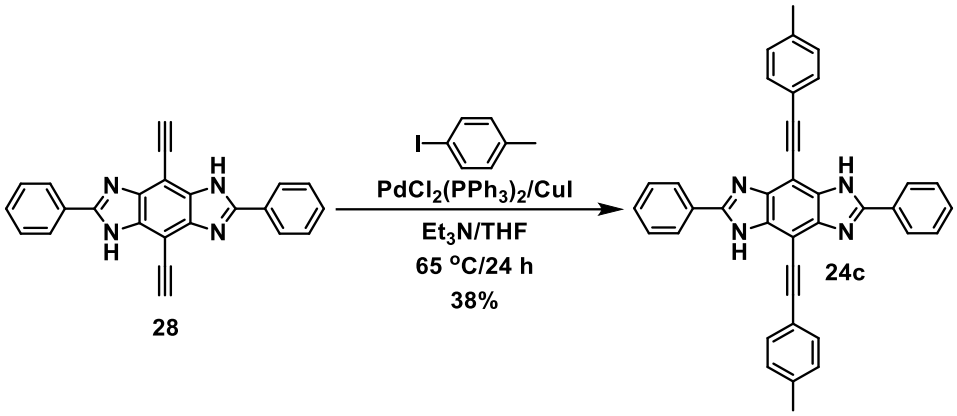

A mixture of compound **28** (300 mg, 0.84 mmol), 4-iodotoluene (913 mg, 4.19 mmol), $PdCl_2(PPh_3)_2$ (50 mg, 0.07 mmol) and CuI (27 mg, 0.14 mmol) was added to a 100 mL pear-shaped Schlenk flask. The flask was sealed, and then evacuated and backfilled with nitrogen three times. In a separate flask, a mixture of Et_3N (25 mL) and THF (17 mL) was degassed for 30 min and transferred slowly under positive N_2 pressure via cannula to the reaction flask. The reaction mixture was stirred and heated at 65 °C for 24 h and then cooled to 20 °C. Afterwards, aluminum oxide was added to the reaction mixture and the solvent was removed under reduced pressure until a brown powder was formed, which was subsequently purified by gradient elution column chromatography on alumina, using EtOAc/hexane eluent system (volume ratios ranging from 3:17 to 9:11). The solvent was removed *in vacuo* to give the crude product, which was further purified by recrystallization from THF to afford cruciform **24c** as a yellow powder (174 mg, 38%, mp 293 °C).

24c: UV/Vis (THF): λ_{max} (log ε) 386 (4.91) nm. IR (neat): 3000 (w, $\tilde{\nu}_{N-H}$), 2188 (w, $\tilde{\nu}_{C\equiv C}$), 1603 (m, $\tilde{\nu}_{C=N}$), 1560 (w), 1528 (w), 1505 (m), 1480 (s), 1454 (s), 1401 (m), 1336

(s), 1286 (m), 1254 (m), 1236 (m), 1176 (m), 1109 (w), 1070 (w), 1030 (m), 987 (w), 935 (m), 809 (s), 774 (s), 738 (w), 723 (m), 692 (s), 632 (w) cm^{-1}. ^1H NMR (DMSO-d_6, 500 MHz): δ 12.97 (s, 2H), 8.34 (d, $^3J_{H–H}$ = 7.5 Hz, 4H), 8.57 (m, 10H), 7.32 (d, $^3J_{H–H}$ = 5.7 Hz, 4H), 2.38 (s, 6H) ppm. ^{13}C NMR (DMSO-d_6, 125 MHz, 90 °C): δ 153.3, 138.9, 132.1, 130.7, 130.5, 129.8, 129.2, 128.0, 120.9, 21.6 ppm. HRMS (ESI/$[M]^+$): calcd for $C_{38}H_{26}N_4^+$: 538.2157, found: 538.2138.

Synthesis of Cruciform **24d**

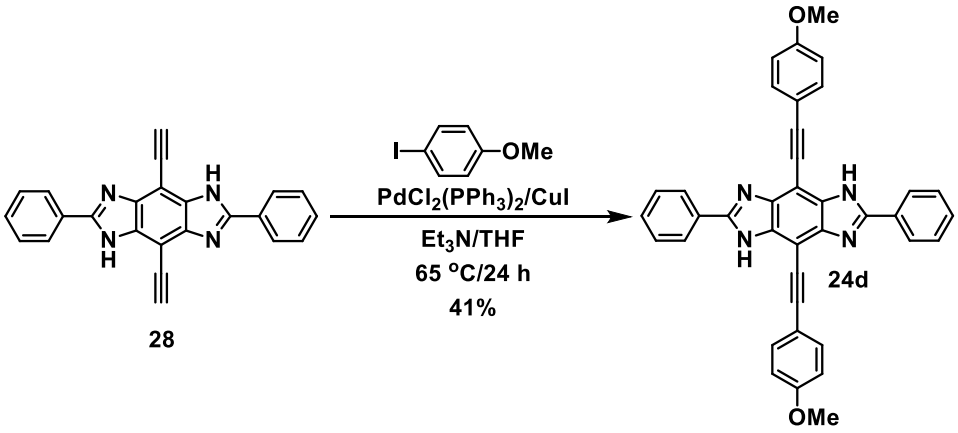

A mixture of compound **28** (300 mg, 0.84 mmol), 4-iodoanisole (979 mg, 4.19 mmol), $PdCl_2(PPh_3)_2$ (50 mg, 0.07 mmol), and CuI (27 mg, 0.14 mmol) was added to a 100 mL pear-shaped Schlenk flask. The flask was sealed, then evacuated and backfilled with nitrogen three times. In a separate flask, a mixture of Et_3N (25 mL) and THF (17 mL) was degassed for 30 min and transferred slowly under positive N_2 pressure via cannula to the reaction flask. The reaction mixture was stirred and heated at 65 °C for 24 h and then cooled to 20 °C. Afterwards, 80 g of aluminum oxide was added to the reaction mixture and the solvent was removed under reduced pressure until a brown

powder was formed. This powder was purified by gradient elution column chromatography on alumina, using EtOAc/hexane eluent system (volume ratio ranging from 7:13 to 4:1). The solvent was removed *in vacuo* to give the crude product, which was further purified by recrystallization from THF to afford cruciform **24d** as a yellow powder (196 mg, 41%, mp 280 °C).

24d: UV/Vis (THF): λ_{max} (log ε) 385 (4.93) nm. IR (neat): 3062 (w, $\tilde{\nu}_{N-H}$), 2834 (w, $\tilde{\nu}_{C-H}$), 2195 (m, $\tilde{\nu}_{C\equiv C}$), 1603 (s, $\tilde{\nu}_{C=N}$), 1567 (w), 1524 (w), 1504 (s), 1478 (s), 1453 (s), 1399 (m), 1340 (s), 1288 (s), 1244 (s), 1169 (s), 1106 (m), 1071 (w), 1027 (s), 942 (m), 827 (s), 774 (s), 727 (m), 689 (s), 644 (w), 633 (w), 589 (s), 564 (m), 546 (m), 529 (s) cm^{-1}. ^{1}H NMR (DMSO-d_6, 500 MHz at 90 ^{o}C): δ 12.69 (s, 2H), 8.33 (d, $^{3}J_{H-H}$ = 6.9 Hz, 4H), 7.71 (s, 4H), 7.52 (m, 6H), 7.05 (d, $^{3}J_{H-H}$ = 8.6 Hz, 4H), 3.84 (s, 6H) ppm. ^{13}C NMR (DMSO-d_6, 125 MHz, 90 °C): δ 160.4, 153.2, 142.0, 133.7, 130.7, 130.4, 129.1, 128.0, 116.0, 115.0, 98.9, 96.9, 83.4, 56.0 ppm. HRMS (ESI/$[M]^{+}$): calcd for $C_{38}H_{26}N_4O_2^{+}$: 570.2056, found: 570.2056.

Synthesis of Cruciform **24e**

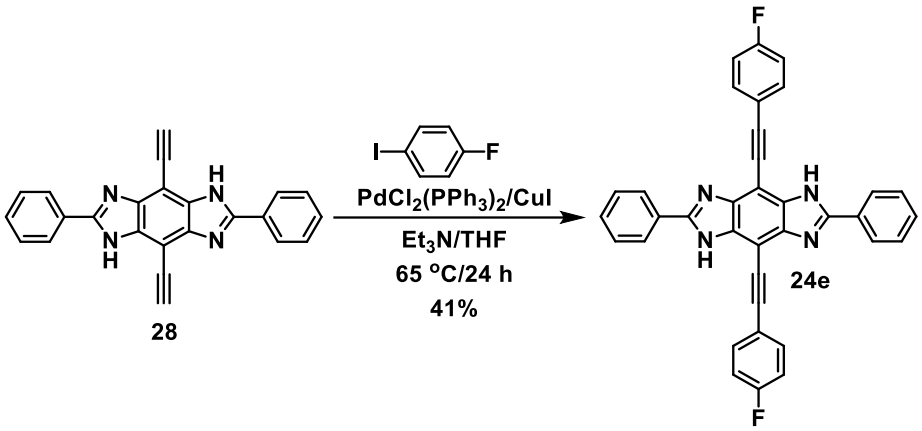

A mixture of compound **28** (300 mg, 0.84 mmol), 4-fluoroiodobenzene (0.56 mL, 4.85 mmol), $PdCl_2(PPh_3)_2$ (50 mg, 0.07 mmol), and CuI (27 mg, 0.14 mmol) was added to a 100 mL pear-shaped Schlenk flask. The flask was sealed, then evacuated and backfilled with nitrogen three times. In a separate flask, a mixture of Et_3N (25 mL) and THF (17 mL) was degassed for 30 min and then transferred slowly under positive N_2 pressure via cannula to the reaction flask. The reaction mixture was stirred and heated at 65 °C for 24 h and then cooled to 20 °C. Afterwards, alumina was added to reaction mixture and the solvent was removed under reduced pressure until a brown powder was formed. This powder was then purified by gradient elution column chromatography on alumina, using EtOAc/hexane eluent system (volume ratio ranging from 1:3 to 1:1). The solvent was removed by vacuum to give the orange crude product which was further purified by recrystallization from EtOAc, to afford cruciform **24e** (187 mg, 41%, mp 287 °C).

24e: UV/Vis (THF): λ_{max} (log ε) 383 (4.89) nm. IR (neat): 3066 (w, $\tilde{\nu}_{N-H}$), 2158 (w, $\tilde{\nu}_{C\equiv C}$), 1602 (m, $\tilde{\nu}_{C=N}$), 1558 (w), 1525 (w), 1503 (s), 1477 (s), 1455 (s), 1402 (m), 1342 (s), 1317 (w), 1288 (s), 1235 (s), 1169 (s), 1105 (m), 1064 (w), 1028 (s), 943 (m), 832 (s), 775 (s), 747 (w), 728 (m), 689 (s), 634 (w), 582 (s), 566 (w), 556 (w), 547 (w), 530 (s) cm^{-1}. ^1H NMR (DMSO-d_6, 500 MHz): δ 13.05 (d, $^3J_{H-H}$ = 8.0 Hz, 2H), 8.33 (m, 4H), 7.84 (m, 4H), 7.55 (m, 6H), 7.36 (m, 4H) ppm. ^{13}C NMR (DMSO-d_6, 125 MHz): δ 163.7, 161.6, 153.4, 142.3, 134.5, 130.7, 129.3, 127.7, 120.0, 116.6, 97.6, 96.4, 84.3 ppm. HRMS (ESI/$[M]^+$): calcd for $C_{36}H_{20}F_2N_4^+$: 546.1656, found: 546.1656.

Synthesis of Cruciform **24f**

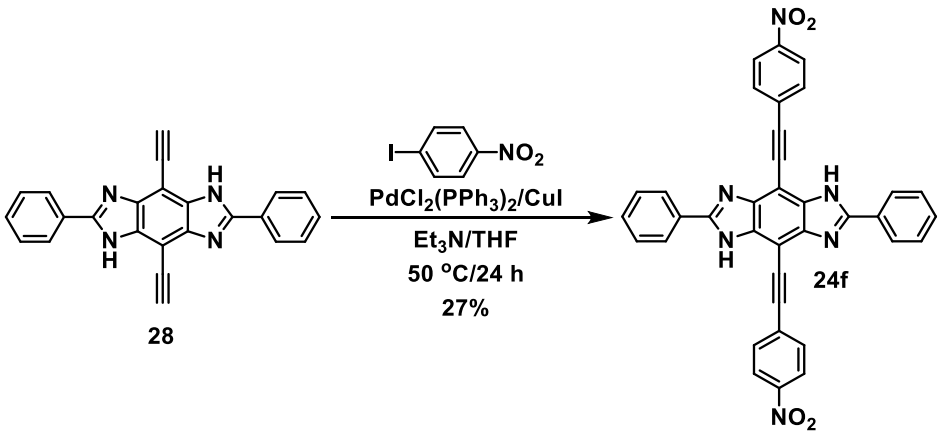

A mixture of compound **28** (300 mg, 0.84 mmol), 1-iodo-4-nitrobenzene (834 mg, 3.35 mmol), $PdCl_2(PPh_3)_2$ (50 mg, 0.07 mmol), and CuI (27 mg, 0.14 mmol) was placed in a 100 mL pear-shaped Schlenk flask. The flask was sealed, then evacuated and backfilled with nitrogen three times. In a separate flask, a mixture of Et_3N (30 mL) and THF (20 mL) was degassed for 30 min and then transferred slowly under positive nitrogen pressure via cannula into the reaction flask. The reaction mixture was stirred and

heated at 50 °C for 24 h, then cooled to 20 °C, filtered, and washed with THF (5 mL). The residue collected was recrystallized from THF to give the crude product, which was then mixed with H_2O (150 mL), sonicated for 30 min, filtered, and dried in air to give cruciform **24f** (136 mg, 27%) as a red powder (mp 327 ^{o}C, with decomposition).

24f: UV/Vis (THF): λ_{max} (log ε) 388 (4.80) nm. IR (neat): 3060 (w, $\tilde{\nu}_{N-H}$), 2199 (w, $\tilde{\nu}_{C\equiv C}$), 1591 (m, $\tilde{\nu}_{C=N}$), 1514 (s, $\tilde{\nu}_{NO2}$), 1476 (m), 1454 (m), 1402 (w), 1337 (s, $\tilde{\nu}_{NO2}$), 1175 (w), 1106 (m), 1028 (w), 994 (w), 943 (w), 854 (s), 775 (m), 748 (m), 728 (w), 687 (s), 568 (w) cm^{-1}. ^{1}H NMR (DMSO-d_6, 500 MHz): δ 13.29 (s, 2H), 8.34 (apparent d, $^{3}J_{H-H}$ = 6.9 Hz, 8H), 8.01 (br s, 4H), 7.57 (m, 6H) ppm. ^{13}C NMR (DMSO-d_6, 125 MHz): δ 133.2, 131.1, 130.0, 129.5, 128.1, 124.4 ppm (because of the low solubility of cruciform **24f**, a satisfactory ^{13}C NMR spectrum could not be obtained; listed are all the observed peaks). HRMS (ESI/$[M]^{+}$): calcd for $C_{36}H_{20}N_6O_4^{+}$: 600.1546, found: 600.1526.

Synthesis of Cruciform **24g**

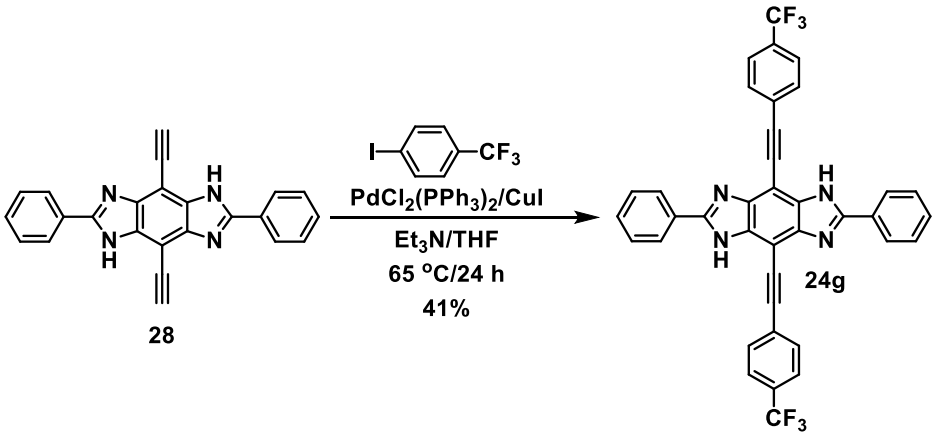

A mixture of compound **28** (300 mg, 0.84 mmol), 4-iodobenzotrifluoride (0.50 mL, 3.40 mmol), $PdCl_2(PPh_3)_2$ (50 mg, 0.07 mmol), and CuI (27 mg, 0.14 mmol) was

placed in a 100 mL pear-shaped Schlenk flask. The flask was sealed, then evacuated and backfilled with nitrogen three times. A mixture of Et_3N (30 mL) and THF (20 mL) was degassed for 30 min and transferred slowly under positive nitrogen pressure via cannula into the reaction flask. The reaction mixture was stirred and heated at 65 °C for 24 h, then cooled to 20 °C. Afterwards, silica gel was added to the reaction mixture, and the solvent was removed under reduced pressure until a brown powder was formed. This powder was purified by gradient elution column chromatography on silica gel, using EtOAc/hexane eluent system (volume ratio ranging from 1:3 to 1:1). The solvent was removed *in vacuo* to give the yellow crude product, which was further purified by recrystallization from Et_2O, to yield cruciform **24g** (220 mg, 41%) as a yellow powder (mp 245 °C, with decomposition).

24g: UV/Vis (THF): λ_{max} (log ε) 392 (4.86) nm. IR (neat): 3062 (w, $\tilde{\nu}_{N-H}$), 2201 (w, $\tilde{\nu}_{C\equiv C}$), 1613 (m, $\tilde{\nu}_{C=N}$), 1563 (w), 1529 (w), 1505 (w), 1478 (s), 1455 (s), 1403 (m), 1341 (s), 1317 (s), 1290 (s), 1246 (m), 1167 (s), 1119 (s), 1103 (s), 1064 (s), 1028 (s), 1018 (s), 945 (m), 837 (s), 774 (s), 747 (w, $\tilde{\nu}_{CF3}$), 728 (m), 689 (s), 634 (w), 592 (s), 537 (m) cm^{-1}. ^1H NMR (DMSO-d_6, 500 MHz): δ 13.16 (s, 2H), 8.34 (d, $^3J_{H-H}$ = 7.5 Hz, 4H), 8.00 (m, 8H), 7.55 (m, 6H) ppm.^{13}C NMR (DMSO-d_6, 125 MHz): δ 153.5, 142.6, 134.2, 132.9, 130.9, 130.2, 129.4, 127.9, 126.2, 125.7, 123.5, 97.4, 96.3, 87.1 ppm. HRMS (ESI/$[M]^+$): calcd for $C_{38}H_{20}F_6N_4^+$: 646.1592, found: 646.1592.

Synthesis of Cruciform **24h**

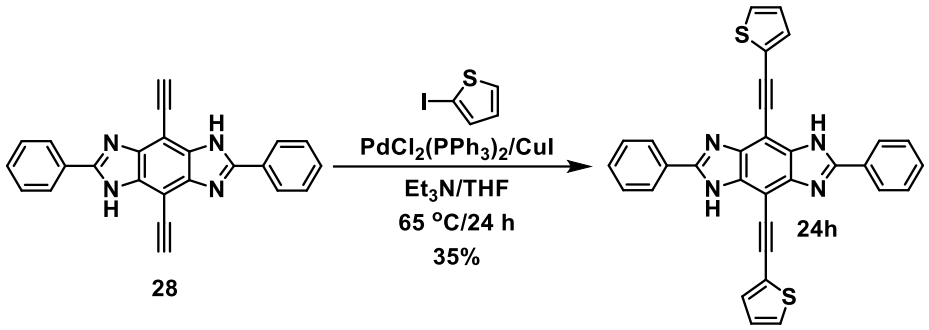

A mixture of compound **28** (300 mg, 0.84 mmol), 2-iodothiophene (0.55 mL, 4.98 mmol), $PdCl_2(PPh_3)_2$ (50 mg, 0.07 mmol), and CuI (27 mg, 0.14 mmol) was placed in a 100 mL pear-shaped Schlenk flask. The flask was sealed, then evacuated and backfilled with nitrogen three times. A solution of Et_3N (25 mL) and THF (17 mL) was degassed for 30 min and then transferred slowly under positive nitrogen pressure via cannula into the reaction flask. The reaction mixture was stirred and heated at 65 °C for 24 h and then cooled to 20 °C. Afterwards, alumina was added to the reaction mixture and the solvent was removed under reduced pressure until a brown powder was formed. This powder was purified by gradient elution column chromatography on alumina, using EtOAc/hexane eluent system (volume ratio ranging from 1:4 to 3:2). The solvent was removed *in vacuo* to give the crude product which was further purified by recrystallization from THF/hexane to yield cruciform **24h** (153 mg, 35%) as a dark yellow powder (mp 268 °C, with decomposition).

24h: UV/Vis (THF): λ_{max} (log ε) 391 (4.89) nm. IR (neat): 3111 (w, $\tilde{\nu}_{C\text{-}H\text{-}thiophene}$), 3060 (w, $\tilde{\nu}_{N-H}$), 2190 (w, $\tilde{\nu}_{C\equiv C}$), 1613 (w, $\tilde{\nu}_{C=N}$), 1562 (w), 1531 (w), 1506 (w), 1479 (m), 1454 (s), 1396 (w), 1341 (s), 1325 (s), 1276 (m), 1226 (s), 1174 (w), 1071 (w), 1043 (s), 1029

(m), 965 (w), 942 (m), 918 (w), 851 (s), 831 (m), 774 (s), 744 (w), 686 (s), 625 (m) cm^{-1}. ^1H NMR (DMSO-d_6, 500 MHz): δ 13.12 (s, 2H), 8.32 (d, $^3J_{H-H}$ = 7.5 Hz, 4H), 8.56 (m, 10H), 7.20 (m, 2H) ppm.^{13}C NMR (Me_2CO-d_6 and 200 mg of TBAF trihydrate, 150 MHz): δ 131.2, 128.0, 127.2, 127.1, 126.2, 125.8, 88.7 ppm. HRMS (ESI/$[M]^+$): calcd for $C_{32}H_{18}N_4S_2^+$: 522.0973, found: 522.0959.

Synthesis of Cruciform **24i**

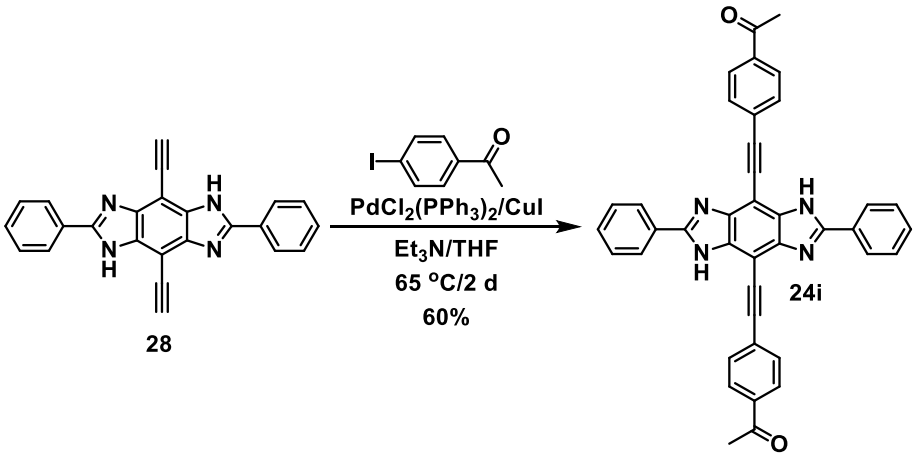

A mixture of compound **28** (300 mg, 0.84 mmol), 4-iodoacetophenone (618 mg, 2.51 mmol), $PdCl_2(PPh_3)_2$ (50 mg, 0.07 mmol), and CuI (27 mg, 0.14 mmol) was placed in a 100 mL pear-shaped Schlenk flask. The flask was sealed, then evacuated and backfilled with nitrogen three times. In a separate flask, a mixture of Et_3N (30 mL) and THF (20 mL) was degassed for 30 min and transferred slowly under positive nitrogen pressure via cannula into the reaction flask. The reaction mixture was stirred and heated at 65 °C for 2 d, then cooled to 20 °C, filtered, and washed with THF (5 mL). The residue collected was recrystallized from THF to give the crude product, which was mixed with

H_2O (150 mL), sonicated for 30 min, filtered, and dried in air to give cruciform **24i** (300 mg, 60%) as a yellow powder (mp 352 °C, with decomposition).

24i: UV/Vis (THF): λ_{max} (log ε) 382 (4.60) nm. IR (neat): 3199 (w, $\tilde{\nu}_{N-H}$), 2204 (w, $\tilde{\nu}_{C\equiv C}$), 1668 (s), 1602 (s, $\tilde{\nu}_{C=N}$), 1557 (w), 1505 (w), 1480 (m), 1455 (s), 1402 (m), 1336 (s), 1312 (w), 1273 (s), 1168 (m), 1105 (m), 1064 (m), 1029 (m), 1017 (w), 940 (w), 829 (s), 777 (s), 747 (w), 728 (m), 689 (s), 593 (m) cm^{-1}. ^1H NMR (DMSO-d_6, 500 MHz, 40 °C): δ 13.10 (s, 2H), 8.35 (d, $^3J_{H-H}$ = 6.9 Hz, 4H), 8.06 (d, $^3J_{H-H}$ = 7.5 Hz, 4H), 7.90 (s, 4H), 7.55 (m, 6H), 2.62 (s, 6H) ppm.^{13}C NMR (DMSO-d_6, 125 MHz, 40 °C): δ 197.8, 154.1, 136.8, 132.3, 130.8, 130.3, 129.3, 129.0, 128.0, 98.3, 27.3 ppm (because of the low solubility of cruciform **4i**, a satisfactory ^{13}C NMR spectrum could not be obtained; listed are all the observed peaks). HRMS (ESI/$[M]^+$): calcd for $C_{40}H_{26}N_4O_2^+$: 594.2056, found: 594.2050.

Synthesis of Cruciform **24j**

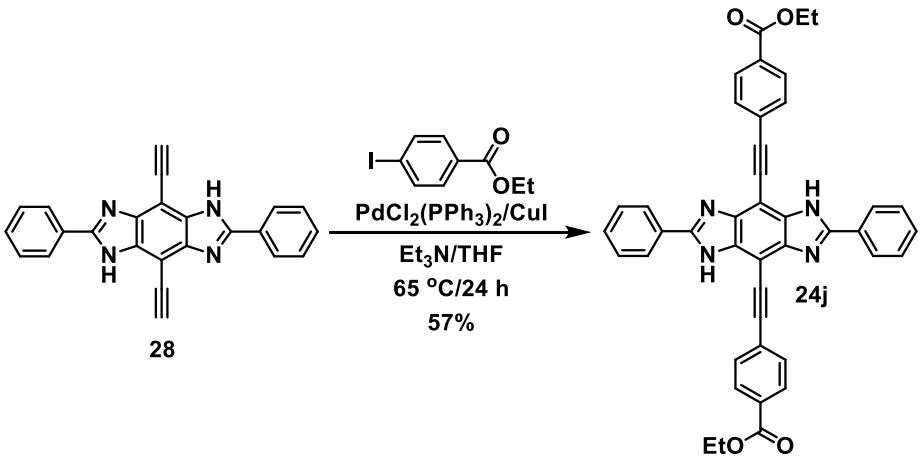

A mixture of compound **28** (300 mg, 0.84 mmol), ethyl 4-iodobenzoate (0.56 mL, 3.33 mmol), $PdCl_2(PPh_3)_2$ (50 mg, 0.07 mmol), and CuI (27 mg, 0.14 mmol) was added

to a 100 mL pear-shaped Schlenk flask. The flask was sealed, then evacuated and backfilled with nitrogen three times. In a separate flask, a solution of Et_3N (30 mL) and THF (20 mL) was degassed for 30 min and then transferred slowly under positive nitrogen pressure via cannula into the reaction flask. The reaction mixture was stirred and heated at 65 °C for 24 h and then cooled to 20 °C, filtered and washed with THF (5 mL). The residue collected was recrystallized from a THF/EtOAc mixture (volume ratio 2:3), to give the crude product which was then mixed with H_2O (150 mL), sonicated for 30 min, filtered and dried in air, to finally give cruciform **24j** (310 mg, 57%) as a yellow powder (mp 268 °C, with decomposition).

24j: UV/Vis (THF): λ_{max} (log ε) 394 (4.89) nm. IR (neat): 3253 (m), 2981 (w, $\tilde{\nu}_{N–H}$), 2205 (w, $\tilde{\nu}_{C\equiv C}$), 1694 (s, $\tilde{\nu}_{C=O}$), 1605 (m, $\tilde{\nu}_{C=N}$), 1561 (w), 1524 (w), 1504 (m), 1480 (s), 1454 (s), 1404 (m), 1365 (w), 1339 (s), 1308 (w), 1287 (s, $\tilde{\nu}_{CO–O}$), 1275 (s), 1172 (m), 1128 (m), 1106 (s), 1071 (w), 1021 (m), 987 (w), 941 (m), 853 (m), 830 (w), 773 (s), 765 (m), 725 (m), 687 (s), 652 (w) cm^{-1}. ^1H NMR (DMSO-d_6, 400 MHz): δ 13.15 (d, $^3J_{H–H}$ = 5.0 Hz, 2H), 8.35 (m, 4H), 8.00 (m, 8H), 7.55 (m, 6H), 4.33 (q, $^3J_{H–H}$ = 7.3 Hz, 4H), 1.33 (t, $^3J_{H–H}$ = 7.3 Hz, 6H) ppm.^{13}C NMR (DMSO-d_6, 100 MHz): δ 165.8, 153.6, 142.7, 134.1, 132.4, 130.9, 130.2, 129.9, 129.4, 128.0, 98.1, 96.3, 87.6, 61.6, 14.7 ppm. HRMS (ESI/$[M]^+$): calcd for $C_{42}H_{30}N_4O_4^+$: 654.2267, found: 654.2270.

Synthesis of Cruciform **24l**

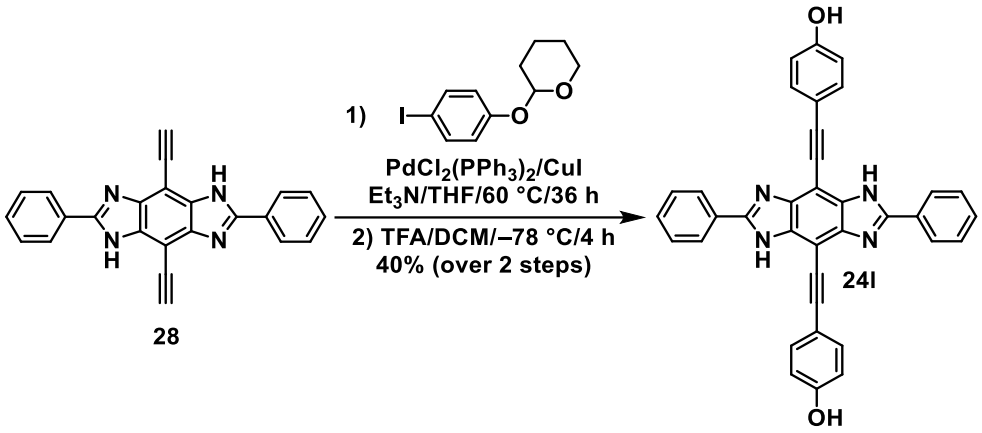

A mixture of compound **28** (500 mg, 1.39 mmol), 4-(iodophenyl)tetrahydropyran-2-yl ether[5] (1.73 g, 5.58 mmol), $PdCl_2(PPh_3)_2$ (83 mg, 0.12 mmol), and CuI (45 mg, 0.24 mmol) was added to a 100 mL pear-shaped Schlenk flask. The flask was sealed, then evacuated and backfilled with nitrogen three times. In a separate flask, a solution of Et_3N (40 mL) and THF (27 mL) was degassed for 30 min and then transferred slowly under positive N_2 pressure via cannula into the reaction flask. The reaction mixture was stirred and heated at 60 °C for 36 h, then cooled to 20 °C. Afterwards, alumina was added to the reaction mixture, and the solvent was removed under reduced pressure until a brown powder was formed. This powder was purified by gradient elution column chromatography on alumina, using EtOAc/hexane eluent system (volume ratio ranging from 25:75 to 55:45). The solvent was removed *in vacuo* to give 590 mg of the crude cruciform **24k** as the intermediate.

In a 250 mL round-bottom flask, trifluoroacetic acid (4.5 mL) was added to a solution of the aforementioned cruciform **2k** (590 mg, 0.83 mmol) in DCM (150 mL),

which was kept in a dry ice/Me_2CO bath. The reaction was stirred for 2 h at –78 °C and then warmed up to 20 °C.[148] The precipitate formed in the reaction was collected by filtration and washed with DCM. Afterwards, it was mixed with water (500 mL), sonicated for 30 min, filtered, and dried in air to give the crude product, which was further purified by recrystallization from THF to afford cruciform **24l** (310 mg, 41%) as a yellow powder (mp 320 °C, with decomposition).

24l: UV/Vis (THF): λ_{max} (log ε) 383 (4.95) nm. IR (neat): 3410 (w, $\tilde{\nu}_{O-H}$), 3063 (w, $\tilde{\nu}_{N-H}$), 2204 (w, $\tilde{\nu}_{C\equiv C}$), 1604 (s, $\tilde{\nu}_{C=N}$), 1525 (w), 1505 (s), 1479 (s), 1454 (s), 1402 (w), 1380 (w), 1345 (m), 1278 (m), 1265 (w), 1243 (s), 1169 (s), 1105 (w), 1072 (w), 1028 (m), 946 (w), 828 (s), 776 (s), 727 (w), 692 (s), 684 (s), 634 (w), 616 (w), 591 (s), 567 (w), 534 (s) cm^{-1}. ^1H NMR (DMSO-d_6, 500 MHz): δ 12.95 (s, 2H), 9.97 (s, 2H), 8.33 (d, $^3J_{H-H}$ = 7.5 Hz, 4H), 8.52 (m, 10H), 6.87 (d, $^3J_{H-H}$ = 8.0 Hz, 4H) ppm.^{13}C NMR (DMSO-d_6, 125 MHz): δ 158.7, 153.1, 142.4, 133.9, 130.6, 129.3, 127.8, 116.3, 113.9, 99.4, 96.6, 82.5 ppm. HRMS (ESI/$[M]^+$): calcd for $C_{36}H_{22}N_4O_2^+$: 542.1743, found: 542.1742.

Synthesis of Cruciform **24m**

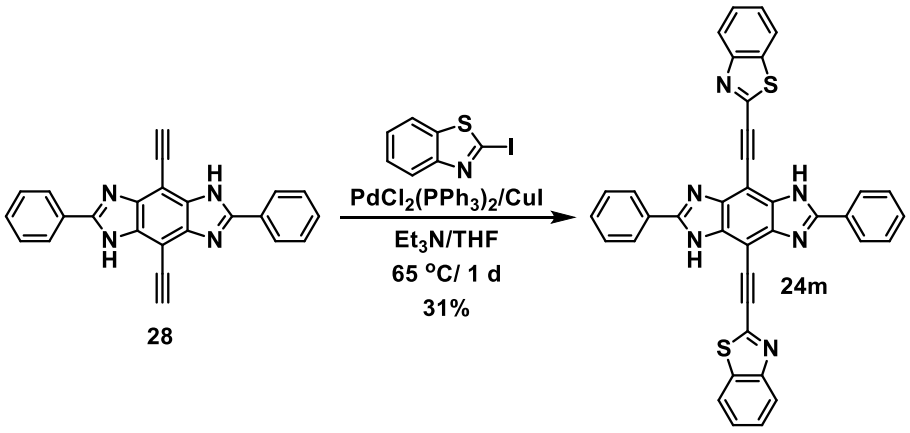

The mixture of compound **28** (300 mg, 0.837 mmol), 2-iodo-benzothiazole (874.6 mg, 3.35 mmol),[7] $PdCl_2(PPh_3)_2$ (50 mg, 0.071 mmol), and CuI (27 mg, 0.142 mmol) was added to 100-mL pear-shaped Schlenk flask. The flask was sealed, then vacuumed and backfilled with N_2 (three times). A solution of 25 mL Et_3N and 17 mL THF was degassed for 30 min and transferred slowly under positive N_2 pressure via cannula to the reaction flask. The reaction mixture was stirred and heated at 65 ^oC for 1 day and cooled to room temperature. Afterward, 80 mL of aluminum oxide was added to the reaction mixture and the solvent was removed under reduced pressure until a brown powder formed, which was purified by gradient elution column chromatography using aluminum oxide (250 mL) and the ethyl acetate (EtOAc)/hexane eluent system (8:2–10:1). The solvent was removed by vacuum to give the orange crude product which was further purified by recrystallization (THF) to afford 162 mg (31%, 0.26 mmol) of an orange-red powder (**24m,** mp 350 ^oC, with decomposition).

24m: UV−Vis (THF): λ_{max} (log ε) = 292 (4.97), 422 (5.1)7 nm. IR (neat): 3048 (w, $\tilde{\nu}_{N-H}$), 2193 (w, $\tilde{\nu}_{C\equiv C}$), 1603 (w, $\tilde{\nu}_{C=N}$), 1556 (w), 1526 (w), 1504 (w), 1481 (w), 1455 (s), 1436 (w), 1400 (m), 1334 (s), 1314 (w), 1281 (m), 1249 (m), 1181 (m), 1111 (w), 1070 (w), 1030 (m), 1015 (w), 973 (m), 940 (m), 921 (m), 869 (w), 828 (m), 778 (s), 761 (s), 726 (s), 691 (s), 630 (w) cm^{-1}. ^{1}H NMR ($(CD_3)_2SO$, 500 MHz): δ 12.53 (s, 2H), 8.37 (d, J = 8.0 Hz, 4H), 8.22 (m, 2H), 8.14 (m, 2H), 7.59 (m, 10H) ppm. ^{13}C NMR ($(CD_3)_2SO$, 500 MHz): δ 154.3, 153.2, 148.7, 143.2, 142.8, 135.7, 134.6, 134.1, 131.1, 129.9, 129.5, 127.9, 127.2, 123.8, 122.9, 95.6, 92.3, 91.1 ppm. HRMS (ESI/$[M]^+$): calcd for $C_{38}H_{20}N_6S_2^+$ 624.1191, found 624.1171.

2.4.3 HOMOs and LUMOs of Cruciforms 24a–j, 24l and 24m

	HOMO	LUMO		HOMO	LUMO
24a	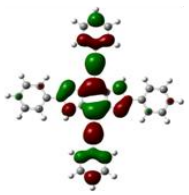	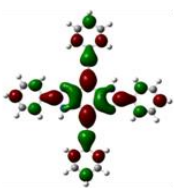	24g	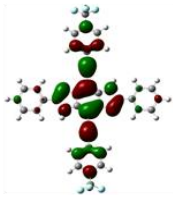	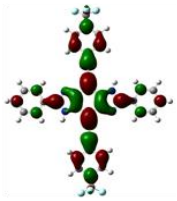
24b	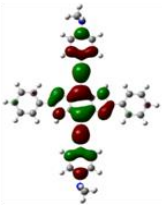	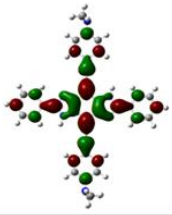	24h	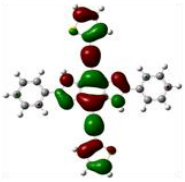	
24c	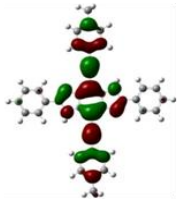	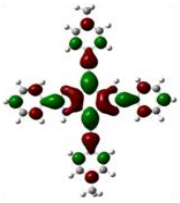	24i	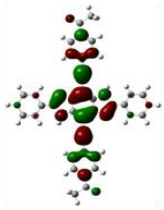	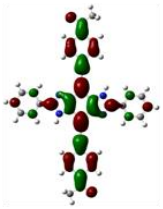
24d	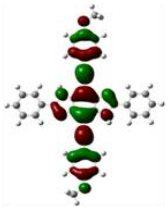	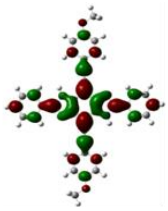	24j	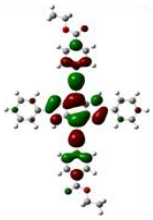	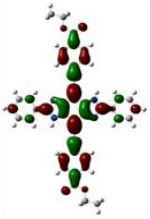
24e	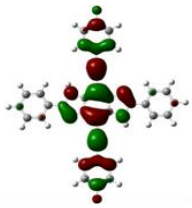	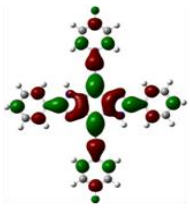	24l	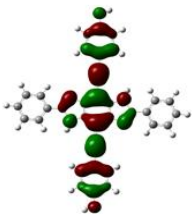	
24f	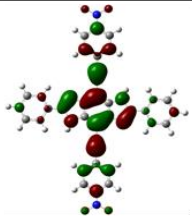	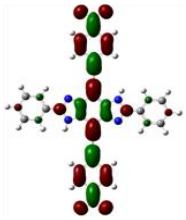	24m	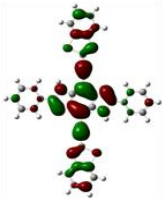	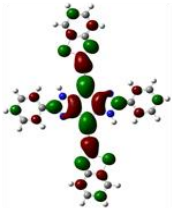

Figure 3.13 Images of HOMOs and LUMOs of cruciform **4a**–**4j**, **4l and 4m**.

FMO calculations of BBI cruciforms were performed using Gaussian 09W software package and its accompanying graphical interface program GaussView 5.0.[108] The B3LYP hybrid density functional and a standard 3-21G basis set were used for the geometry optimizations. All structures were optimized within a C_s symmetry constraint.

3.4.4 UV/Vis Absorption and Fluorescence Titrations of Cruciforms 24a–m with Acid—TFA and Base—*n*-Bu_4NOH

UV-visible and fluorescence titrations of BBI cruciforms were performed using Perkin-Elmer LAMBDA 25 UV/VIS Spectrometer and Perkin-Elmer Fluorescence Spectrometer LS-55, respectively. In a quartz cuvette, 3 mL of 1×10^{-5} M solutions of cruciform in THF were titrated with increasing amount of TFA, or 40% aqueous solution of TBAOH, prepared in spectroscopic grade THF.

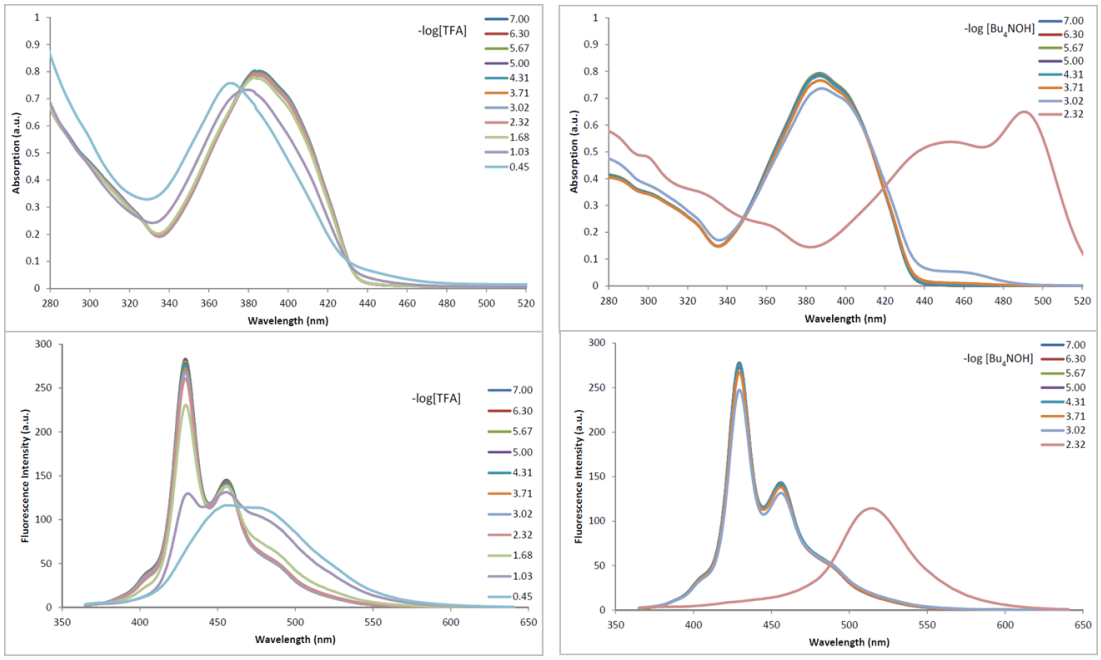

Figure 3.14 Absorption (top) and emission (bottom) spectra for the TFA titration (left, λ_{exc}=335 nm) and for TBAOH titration (right, λ_{exc}=335 nm) of **24a**.

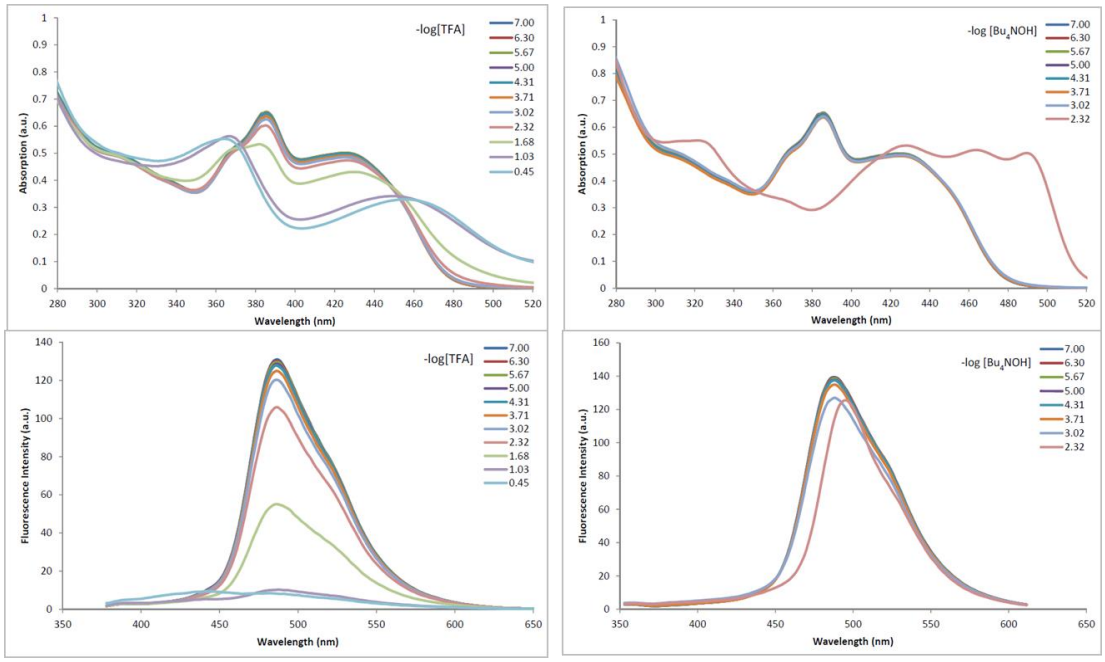

Figure 3.15 Absorption (top) and emission (bottom) spectra for the for TFA titration (left, λ_{exc}=348 nm) and for TBAOH titration (right, λ_{exc}=340 nm) of **24b**.

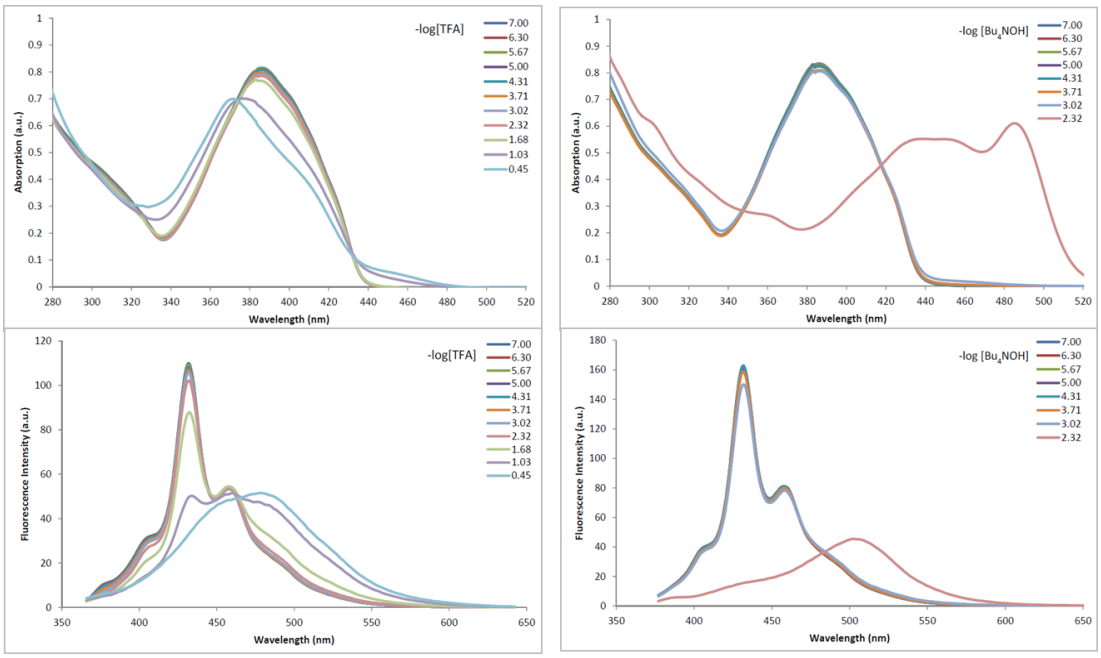

Figure 3.16 Absorption (top) and emission (bottom) spectra for the the TFA titration (left, λ_{exc}=336 nm) and for TBAOH titration (right, λ_{exc}=340 nm) of **24c**.

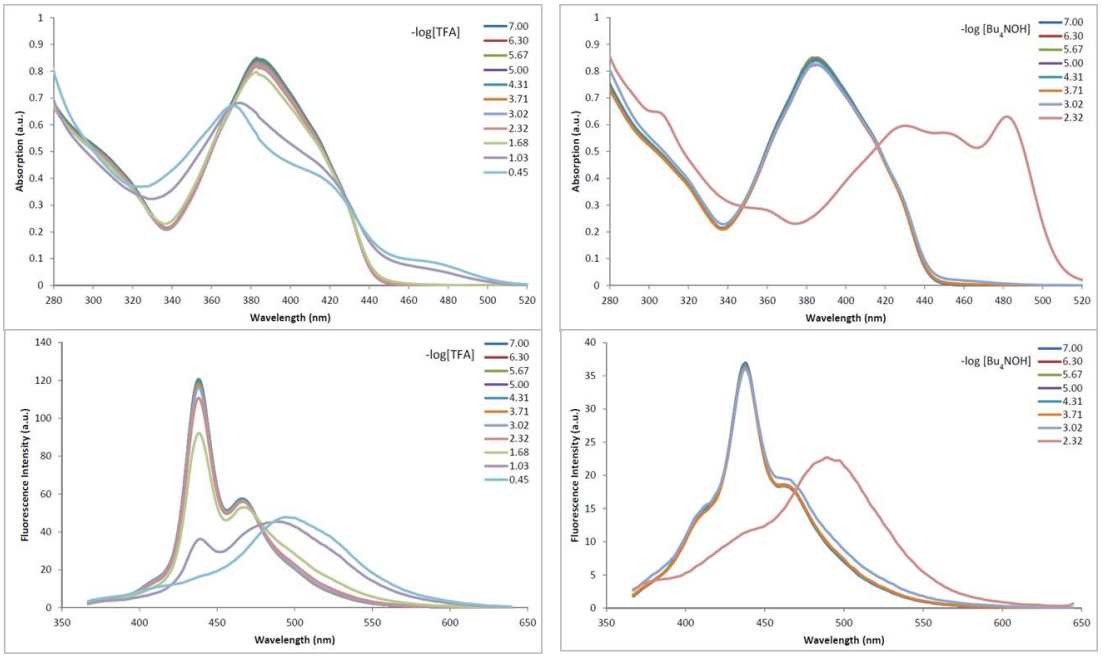

Figure 3.17 Absorption (top) and emission (bottom) spectra for the the TFA titration (left, λ_{exc}=337 nm) and for TBAOH titration (right, λ_{exc}=340 nm) of **24d**.

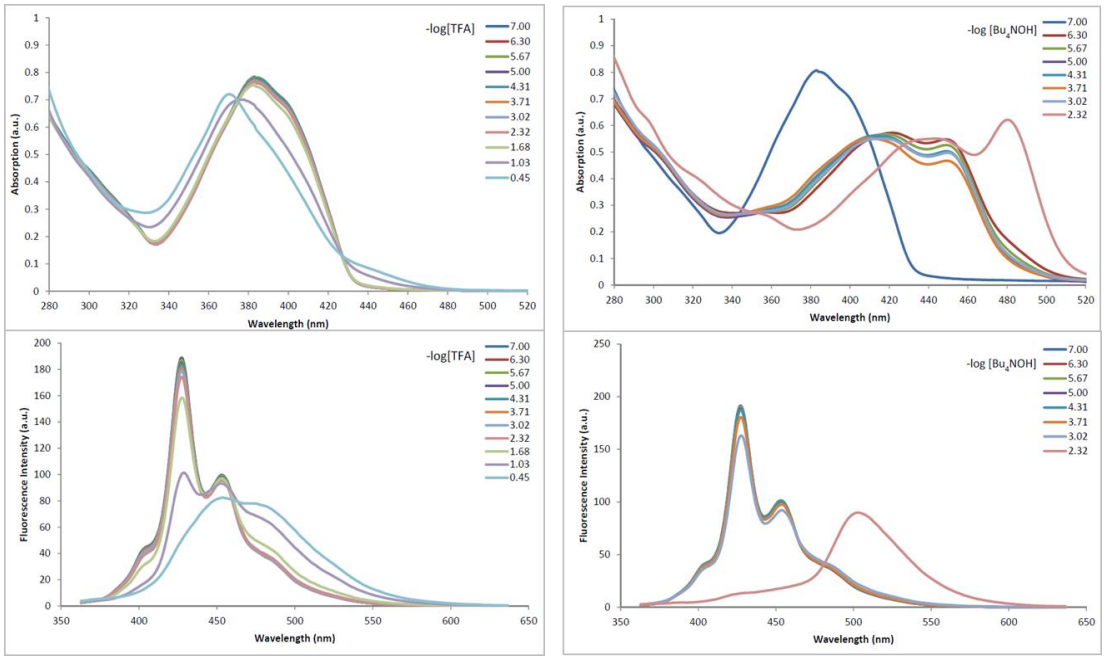

Figure 3.18 Absorption (top) and emission (bottom) spectra for the the TFA titration (left, λ_{exc}=333 nm) and for TBAOH titration (right, λ_{exc}=333 nm) of **24e.**

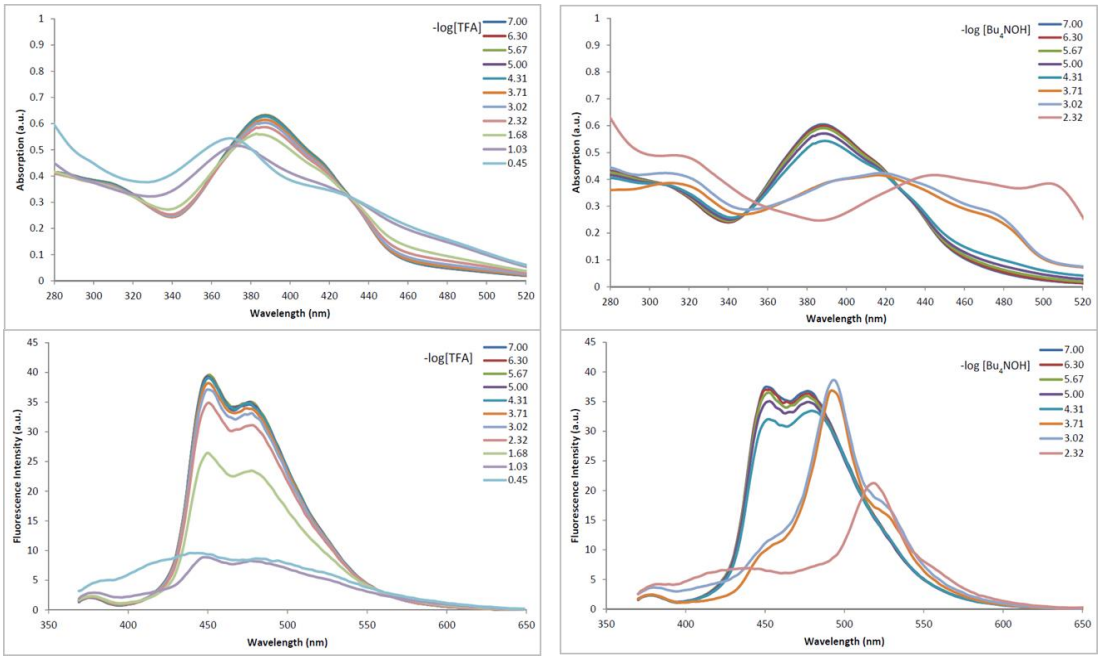

Figure 3.19 Absorption (top) and emission (bottom) spectra for the the TFA titration (left, λ_{exc}=339 nm) and for TBAOH titration (right, λ_{exc}=340 nm) of **24f.**

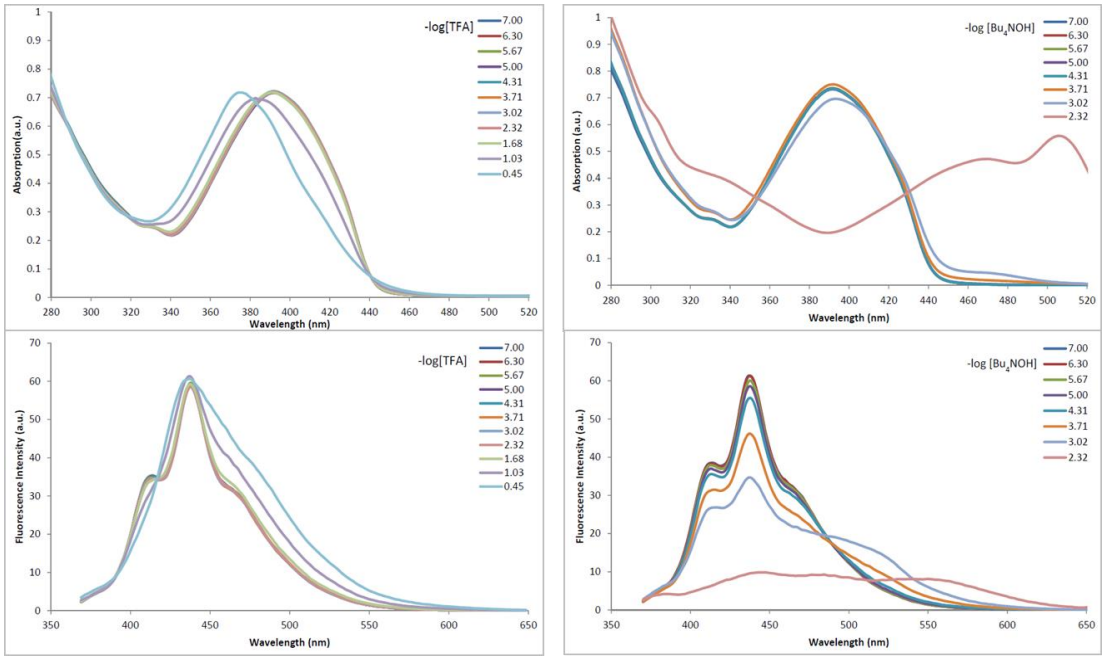

Figure 3.20 Absorption (top) and emission (bottom) spectra for the the TFA titration (left, λ_{exc}=339 nm) and for TBAOH titration (right, λ_{exc}=340 nm) of **24g.**

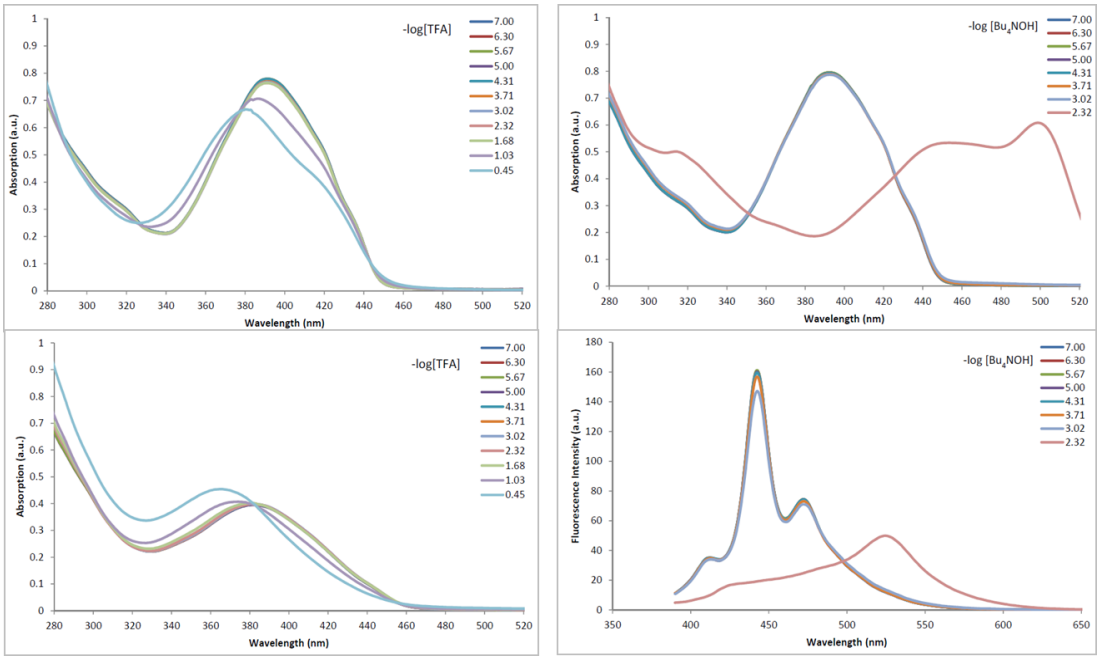

Figure 3.21 Absorption (top) and emission (bottom) spectra for the the TFA titration (left, λ_{exc}=339 nm) and for TBAOH titration (right, λ_{exc}=350 nm) of **24h.**

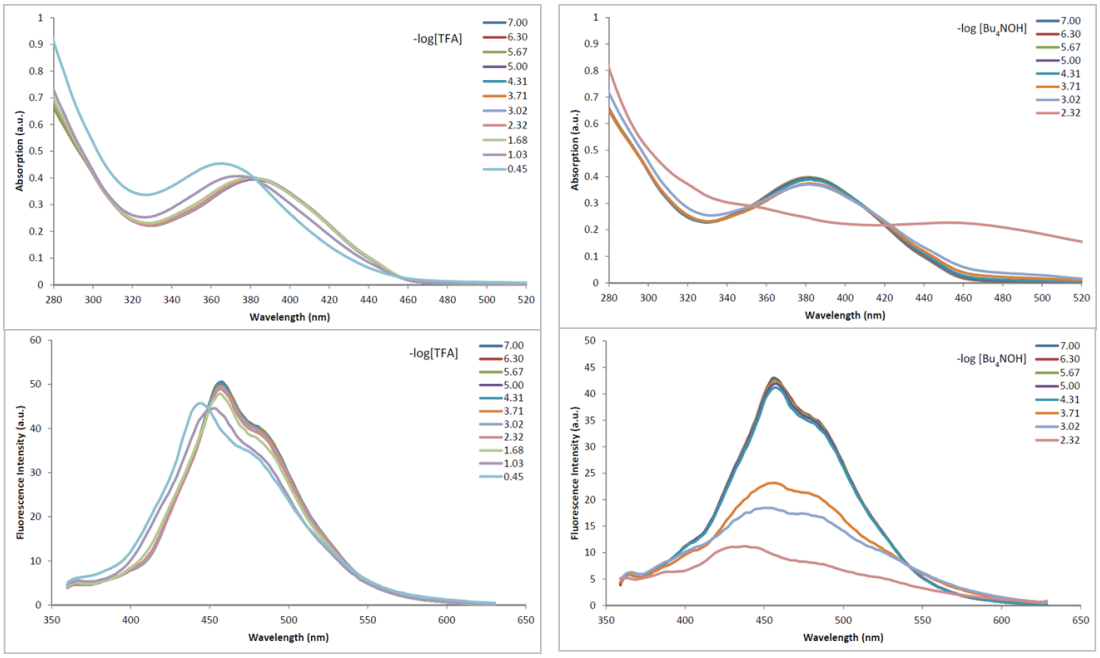

Figure 3.22 Absorption (top) and emission (bottom) spectra for the the TFA titration (left, λ_{exc}=330 nm) and for TBAOH titration (right, λ_{exc}=340 nm) of **24i.**

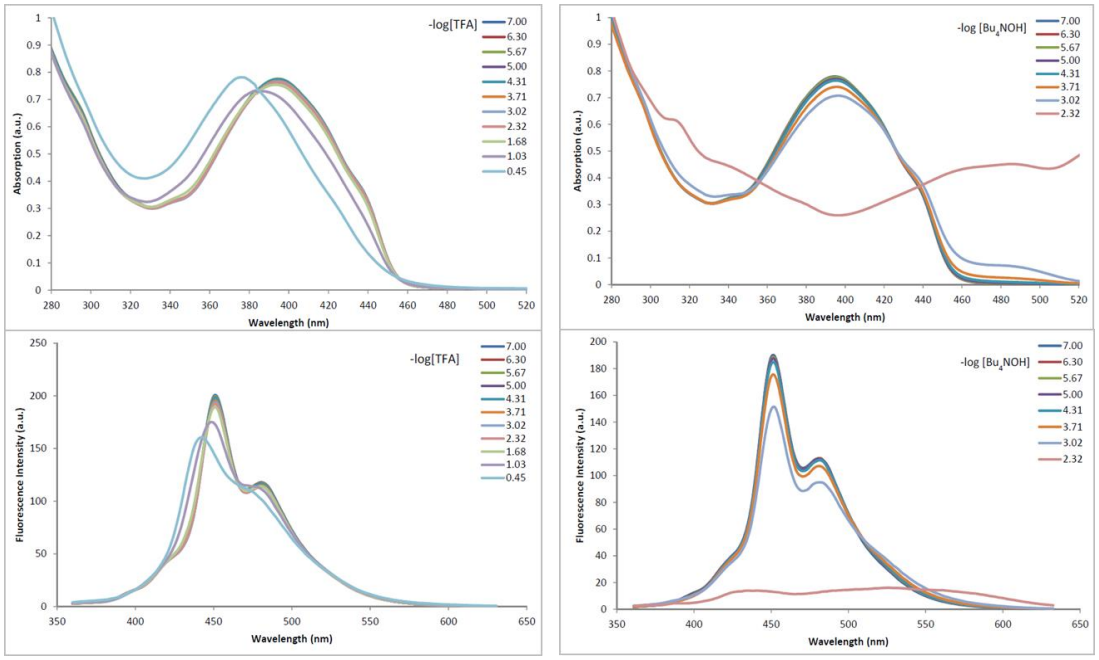

Figure 3.23 Absorption (top) and emission (bottom) spectra for the the TFA titration (left, λ_{exc}=330 nm) and for TBAOH titration (right, λ_{exc}=331 nm) of **24j.**

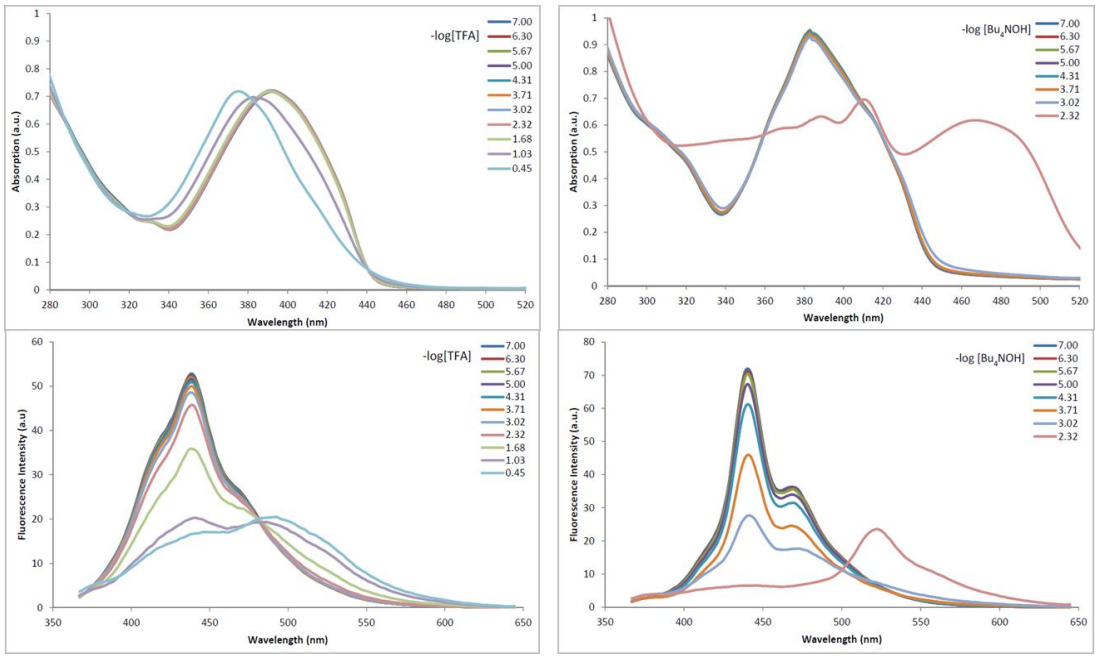

Figure 3.24 Absorption (top) and emission (bottom) spectra for the the TFA titration (left, λ_{exc}=337 nm) and for TBAOH titration (right, λ_{exc}=337 nm) of **24l.**

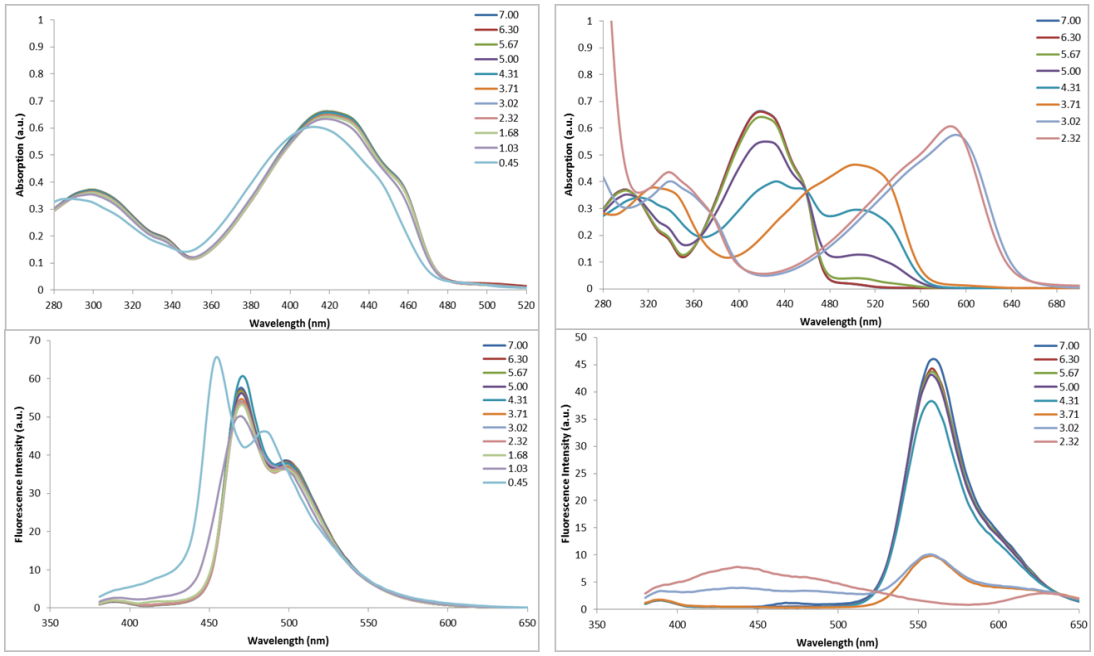

Figure 3.25 Absorption (top) and emission (bottom) spectra for the the TFA titration (left, λ_{exc}=351 nm) and for TBAOH titration (right, λ_{exc}=350 nm) of **24m.**

3.4.5 Sensing of Anions in Organic Media with Cruciform 24m

Rapid recognition of analytes was accomplished utilizing digital photography of emission colors. From each of the digital photographs of emission colors, representative 75×75 pixel segments were cut out using Corel PHOTO-PAINT X5 and arranged into a panel of emission colors. The emission color photographs of cruciform **24m** (10^{-5} M solutions) upon exposure to excess analytes (2 g L^{-1}) were taken under visible light (two left columns) and UV lamp excitation ($\lambda_{excitation}$=365 nm; shutter speed 1/10 s–two right columns) in THF and DMSO (Figure 3.8, left).

Ten anions were analyzed using the methodology developed by Bunz. Using Colour Contrast Analyser software, *R*(ed), *G*(reen) and *B*(lue) values were extracted from for each analyte under each set of conditions. Therefore, each analyte was assigned 12 numbers: *R*, *G* and *B* values for each of the four conditions. To evaluate the correlation between the R/G/B values of different analytes, the relative standard deviations σ was calculated. For arbitrary analytes **A1** and **A2**, this $\sigma_{\mathbf{A1@A2}}$ was defined as:

$$\sigma'_{A1@A2} = \sqrt{\frac{\sum_{cond.}^{i}(R_{A1}-R_{A2})^2+(G_{A1}-G_{A2})^2+(B_{A1}-B_{A2})^2}{3^*i}}$$

Figure 3.26 plots relative standard deviation value of any arbitrary analyte pair describing the difference between all analytes.

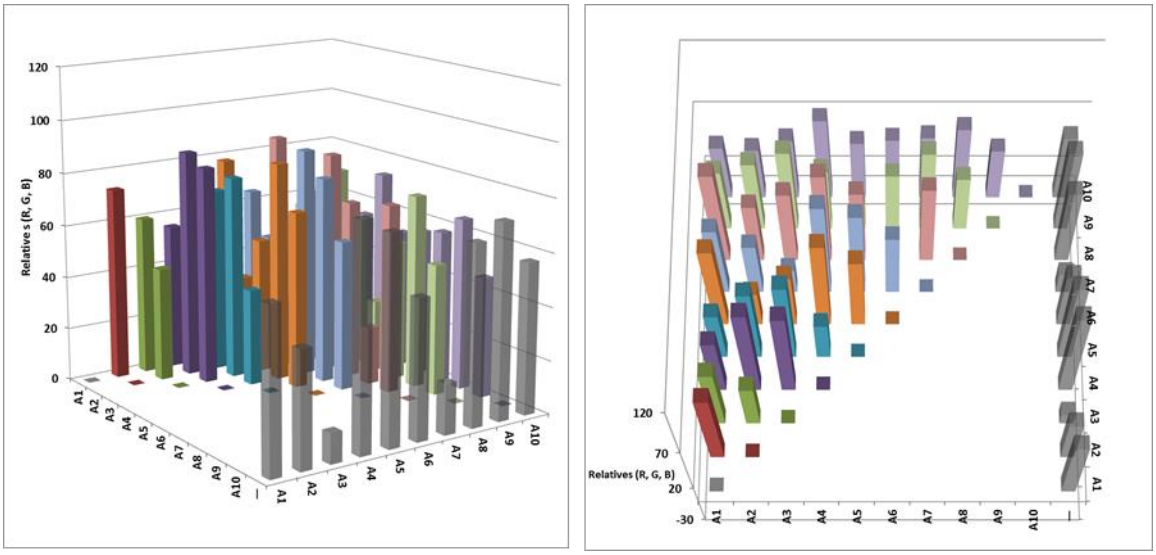

Figure 3.26 The correlation diagram shows standard deviations of R/G/B values for analytes A1–A10 (summed over four conditions−two solvent with and without UV lamp irradiation), relative to all other analytes. The anions in the order listed above were labeled corresponding to A1−A10. The semi-transparent bars in the row marked with "—" indicate standard deviations relative to the blank solution of **24m**, summed over all four conditions.

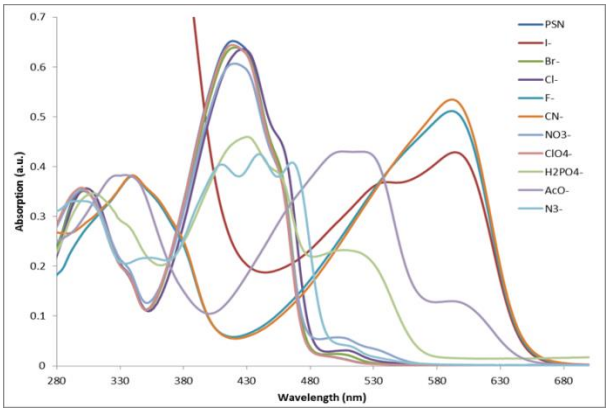

Figure 3.27 UV-Vis response of cruciform **24m** to addition of 50 equiv. of 10 different anions in THF.

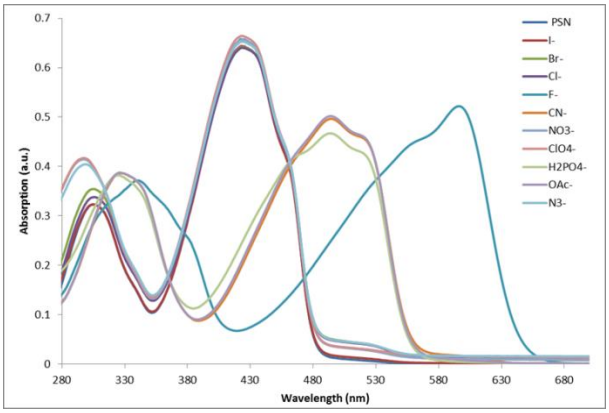

Figure 3.28 UV-Vis response of cruciform **3** to addition of 50 equiv. of 10 different anions in DMSO.

3.4.6 Sensing of Anions in Aqueous Organic Media Using Cruciform 24m

Rapid recognition of analytes was accomplished utilizing digital photography of emission colors: panel of emission color (Figure 3.11) of **24m** (10^{-5} M solutions) upon exposure to excess analytes (2 g L^{-1}) under visible light (two left columns) and UV lamp excitation ($\lambda_{excitation}$=365 nm; shutter speed 1/10 s–two right columns) in aqueous solutions with 20% water.

Utilizing the method mentioned in a previous section, we obtained Figure 3.29 which plots relative standard deviation value of any arbitrary analyte pair describing the difference between all analytes.

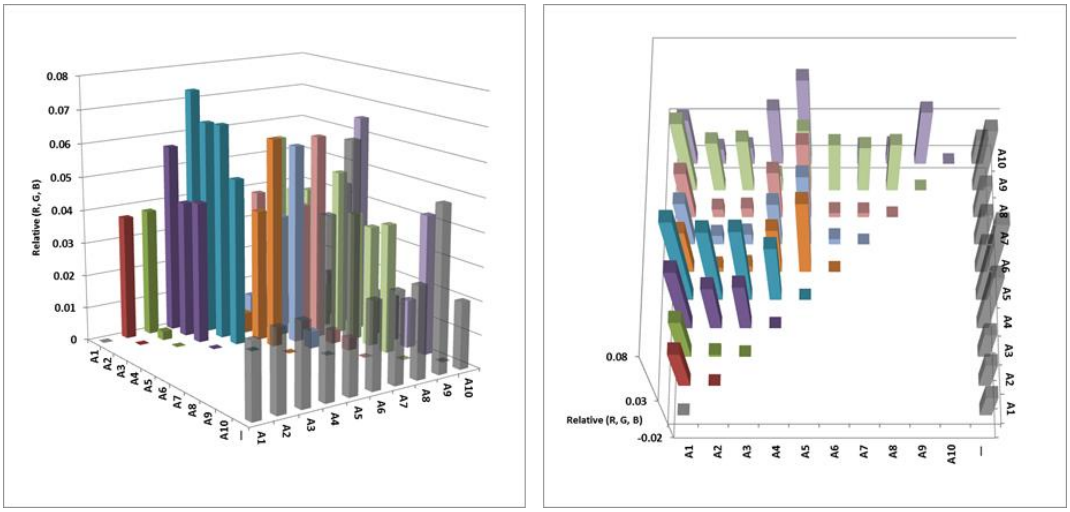

Figure 3.29 The correlation diagram shows standard deviations of R/G/B values for analytes A1–A10 (summed over six conditions−three mixed solvent with and without UV lamp irradiation), relative to all other analytes. The semi-transparent bars in the row marked with "—" indicate standard deviations relative to the blank solution of **24m**, summed over all six conditions.

Chapter Four

Synthesis, Characterization of Precursors for Noncovalent Organic Framework

4.1 Introduction

Porous materials, such as metal-organic frameworks (MOFs), covalent organic frameworks (COFs), and porous organic polymers (POPs),[149] have numerous applications in the fields of energy and catalysis. Among these fascinating structures, porous materials composed of discrete molecules are still quite rare.[150] MOFs are constructed from coordination bonds of metal ions or clusters and an organic linker, acting as "infinite" one-, two-, or three-dimensional structures.[151] COFs are built from light elements (H, B, C, N, and O) and held together by strong covalent bonds.[152] POPs are a class of highly crosslinked amorphous polymers containing nanopores, which have recently appeared as a versatile platform for catalyst development.[149] Discrete molecules forming a porous molecular crystal framework need to be connected in the solid state exclusively through weak, noncovalent interactions such as hydrogen bonds.[153] In the solid state, molecules generally tend to closely pack, leaving no significant empty space between the molecules; it is because of this that porous molecular crystals are very atypical.

MOFs and COFs are characterized by large internal surface areas, permanent porosity, high thermal stability, and modular synthesis which allow tunability over geometry of metal cluster, size, structure, and thermal stability. Furthermore, the possibility for postsynthetic modifications[154] creates even greater synthetic variability. These properties make them important in applications like gas storage,[155] molecular

separation,[156] catalysis,[157] sensing,[158] and drug delivery.[159] In comparison to MOFs and COFs synthesis, the porous molecular crystals assembly is hard to predict, making these materials difficult to design and produce;[160] furthermore, even when a small molecule can be organized into a porous structure, such structures usually collapse when the guest or solvent molecules are removed. However, once these materials are successfully formed by proper arrangement and efficient noncovalent bonding, their lightweight, porous, metal-free structures can have significant advantages over MOFs and COFs. For example, extended crystalline materials, such as MOFs and COFs, are impossible to dissolve without decomposition, and their solution-phase characterization and processability are essentially impossible due to their poor solubility. Porous molecular crystals can be dissolved in select solvents, allowing their easy purification and solution characterization, as well as easy regeneration through simple recrystallization.[161]

In the past ten years, this class of material was extensively studied by Cooper,[162] Mastalerz,[163] Chen,[161,164] and others.[165,166,167] The most common interactions observed in porous molecular crystals are hydrogen bonding,[163b] [$\pi\cdots\pi$],[163d] van de Waals,[168] and hydrophobic/hydrophilic interactions[169].[170] There are multiple ways that porous materials can be assigned into a subgroup depending on the specific concerns, such as pore size, degree of long-range order, the relative strength of the bonds between the atomic or molecular building blocks, or functional properties.[171] Among them, the most basic classification is their pore diameters in the ranges of microporous (poresize <2 nm), mesoporous (2–50 nm), and macroporous (>50 nm). In this chapter, porous molecular

crystals will be discussed as intrinsically porous organic crystals and extrinsically porous organic crystals.

4.1.1 Intrinsically Porous Organic Crystals

Intrinsically porous organic crystals are engineered by discrete molecules having permanent covalent cavities themselves in view of isolation, these molecules arrange in long-range order rendering an extended porous structure. The more prevalent motifs found in these individual building blocks were the macrocycle or the molecular capsule.[162d]

An early example in this category was the hexagonal closely packed arrangement of a calix[4]arene macrocycle that was found to occlude small, highly volatile molecules in its lattice voids (Figure 4.1).[172] Hydrogen bonds between adjacent OH groups at the lower rim hold the cone conformation of calix[4]arene, and three cones arrange to form an approximately spherical trimer (Figure 4.1b). These molecule spheres then pack in a fashion that generates two parallel and oblique channels linking interstitial voids. The van der Waals forces retained the stabilization of adsorbates in the solid matrix, allowing this material to capture a range of Freons and methane, not only well above their normal boiling points, but also at relatively high temperatures and low pressure, as exemplified by CF_4@calix[4]arene complex, which was found to be stable up to 240 °C.

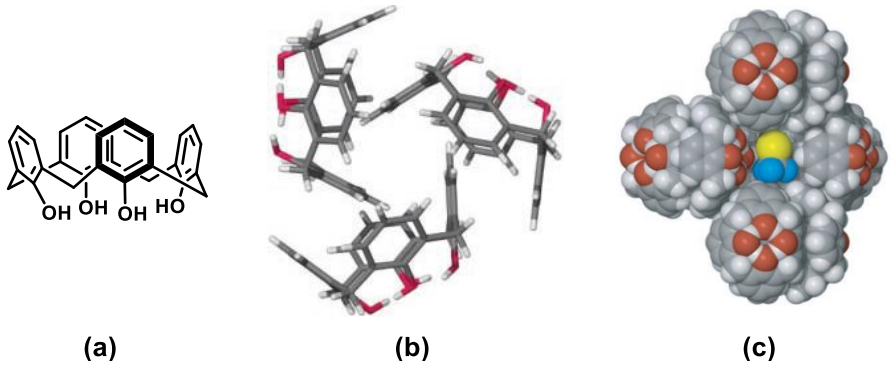

Figure 4.1 (a) Chemical structure of calix[4]arene. (b) Capped-stick representation of its crystal structure viewed along the threefold axis. (c) Space-filling representation of CF_3Br@calix[4]arene viewed perpendicular to the crystallographic *c* axis. Element colors: C, gray; H, white; O, red; F, blue; Br, yellow.

Macrocycle arrangement within crystal generates can generate supramolecular nanotubes, which was demonstrated in the case of cucurbit[6]uril and bis-urea macrocycles (Figure 4.2) synthesized by Kim[173] and Shimizu[174] groups, respectively. The cucurbit[6]uril is a hexamic cavitand produced by acidic condensation of paraformaldehyde and glycoluril, and its cavity is highly hydrophobic. In the solid state, each macrocycle communicates with its neighbors through [C–H···O] hydrogen bonding and van der Waal interactions, to afford a honeycomb-like structure with remarkable stability and porosity (Figure 4.2b). 1D channels established by hexagonal arrangement of cucurbit[6]urils show useful application in the storage of gases, in particular acetylene. The larger bis-urea macrocycles were held together mainly by hydrogen bonding and π-stacking of rigid spacers (Figure 4.2a,b) to a form nanotubular structure which exhibits reversible binding affinity toward the acetic acid guest,[174a] ability to adsorb CO_2, and

preferential binding of *p*-xylene from a mixtrure of xylene isomers.[174b] Alternative examples of porous materials constituted from macrocycles[175] were explored and were used for gas adsorption or other applications.

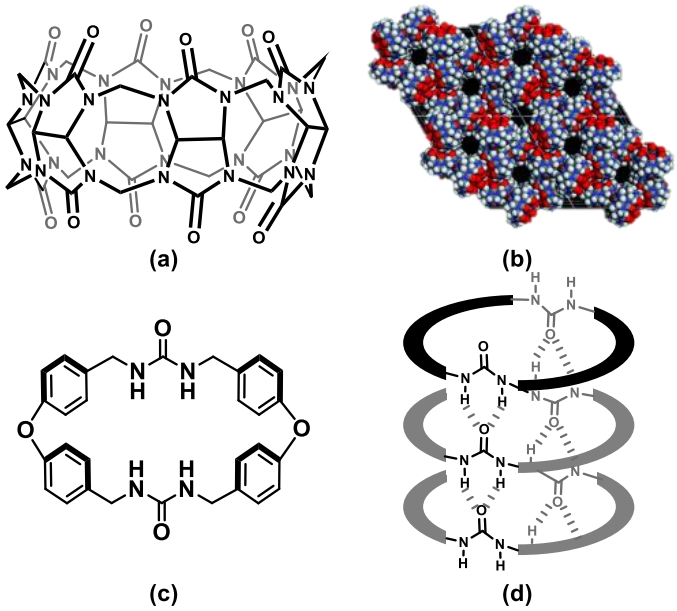

Figure 4.2 (a) Chemical structure of cucurbit[6]uril.[176] (b) X-ray crystal structure of as-synthesized cucurbit[6]uril. (c) Chemical tructure of a bis-urea macrocycle. (d) The self-assembly of bis-urea macrocycles into a nanotube.

Cooper and colleagues reported the first case in which tetrahedral covalent organic cages were assembled into microporous materials in 2009.[162] General synthetic strategy used to produce these organic cages involved [4+6] cycloimination reactions between 1,3,5-triformylbenzene and corresponding vicinal diamines. By alternating the functional substituent of molecular cage, the three-dimensional stacking between the cage windows could be changed to yield either permanently porous or non-porous structures;

for the most part, new designs were integrated carefully by atomistic and solid-state molecular dynamic simulations. The porosity in these crystalline materials is attributed to the molecular voids in the cages (intrinsic porosity) and the inefficient packing of tetrahedral cages (extrinsic porosity), reflecting that both intrinsic and extrinsic porosity can exist in the same porous molecular crystal. Taking cage **CC3** (Figure 4.3) as an example, the window-to-window arrangement due to interlocking of cyclohexyl groups resulted in an interconnected 3D diamondoid homochiral pore network (Figure 4.3c) which is highly thermally stable. Interestingly, some of imine cages can experience morphology changes in response to chemical stimuli under different recrystallization conditions[162e,f] or single-crystal-to-single-crystal transformation when the trapped mother liquor was evacuated.[162g] A mix-and-match strategy was successfully implemented to generate a new porous single-phase molecular co-crystal from two different cages, which is an encouraging strategy to produce functionalized molecules with two incompatible chemical entities by co-crystalization.[162a] Moreover, with the advantages in solution processing compared to MOFs, cage **CC3** originated from 1,3,5-triformylbenzene was able to separate a common aromatic feedstock (mesitylene) from its structural isomer (4-ethyltoluene). Based on the fact that 1,3,5-triformylbenzene was synthesized from mesitylene, the selective separation can be attributed to the similarity between host and guest[177]. Cage **CC3** is a rigid enough to maintain $\pi\cdots\pi$ stacking between mesitylene and the **CC3** face. On the other hand, vapor adsorption study shows that cages **CC3** in the solid state can trap linear 4-ethyltoluene, but reject mesitylene. In the solid state, imine bonds are not broken by hydrolysis, preventing mesitylene diffusion.

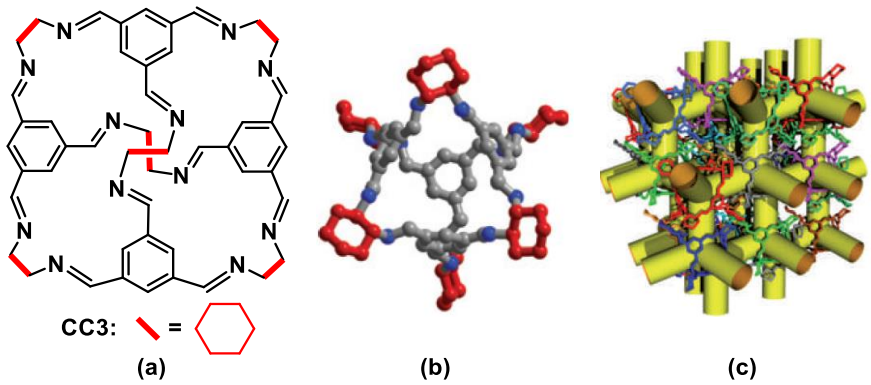

Figure 4.3 (a) Chemical structure of cage **CC3**. (b) Crystal structure of an individual molecule. (c) Crystal packing of tetrahedral imine cages.

Utilizing similar reversible imine bond or boronic ester formation, Mastalerz and coworkers constructed a series of intrinsically porous cages.[163] The adamantoid cage compound (Figure 4.4a) was constructed by [4+6] imine cage formation between four triaminotriptycenes and six salicylic dialdehydes, and it showed selective adsorption of CO_2 versus methane with a weight selectivity of 10 to 1. This cage is also ready for post-modification planning like nucleophilic substitution and reduction to afford new structures with methoxy and amine-functionalization, respectively.[163d,h] Other than [4+6] cage formation, [4+4] reaction between four triaminotriptycenes and four trissalicylaldehydes leads to an amorphous cage molecule.[163i] Recently, they reported a permanent mesoporous organic cage with an exceptionally high surface area (BET surface area of 3,758 $m^2\ g^{-1}$).[163f] This [12+8] cage (Figure 4.4b), possessing 24 boronic esters, resulted from the combination of twelve triptycene tetraols and eight triboronic acids (94% yield). Its single-crystal structure allowed estimation of the inner and outer

diameters at 2.6 and 3.1 nm, respectively. Moreover, crystalizing one of these monomer cages unprecedentedly leads to the giant shape-persistent porous cage catenane with high surface area contributed by defined micropores and mesopores inside its structure. This is the first example of one-step 96-fold condensation to form porous molecular catenane.[163e]

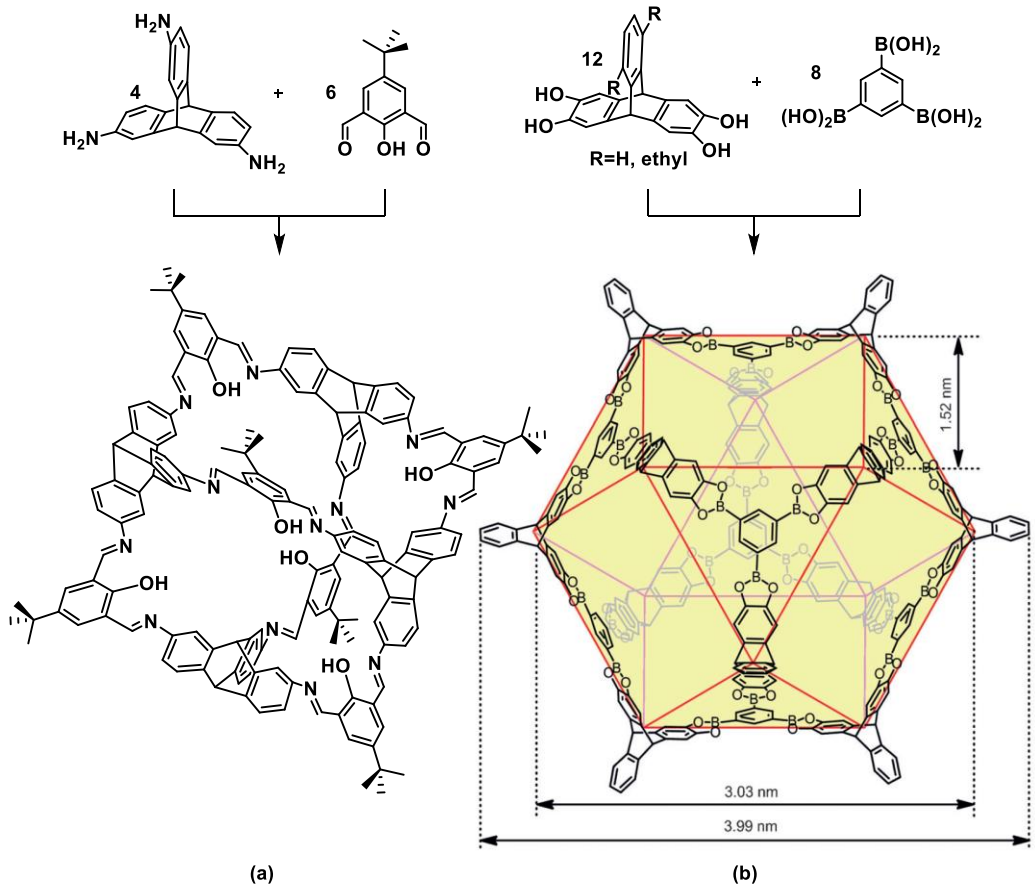

Figure 4.4 (a) Synthesis of [4+6] imine cage compound. (b) The synthesis of cuboctahedral [12+8] boronic ester cage.

4.1.2 Extrinsically Porous Organic Crystals

Extrinsically porous organic crystals have porosity established from inefficient packing of individual molecule generating pores with long-range order in the solid state, with the molecule itself being inherently nonporous.

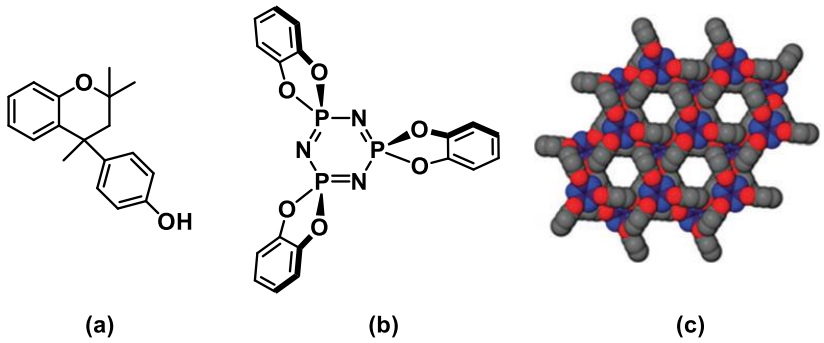

Figure 4.5 (a) Chemical structure of Dianin's compound. (b) Chemical structure of TPP. (c) Hexagonal porous phase of TPP.[178]

One of the earliest examples for this category was Dianin's compound–4-(4'-hydroxyphenyl)-2,2,4-trimethylchroman (Figure 4.5a) which was synthesized in 1914.[179] Its trigonal structure can form inclusion complexes with many molecules in solution[180] and can adsorb a large variety of guests such as Ar, Kr, Xe, CO_2, CH_4, C_2H_6, C_3H_8, C_4H_{12}, *iso*-C_4H_{12}, and neo-C_5H_{12} in its unsolvated form.[181] The crystal structure of this molecule is composed of a columnar arrangement of cages which are formed by six host molecules held together by hydrogen bonding. The forming cage void has an hourglass shape with maximum 11 Å in length and maximum and minimum diameters of 6.5 Å and 4.4 Å, respectively; however, the guest molecules enter the void only through the interconnecting channels of minimum diameter = 2.5 Å, which is smaller than the kinetic

diameter of adsorbates in general. Therefore, cooperative diffusion mechanism involving dynamic processes is a good rationalization.[182]

Tris-o-phenylenedioxycyclotriphosphazene (TPP) featuring a phosphazene (P_3N_3) core with three orthogonal catechol rings (Figure 4.5b) has been well-known to act as a host for many guests such as Ar, N_2, O_2, H_2, CH_4, and CO_2; selective adsorption was found in the case of CO_2 and CH_4. TPP's crystal structure with one-dimension channels of 6 Å in diameter (Figure 4.5c) were first confirmed by Sozzani *et al.*[183] Furthemore, the a proper strategy, evacuation of the solvent molecule included at relatively low temperature can result in a guest-free metastable form instead of the collapsed host lattice–dense-pack monoclinic system.

The hydrogen bonds were extensively used in the self-assembly of organic frameworks, which is reflected from hydrogen-bonded organic frameworks (HOFs) synthesized by Chen[161,164] and Zhong[165] group. The first example of microporous hydrogen-bonded organic framework—HOF-1 (Figure 4.6a) was reported by the Chen group; they employed a 2,4-diaminotriazine group as a sticky end group, which launches multiple hydrogen bonds, forming permanently porous material with one-dimensional channels. This flexible scaffold shows extraordinarily selective adsorptive separation of C_2H_2 and C_2H_4 at ambient temperature. An extended version of HOF-1, dubbed HOF-4 (Figure 4.6b) was also synthesized and shown to be a six-fold interpenetrated framework (Figure 4.6c) that tunes the channel size and allows C_2H_4/C_2H_6 separation applications. Zhong's group also contributed to the HOFs library with very stable HOF-8 fabricated from a N^1,N^3,N^5-tris(pyridin-4-yl)benzene-1,3,5-tricarboxamide (TPBTC) building block (Figure 4.6d). This material is remarkably stable in water and common organic solvents and displays high CO_2

adsorption as well as highly selective CO_2 and benzene adsorption at ambient temperature.

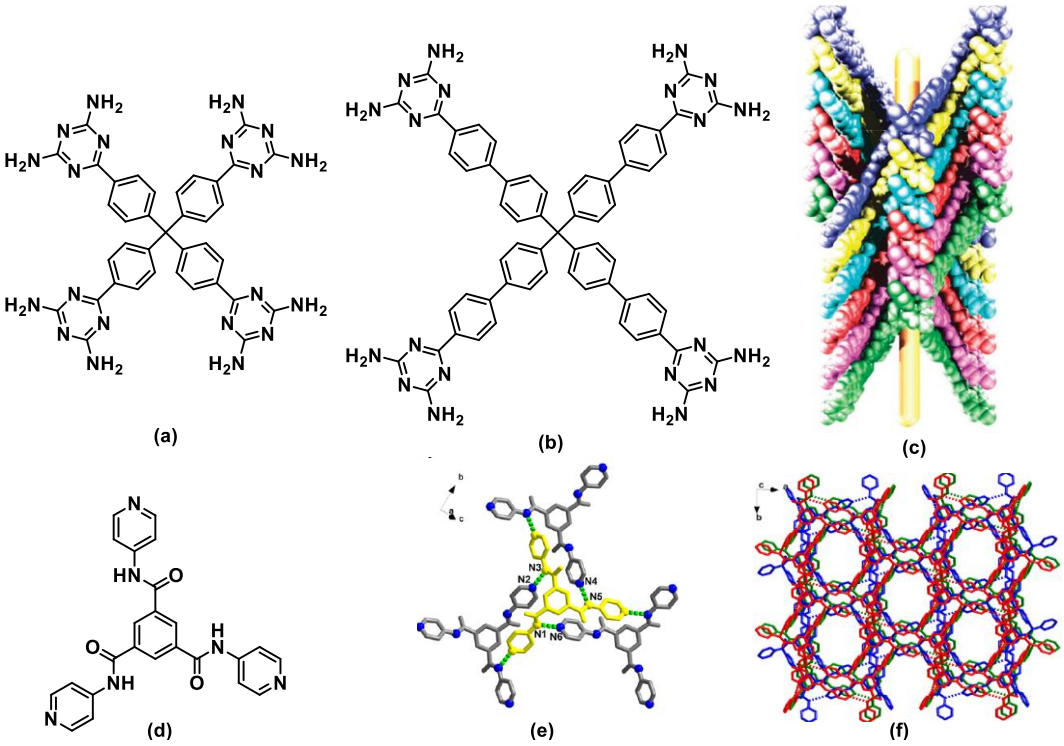

Figure 4.6 (a) Chemical structure of HOF-1. (b) Chemical structure of HOF-4. (c) Six-fold interpenetrated frameworks of HOF-4. (d) Molecular structure of organic building block TPBTC. (e) H-bonding interactions observed in HOF-8. (f) 3D supramolecular microporous structure of HOF-8.

Mastalerz's group also made advances in the area of extrinsically porous crystals. Their extrinsically porous cage utilized benzimidazolone units which could provide directed H-bonds forming a ribbon-like motif (Figure 4.7a) and incorporated into a rigid triptycene scaffold. An extrinsically permanent porous crystal was formed, and was characterized by one-dimensional pore channel and a very high BET surface area of

2,796 $m^2 g^{-1}$—the highest recorded for extrinsic molecular cages so far (Figure 4.7b).[184] The porous solid was activated by multiple solvent exchange and showed preferable adsorption toward CO_2 than CH_4.

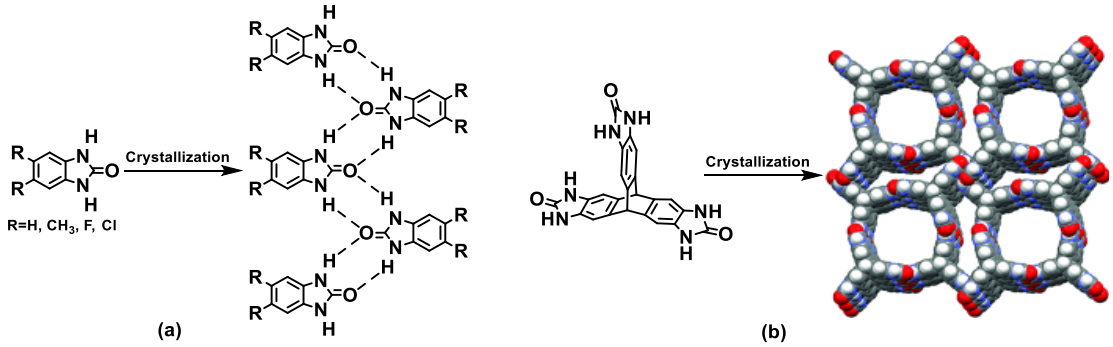

Figure 4.7 (a) Formation of ribbon-like structures of 4,5-disubstituted benzimidazolones by H-bonding. (b) Single crystal structure of porous molecular crystal made from triptycenetrisbenzimidazolone. Element colors: C, gray; H, white; O, red; N, blue.

Our group recently has succeeded in synthesis and characterization of a fluorinated trispyrazole (Figure 4.8a) that organizes into a robust, extrinsically porous noncovalent organic framework (nCOF) with an accessible surface area of 1,159 $m^2 g^{-1}$.[185] This structure (nCOF-1) is held together by a combination of hydrogen bonding between the terminal pyrazole ring and [π···π] stacking between the electron-rich pyrazoles and electron-poor tetrafluorobenzenes (Figure 4.8). This material is lightweight, thermally and hydrolytically stable (structure stable to at least 250 °C), and is a superb adsorbent for hydrocarbons and their halogenated derivatives, many of which are potent greenhouse gases or inhalation anesthetics—enflurane, isoflurane, sevoflurane, halothane, and methoxyflurane.[186]

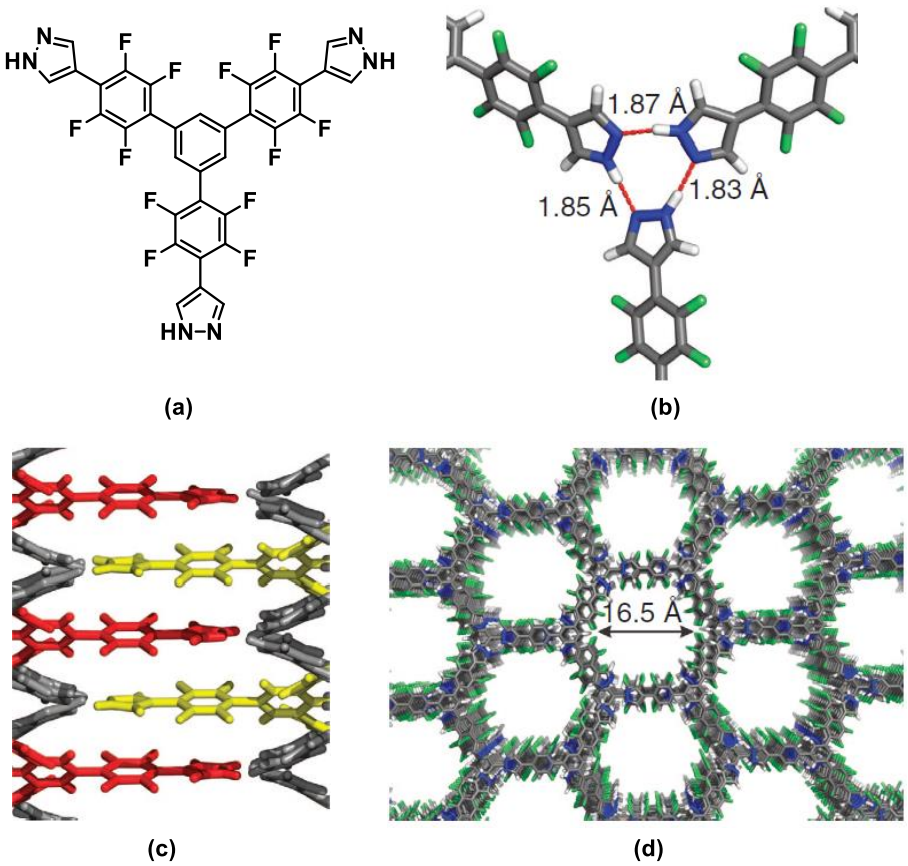

Figure 4.8 (a) Fluorinated trispyrazole ligand. Three pyrazoles come together in each of the layers (b) forming a triplet of hydrogen bonds. (c) Each pyrazole engages in [π···π] stacking interactions with six of its neighbours. Overall, a hexagonal network results, with infinite fluorine-lined channels protruding throughout the structure along the crystallographic *c* axis (d).

In this chapter, I will discuss the synthesis of new precursors to nCOFs and the study of their self-assembly into an isoreticular series of nCOFs. The goal of this project was to dissect the relative importance of [π···π] stacking and hydrogen bonding in the formation of this robust porous structure. A battery of new ligands was synthesized using

C–H functionalization chemistry.[187] Their design was developed based on the first successful ligand by either replacement of components, alteration of the number of arms, and changes in arm length.

4.2 Result and Discussion

4.2.1 Synthesis of Precursors for Noncovalent Organic Framework

4.2.1.1 Synthesis of Bent Precursors

As described above, our target was to diversify the structure of stock ligands inspired by nCOF-1. We first synthesized symmetrically bent **31** (Scheme 4.1) and asymmetrically bent **37** (Scheme 4.2), which are similar in geometry to the trigonal nCOF-1, but with one arm eliminated. Employing an analogous method developed by Daugulis'group[187] we were able to prepare structures **31** and **37**. Synthesis of **31** is accomplished by palladium-catalysed coupling of 1,3-diiodobenzene with an excess of perfluorinated aromatic **29**[187] followed by replacement of the trityl (Ph_3C–) group with a Boc protecting group. In the last step, the general method applying to all precursors for de-protection of Boc and generating NH free pyrazole was a solvothermal method in proper solvent, and this step will be presented only in the cases when single crystals formed after solvothermal treatment. Single crystals of compound **32** were obtained after heating of a solution of **31** in *N*,*N*-dimethylformamide (DMF) and MeOH for 1 day at 80 °C.

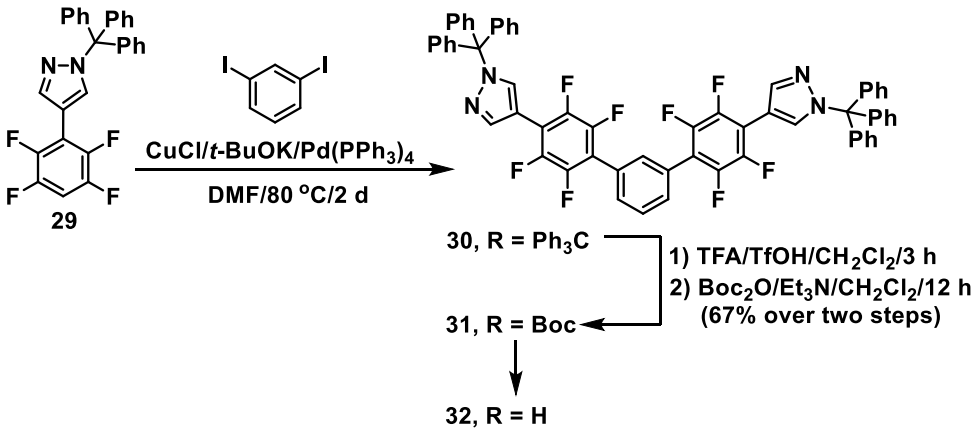

Scheme 4.1 Synthesis of a symmetrically bent potential precursor to nCOF.

The first step in the synthesis of an asymmetrically bent precursor (Scheme 4.2) was conducted by coupling **29** with 3-bromoiodobenzene; thanks to the difference in activity of bromide and iodide, the monocoupled product **33** was furnished. The aryl bromide **33** was then converted to aryl iodide **34** in the presence of NaI, CuI, and *N,N'*-dimethylethylenediamine (DMEDA). The subsequent coupling of **34** with a longer perfluorinated aromatic arm **35**[188] afforded trityl-protected intermediate **36**. Finally, the trityl group was transferred to Boc protecting group in **37**; compound **37** was heated at 80 °C in *N*,*N*-dimethylacetamide (DMA) and EtOH for one day and left at room temperature for one more day to give single crystals of compound **38**.

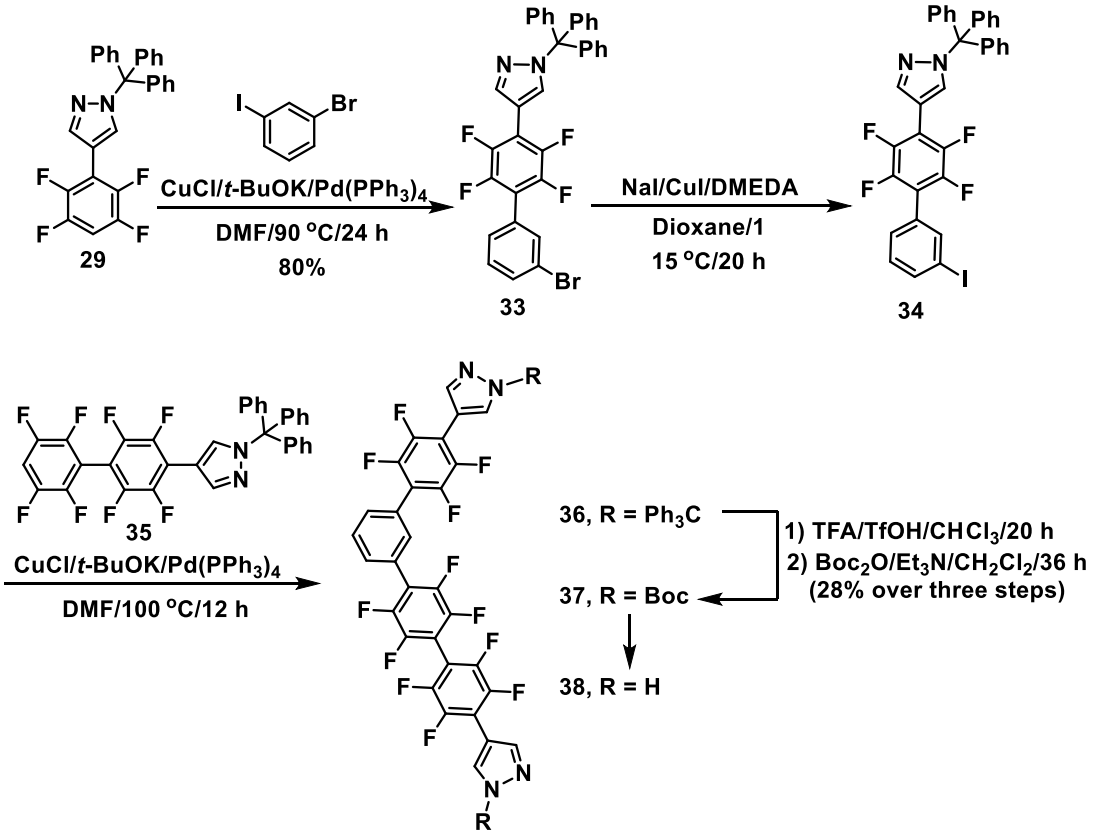

Scheme 4.2 Synthesis of an asymmetrically bent precursor to nCOF.

4.2.1.1 Trigonal Precursors with Alternate Components

We are also interested in establishing new trigonal precursors with alternate components; by this way, we are able to evaluate the relative importance of nCOF-1's components in fabricating porous materials. A new set of precursors, **43** (Scheme 4.3), **48** (Scheme 4.4), and **50** (Scheme 4.5) were successfully synthesized. Compound **43** is derived from nCOF-1 by the replacement of a perfluorinated aromatic ring with an alkyne. The Sonogashira coupling of *N*-trityl pyrazole **39** followed by TMS deprotection to provide terminal alkyne intermediate **41**, which was ready for consecutive Sonogashira coupling with 1,3,5-triiodobenzene to afford **42**. Finally, the trityl group of **42** was

exchanged to a Boc protecting group in compound **43**. Heating of **43** in MeOH at 80 ^{o}C resulted in deprotection of the Boc protecting group, and single crystals of compound **44** were formed.

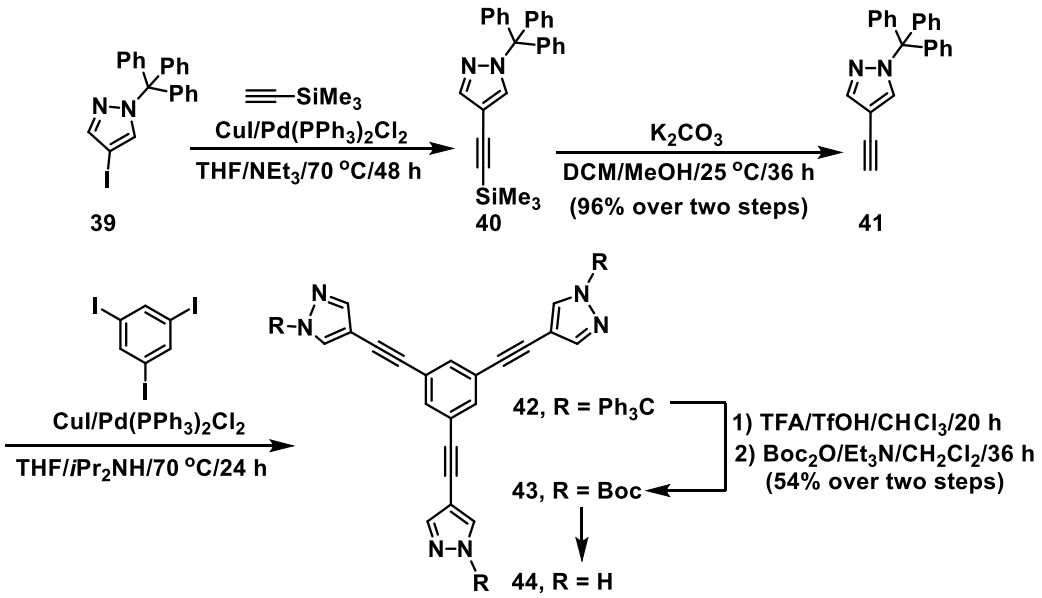

Scheme 4.3 Synthesis of trigonal precursor **43.**

When the perfluorinated benzene in nCOF-1 was substituted by a phenyl ring, we got new ligand **48**, depicted in Scheme 4.4. 1,3,5-tris(*p*-bromophenyl)benzene **45** was functionalized with boronic ester by a Miyaura borylation reaction to generate corresponding boronic ester **46**. Another palladium-catalyzed Suzuki-Miyaura coupling between **46** and iodopyrazole **39** provided *N*-trityl intermediate **47**, which was further converted to the Boc-protected trigonal precursor **48** at the end.

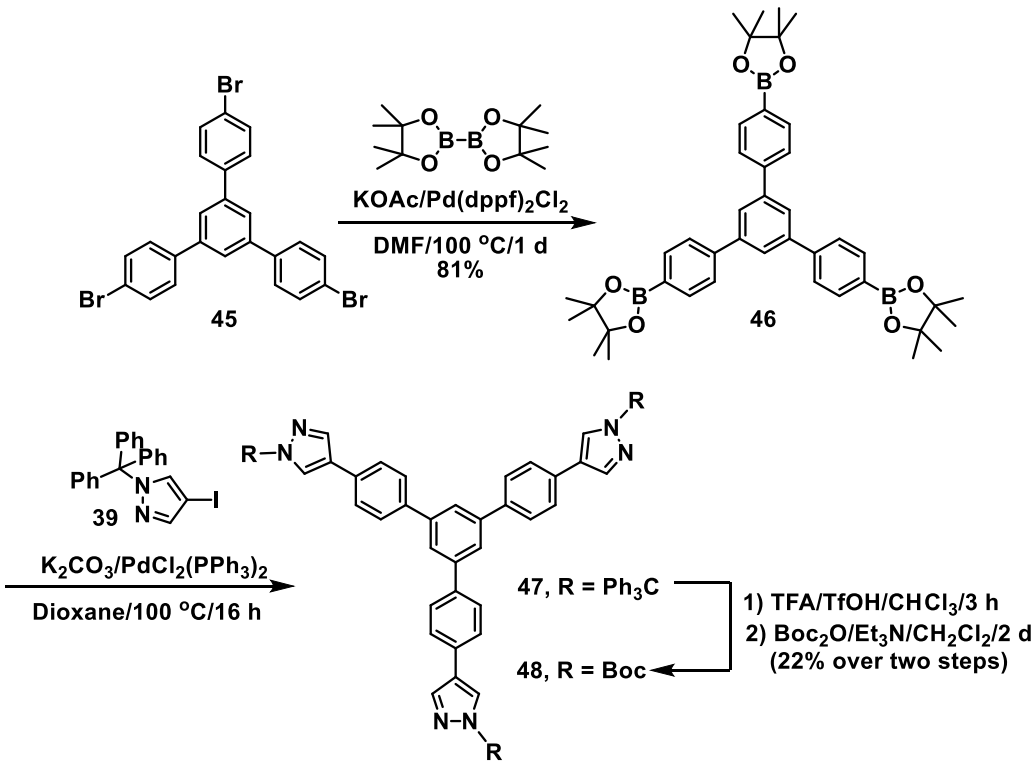

Scheme 4.4 Synthesis of trigonal precursor **48.**

Another new trigonal precursor, compound **50,** in which mesitylene was chosen to replace the phenyl ring core was chosen as the next target. The benzylic position in the new precursor is active and promising for post modification.[189] The synthesis scheme of this compound was similar to the nCOF-1 ligand, but 1,3,5-iodobenzene was replaced by 1,3,5-triiodo-2,4,6-trimethylbenzene in the Scheme 4.5.

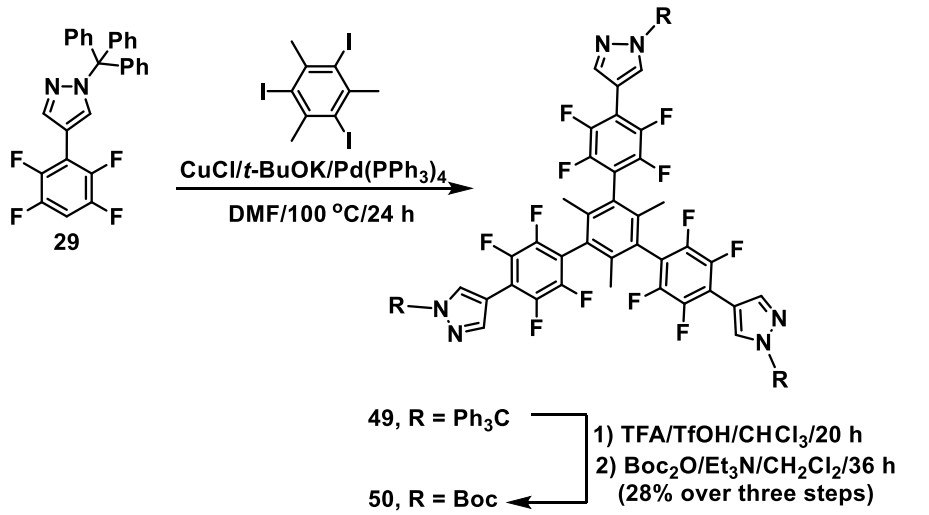

Scheme 4.5 Synthesis of trigonal precursor **50.**

4.2.1.3 Synthesis of Extended Trigonal Precursors

Another set of precursors, whose structures were analogous to nCOF-1 but with longer arms, was also introduced. These scaffolds were designed by adding organic spacers between perfluorinated benzene and pyrazole rings. Dr. Popov were successful in the synthesis of precursor **51** (Scheme 4.6) having one more perfluorinated benzene in its arm. Next, Dr. Chen successfully grew single crystals of Boc-deprotected compound **52** by heating of compound **51** in a mixture of DMF and MeOH at 80 ^{o}C.

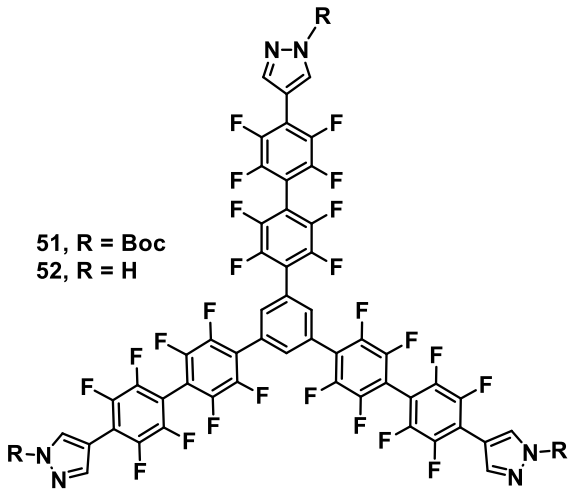

Scheme 4.6 Extended trigonal precursor **51.**

Precursor **56**, featuring an ethynylbenzene spacer between perfluorinated benzene and pyrazole, was synthesized as described in Scheme 4.7. Starting with 1,2,4,5-tetrafluorobenzene, coupling with 1-bromo-4-iodobenzene in the presence of palladium catalyst delivered a mono-coupling product **53**. The structure was extended by Sonogashira coupling at aryl halide position with terminal alkyne **41**, to generate a single arm **54**. Fully trigonal structure **55** was afforded by subsequently coupling of **54** with triiodobenzene. Finally, replacement of the trityl group by a Boc protecting group produced precursor **56**, ready for solvothermal processing.

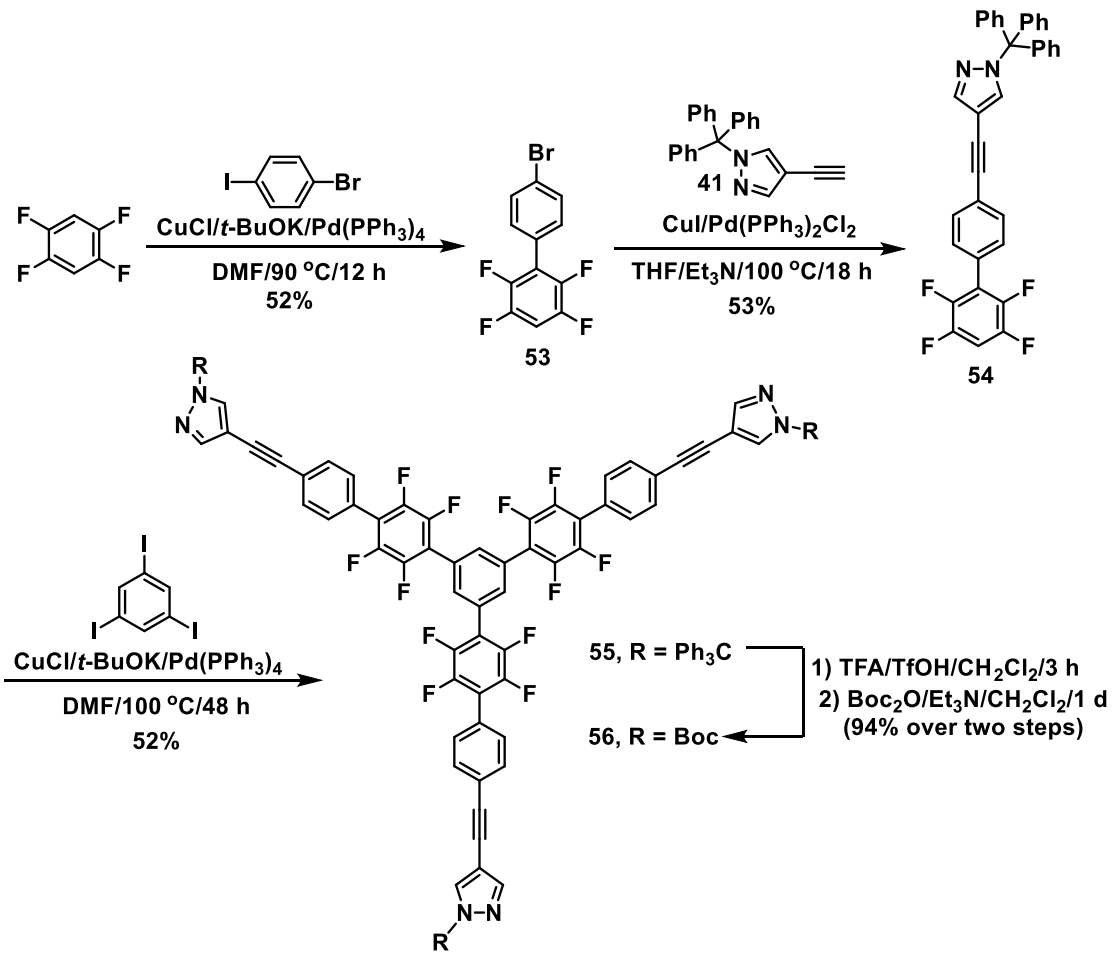

Scheme 4.7 Extended trigonal precursor **56.**

4.2.2 Crystal Structures of Precursors for Noncovalent Organic Framework

Although a great deal of effort was put into growing crystals of all the precursors in hand, we were to get single crystals of only **32**, **38**, **44**, and **52**. Among them, only one crystalline material possessed pores in its extended structure: **52**.

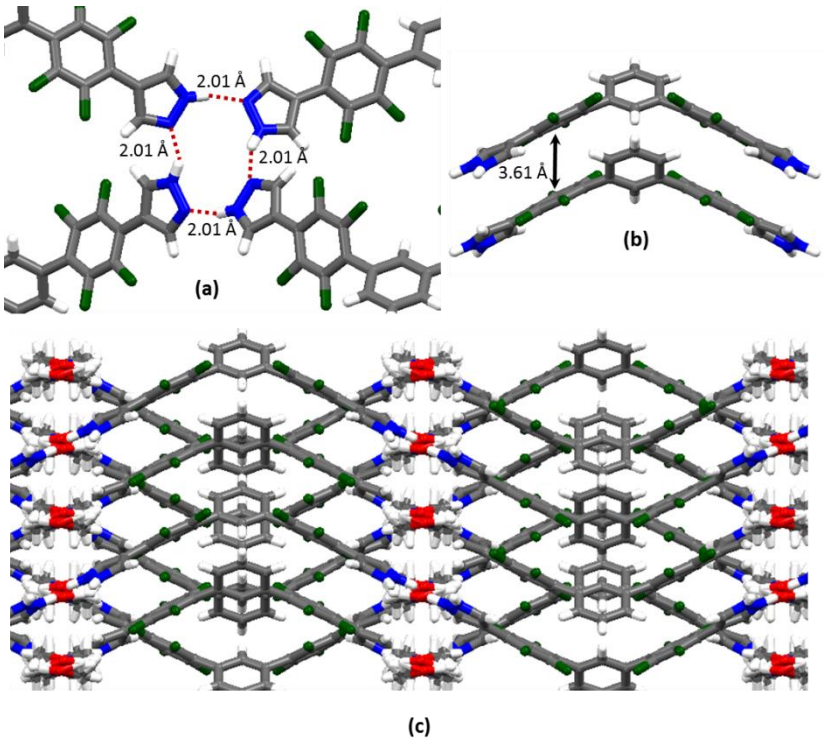

Figure 4.9 Crystal structure of compound **32**. Four pyrazoles come together in each of the wavy layers (a) forming a quartet of hydrogen bonds. (b) [π···π] stacking interaction between two molecules. (c) Interweaving network along the crystallographic *b* axis.

The crystal structure of compound **32** is displayed in Figure 4.9. In spite of resemblance in structure between **32** and the nCOF-1 ligand, the hydrogen bond triplet of neighboring pyrazoles was not observed; instead, a quartet was formed, and [NH···N] hydrogen bonds revealed the distance of 2.0 Å. It is noticeable that there is [π···π] stacking interaction between wavy layers of molecule (Figure 4.9b), reflected by plane distance of 3.61 Å and interplanar angle of 9.2° measured from tetrafluorinated aromatic rings of two consecutive layers. However, these layers interweave (Figure 4.9c),

cancelling the possible pores between molecule and leaving the crystal structure with no pore at the end.

We were also successful in growing a single crystal of compound **38** suitable for X-ray diffraction experiments. Initial results revealed that there is no pore in this crystal structure; therefore, the experiment was discontinued.

Trigonal precursor **44** with no of perfluorinated benzenes in the scaffold also did not show a porous structure (Figure 4.10b). The triplet of hydrogen bonds between the pyrazole end groups was maintained (Figure 4.10a), with [NH···N] distances between 1.86 and 1.93 Å. These consecutive hydrogen bonds fabricated wavy molecular sheets, however, they interweaved with each other, leaving the structure with no pores.

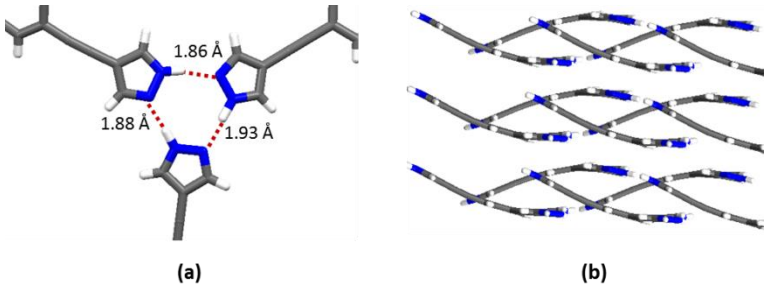

Figure 4.10 Crystal structure of compound **44**. Three pyrazoles come together in each of the wavy layers (a) forming a triplet of hydrogen bonds. (b) Side view of the interweaving network.

The single-crystal X-ray structure of compound **52** is shown in Figure 4.11. Several aspects of this structure share similarity with nCOF-1, such as the fact that the perfluorinated benzene close to the central ring twists in a propeller-like fashion out of

the plane of the core. Every molecule of **52** participates in short contacts with twelve neighboring molecules: six [NH···N] hydrogen bonds generate a hexagonal two-dimensional lattice and its [π···π] stacking pattern is more complicated than nCOF-1. As depicted in Figure 4.11b, there are two sorts of molecules packing—yellow and red, interspersed with each other. Molecules having the same color code are arranged in the same fashion, considered almost parallel in pair. Overall, each arm of molecule **52** establishes four [π···π] stacking arrangements: two sandwich stacks with molecules of the same color and two offset stacks with molecules of different color. In the case of same color code, [π···π] stacking interactions between two pyrazoles or their adjacent perfluorinated benzenes were characterized of centroid-centroid distances of 3.69 and 3.74 Å, respectively, and interplanar angles vary between 1.6 and 10.1^{o}. In the different color code scenario, offset stacking was observed between electron-poor tetrafluorinated aromatic rings with the relatively electron-rich pyrazoles, denoted by centroid-centroid distance vary between 3.70 and 3.74 Å and interplanar angles in the range of 20.6 and 20.8^{o}. Pyrazoles at the end of each arm interact through hydrogen bonding with two adjacent molecules, and N···H distances vary between 1.92 and 1.97 Å, while N···N distances are between 2.79 and 2.82 Å. These short contacts resulted in a three-dimensional network, with infinite one-dimensional channels, diameter of ~26.9 Å, protruding throughout the crystal along the crystallographic *c* axis (Figure 4.11d).

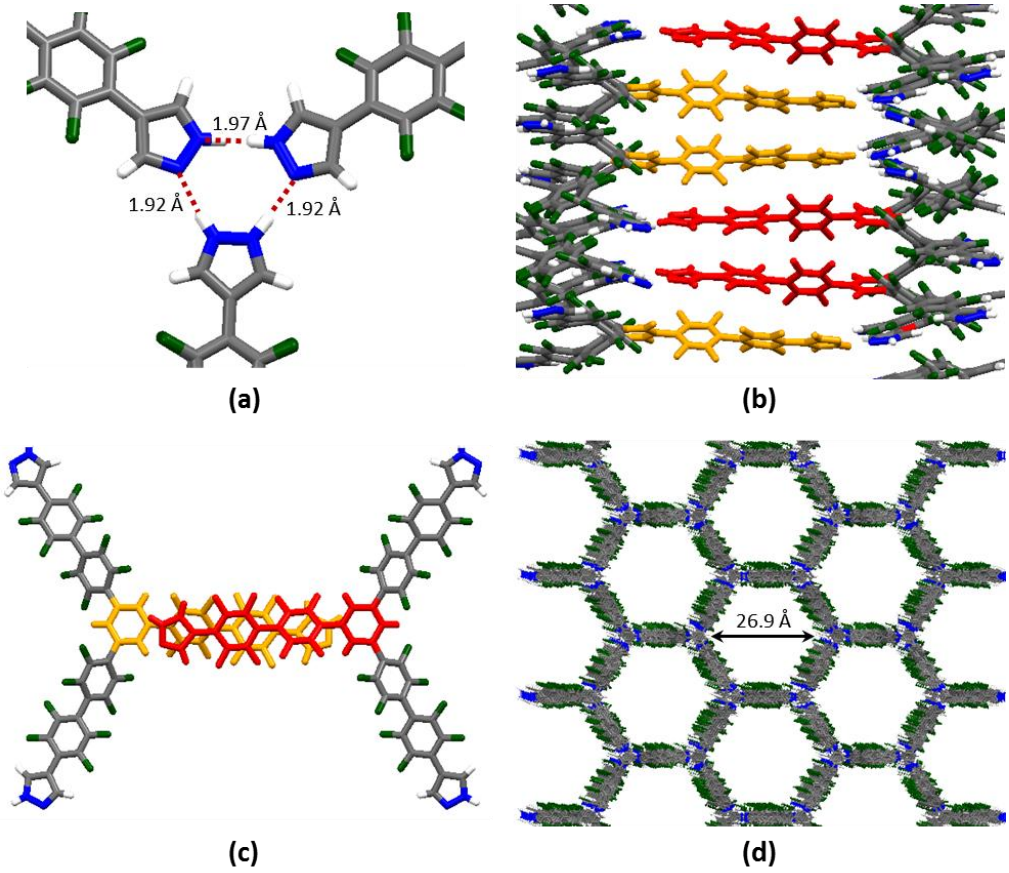

Figure 4.11 Crystal structure of compound **52**. Three pyrazoles come together in each of the wavy layers (a) forming a triplet of hydrogen bonds. (b) [π···π] stacking interaction between arms. (c) Offset [π···π] stacking of two neighbor molecules along the crystallographic *c* axis. (d) Hexagonal network with infinite fluorine-lined channels along the crystallographic *c* axis.

4.2.3 Gas Sorption for Noncovalent Organic Framework 52

The BET surface area of compound **52** was determined to be 258.5 m^2 g^{-1}, which is much lower than nCOF-1 and needs further investigation.

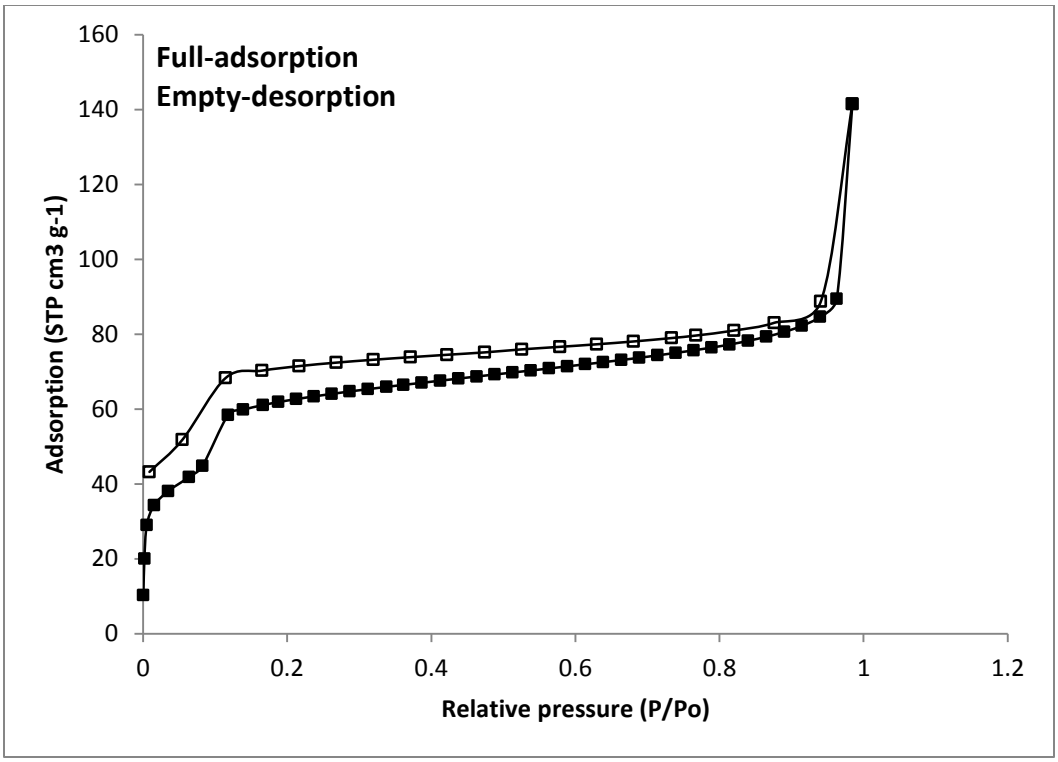

Figure 4.12 Gas sorption of compound **52** uptake of N_2 (77K)

To examine the structural changes that occur with heating, we performed PXRD studies of compound **52** after obtaining porosity measurements; results, shown in Figure 4.13, suggest the crystal phase does not change when the mode of activation is switched from supercritical CO_2 drying to heating up to 120 °C before porosity measurements.

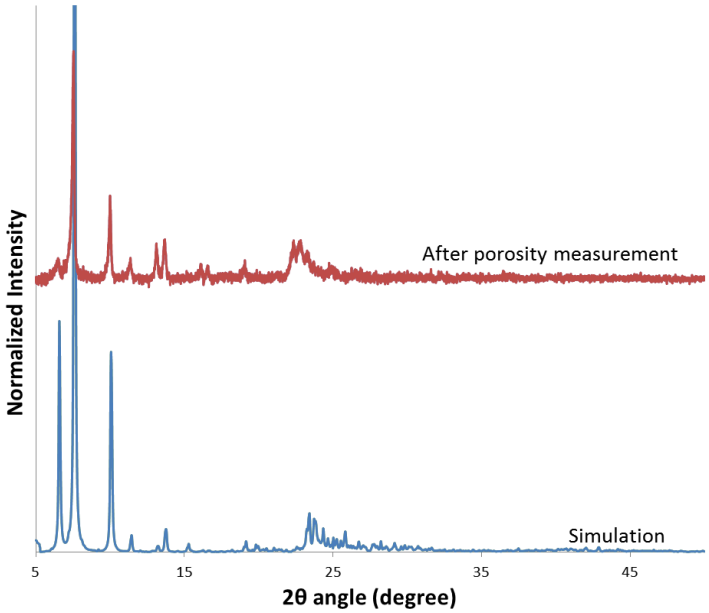

Figure 4.13 Powder X-ray diffraction (PXRD) revealed no change in the structure after porosity measurement.

4.3 Conclusions and Outlook

We were successful in the synthesis of a series of precursors readily to build up noncovalent organic frameworks. These new structures were inspired by the scaffold of nCOF-1, making them share some similar packing fashions of this porous material. Single crystals of compounds **32**, **38**, **44**, **52** were obtained by solvothermal treatment in proper solvents and compound **52** was the only one to exhibit a porous structure proved by single crystal data as well as gas sorption. With these results in hands, we suggest the trigonal geometry molecule is a better choice compared to the bent shape molecule in order to design molecules with pores, and perfluorinated aromatic rings as well as pyrazoles play important roles in short interactions building these scaffolds.

This result encourages us in growing crystals of all the synthesized precursors to fully understand the driving force behind porosity in these successful cases. Although precursors **32**, **38**, and **44** provided structures without pores, growing their single crystals in different conditions may change their phases, leading to porous crystals.[162e,f] These precursors cam also can serve as linkers in building MOF structures.[190]

4.4 Experimental Section

4.4.1 General Experimental Methods

Schlenk flasks and standard scintillation bottles were used as reaction vessels for the synthesis, while vials with PTFE/Liner caps were used as vessels for deprotection of the Boc group. Column chromatography was carried out on silica gel 60, 32–63 mesh and basic aluminum oxide Act.1, 50–200 μm (Sorbent Technologies). Analytical TLC was performed on J. T. Baker plastic-backed silica gel IB-F plates and aluminum oxide IB-F plates. The ^{1}H and ^{19}F NMR spectra were recorded on JEOL ECA-500, ECX-400P spectrometers using the peaks of tetramethylsilane or residual solvent as standards. Trifluorotoluene ($PhCF_3$, $\delta = -63.72$ ppm) was used as the internal standard in ^{19}F NMR spectra. All ^{13}C NMR spectra were recorded with simultaneous decoupling of ^{1}H nuclei. Some ^{13}C Spectra were not included since they are not informative, due to poor solubility of the prepared compounds and extensive coupling between ^{13}C and ^{19}F nuclei, low intensities and many missing peaks were observed. Analytical thin-layer chromatography was performed on Fluka silica gel/TLC plates with a fluorescent indicator that emitted when irradiated at 254 nm.

All reactions were performed under nitrogen atmosphere in oven-dried glassware. The starting materials and solvents were obtained from the respective commercial sources and used without further purification. All gases were purchased from Matheson Tri-Gas. In Sonogashira couplings, tetrahydrofuran (THF) and triethylamine (Et_3N) were degassed by a 30 minute nitrogen purge prior to use.

4.4.2 Synthesis of Precursors for Noncovalent Organic Framework

Synthesis of Compound **30**

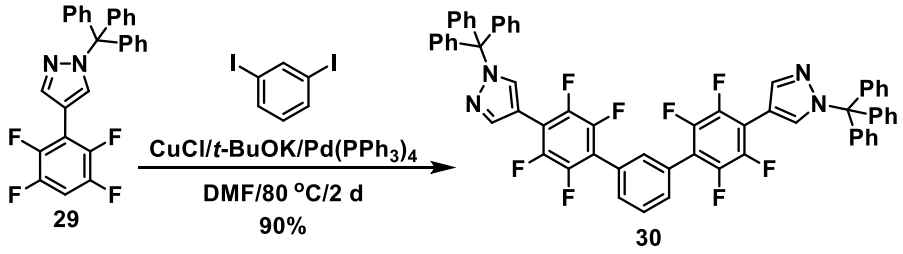

Inside a glovebox, a 100 mL screw cap pressure vessel was equipped with magnetic stir bar and charged with CuCl (2.18 g, 22.0 mmol) and *t*-BuOK (2.47 g, 22.0 mmol). Dry DMF (40 mL) was added. After that, reaction mixture was sealed, and vigorously stirred at 25 °C for 1 h inside glovebox. *N*-Trityl pyrazole **29**[185] (12.5 g, 27.3 mmol) was added in one portion, after that reaction mixture was sealed, and stirred at 25 °C for 1 h inside glovebox. Catalyst $Pd(PPh_3)_4$ (230 mg, 0.20 mmol) was added next, followed by 1,3-diiodobenzene (3.3 g, 10.0 mmol). Reaction mixture was sealed, taken out of the glovebox and then placed inside an oil bath preheated to 80 °C, where it was stirred vigorously for 48 h Reaction mixture was cooled to 25 °C, poured into a 1 L beaker containing NH_4OH (100 mL), NH_4Cl (14 g), and H_2O (300 mL). Mixture of

CH_2Cl_2/hexane (200 mL/200 mL) was added to the beaker. Whole solution was vigorously stirred, filtered and washed with water (3×50 mL). The collected solid after drying in air afforded white powder as the desired product **30** (8.9 g, 90%).

30: ^{1}H NMR (500 MHz, $CDCl_3$) δ 8.20 (s, 2H), 7.95 (s, 2H), 7.56 (m, 4H), 7.34 (m, 18H), 7.19 (m, 12H) ppm.^{19}F NMR (500 MHz, CDCl3) δ −141.07 to −141.13 (m, 4F), −144.95 to −145.02 (m, 4F) ppm. This compound was used as crude in the next step.

Synthesis of Compound **31**

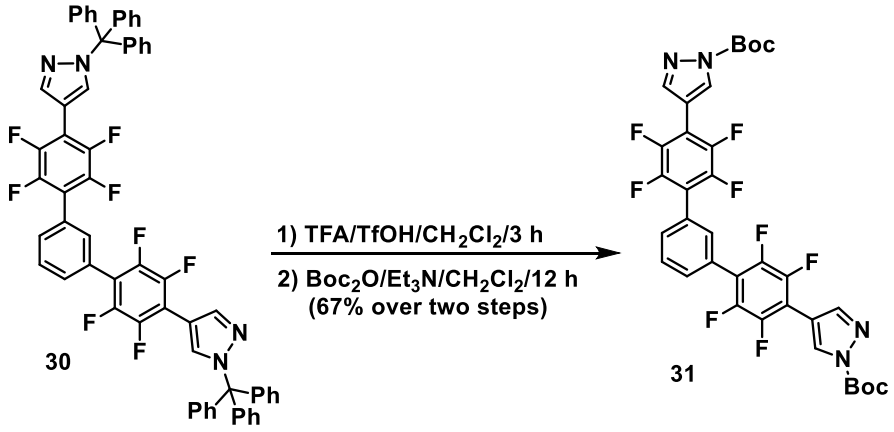

A 250 mL flask equipped with magnetic stirring bar was charged with trityl-protected tripyrazole intermediate **30** (8.90 g, 9.00 mmol) and CH_2Cl_2 (125 mL). Resulting clear solution was treated with TFA (12 mL), followed by TfOH (12 mL), causing solution turn to cloudy. Reaction mixture was vigorously stirred at 25 °C for 3 h. Resulting solution was poured into a beaker containing K_2CO_3 (60.0 g) and water (300 mL). Whole solution was stirred well and the precipitates were filtered off and washed with CH_2Cl_2 (2×20 mL). Obtained solid was dried in air over night and dried *in vacuo* for 30 min.

Next, a 250 mL flask equipped with magnetic stirring bar was charged with previously isolated salt and CH_2Cl_2 (60 mL) was added. Resulting suspension was treated with Et_3N (12 mL), followed by the addition of DMAP (1.79 g, 14.7 mmol). To the open flask, Boc_2O (28.8 g, 132 mmol) was added via syringe over 5 min. CAUTION: rapid evolution of CO_2 is observed during the addition! After addition of Boc_2O was complete, reaction flask was capped with a septum connected to a bubbler. Reaction mixture was stirred vigorously at 25 °C until the evolution of CO_2 ceased (12 h). Upon completion, reaction mixture was dry-absorbed on silica gel. After purification by column chromatography on silica gel, eluting first with CH_2Cl_2/Hexanes (1/1) slowly increased to pure CH_2Cl_2 as eluent and evaporation of the fractions containing the product, compound **31** was obtained as a white solid (4.7 g, 67 % over two steps).

31: ^{1}H NMR (500 MHz, $CDCl_3$) δ 8.63 (s, 2H), 8.23 (s, 2H), 7.62 (m, 4H), 1.70 (m, 18H) ppm. ^{19}F NMR (500 MHz, $CDCl_3$) δ −140.33 to −140.40 (m, 4F), −143.92 to −143.98 (m, 4F) ppm.

Synthesis of Compound **33**

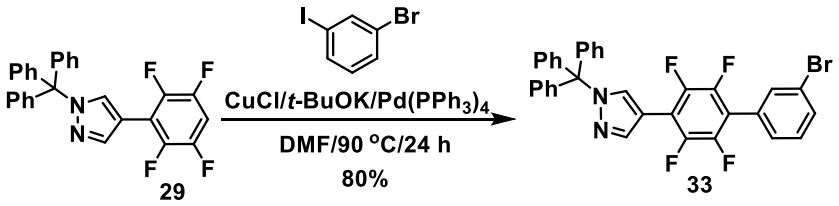

Inside a glovebox, a 100 mL screw cap pressure vessel was equipped with magnetic stir bar and charged with CuCl (2.86 g, 28.9 mmol) and *t*-BuOK (3.24 g, 28.9 mmol). Dry DMF (50 mL) was added, after that reaction mixture was sealed, and

vigorously stirred at 25 °C for 1 h inside glovebox. *N*-Trityl pyrazole **29**[185] (12.0 g, 26.2 mmol) was added in one portion, after that reaction mixture was sealed and vigorously stirred at 25 °C for 1 h inside glovebox. Catalyst $Pd(PPh_3)_4$ (1.00 g, 0.86 mmol) was added, followed by 3-bromoiodobenzene (8.14 g, 28.8 mmol). Reaction mixture was sealed, taken out of the glovebox and then placed inside an oil bath preheated to 90 °C, where it was stirred vigorously for 24 h. Reaction mixture was cooled to 25 °C, and then poured into a 2 L beaker containing NH_4OH (100 mL), NH_4Cl (14 g), and H_2O (1 L). Subsequently, CH_2Cl_2 (300 mL) was added to the beaker and the whole solution was vigorously stirred, the layers were separated, and the aqueous layer was extracted with CH_2Cl_2. The combined organic layers were washed with more H_2O until blue color disappeared; after that, the collected organic layer was dried over $MgSO_4$, and concentrated *in vacuo*. The residue was purified by column chromatography (SiO_2, gradient eluent: 30–45% CH_2Cl_2/hexane) providing **33** (12.8 g, 80%) as a white solid.

33: ^{1}H NMR (600 MHz, $CDCl_3$) δ 8.19 (s, 1H), 7.95 (s, 1H), 7.61 (s, 1H), 7.56 (d, 2H), 7.39 (d, 1H), 7.35 (m, 10H), 7.19 (m, 6H) ppm. ^{19}F NMR (600 MHz, CDCl3) δ −140.92 to −140.98 (m, 2F), −144.76 to −144.82 (m, 2F) ppm.

Synthesis of Compound **34**

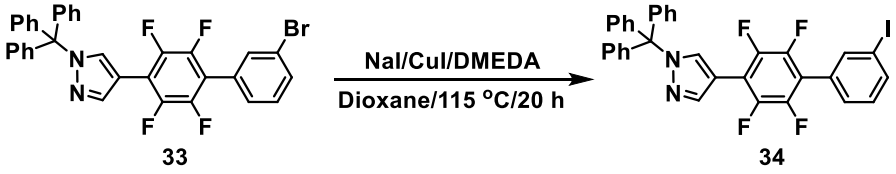

Inside a glovebox, a 150 mL heavy wall pressure vessel was equipped with magnetic stir bar and charged with CuI (3.55 g, 18.6 mmol), NaI (5.6 g, 37.4 mmol),

N,N′-dimethylethylenediamine (DMEDA) (2.20 g, 18.9 mmol), and **33** (11.4 g, 18.6 mmol). Dioxane (60 mL) was added, after that reaction mixture was sealed, taken out of the glovebox and then placed inside an oil bath, heated to 115 °C, and stirred vigorously for 22 h. At the end, the suspension turns purple in brown solution. Reaction mixture was cooled to 25 °C while stirring, followed by silica gel addition. Whole mixture was concentrated *in vacuo* to give brown powder which subjected to column chromatography (SiO_2, gradient eluent: 30–55% CH_2Cl_2/hexane) to afford **34** (6.6 g, 54%) as a white solid.

34: ^{1}H NMR (600 MHz, $CDCl_3$) δ 8.19 (s, 1H), 7.95 (s, 1H), 7.81 (s, 1H), 7.78 (d, 2H), 7.42 (d, 1H), 7.35 (m, 9H), 7.19 (m, 7H) ppm. ^{19}F NMR (600 MHz, CDCl3) δ −140.91 to −140.96 (m, 2F), −144.73 to −144.82 (m, 2F) ppm. This compound was used as crude in the next step.

Synthesis of Compound **36**

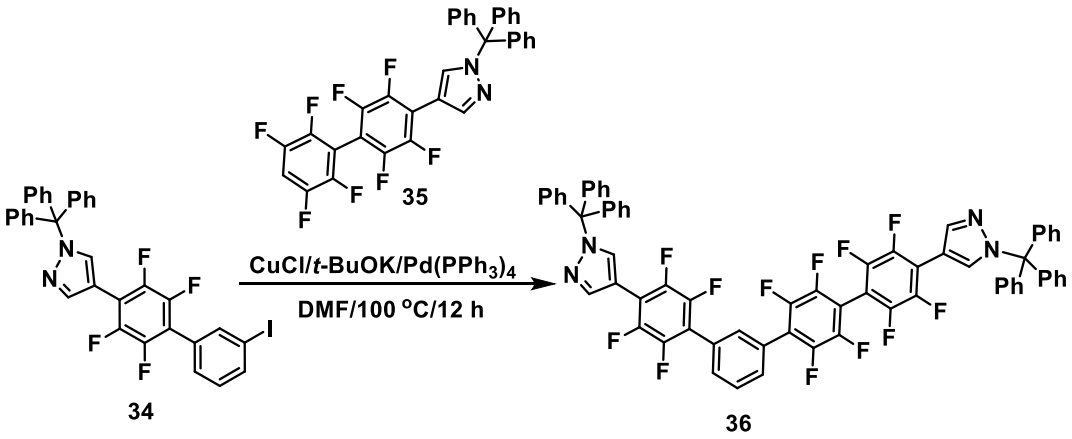

Inside a glovebox, a 100 mL screw cap pressure vessel was equipped with magnetic stir bar and charged with CuCl (1.1 g, 11.1 mmol) and *t*-BuOK (1.23 g, 11

mmol). Dry DMF (40 mL) was added, after that reaction mixture was sealed, and vigorously stirred at 25 °C for 1 h inside glovebox. *N*-Tritylpyrazole **35** (6.67 g, 11 mmol) was added in one portion, after that reaction mixture was sealed, vigorously stirred at 25 °C for 1 h inside glovebox. $Pd(PPh_3)_4$ (346.6 mg, 0.3 mmol) was added, followed by **34** (6.6 g, 10 mmol). Reaction mixture was sealed, taken out of the glovebox and then placed inside an oil bath preheated to 100 °C, where it was stirred vigorously for 24 h. Reaction mixture was cooled to 25 °C, poured into a 2 L beaker containing 100 mL NH_4OH, 14 g NH_4Cl, and 1 L H_2O. Subsequently, 300 mL CH_2Cl_2 was then added to the beaker and whole solution was vigorously stirred, the layers were separated, and the aqueous layer was extracted with CH_2Cl_2. The combined organic layers were washed with more H_2O until blue color dismissed, after that the collected organic layer was dried over $MgSO_4$, and concentrated *in vacuo*. The residue was purified by column chromatography (SiO_2, gradient eluent: 30–55% CH_2Cl_2/hexane) providing **36** (8.3 g, 73%) as a white solid.

36: ^{1}H NMR (500 MHz, $CDCl_3$) δ 8.22 (d, 2H), 7.98 (d, 2H), 7.64 (m, 4H), 7.35 (m, 18H), 7.20 (m, 12H) ppm. ^{19}F NMR (500 MHz, $CDCl_3$) δ −137.98 to −138.09 (m, 2F), −139.19 to −139.29 (m, 2F), −140.16 to −140.23 (m, 2F), −140.95 to −141.02 (m, 2F), −142.67 to −142.74 (m, 2F), −144.93 to −145.00 (m, 2F) ppm. This compound was used as crude in the next step.

Synthesis of Compound **37**

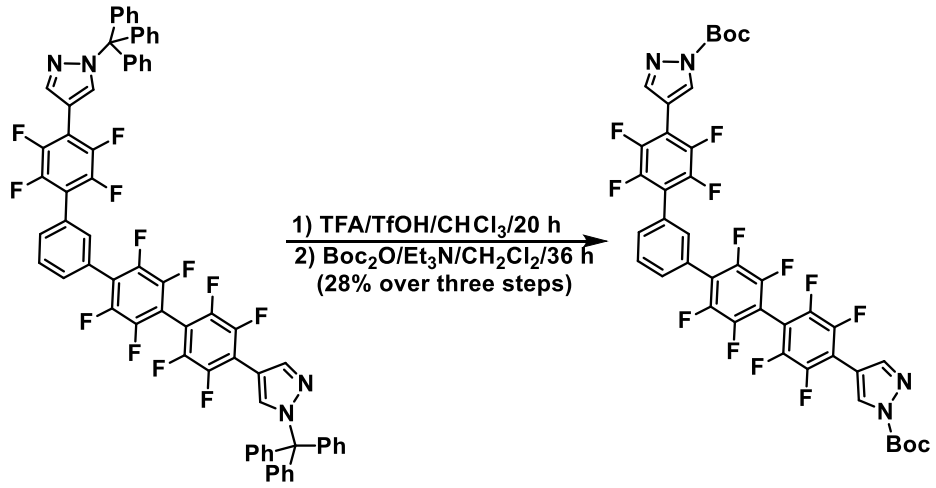

A 250 mL flask equipped with magnetic stirring bar was charged with trityl-protected tripyrazole intermediate **36** (8.3 g, 7.29 mmol) and CH_2Cl_2 (125 mL). Resulting clear solution was treated with trifluoroacetic acid (12 mL), followed by TfOH (12 mL) causing the solution turn to cloudy. Reaction mixture was vigorously stirred at 25 °C for 3 h. Resulting solution was poured into a beaker containing K_2CO_3 (53 g) and H_2O (300 mL). Whole solution was stirred well and the precipitates were filtered off, washed with CH_2Cl_2 (2×20 mL). Obtained solid was dried in air over night and dried *in vacuo* for 30 min.

Next, a 250 mL flask equipped with magnetic stirring bar was charged with previously isolated salt and CH_2Cl_2 (60 mL) was added. Resulting suspension was treated with Et_3N (10 mL), followed by the addition of DMAP (1.47 g, 12.03 mmol). To the open flask, Boc_2O (15.4 g, 70.56 mmol) was added via syringe over 5 min. CAUTION: rapid evolution of CO_2 is observed during the addition! After addition of Boc_2O was complete, reaction flask was capped with a septum connected to a bubbler. Reaction

mixture was stirred vigorously at 25 °C until the evolution of CO_2 ceased (12 h). Upon completion, reaction mixture was dry-absorbed on silica gel. After purification by column chromatography on silica gel, eluting first with CH_2Cl_2/ Hexanes (3/1), then pure CH_2Cl_2 and finally EtOAc/CH_2Cl_2 (1% of EtOAc) as eluent, and evaporation of the fractions containing the product, compound **37** was obtained as a white solid (4.4 g, 28 % over three steps).

37: ^{1}H NMR (500 MHz, $CDCl_3$) δ 8.63 (s, 2H), 8.21 (s, 2H), 7.64 (m, 4H), 1.67 (m, 18H) ppm. ^{19}F NMR (470 MHz, $CDCl_3$) δ −137.85 to −137.96 (m, 2F), −138.18 to −138.28 (m, 2F), −139.49 to –139.57 (m, 2F), −140.34 to −140.41 (m, 2F), –142.48 to –142.56 (m, 2F), –143.96 to −144.03 (m, 2F) ppm.

Synthesis of Compound **40**

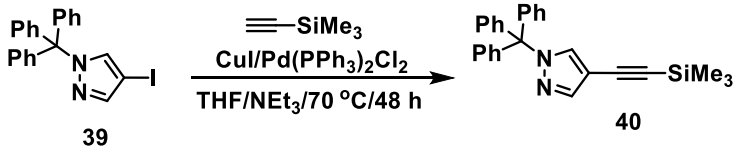

A 500 mL pear-shaped Schlenk flask was charged with compound **39**[185] (18.0 g, 41.3 mmol), $PdCl_2(PPh_3)_2$ (450 mg, 0.64 mmol), and CuI (236 mg, 1.24 mmol). The flask was sealed, then evacuated and backfilled with N_2 three times. In a separate flask, a mixture of NEt_3 (100 mL), THF (100 mL), and TMSA (17.5 mL, 124 mmol) was degassed for 20 min and then slowly transferred, under positive N_2 pressure, via cannula to the reaction flask. The reaction mixture was stirred and heated at 70 °C for 2 d, and then cooled to 25 °C. Afterwards, silica gel (200 mL) was added to the reaction mixture, and the solvent was removed under reduced pressure until a brown powder was formed.

This powder was subjected to short silica gel column chromatography, using CH_2Cl_2/hexane (1/1) as an eluent. The solvent was removed *in vacuo* to give an off-white powder; this compound was used for the next step without further purification.

Synthesis of Compound **41**

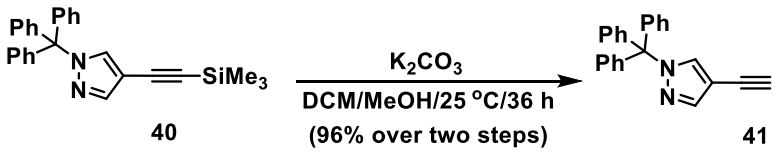

In a nitrogen-flushed 500 mL flask, trimethylsilyl-substituted alkyne produced in the previous step (16.7 g, 41 mmol) was dissolved in a mixture of DCM (200 mL) and MeOH (150 mL), and treated with anhydrous K_2CO_3 (10.0 g, 72.0 mmol). The resulting solution was stirred at 25 °C for 36 h. The whole mixture was filtered over a plug of Celite (bottom), silica (middle), sand (top); the residue was washed by DCM. The collected filtrate was concentrated under vacuum to afford **41** as a white powder (13.2 g, 96% over two steps).

41: ^{1}H NMR (400 MHz, CD_3OD) δ 7.74 (s, 1H), 7.53 (s, 1H), 7.30 (m, 10H), 7.13 (m, 5H), 2.97 (s, 1H) ppm. This data agrees with a previous literature report.[191]

Synthesis of Compound **42**

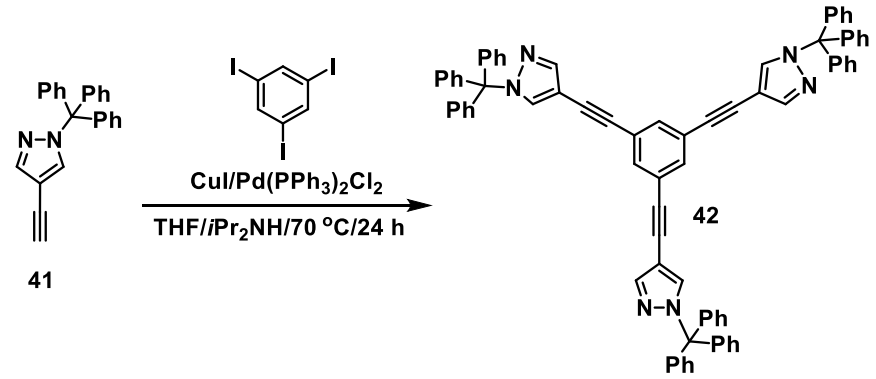

A mixture of compound **41** (11.0 g, 32.9 mmol), 1,3,5-triiodobenzene (4.56 g, 10 mmol), $PdCl_2(PPh_3)_2$ (211 mg, 0.30 mmol), and CuI (190 mg, 1.00 mmol) was added to a 500 mL pear-shaped Schlenk flask. The flask was sealed, and then evacuated and backfilled with nitrogen three times. In a separate flask, a mixture of *i*Pr_2NH (200 mL) and THF (120 mL) was degassed for 30 min and transferred slowly under positive N_2 pressure via cannula to the reaction flask. The reaction mixture was stirred and heated at 70 °C for 20 h and then cooled to 20 °C. Afterwards, silica gel (100 g) was added to the reaction mixture and the solvent was removed under reduced pressure until a brown powder was formed, which was subsequently purified by gradient elution column chromatography on silica gel, using DCM/hexane eluent system (volume ratios ranging from 1:1 to 10:0). The solvent was removed *in vacuo* to give the white powder **42** (7.5 g, 70%).

42: ^{1}H NMR (600 MHz, $CDCl_3$) δ 7.79 (s, 3H), 7.58 (s, 3H), 7.42 (s, 3H), 7.33 (m, 27H), 7.15 (m, 18H) ppm. ^{13}C NMR (600 MHz, $CDCl_3$) δ 142.7, 142.3, 135.5, 133.1, 130.2,

128.1, 127.9, 124.1, 101.7, 88.9, 82.2, 79.3 ppm. This compound was used as crude in the next step.

Synthesis of Compound **43**

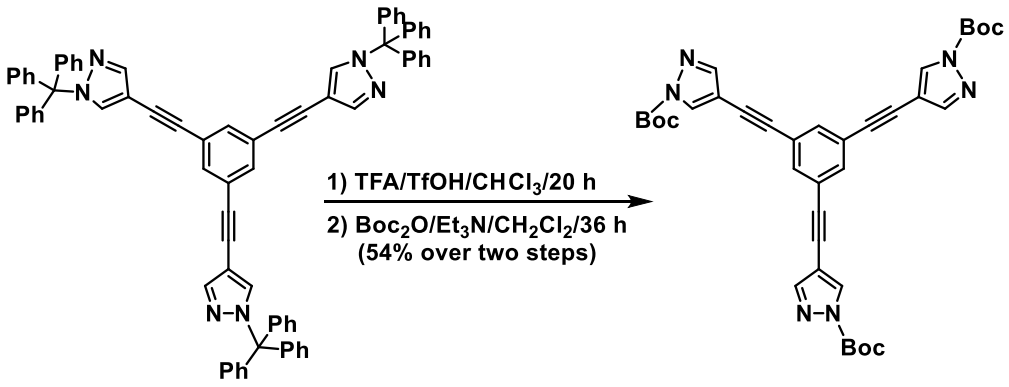

A 1 L flask equipped with magnetic stirring bar was charged with trityl-protected tripyrazole intermediate **42** (7.5 g) and CH_2Cl_2 (600 mL). Resulting solution was treated with trifluoroacetic acid (12 mL), followed by TfOH (12 mL) causing salt to precipitate. Reaction mixture was vigorously stirred at 25 °C for 20 h. Resulting salt that was formed during the reaction was filtered off and the solid was washed with fresh CH_2Cl_2 (3×50 mL). Obtained light tan solid was dried in vacuum for 2 h.

Next, a 250 mL flask equipped with magnetic stirring bar was charged with previously isolated salt and CH_2Cl_2 (175 mL) was added. Resulting suspension was treated with Et_3N (14 mL), followed by the addition of DMAP (1.42 g, 11.6 mmol). To the open flask Boc_2O (15.2 g, 69.6 mmol) was slowly added over 5 min. CAUTION: rapid evolution of CO_2 is observed during the addition! After addition of Boc_2O was complete reaction flask was capped with a septum connected to a bubbler. Reaction mixture was stirred vigorously at 25 °C until the evolution of CO_2 ceased—18 h. Upon

completion, reaction mixture was dry-absorbed on silica gel. After purification by column chromatography on silica gel using eluting first with CH_2Cl_2, then EtOAc/CH_2Cl_2 (from 5:95 to 1:9) as eluent and evaporation of the fractions containing the product, compound **43** was obtained as a white solid (3.5 g, 54 % over two steps).

43: ^{1}H NMR (400 MHz, $CDCl_3$) δ 8.20 (s, 3H), 7.76 (s, 3H), 7.51 (s, 3H), 1.61 (s, 27H) ppm. ^{13}C NMR (400 MHz, $CDCl_3$) δ 146.86, 145.60, 133.91, 133.03, 123.74, 106.12, 90.13, 86.39, 80.59, 27.93 ppm.

Synthesis of Compound **46**[192]

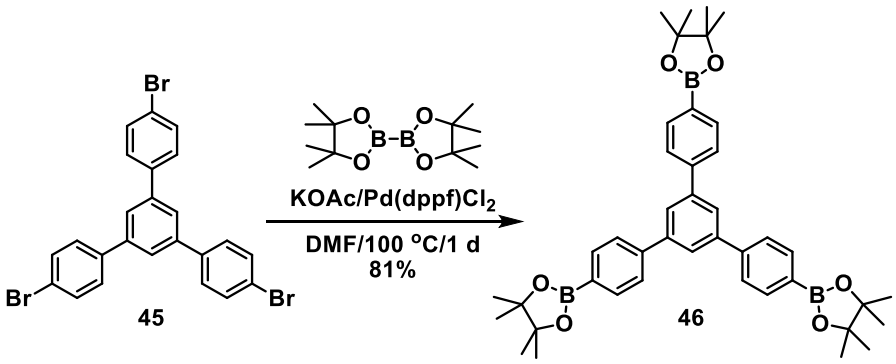

To a 100 mL Schlenk flask were added KOAc (6.50 g, 66.2 mmol), which was flame-dried under vacuo in 5 min and allowed to cool down to room temperature. Bis(pinacolato)diboron (8.42 g, 33.2 mmol), 1,3,5-tris(*p*-bromophenyl)benzene **45** (5 g, 9.2 mmol), Pd(dppf)Cl_2 (376 mg, 0.46 mmol), and dry DMF (20 mL) were added under N_2 flow. The reaction was stirred at 25 °C for 15 min then increased to 100 °C and stirred for 24 h. After cooling to room temperature, the resulting mixture was diluted with water and extracted with diethyl ether, the combined organic layer was washed with water, dried over $MgSO_4$ and dry-absorbed onto silica gel. The residue was purified by column

chromatography (SiO_2, gradient eluent: 20–100% CH_2Cl_2/hexane) to afford **46** (5.1 g, 81%) as a white solid.

46: ^{1}H NMR (400 MHz, $CDCl_3$) δ 7.93 (d, 6H), 7.81 (s, 3H), 7.71 (d, 6H), 1.37 (s, 36H) ppm. The NMR data is consistent with the literature report.[192]

Synthesis of Compound **47**

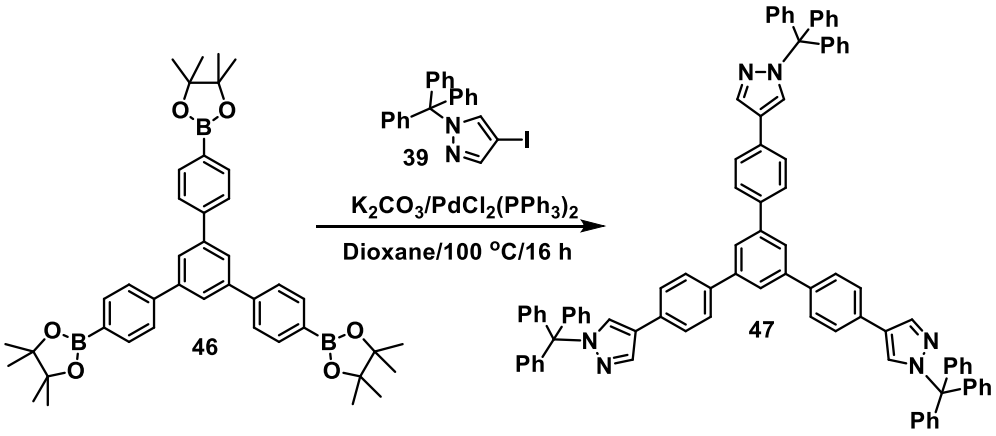

To a 250 mL flask was added dioxane (130 mL), boronic ester **46** (5.10 g, 7.45 mmol), iodopyrazole **39** (16.2 g, 37.2 mmol), and K_2CO_3 (5.15 g, 37.2 mmol). The resulting mixture was flushed with nitrogen for 15 min before H_2O (10 mL) and $Pd(PPh_3)_2Cl_2$ were added to it. The reaction was then purged again with nitrogen for 15 min and heated to 100 °C for 16 h. The mixture was allowed to cool to room temperature and the solvent was removed by vacuum evaporation. The crude reaction mixture was dissolved in CH_2Cl_2 and washed with H_2O. The organic solution were dried over $MgSO_4$, and concentrated. The residue was purified by flash column chromatography chromatography (SiO_2, gradient eluent: 50–100% CH_2Cl_2/hexane) to give product **47** as a white solid (5.3 g, 58% yield). This compound was used as crude for the next step.

Synthesis of Compound **48**

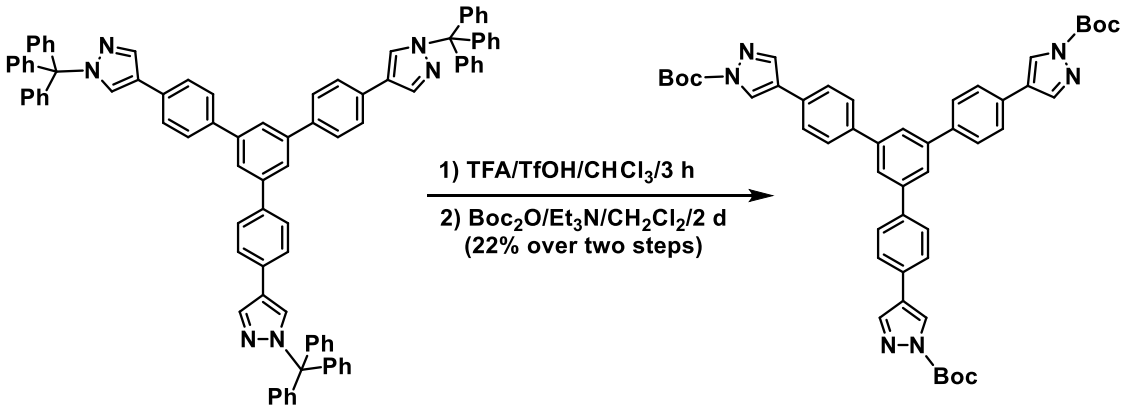

A 250 mL flask equipped with magnetic stirring bar was charged with trityl-protected tripyrazole intermediate **47** (5.30 g, 4.30 mmol) and CH_2Cl_2 (100 mL). Resulting solution was treated with TFA (12 mL), followed by TfOH (12 mL), causing salt to precipitate. Reaction mixture was vigorously stirred at 25 °C for 3 h. Resulting solution was poured into a beaker containing 30 g of K_2CO_3 and 300 mL of water. Whole solution was stirred well and the precipitates were filtered off, and washed with CH_2Cl_2 (20 mL). Obtained solid was dried in air over night and dried *in vacuo* for 30 min.

Next, a 1250 mL flask equipped with magnetic stirring bar was charged with previously isolated solid and CH_2Cl_2 (50 mL) was added. Resulting suspension was treated with Et_3N (9 mL), followed by the addition of DMAP (0.95 g, 7.80 mmol). To the open flask Boc_2O (10.0 g, 45.8 mmol) was slowly added over 5 min. CAUTION: rapid evolution of CO_2 is observed during the addition! After addition of Boc_2O was complete reaction flask was capped with a septum connected to a bubbler. Reaction mixture was stirred vigorously at 25 °C until the evolution of CO_2 ceased—2 days. Upon completion, reaction mixture was dry-absorbed on silica gel. After purification by column

chromatography on silica gel using gradient eluent: 30–70% EtOAc/hexane and evaporation of the fractions containing the product, compound **48** was obtained as a white solid (1.32 g, 22 % over two steps).

48: ^{1}H NMR (500 MHz, $CDCl_3$) δ 8.37 (d, 3H), 8.06 (d, 3H), 7.81 (s, 3H), 7.74 (d, 6H), 7.65 (d, 6H), 1.69 (s, 27H) ppm. ^{13}C NMR (400 MHz, $CDCl_3$) δ 147.7, 142.0, 140.2, 130.4, 128.0, 126.6, 125.1, 125.0, 85.9, 28.1 ppm.

Synthesis of Compound **49**

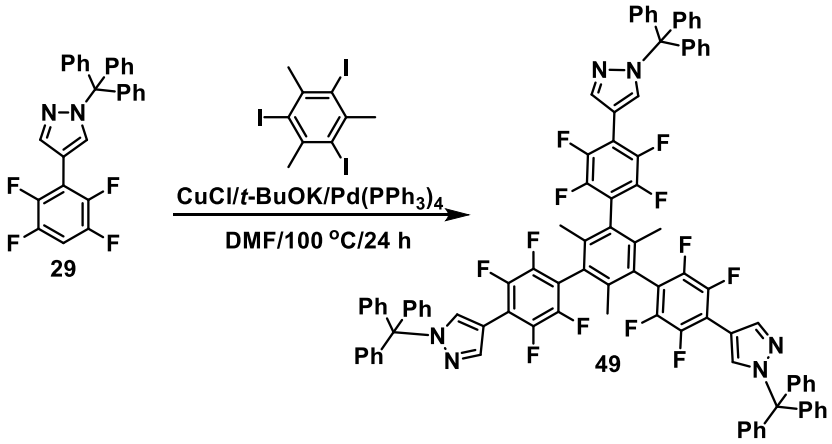

Inside a glovebox a 100 mL screw cap pressure vessel was equipped with magnetic stir bar and charged with CuCl (1.97 g, 19.9 mmol) and *t*-BuOK (2.23 g, 19.9 mmol). Dry DMF (30 mL) was added, after that reaction mixture was sealed, vigorously stirred at 25 °C for 1 h inside glovebox. *N*-Trityl pyrazole **29**[185] (9.1 g, 19.8 mmol) was added in one portion, after that reaction mixture was sealed, vigorously stirred at 25 °C for 1 h inside glovebox. Compound $Pd(PPh_3)_4$ (689 mg, 0.6 mmol) was added, followed by 2,4,6-triiodomesitylene[193] (3.00 g, 6.00 mmol). Reaction mixture was sealed, taken out of the glovebox and then placed inside an oil bath preheated to 100 °C, where it was

stirred vigorously for 48 h Reaction mixture was cooled to 25 °C, and then poured into a 1 L beaker containing NH_4OH (100 mL), NH_4Cl (14 g), and H_2O (300 mL). Subsequently, CH_2Cl_2 (300 mL) was then added to the beaker and whole solution was vigorously stirred, the layers were separated, and the aqueous layer was extracted with CH_2Cl_2. The combined organic layers were washed with more H_2O until blue color disappeared, after that the collected organic layer was dried over $MgSO_4$, and concentrated *in vacuo*. The residue was purified by column chromatography (SiO_2, gradient eluent: 40–80% CH_2Cl_2/hexane) providing **49** (4.13 g, 46%) as a white solid.

49: ^{1}H NMR (500 MHz, $CDCl_3$) δ 8.28 (s, 3H), 8.05 (s, 3H), 7.38 (m, 27H), 7.26 (m, 18H), 1.97 (s, 9H) ppm.^{19}F NMR (500 MHz, CDCl3) δ −140.60 to −140.62 (m, 12F) ppm. This compound was used as crude in the next step.

Synthesis of Compound **50**

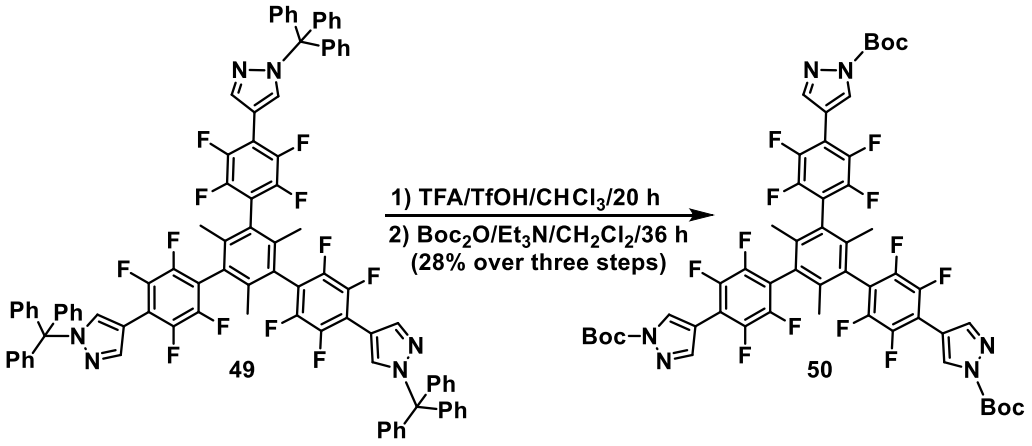

A 250 mL flask equipped with magnetic stirring bar was charged with trityl-protected tripyrazole intermediate **49** (4.13 g, 2.77 mmol) and CH_2Cl_2 (70 mL). Resulting solution was treated with TFA (12 mL), followed by TfOH (12 mL) causing salt to

precipitate. Reaction mixture was vigorously stirred at 25 °C for 3 h. Resulting solution was poured into a beaker containing K_2CO_3 (30 g) and water (300 mL). Whole solution was stirred well and the precipitates were filtered off, washed with CH_2Cl_2 (20 mL). Obtained solid was dried in air over night and dried *in vacuo* for 30 min.

Next, a 1250 mL flask equipped with magnetic stirring bar was charged with previously isolated solid and CH_2Cl_2 (50 mL) was added. Resulting suspension was treated with Et_3N (10 mL), followed by the addition of DMAP (1.13 g, 9.2 mmol). To the open flask Boc_2O (12 g, 55 mmol) was slowly added over 5 min. CAUTION: rapid evolution of CO_2 is observed during the addition! After addition of Boc_2O was complete reaction flask was capped with a septum connected to a bubbler. Reaction mixture was stirred vigorously at 25 °C until the evolution of CO_2 ceased—2 days. Upon completion, reaction mixture was dry-absorbed on silica gel. After purification by column chromatography on silica gel using gradient eluent: 0–15% EtOAc/CH_2Cl_2 and evaporation of the fractions containing the product, compound **50** was obtained as a white solid (1.1 g, 17 % over two steps).

50: ^{1}H NMR (500 MHz, $CDCl_3$) δ 8.61 (d, 3H), 8.21 (d, 3H), 1.95 (s, 6H), 1.67 (s, 27H) ppm. ^{19}F NMR (500 MHz, $CDCl_3$) δ −139.85 to −139.9 (m, 12F) ppm.

Synthesis of Compound **53**

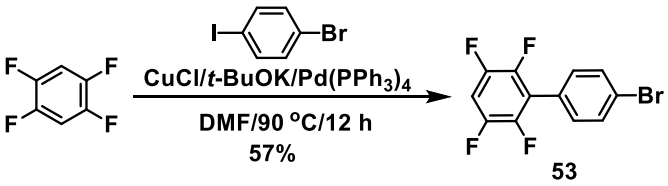

Inside a glovebox a 100 mL screw cap pressure vessel was equipped with magnetic stir bar and charged with CuCl (7.80 g, 78.4 mmol) and *t*BuOK (8.80 g, 78.4 mmol). Dry DMF (40 mL) was added, after that reaction mixture was sealed, vigorously stirred at 25 °C for 1 h inside glovebox. Compound 1,2,4,5-tetrafluorobenzene (10.7 g, 71.3 mmol) was added in one portion, after that reaction mixture was sealed, vigorously stirred at 25 °C for 1 h inside glovebox. Catalyst $Pd(PPh_3)_4$ (823 mg, 0.70 mmol) was added, followed by 1-bromo-4-iodobenzene (22.2 g, 78.4 mmol). Reaction mixture was sealed, taken out of the glovebox and then placed inside an oil bath preheated to 90 °C, where it was stirred vigorously for 12 h. Reaction mixture was cooled to 25 °C, poured into a 2 L beaker containing NH_4OH (100 mL), NH_4Cl (14 g), and H_2O (1 L). Subsequently, CH_2Cl_2 (300 mL) was then added to the beaker and whole solution was vigorously stirred, the layers were separated, and the aqueous layer was extracted with CH_2Cl_2. The combined organic layers were washed with more H_2O until blue color disappeared, after that the collected organic layer was dried over $MgSO_4$, and concentrated *in vacuo*. The residue was purified by column chromatography (SiO_2, gradient eluent: 0–40% CH_2Cl_2/hexane) providing **53** (12.4 g, 52%) as a white solid.

53: ^{1}H NMR (500 MHz, $CDCl_3$) δ 7.64 (d, 2H), 7.32 (d, 2H), 7.08 (m, 1H) ppm. ^{19}F NMR (500 MHz, CDCl3) δ −138.51 to −138.61 (m, 2F), −143.60 to −144.70 (m, 2F) ppm. This compound was used as crude in the next step.

Synthesis of Compound **54**

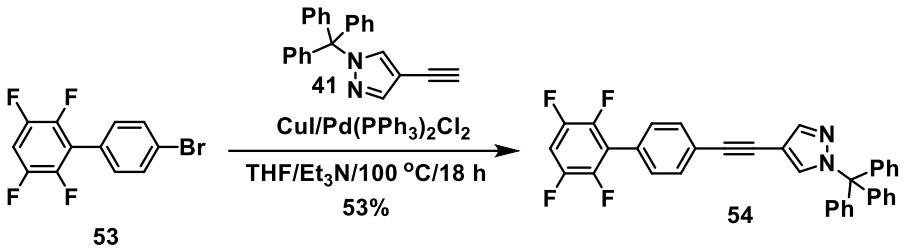

A 500 mL pear-shaped Schlenk flask was charged with compound **53** (9.13 g, 29.9 mmol), compound **41** (13 g, 38.9 mmol), $PdCl_2(PPh_3)_2$ (1.0 g, 1.4 mmol), and CuI (572 mg, 3.0 mmol). The flask was sealed, then evacuated and backfilled with N_2 three times. In a separate flask, a mixture of NEt_3 (100 mL) and THF (100 mL) was degassed for 20 min and then slowly transferred, under positive N_2 pressure, via cannula to the reaction flask. The reaction mixture was stirred and heated at 100 °C for 18 h and then cooled to 25 °C. Afterwards, silica gel (200 mL) was added to the reaction mixture, and the solvent was removed under reduced pressure until a brown powder was formed. This powder was subjected to column chromatography (SiO_2, gradient eluent: 25–35% CH_2Cl_2/hexane) to afford **54** (8.8 g, 53%) as a white solid.

54: ^{1}H NMR (500 MHz, $CDCl_3$) δ 7.83 (s, 1H), 7.62 (s, 1H), 7.54 (d, 2H), 7.42 (d, 2H), 7.33 (m, 9H), 7.16 (m, 6H), 7.07 (m, 1H) ppm. ^{19}F NMR (500 MHz, CDCl3) δ −138.71 to −138.81 (m, 2F), −143.56 to −143.65 (m, 2F) ppm.

Synthesis of Compound **55**

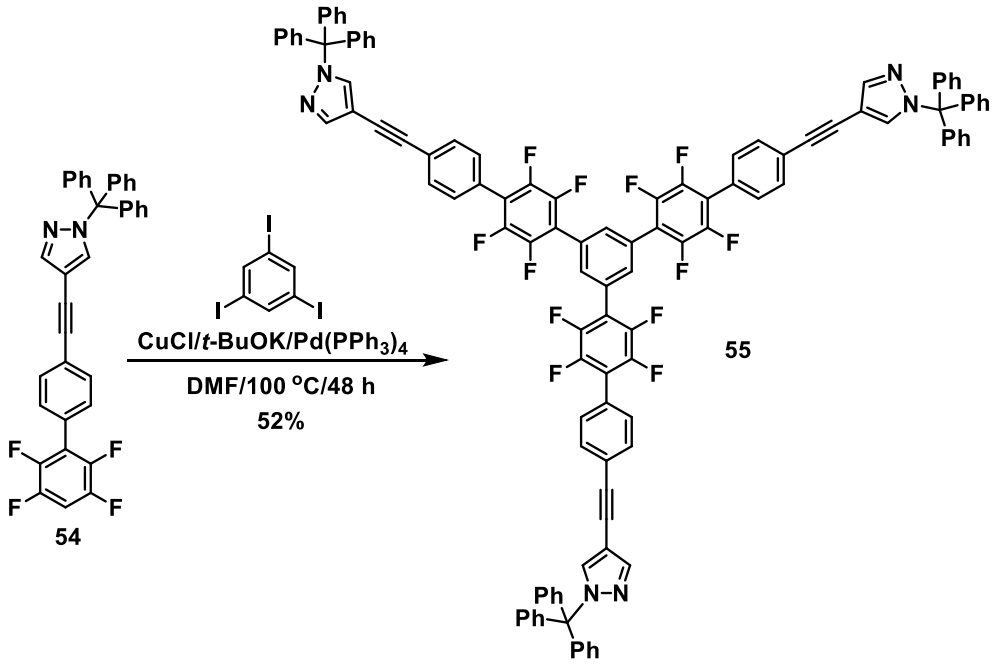

Inside a glovebox, a 100 mL screw cap pressure vessel was equipped with magnetic stir bar and charged with CuCl (1.50 g, 15.2 mmol) and *t*-BuOK (1.70 g, 15.2 mmol). Dry DMF (35 mL) was added, after that reaction mixture was sealed, vigorously stirred at 25 °C for 1 h inside glovebox. *N*-Trityl pyrazole **54** (8.50 g, 15.2 mmol) was added in one portion, after that reaction mixture was sealed, vigorously stirred at 25 °C for 1 h inside glovebox. Catalyst$Pd(PPh_3)_4$ (207 mg, 0.17 mmol) was added, followed by 1,3,5-triiodobenzene (2.04 g, 4.4 mmol). Reaction mixture was sealed, taken out of the glovebox and then placed inside an oil bath preheated to 100 °C, where it was stirred vigorously for 48 h. Reaction mixture was cooled to 25 °C, poured into a 2 L beaker containing NH_4OH (100 mL), NH_4Cl (14 g), and H_2O (1 L). Subsequently, CH_2Cl_2 (300 mL) was added to the beaker and the whole solution was vigorously stirred, the layers were separated, and the aqueous layer was extracted with CH_2Cl_2. The combined organic

layers were washed with more H_2O until blue color dissipated, after that the collected organic layer was dried over $MgSO_4$, and concentrated *in vacuo*. The residue was purified by column chromatography (SiO_2, gradient eluent: 30–90% CH_2Cl_2/hexane) providing **55** (4.1 g, 52%) as a white solid.

55: ^{1}H NMR (500 MHz, $CDCl_3$) δ 7.87 (s, 3H), 7.83 (s, 3H), 7.66 (s, 3H), 7.60 (d, 6H), 7.52 (d, 6H), 7.34 (m, 27H), 7.19 (m, 18H) ppm.^{19}F NMR (500 MHz, CDCl3) δ −143.07 to −143.14 (m, 6F), −143.55 to −143.63 (m, 6F) ppm. This compound was used as crude in the next step.

Synthesis of Compound **56**

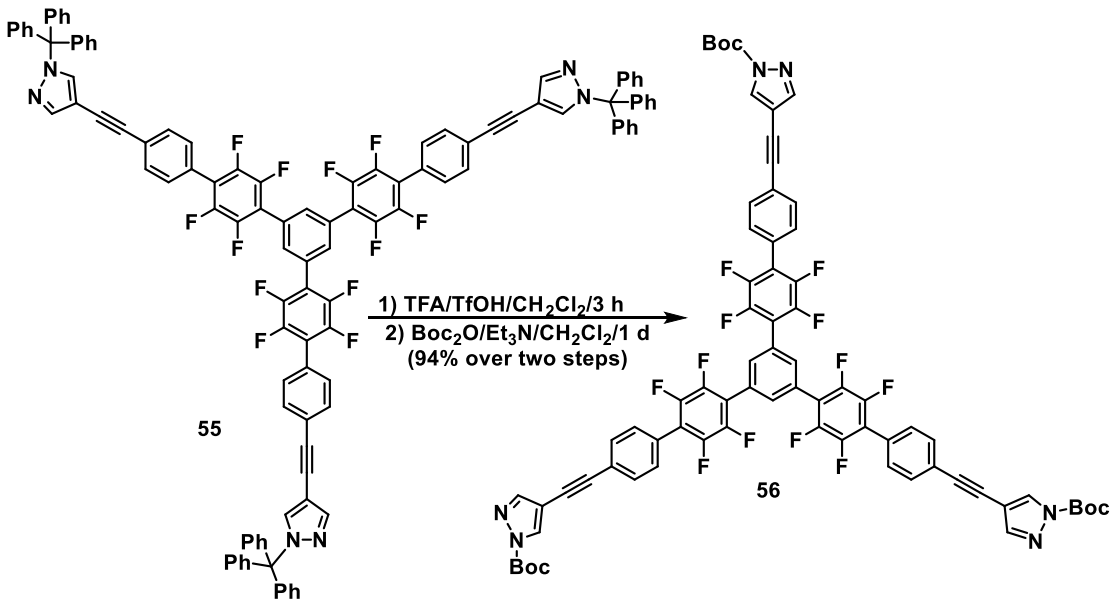

A 250 mL flask equipped with magnetic stirring bar was charged with trityl-protected tripyrazole intermediate **55** (3.80 g, 2.17 mmol) and CH_2Cl_2 (80 mL). Resulting solution was treated with trifluoroacetic acid (12 mL), followed by TfOH (12 mL) causing salt to precipitate. Reaction mixture was vigorously stirred at 25 °C for 3 h.

Resulting solution was poured into a beaker containing K_2CO_3 (30 g) and water (300 mL). Whole solution was stirred well and the precipitates were filtered off, washed with CH_2Cl_2 (20 mL). Obtained solid was dried in air over night and dried *in vacuo* for 30 min.

Next, a 1250 mL flask equipped with magnetic stirring bar was charged with previously isolated solid and CH_2Cl_2 (50 mL) was added. Resulting suspension was treated with Et_3N (9.4 mL), followed by the addition of DMAP (1.20 g, 9.80 mmol). To the open flask Boc_2O (13.2 g, 60.7 mmol) was slowly added over 5 min. CAUTION: rapid evolution of CO_2 is observed during the addition! After addition of Boc_2O was complete, reaction flask was capped with a septum connected to a bubbler. Reaction mixture was stirred vigorously at 25 °C until the evolution of CO_2 ceased—one day. Upon completion, reaction mixture was dry-absorbed on silica gel. After purification by column chromatography on silica gel using gradient eluent: 50–100% CH_2Cl_2/hexane then 5% EtOAc/ CH_2Cl_2 and evaporation of the fractions containing the product, compound **56** was obtained as a white solid (2.7 g, 94 % over two steps).

56: ^{1}H NMR (500 MHz, $CDCl_3$) δ 8.28 (s, 3H), 7.83 (d, 6H), 7.65 (d, 6H), 7.55 (d, 6H), 7.65 (d, 6H), 1.67 (s, 27H) ppm. ^{19}F NMR (500 MHz, CDCl3) δ −143.07 to −143.15 (m, 6F), −143.49 to −143.57 (m, 6F) ppm**.**

4.4.3 Gas Sorption for Noncovalent Organic Framework 52

Crystals of compound **52** were activated by solvent removal using supercritical CO_2. Absolute EtOH was added to the crystals of compound **52** after the mother liquor was decanted. The EtOH was then decanted and replaced repeatedly for 1 d and the crystals were left in EtOH until the next step. Approximately 200 mg of crystals were transferred into a Tousimis Samdri-PVT-3D super-critical CO_2 dryer. Excess EtOH was decanted, the temperature was lowered to 0 ºC, and the chamber was filled with liquid CO_2 (ultrahigh grade CO_2 with a siphon tube from Matheson Tri-Gas Inc. was used). The sample was soaked for 16 h total, venting for 10 min for 10 times. The chamber was then heated to 40 ºC and the pressure in the chamber was above 1300 psi. The supercritical CO_2 was bled off for 12 h until the chamber was at ambient pressure. The chamber was opened and the sample was quickly sealed and taken into an Ar atmosphere glove box for further manipulations. Dried crystals were transferred into a pre-weighed glass sample tube. The tube was sealed and quickly transferred to a system providing 10^{-4} Torr dynamic vacuum. The sample was kept under vacuum at 120 ºC for 15 h then used for gas adsorption measurements.

A Micromeritics ASAP 2020 Surface Area and Porosity Analyzer was used to measure N_2 adsorption isotherms. Oven-dried sample tubes equipped with TranSeals™ (Micrometrics) were evacuated and tared. Sample (178.1 mg) was transferred to the sample tube, which was then capped by a TranSeal™. Samples were heated to 120 ˚C under high vacuum (10−3–10−4 Torr) and held until the outgas rate was less than 2 mTorr/minute. The evacuated sample tube were weighed again, and the sample mass was

determined by subtracting the mass of the previously tared tubes. N_2 isotherms were measured using a liquid nitrogen bath (77 K). Ultrahigh purity grade (99.999% purity) N_2 and He, oil-free valves, and gas regulators were used for all free space corrections and measurements. Relative pressure (P/P_0) range for BET analysis was taken from 5.10^{-5} to 0.1.

4.4.4 Crystal Data of Crystalline Precursors and Noncovalent Organic Framework

Table 4.1 Crystallographic Data of compound **32**

Empirical formula	$C_{24}H_{10}F_8N_4 \cdot ½C_3H_7NO$	
Formula weight	542.91	
Temperature	123(2) K	
Wavelength	1.54178 Å	
Crystal system	Orthorhombic	
Space group	*I*bam	
Unit cell dimensions	a = 7.5844(1) Å	α = 90°
	b = 15.3613(3) Å	β = 90°
	c = 37.0130(6) Å	γ = 90°
Volume	4312.25(12) Å^3	
Z	8	
Density (calculated)	1.672 Mg/m^3	
Absorption coefficient	1.339 mm^{-1}	
F(000)	2192	
Crystal size	0.35×0.15×0.08 mm^3	
θ range for data collection	2.39° to 66.55°	
Index ranges	$0 \le h \le 8$, $0 \le k \le 18$, $0 \le l \le 43$	
Reflections collected	14594	
Independent reflections	2144 [R(int) = 0.0174]	
Completeness to θ = 66.55°	98.7 %	
Absorption correction	Empirical	
Max. and min. transmission	0.7528 and 0.6173	
Refinement method	Full-matrix least-squares on F^2	
Data / restraints / parameters	1867 / 3 / 188	
Goodness-of-fit on F^2	1.284	
Final R indices [$I > 2\sigma(I)$]	R_1 = 0.0500, wR_2 = 0,1237	
R indices (all data)	R_1 = 0.0508, wR_2 = 0.1240	
Absolute structure parameter	0.50	
Extinction coefficient	none	
Largest diff. peak and hole	0.285 and −0.333 e / Å^3	

Table 4.2 Crystallographic Data of Compound **44**

Empirical formula	$C_{21}H_{12}N_6$	
Formula weight	348.37	
Temperature	123(2) K	
Wavelength	1.54178 Å	
Crystal system	Monoclinic	
Space group	*P*2(1)	
Unit cell dimensions	a = 9.5700(3) Å	α = 90°
	b = 9.4056(3) Å	β = 106.840(1)°
	c = 10.6320(3) Å	γ = 90°
Volume	915.96(5) Å^3	
Z	2	
Density (calculated)	1.263 Mg/m^3	
Absorption coefficient	0.641 mm^{-1}	
F(000)	360	
Crystal size	0.45×0.30×0.20 mm^3	
θ range for data collection	4.34° to 66.47°	
Index ranges	$-11 \le h \le 10$, $-10 \le k \le 9$, $0 \le l \le 12$	
Reflections collected	6148	
Independent reflections	2590 [R(int) = 0.0198]	
Completeness to θ = 66.47°	95.1 %	
Absorption correction	Empirical	
Max. and min. transmission	0.7528 and 0.6314	
Refinement method	Full-matrix least-squares on F^2	
Data / restraints / parameters	2572 / 1 / 254	
Goodness-of-fit on F^2	1.058	
Final R indices [$I > 2\sigma(I)$]	R_1 = 0.0262, wR_2 = 0.0732	
R indices (all data)	R_1 = 0.0262, wR_2 = 0.0733	
Absolute structure parameter	0.3(3)	
Extinction coefficient	0.0137(16)	
Largest diff. peak and hole	0.169 and −0.110 e / Å^3	

Table 4.3 Crystallographic Data of Compound **52**

Empirical formula	$C_{102}H_{25}F_{48}N_{12}$
Formula weight	2330.34
Temperature	100(2) K
Wavelength	1.54178 Å
Crystal system	Orthorhombic
Space group	*C*ccm
Unit cell dimensions	a = 15.3843(10) Å α = 90°
	b = 93.285(7) Å β = 90°
	c = 53.370(4) Å γ = 90°
Volume	76592(9) Å^3
Z	16
Density (calculated)	0.808 Mg/m^3
Absorption coefficient	0.735 mm^{-1}
F(000)	18448
Crystal size	0.35×0.10×0.10 mm^3
θ range for data collection	0.947° to 50.557°
Index ranges	$-14 \leq h \leq 15$, $-93 \leq k \leq 91$, $-53 \leq l \leq 53$
Reflections collected	101140
Independent reflections	20264 [R(int) = 0.1896]
Completeness to θ = 67.679°	57.7 %
Absorption correction	None
Refinement method	Full-matrix least-squares on F^2
Data / restraints / parameters	10627 / 1757 / 1624
Goodness-of-fit on F^2	1.088
Final R indices [$I > 2\sigma(I)$]	R_1 = 0.1250, wR_2 = 0.3162
R indices (all data)	R_1 = 0.1844, wR_2 = 0.3553
Extinction coefficient	None
Largest diff. peak and hole	0.711 and −0.617 e / Å^3

References

[1] Wang, B.; Anslyn, B. V. *Chemosensors: Principles, Strategies, and Applications*, John Wiley and Sons, Inc., Hoboken, NJ, **2011**.

[2] Czarnik, A. W. *Advances in Supramolecular Chemistry*, ed. G. W. Gokel, JAI Press, Greenwich, CT, **1993**.

[3] Kim, S. K.; Lee, D. H.; Hong, J.-I.; Yoon, J. *Acc. Chem. Res.* **2009**, *42*, 23–31.

[4] Santos-Figueroa, L. E.; Moragues, M. E.; Climent, E.; Agostini, A.; Martínez-Máñez, R.; Sancenón, F. *Chem. Soc. Rev.* **2013**, *42*, 3489–3613.

[5] Bell, T. W.; Hext, N. M. *Chem. Soc. Rev.* **2004**, *33*, 589–598.

[6] Hulanicki, A.; Glab, S.; Ingman, F. *Pure & Appl. Chem.* **1991**, *63*, 1247–1250.

[7] Kim, H. N.; Ren, W. X.; Kim, J. S.; Yoon, J. *Chem. Soc. Rev.* **2012**, *41*, 3210–3244.

[8] Silva, A. P.; Nimal Gunaratne, H. Q.; Gunnlaugsson, T.; Huxley, A. J. M.; McCoy, C. P.; Rademacher, J. T.; Rice, T. E. *Chem. Rev.* **1997**, *97*, 1515–1566.

[9] Czarnik, A. W. *Fluorescent Chemosensors for Ion and Molecule Recognition*, ACS Symposium Series **1993**, *chapter 1*, 1–9.

[10] Boens, N.; Leen, V.; Dehaen, W.; *Chem. Soc. Rev.* **2012**, *41*, 1130–1172.

[11] Lakowicz, J. R. *Principles of Fluorescence Spectroscopy*, Springer Science+Business Media, LLC, NY, **2006**.

[12] Coble, P. G.; Lead, J.; Baker, A.; Reynolds, D. M.; Spencer, R. G. M. *Aquatic Organic Matter Fluorescence*, Cambridge University Press, NY, **2014**.

[13] Lingeman, H.; Underberg, W. J. M.; Takadate, A.; Hulshoff, A. *J. Liq. Chromatogr.* **1985**, *8*, 789–874.

[14] Valeur, B. *Molecular Fluorescence: Principles and Applications*, WILEY-VCH Verlag GmbH, Weinheim, **2002**.

[15] Gleiter, R.; Haberhauer, G. *Aromaticity and Other Conjugation Effects*, Wiley-VCH: Weinheim, **2012**.

[16] Krygowski, T. M.; Cyrański, M. K. *Aromaticity in Heterocyclic Compounds*, Springer-Verlag Berlin Heidelberg, **2009**.

[17] Orchin, M.; Macomber, R. S.; Pinhas, A. R.; Wilson, R. M. *The Vocabulary and Concepts of Organic Chemistry*, John Wiley & Sons, Inc., NJ, **2005**.

[18] Köhler, A.; Bässler, H. *Electronic Processes in Organic Semiconductor*, Wiley-VCH Verlag GmbH & Co. KGaA, Weinheim, **2015**.

[19] Delhaes, P. *Carbon-based Solids and Materials*, ISTE Ltd and John Wiley & Sons, Inc. **2011**.

[20] (a) Burroughes, J. H.; Bradley, D. D. C.; Brown, A. R.; Marks, R. N.; Mackay, K.; Friend, R. H.; Burns, P. L.; Homes, A. B. *Nature* **1990**, *347*, 539–541. (b) Gross, M.; Müller, D. C.; Nothofer, H.-G.; Scherf, U.; Neher, D.; Bräuchle, C.; Meerholz, K. *Nature* **2000**, *405*, 661–665. (c) O'Neill, M.; Kelly, S. M. *Adv. Mater.* **2003**, *15*, 1135–1146.

[21] (a) Segura, J. L.; Martín, N.; Guldi, D. M. *Chem. Soc. Rev*. **2005**, *34*, 31–47. (b) Günes, S.; Neugebauer, H.; Sariciftci, N. S. *Chem. Rev.* **2007**, *107*, 1324–1338. (c) Cheng, Y.-J.; Yang, S.-H.; Hsu, C.-S. *Chem. Rev*. **2009**, *109*, 5868–5923.

[22] Sariciftci, N. S. *Curr. Opin. Solid-State Mater. Sci.* ***1999***, *4*, 373–378.

[23] (a) Klauk, H. *Chem. Soc. Rev.* **2010**, *39*, 2643–2666. (b) Platt, A. D.; Kendrick, M. J.; Loth, M.; Anthony, J. E.; Ostroverkhova, O. *Phys. Rev. B* **2011**, *84*, 235–209. (c) Wang, C.; Dong, H.; Hu, W.; Liu, Y.; Zhu, D. *Chem. Rev.* **2012**, *112*, 2208–2267.

[24] Li, Y. *Organic Optoelectronic Materials*, Springer International Publishing Switzerland, **2015**.

[25] Barford, W. *Electronic and Optical Properties of Conjugated Polymers*, Oxford University Press, UK, **2013**.

[26] Brédas, J. L.; Silbey, R.; Boudreaux, D. S.; Chance, R. R. *J. Am. Chem. Soc.* **1983**, *105*, 6555–6559.

[27] Fleming, I. *Molecular Orbitals and Organic Chemical Reactions*, John Wiley and Sons Ltd, UK, **2010**.

[28] Clayden, J.; Greeves, N.; Warren, S. *Organic Chemistry*, Oxford University Press Inc., NY, **2012**.

[29] (a) Anthony, J.; Boldi, A. M.; Rubin, Y.; Hobi, M.; Gramlich, V.; Knobler, C. B.; Seiler, P.; Diederich, F. *Helv. Chim. Acta.* **1995**, *78*, 13–45. (b) Jung, K. H.; Bae, S. Y.; Kim, K. H.; Cho, M. J.; Lee, K.; Kim, Z. H.; Choi, D. H.; Lee, D. H.; Chung, D. S.; Park,

C. E. *Chem. Commun.* **2009**, *35*, 5290–5292. (c) Tolosa, J.; Solntsev, K. M.; Tolbert, L. M.; Bunz, U. H. F. *J. Org. Chem.* **2010**, *75*, 523–534.

[30] (a) Klare, J. E.; Tulevski, G.S; Sugo, K.; Picciotto, A. D.; White, K. A.; Nuckolls, C. *J. Am. Chem. Soc.* **2003**, *125*, 6030–6031. (b) Grunder, S.; Huber, R.; Horhoiu, V.; González, M. T.; Schönenberger, C.; Calame, M.; Mayor, M. *J. Org. Chem.* **2007**, *72*, 8337–8344.

[31] Wilson, J. N.; Smith, M. D.; Enkelmann, V.; Bunz, U. H. F. *Chem. Commun.* **2004**, 1700–1701.

[32] (a) Saragi, T. P. I.; Spehr, T.; Siebert, A.; Fuhrmann-Lieker, T.; Salbeck, J. *Chem. Rev*. **2007**, *107*, 1011–1065. (b) Shirota, Y.; Kageyama, H. *Chem. Rev*. **2007**, *107*, 953–1010.

[33] (a) Bartholomew, G. P.; Bazan, G. C. *Acc. Chem. Res.* **2001**, *34*, 30–39. (b) Bartholomew, G. P.; Rumi, M.; Pond, S. J. K.; Perry, J. W.; Tretiak, S.; Bazan, G. C. *J. Am. Chem. Soc.* **2004**, *126*, 11529–11542.

[34] (a) Zen, A.; Pingel, P.; Jaiser, F.; Neher, D.; Grenzer, J.; Zhuang, W.; Rabe, J. P.; Bilge, A.; Galbrecht, F.; Nehls, B. S.; Farrell, T.; Scherf, U.; Abellon, R. D.; Grozema, F. C.; Siebbeles, L. D. A. *Chem. Mater*. **2007**, *19*, 1267–1276. (b) Bilge, A.; Zen, A.; Forster, M.; Li, H.; Galbrecht, F.; Nehls, B. S.; Farrell, T.; Neher, D.; Scherf, U. *J. Mater. Chem.* **2006**, *16*, 3177–3182.

[36] Tolosa, J.; Díez-Barra, E.; Sánchez-Verdú, P.; Rodríguez-López, J. *Tetrahedron Lett.* **2006**, *47*, 4647–4651.

[37] (a) Hsu, H.-F.; Kuo, C.-H.; Chen, C.-F.; Lin, Y.-H.; Huang, L.-Y.; Chen, C.-H.; Cheng, K.-C.; Chen, H.-H. *Chem. Mater.* **2004**, *16*, 2379–2385. (b) Sun, X. B.; Zhou, Y. H.; Wu, W. C.; Liu, Y. Q.; Tian, W. J.; Yu, G.; Qiu, W. F.; Chen, S. Y.; Zhu, D. B. *J. Phys. Chem. B* **2006**, *110*, 7702–7707.

[38] (a) Kim, I. T.; Lee, S. W.; Kim, S. Y.; Lee, J. S.; Park, G. B.; Lee, S. H.; Kang, S. K.; Kang, J. G.; Park, C.; Jin, S. H. *Synth. Met.* **2006**, *156*, 38–41. (b) Kang, J. G.; Cho, H. G.; Kang, S. K.; Park, C.; Lee, S. W.; Park, G. B.; Lee, J. S.; Kim, I. T. *J. Photochem. Photobiol. A* **2006**, *183*, 212–215. (c) Kang, J. G.; Kim, H. J.; Jeong, Y. K.; Nah, M. K.; Park, C.; Bae, Y. J.; Lee, S. W.; Kim, I.T. *J. Phys. Chem. B*, **2010**, *114*, 3791–3798.

[39] (a) Zhao, H.-P.; Tao, X.-T,; Wang, F. –Z.; Ren, Y.; Sun, X.-Q.; Yang, J.-X.; Yan, Y.-X.; Zou, D.-C.; Zhao, X.; Jiang, M.-H. *Chem. Phys. Lett.* **2007**, *439*, 132–137. (b) Gu, R.; Snick, S. V.; Robeyns, K.; Meervelt, L. V.; Dehaen, W. *Org. Biomol. Chem.* **2009**, *7*, 380–385. (c) Gu, R.; Robeyns, K.; Meervelt, L. V.; Toppet, S.; Dehaen, W. *Org. Biomol. Chem*. **2008**, *6*, 2484–2487.

[40] (a) Huo, L.; Hou, J.; Zhang, S.; Chen, H.-Y.; Yang, Y. *Angew. Chem., Int. Ed.* **2010**, *49*, 1500–1503. (b) Liu, Y.; Wang, H.; Dong, H.; Tan, J. Hu, W.; Zhan, X. *Macromolecules* **2012**, *45*, 1296–1302.

[41] (a) Tlach, B. C.; Tomlinson, A. L.; Bhuwalka, A.; Jeffries-EL, M. *J. Org. Chem.* **2011**, *76*, 8670–8681. (b) Mike, J. F.; Nalwa, K.; Makowski, A. J.; Putnam, D.;

Tomlinson, A.; Chaudhary, S.; Jeffries-EL, M. *Phys. Chem. Chem. Phys.* **2011**, *13*, 1338–1344; (c) Intemann, J. J.; Mike, J. F.; Cai, M.; Bose, S.; Xiao, T.; Mauldin, T.; Shinar, J.; Shinar, R.; Jeffries-EL, M. *Macromolecules* **2011**, *44*, 248–255.

[42] Zucchero, A. J.; Mcgrier, P. L.; Bunz, U. H. F. *Acc. Chem. Res.* **2010**, *43*, 397–408.

[43] (a) Wilson, J. N.; Windscheif, P. M.; Evans, U.; Myrick, M. L.; Bunz, U. H. F. *Macromolecules* **2002**, *35*, 8681–8683. (b) Wilson, J. N.; Josowicz, M.; Wang, Y.; Bunz, U. H. F. *Chem. Commun.* **2003**, 2962–2963.

[44] Gerhardt, W. W.; Zucchero, A. J.; Wilson, J. N.; South, C. R.; Bunz, U. H. F.; Weck, M. *Chem. Commun.* **2006**, 2141–2143.

[45] Gerhardt, W. W.; Zucchero, A. J.; South, C. R.; Bunz, U. H. F.; Weck, M. *Chem. Eur. J.* **2007**, *13*, 4467–4474.

[46] Grunder, S.; Huber, R.; Horhoiu, V.; González, M. T.; Schönenberger, C.; Calame, M.; Mayor, M. *J. Org. Chem.* **2007**, *72*, 8337–8344.

[47] Wilson, J. N.; Bunz, U. H. F. *J. Am. Chem. Soc.* **2005**, *127*, 4124–4125.

[48] Zucchero, A. J.; Wilson, J. N.; Bunz, U. H. F. *J. Am. Chem. Soc.* **2006**, *128*, 1872–1881.

[49] Tolosa, J.; Zucchero, A. J.; Bunz, U. H. F. *J. Am. Chem. Soc.* **2008**, *130*, 6498–6506.

[50] (a) Schwaebel, T.; Trapp, O. Bunz, U. H. F. *Chem. Sci*. **2013**, *4*, 273–281. (b)Schwaebel, T.; Menning, S.; Bunz, U. H. F. *Chem. Sci.* **2014**, *5*, 1422–1428.

[51] Hauck, M.; Schönhaber, J.; Zucchero, A. J.; Hardcastle, K. I.; Müller, T. J. J.; Bunz, U. H. F. *J. Org. Chem.* **2007**, *72*, 6714–6725.

[52] Davey, E. A.; Zucchero, A. J.; Trapp, O.; Bunz, U. H. F. *J. Am. Chem. Soc.* **2011**, *133*, 7716–7718

[53] Tolosa, J.; Zucchero, A. J.; Bunz, U. H. F. *J. Am. Chem. Soc.* **2008**, *130*, 6498–6506.

[54] McGrier, P. L.; Solntsev, K. M; Schöhaber, J.; Brombosz, S. M.; Tolbert, L. M.; Bunz, U. H. F. *Chem. Commun.* **2007**, 2127–2129.

[55] McGrier, P. L.; Solntsev, K. M.; Miao, S.; Tolbert, L. M.; Miranda, O. R.; Rotello, V. M.; Bunz, U. H. F. *Chem. Eur. J.* **2008**, *14*, 4503–4510.

[56] Zucchero, A. J.; Shiels, R. A.; McGrier, P. L.; To, M. A.; Jones, C. W.; Bunz, U. H. F. *Chem. Asian. J.* **2009**, *4*, 262–269.

[57] Patze, C.; Broedner, K.; Rominger, F.; Trapp, O.; Bunz. U. H. F. *Chem. Eur. J.* **2011**, *17*, 13720–13725.

[58] Schwaebel, T.; Schäfer, V.; Wenz, J.; Coombs, B. A.; Tolosa, J.; Bunz, U. H. F. *J. Org. Chem.* **2013**, *78*, 960−965.

[59] Freudenberg, J.; Kumpf, J.; Schäfer, V.; Sauter, E.; Wörner, S. J.; Brödner, K.; Dreuw, A.; Bunz, U. H. F. *J. Org. Chem.* **2013**, *78*, 4949−4959.

[60] Brombosz, S. M.; Zucchero, A. J.; Phillips, R. L.; Vazquez, D.; Wilson, A.; Bunz, U. H. F. *Org. Lett.* **2007**, *9*, 4519–4522.

[61] McGrier, P. L.; Solntsev, K. M.; Zucchero, A. J.; Miranda, O. R.; Rotello, V. M.; Tolbert, L. M.; Bunz, U. H. F. *Chem. Eur. J.* **2011**, *17*, 3112–3119.

[62] Wilson, J. N.; Hardcastle, K. I.; Josowicz, M.; Bunz, U. H. F. *Tetrahedron* **2004**, *60*, 7157–7167.

[63] Tolosa, J.; Solntsev, K. M.; Tolbert, L. M.; Bunz, U. H. F. *J. Org. Chem.* **2010**, *75*, 523–534

[64] (a) Ohta, K.; Yamada, S.; Kamada, K.; Slepkov, A. D.; Hegmann, F. A.; Tykwinski, R. R.; Shirtcliff, L. D.; Haley, M. M.; Sałek, P.; Gel'mukhanov, F.; Ågren, H. *J. Phys. Chem. A* **2011**, *115*, 105–117. (b) Spitler, E. L.; Haley, M. M. *Tetrahedron* **2008**, *64*, 11469–11474. (c) Samori, S.; Tojo, S.; Fujitsuka, M.; Spitler, E. L.; Haley, M. M.; Majima, T. *J. Org. Chem.* **2008**, *73*, 3551–3558. (d) Slepkov, A. D.; Hegmann, F. A.; Tykwinski, R. R.; Kamada, K.; Ohta, K.; Marsden, J. A.; Spitler, E. L.; Miller, J. J.; Haley, M. M. *Opt. Lett.* **2006**, *31*, 3315–3317.

[65] (a) Marsden, J. A.; Miller, J. J.; Shirtcliff, L. D.; Haley, M. M. *J. Am. Chem. Soc.* **2005**, *127*, 2464–2476. (b) Miller, J. J.; Marsden, J. A.; Haley, M. M. *Synlett.* **2004**, 165–168.

[66] Spitler, E. L.; Shitcliff, L. D.; Haley, M. M. *J. Org. Chem.* **2007**, *72*, 86–96.

[67] Samori, S.; Tojo, S.; Fujitsuka, M.; Spitler, E. L.; Haley, M. M.; Majima, T. *J. Org. Chem.* **2007**, *72*, 2785–2793.

[68] Spitler, E. L.; Monson, J. M.; Haley, M. M. *J. Org. Chem.* **2008**, *73*, 2211–2223.

[69] Chase, D. T.; Young, B. S.; Haley, M. M. *J. Org. Chem.* **2011**, *76*, 4043–4051.

[70] Zhang, X.-B.; Feng, J.-K.; Ren, A.-M.; Sun, C.-C. *Opt. Mater.* **2007**, *29*, 955–962.

[71] Hori, Y.; Noda, K.; Kobayashi, S.; Taniguchi, H. *Tetrahedron Lett.* **1969**, *40*, 3563–3566.

[72] (a) Hauptmann, V. H. *Angew. Chem.* **1975**, *87*, 490–491. (b) Hauptmann, H. Tetrahedron Lett. **1975**, 1931–1934. (c) Hauptmann, H. *Tetrahedron* **1976**, *32*, 1293–1297.

[76] (a) Diederich, F.; Philp, D.; Seiler, P. J. *Chem. Soc., Chem. Commun.* **1994**, 205–208. (b) Philp, D.; Gramlich, V.; Seiler, P.; Diederich, F. *J. Chem. Soc. Perkin Trans. 2* **1995**, 875–886.

[77] Rubin, Y.; Knobler, C. B.; Diederich, F. *Angew. Chem. Int. Ed.* **1991**, *30*, 698–670.

[78] Anthony, J.; Boldi, A. M.; Rubin, Y.; Hobi, M.; Gramlich, V.; Knobler, C. B.; Seiler, P.; Diederich, F. *Helv. Chim. Acta* **1995**, *78*, 13–45.

[79] Hilger, A.; Gisselbrecht, J.-P.; Tykwinski, R. R.; Boudon, C.; Schreiber, M.; Martin, R. E.; Lüthi, H. P.; Gross, M.; Diederich, F. *J. Am. Chem. Soc.* **1997**, *119*, 2069–2078.

[80] Boudon, C.; Gisselbrecht, J. P.; Gross, M.; Anthony, J.; Boldi, A. M.; Faust, R.; Lange, T.; Philp, D.; Van Loon, J.-D.; Diederich, F. *J. Electroanal. Chem.* **1995**, *394*, 187–197.

[81] (a) Bosshard, C.; Spreiter, R.; Günter, P.; Tykwinski, R. R.; Schreiber, M.; Diederich, F. *Adv. Mater*. **1996**, *8*, 231–234. (b) Tykwinski, R. R.; Schreiber, M.; Carlón, R. P.; Diederich, F.; Gramlich, V. *Helv. Chim. Acta* **1996**, *79*, 2249–2281.

[82] Gobbi, L.; Seiler, P.; Diederich, F. *Angew. Chem. Int. Ed.* **1999**, *38*, 674–678.

[83] Saeed, M. A.; Le, H. T. M.; Miljanić, O. Š. *Acc. Chem. Res.* **2014**, *47*, 2074–2083.

[84] Feldman, A. K.; Steigerwald, M. L.; Guo, X.; Nuckolls, C. *Acc. Chem. Res.* **2008**, *41*, 1731−1741.

[85] Intemann, J. J.; Hellerich, E. S.; Tlach, B. C.; Ewan, M. D.; Barnes, C. A.; Bhuwalka, A.; Cai, M.; Shinar, J.; Shinar, R.; Jeffries-EL, M. *Macromolecules* **2012**, *45*, 6888−6897.

[86] Klare, J. E.; Tulevski, G. S.; Sugo, K.; de Picciotto, A.; White, K. A.; Nuckolls, C. *J. Am. Chem. Soc.* **2003**, *125*, 6030−6031.

[87] Hegedus, L. S.; Odle, R. R.; Winton, P. M.; Weider, P. R. *J. Org. Chem.* **1982**, *47*, 2607−2613.

[88] Lim, J.; Albright, T. A.; Martin, B. R.; Miljanić, O. Š. *J. Org. Chem*. **2011**, *76*, 10207−10219.

[89] Mike, J. F.; Makowski, A. J.; Jeffries-EL, M. *Org. Lett.* **2008**, *10*, 4915−4918.

[90]Tlach, B. C.; Tomlinson, A. L.; Ryno, A. G.; Knoble, D. D.; Drochner, D. L.; Krager, K. J.; Jeffries-EL, M. *J. Org. Chem.* **2013**, *78*, 6570−6581.

[91] Troegel, D.; Möller, F.; Burschka, C.; Tacke, R. *Organometallics* **2009**, *28*, 3218−3224.

[92] Schwaebel, T.; Lirag, R. C.; Davey, E. A.; Lim, J.; Bunz, U. H. F.; Miljanić, O. Š. *J. Visualized Exp.* **2013**, *78*, No. e50858.

[93] Lim, J.; Miljanić, O. Š. *Chem. Commun*. **2012**, *48*, 10301−10303.

[94] Jo, M.; Lim, J.; Miljanić, O. Š. *Org. Lett.* **2013**, *15*,3518−3521.

[95] Lirag, R. C.; Le, H. T. M.; Miljanić, O. Š. *Chem. Commun.* **2013**, *49*, 4304−4306.

[96] (a) Molina, P.; Tárraga, A.; Otón, F. *Org. Biomol. Chem.* **2012**, *10*, 1711–1711. (b) Benelhadj, K.; Massue, J.; Retailleau, P.; Ulrich, G.; Ziessel, R. *Org. Lett.* **2013,** *15*, 2918–2921. (c) Hung, W.-Y.; Chi, L.-C.; Chen, W.-J.; Chen, Y.-M.; Chou, S.-H.; Wong, K.-T. *J. Mater. Chem.* **2010**, *20*, 10113–10119.

[97] (a) Song, K. C.; Choi, M. G.; Ryu, D. H.; Kim, K. N.; Chang, S. K. *Tetrahedron Lett.* **2007**, *48*, 5397–5400. (b) Lin, W.; Yuan, L.; Tan, W.; Feng, J.; Long, L. *Chem. Eur. J.* **2009**, *15*, 1030–1035. (c) Lin, W.; Long, L.; Chen, B.; Tan, W. *Chem. Eur. J.* **2009**, *15*, 2305–2309. (d) Lin, W.; Long, L.; Yuan, L.; Cao, Z.; Chen, B.; Tan, W. *Org. Lett.* **2008**, *10*, 5577–5580 (e) Wang, J.; Lin, W.; Li, W. *Chem. Eur. J.* **2012**, *18*, 13629– 13632 (f) Zheng, K.; Lin, W.; Tan, L. *Org. Biomol. Chem.* **2012**, *10*, 9683–9688. (g) Yan, Y.; Zhang, R.; Yu, X.; Xu, H. *ChemPlusChem* **2014**, *79*, 1676–1680.

[98] Xue, Z. W.; Chen, M. L.; Chen, J. M.; Han, J. H.; Han, S. F. *RSC Adv.* **2014**, *4*, 374–378.

[99] Kim, H. J.; Heo, C. H.; Kim, H. M. *J. Am. Chem. Soc.* **2013**, *135*, 17969−17977.

[100] Abraham, Y.; Salman, H.; Suwinska, K.; Eichen, Y. *Chem. Commun.* **2011**, *47*, 6087–6089.

[101] Rouffet, M.; Oliveria, C. A. F.; Udi, Y.; Agrawai, A.; Sagi, I.; McCammon, J. A.; Cohen, S. M. *J. Am. Chem. Soc.* **2010**, *132*, 8232–8233.

[102] (a) Song, S.; Ko, S.-J.; Kim, J. A.; Jin, Y.; Kim, I.; Kim, J. Y.; Suh, H. *Polymer Journal* **2013**, *45*, 555–559. (b) Tamilavan, V.; Song, M.; Agneeswari, R.; Kim, S.; Hyun, M. H. *Bull. Korean Chem. Soc.* **2014**, 35, 1098–1104.

[103] Ku, J.; Lansac, Y.; Jang, Y. H. *J. Phys. Chem. C* **2011**, *115*, 21508–21516.

[104] Ravichandran, M. *Chemosphere* **2004**, *55*, 319–331.

[105] Li, A.-F.; Wang, J.-H.; Wang, F.; Jiang, Y.-B. *Chem. Soc. Rev.* **2010**, *39*, 3729–3745.

[106] (a) Wsik, R.; Wińska, P.; Poznański J.; Shugar, J. *J. Phys. Chem. B* **2012**, *116*, 7259–7268; (b) Peng, Q.; Xu, J.; Zheng, W. *J. Polym. Sci., Part A: Polym. Chem.* **2009**, *47*, 3399–3408.

[107] (a) Osowska, K.; Miljanić, O. Š. *J. Am. Chem. Soc.* **2011**, *133*, 724–727. (b) Osowska, K.; Miljanić, O. Š. *Synlett* **2011**, 1643–1648.

[108] Gaussian 09, Revision B.01: Frisch, M. J.; Trucks, G. W.; Schlegel, H. B.; Scuseria, G. E.; Robb, M. A.; Cheeseman, J. R.; Scalmani, G.;Barone, V.; Mennucci, B.;

Petersson, G. A.; Nakatsuji, H.; Caricato, M.; Li, X.; Hratchian, H. P.; Izmaylov, A. F.; Bloino, J.; Zheng, G.; Sonnenberg, J. L.; Hada, M.; Ehara, M.; Toyota, K.; Fukuda, R.; Hasegawa, J.; Ishida, M.; Nakajima, T.; Honda, Y.; Kitao, O.; Nakai, H.; Vreven, T.; Montgomery, J. A., Jr.; Peralta, J. E.; Ogliaro, F.; Bearpark, M.; Heyd, J. J.; Brothers, E.; Kudin, K. N.; Staroverov, V. N.; Keith, T.; Kobayashi, R.; Normand, J.; Raghavachari, K.; Rendell, A.; Burant, J. C.; Iyengar, S. S.; Tomasi, J.; Cossi, M.; Rega, N.; Millam, J. M.; Klene, M.; Knox, J. E.; Cross, J. B.; Bakken, V.; Adamo, C.; Jaramillo, J.; Gomperts, R.; Stratmann, R. E.; Yazyev, O.; Austin, A. J.; Cammi, R.; Pomelli, C.; Ochterski, J. W.; Martin, R. L.; Morokuma, K.; Zakrzewski, V. G.; Voth, G. A.; Salvador, P.; Dannenberg, J. J.; Dapprich, S.; Daniels, A. D.; Farkas, O.; Foresman, J. B.; Ortiz, J. V.; Cioslowski, J.; Fox, D. J. Gaussian, Inc., Wallingford, CT, 2010.

[109] Walba, H.; Isensee, R. W. *J. Org. Chem.* **1961**, *26*, 2789–2791. The only two compounds in the series that respond to deprotonation with a blue shift are **6** and **12**, which have significantly higher LUMO than HOMO densities in the imidazole ring.

[110] These values are quoted for the parent molecules, and may in fact vary significantly in an extensively substituted system such as **10**. See http://www.zirchrom.com/organic.htm.

[111] (a) Carroll, C. N.; Naleway, J. J.; Haley, M. M.; Johnson, D. W. *Chem. Soc. Rev.* **2010**, *39*, 3875–3888. (b) Sessler, J. L.; Gale, P.; Cho, W.-S. *Anion Receptor Chemistry*, RSC Publishing, Cambridge, **2006**. (c) Gale, P. A. *Chem. Commun.* **2011**, *47*, 82–86. (d)

Bayly, S. R.; Beer, P. D. *Top. Curr. Chem.* **2008**, *129*, 45–94. (e) Martinez-Mánez, R.; Sancenon, F. *Chem. Rev.* **2003**, *103*, 4419–4476.

[112] Frantz, D. K.; Linden, A.; Baldridge, K. K.; Siegel, J. S. *J. Am. Chem. Soc.* **2012**, *134*, 1528−1535.

[113] Pilgram, K.; Zupan, M.; Skiles, R. *J. Heterocycl. Chem*. **1970**, *7*, 629–633.

[114] Gearson, R. G. *J. Chem. Educ.* **1968**, *45*, 581–587.

[115] (a) Ashby, C. I. H.; Cheng, C. P.; Duesler, E. N.; Brown, T. L. *J. Am. Chem. Soc.* **1978**, *30*, 6057–6063. (b) Sandmark, C. *Acta Chem. Scand.* **1967**, *21*, 993–999.

[116] (a) Chun, H.; Kim, D.; Dybtsev, D. N.; Kim, K. *Angew. Chem. Int. Ed.* **2004**, *43*, 971–974. (b) Zhu, R.-Q. *Acta Cryst.* **2012**, *E68*, m439.

[117] (a) Wang, B.; Côté, A. P.; Furukawa, H.; O'Keeffe, M.; Yaghi, O. M. *Nature* **2008**, *453*, 207–211. (b) Banerjee, R.; Phan, A.; Wang, B.; Knobler, C.; Furukawa, H.; O'Keeffe, M.; Yaghi, O. M. *Science* **2008**, *319*, 939–943.

[118] Peng, Q.; Xu, J.; Zheng, W. X. *J. Polym. Sci., Part A: Polym. Chem.* **2009**, *47*, 3399–3408.

[119] Pilgram, K.; Zupan, M.; Skiles, R. *J. Heterocycl. Chem.* **1970**, *7*, 629–633.

[120] Abraham, Y.; Salman, H.; Suwinska, K.; Eichen, Y. *Chem. Commun.* **2011**, *47*, 6087–6089.

[121] Osowska, K.; Miljanić, O. Š. *J. Am. Chem. Soc.* **2011**, *133*, 724–727.

[122] Le, H. T. M.; El-Hamdi, N. S.; Miljanić, O. Š. *J. Org. Chem.* **2015**, *80,* 5210–5217.

[123] (a) Lim, J.; Nam, D.; Miljanić, O. Š. *Chem. Sci.* **2012**, *3*, 559–563. (b) Saeed, M. A.; Le, H. T. M.; Miljanić, O. Š. *Acc. Chem. Res.* **2014**, *47*, 2074−2083. (c) Martínez-Martínez, V.; Lim, J.; Bañuelos, J.; López-Arbeloa, I.; Miljanić, O. Š. Phys. Chem. Chem. Phys. **2013**, *15*, 18023−18029. (d) Lim, J.; Albright, T. A.; Martin, B. R.; Miljanić, O. Š. *J. Org. Chem.* **2011**, *76*, 10207−10219.

[124] (a) Boydston, A. J.; Pecinovsky, C. S.; Chao, S. T.; Bielawski, C. W. *J. Am. Chem. Soc.* **2007**, *129*, 14550−14551. (b) Boydston, A. J.; Vu, P. D.; Dykhno, O. L.; Chang, V.; Wyatt, A. R., II; Stockett, A. S.; Ritschdorff, E. T.; Shear, J. B.; Bielawski, C. W. *J. Am. Chem. Soc.* **2008**, *130*, 3143−3156. (c) Boydston, A. J.; Khramov, D. M.; Bielawski, C. W. *Tetrahedron Lett.* **2006**, *47*, 5123−5125. (d) Khramov, D. M.; Boydston, A. J.; Bielawski, C. W. *Org. Lett.* **2006**, *8*, 1831−1834.

[125] Cohen, Y.; Avram, L.; Frish, L. *Angew. Chem. Int. Ed.* **2005**, *44*, 520–554.

[126] Jiang, W.; Schafer, A.; Mohr, P. C.; Schalley, C. A. *J. Am. Chem. Soc.* **2010**, *132*, 2309–2320.

[127] Lavigne, J. J.; Anslyn, E. V. *Angew. Chem. Int. Ed.* **2001**, *40*, 3119–3130.

[128] Anzenbacher, P.; Lubal, P.; Bucek, P.; Palacios, M. A.; Kozelkova, M. E. *Chem. Soc. Rev.* **2010**, *39*, 3954–3979.

[129] Zhang, C.; Bailey, D. P.; Suslick, K. S. *J. Agric. Food. Chem.* **2006**, *54*, 4925–4931.

[130] Buryak, A.; Severin, K. *Angew. Chem. Int. Ed.* **2005**, *44*, 7935–7938.

[131] Palacios, M. A.; Wang, Z.; Montes, V. A.; Zyryanov, G. V.; Anzenbacher, P. *J. Am. Chem. Soc.* **2008**, *130*, 10307–10314.

[132] You, L.; Zha, D.; Anslyn, E. V. *Chem. Rev.* **2015**, *72*, 687–699.

[133] Colour Contrast Analyser can be freely downloaded from: http://www.visionaustralia.org/digital-access-cca. Last accessed on June 25, 2015.

[134] Schwaebel, T.; Lirag, R. C.; Davey, E. A.; Lim, J.; Bunz, U. H.; Miljanić, O. Š. *J. Vis. Exp.* **2013**, e50858.

[135] Hegedus, L. S.; Odle, R. R.; Winton, P. M.; Weider, P. R. *J. Org. Chem.* **1982**, *47*, 2607−2613.

[136] (a) Zhang, L.-P.; Jiang, K.-J.; Li, G.; Zhang, Q.-Q.; Yang, L.-M. *J. Mater. Chem.* A **2014**, *2*, 14852−14857. (b) Li, H.; Kim, F. S.; Ren, G.; Hollenbeck, E. C.; Subramaniyan, S.; Jenekhe, S. A. *Angew. Chem., Int. Ed.* **2013**, *52*, 5513−5517.

[137] Nihei, M.; Kurihara, M.; Mizutani, J.; Nishihara, H. *J. Am. Chem. Soc.* **2003**, *125*, 2964−2973.

[138] For example, cruciform **24j** appears to have a fluorescence quantum yield of 98% (measured using 9,10-diphenylanthracene as the standard). We will elaborate on this

finding and other related studies in a future paper dealing exclusively with the photophysics of benzobisimidazole cruciforms.

[139] Lirag, R. C.; Le, H. T. M.; Miljanić, O. Š. *Chem. Commun.* **2013**, *49*, 4304−4306.

[140] Sun, H.; Wang, B.; DiMagno, S. G. *Org. Lett.*, **2008**, *10*, 4413–4416.

[141] (*a*) Bordwell, F. G. *Acc. Chem. Res.*, 1988, **21**, 456–463. We did not use pK_a values for THF solutions, as those appear much less accurate than their DMSO counterparts. See: (*b*) Bordwell, F. G. *Pure Appl. Chem.*, 1977, **49**, 963–968.

[142] Bordwell, F. G.; Algrim, D. *J. Org. Chem.*, 1976, **41**, 2507–2508.

[143] Hildebrand, J. H. *Principles of Chemistry*, New York, The Macmillan Company, 1940.

[144] Dippy, J. F. J.; Hughes, S. R. C.; Rozanski, A. *J. Chem. Soc.*, 1959, 2492–2498.

[145] Takayama, Y.; Yamada, T.; Tatekabe, S.; Nagasawa, K. *Chem. Commun.* **2013**, *49*, 6519−6521.

[146] Boyer, J. H.; Buriks, R. S.; Toggweiler, U. *J. Am. Chem. Soc.* **1960**, *82*, 2213−2215.

[147] Nihei, M.; Kurihara, M.; Mizutani, J.; Nishihara, H. *J. Am. Chem. Soc*. **2003**, *125*, 2964−297.

[148] McGrier, P. L.; Solntsev, K. M.; Schönhaber, J.; Brombosz, S. M.; Tolbert, L. M.; Bunz, U. H. F. *Chem. Commun.* **2007**, 2127−2129.

[149] (a) Thomas, A. *Angew. Chem. Int. Ed.* **2010**, *49*, 8328–8344. (b) Zhang, Y.; Riduan, S. N. *Chem. Soc. Rev.* **2012**, *41*, 2083–2094.

[150] Mastalerz, M. *Chem. Eur. J.* **2012**, *18*, 10082–10091.

[151] (a) Li, H.; Eddaoudi, M.; O'Keeffe, M.; Yaghi, O. M. *Nature* **1999**, *402*, 276–279. (b) Furukawa, H.; Ko, N.; Go, Y. B.; Aratani, N.; Choi, S. B.; Choi, E.; Yazaydin, A. Ö.; Snurr, R. Q.; O'Keeffe, M.; Kim, J.; Yaghi, O. M. Science **2010**, *329*, 424–427.

[152] (a) Côté, A. P.; Benin, A. I.; Ockwig, N. W.; O'Keeffe, M.; Matzger, A. J.; Yaghi, O. M. *Science* **2005**, *310*, 1166–1170. (b) Ding, S.-Y.; Wang, W. *Chem. Soc. Rev.* **2013**, *42*, 548–568.

[153] Cheng, G.; Hasell, T.; Trewin, A.; Adams, D. J.; Cooper, A. I. *Angew. Chem. Int. Ed.* **2012**, *51*, 7982–7893.

[154] (a) Cohen, S. M. *Chem. Rev.* **2012**, *112*, 970–1000. (b) Wang, Z.; Cohen, S. M. *Chem. Soc. Rev.* **2009**, *38*, 1315–1329.

[155] Mueller, U.; Schubert, M.; Teich, F.; Puetter, H.; Schierle-Arndt, K.; Pastre, J. *J. Mater. Chem.* **2006**, *16*, 626–636.

[156] Li, J.-R.; Kuppler, R. J.; Zhou, H.-C. *Chem. Soc. Rev.* **2009**, *38*, 1477–1504.

[157] (a) MacGillivray, L. R. *Metal-Organic Frameworks: Design and Applications*, Wiley: Hoboken, NJ, **2010**. (b) Lee, J.; Farha, O. K.; Roberts, J.; Scheidt, K. A.; Nguyen, S. T.; Hupp, J. T. *Chem. Soc. Rev.* **2009**, *38*, 1450–1459.

[158] Kreno, L. E.; Leong, K.; Farha, O. K.; Allendorf, M.; Duyne, R. P. V.; Hupp, J. T. | *Chem. Rev.* **2012**, *112*, 1105–1125.

[159] (a) Rocca, J. D.; Liu, D.; Lin, W. *Acc. Chem. Res.* **2011**, *44*, 957–968. (b) Horcajada, P.; Serre, C.; Maurin, G.; Ramsahye, N. A.; Balas, F.; Vallet-Regi, M.; Sebban, M. Taulelle, F.; Férey, G. *J. Am. Chem. Soc.* **2008**, *130*, 6774–6780.

[160] Aoyama, Y. *Top. Curr. Chem.* **1998**, *198*, 131–161.

[161] He, Y.; Xiang, S.; Chen, B. *J. Am. Chem. Soc.* **2011**, *133*, 14570–14573.

[162] (a) Jones, J. T. A.; Hasell, T.; Wu, X.; Bacsa, J.; Jelfs, K. E.; Schmidtmann, M.; Chong, S. Y.; Adams, D. J.; Trewin, A.; Schiffman, F.; Cora, F.; Slater, B.; Steiner, A.; Day, G. M.; Cooper, A. I. *Nature* **2011**, *474*, 367–371. (b) Cooper, A. I. *Angew. Chem., Int. Ed.* **2012**, *51*, 7892–7894. (c) Hasell, T.; Zhang, H.; Cooper, A. I. *Adv. Mater.* **2012**, *24*, 5732–5737. (d) Holst, J. R.; Trewin, A.; Cooper, A. I. *Nat. Chem.* **2010**, *2*, 915–920. (e) Tozawa1, T.; Jones, J. T. A.; Swamy, S. I.; Jiang, S.; Adams, D. J.; Shakespeare, S.; Clowes, R.; Bradshaw, D.; Hasell, T.; Chong, S. Y.; Tang, C.; Thompson, S.; Parker, J.; Trewin, A.; Bacsa, J.; Slawin, A. M. Z.; Steiner, A.; Cooper, A. I. *Nat. Mater.* **2009**, *8*, 973–978. (f) Jones, J. T. A.; Holden, D.; Mitra, T.; Hasell, T.; Adams, D. J.; Jelfs, K. E.; Trewin, A.; Willock, D. J.; Day, G. M.; Bacsa, J.; Steiner, A.; Cooper, A. I. *Angew. Chem. Int. Ed.* **2011**, *50*, 749–753.(g) Mitra, T.; Wu, X.; Clowes, R.; Jones, J. T. A.; Jelfs, K. E.; Adams, D. J; Trewin, A.; Bacsa, J.; Steiner, A.; Cooper, A. I. *Chem. Eur. J.* **2011**, *17*, 10235–10240.

[163] (a) Zhang, G.; Mastalerz, M. *Chem. Soc. Rev.* **2014**, *43*, 1934–1947. (b) Mastalerz, M.; Oppel, I. M. *Angew. Chem., Int. Ed.* **2012**, *51*, 5252–5255. (c) Schneider, M. W.; Oppel, I. M.; Ott, H.; Lechner, L. G.; Hauswald, H.-J.; Stoll, R.; Mastalerz, M. *Chem. Eur. J.* **2012**, *18*, 836–847. (d) Mastalerz, M.; Schneider, M. W.; Oppel, I. M.; Presly, O. *Angew. Chem., Int. Ed.* **2011**, *50*, 1046–1050. (e) Zhang, G.; Presly, O.; White, F.; Oppel, I. M.; Mastalerz, M. *Angew. Chem., Int. Ed.* **2014**, *53*, 5126–5130. (f) Zhang, G.; Presly, O.; White, F.; Oppel, I. M.; Mastalerz, M. *Angew. Chem., Int. Ed.* **2014**, *53*, 1516–1520. (g) Brutschy, M.; Schneider, M. W.; Mastalerz, M.; Waldvogel, S. R. *Adv. Mater.* **2012**, *24*, 6049–6052. (h) Schneider, M. W.; Oppel, I. M.; Griffin, A.; Mastalerz, M. *Angew. Chem. Int. Ed.* **2013**, *52*, 3611–3615. (i) Elbert, S. M.; Rominger, F.; Mastalerz, M. *Chem. Eur. J.* **2014**, *20*, 16707–16720. (j) Mastalerz, M. *Chem. Comm.* **2008**, 4756.

[164] (a) Li, P.; He, Y.; Guang, J.; Weng, L.; Zhao, J. C.-G.; Xiang, S.; Chen, B. *J. Am. Chem. Soc.* **2014**, *136*, 547–549. (b) Wang, H.; Li, B.; Wu, H.; Hu, T.-H.; Yao, Z.; Zhou, Z.; Xiang , Z. and Chen, B. *J. Am. Chem. Soc.* **2015**, *137*, 9963–9970. (c) Li, P.; He, Y.; Arman, H. D.; Krishna, R.; Wang, H.; Weng, L.; Chen, B. *Chem. Commun.* **2014**, *50*, 13081–13084. (d) Xiang, S.; Zhang, Z.; Zhao, C.-G.; Hong, K.; Zhao, X.; Ding, D.-L.; Xie, M.-H.; Wu, C.-D.; Gill, R.; Thomas, K. M.; Chen, B. *Nat. Commun.* **2010,** *2*, 204.

[165] Luo, X.-Z.; Jia, X.-J.; Deng, J.-H.; Zhong, J.-L.; Liu, H.-J.; Wang, K.-J.; Zhong, C. *J. Am. Chem. Soc.* **2013**, *135*, 11684–11687.

[166] Yang, W.; Greenaway, A.; Lin, X.; Matsuda, R.; Blake, A. J.; Wilson, C.; Lewis, W.; Hubberstey, P.; Kitagawa, S.; Champness, N. R.; Schröder, M. *J. Am. Chem. Soc.* **2010**, *132*, 14457–14469.

[167] Brunet, P.; Simard, M.; Wuest, J. D. *J. Am. Chem. Soc.* **1997**, *119*, 2727–2738.

[168] (a) Atwood, J. L.; Barbour, L. J.; Jerga, A. *Science* **2002**, *296*, 2367–2369. (b) MacGillivray, L. R.; Atwood, J. L. *Nature* **1997**, *389*, 469–472. (c) Orr, G. W.; Barbour, L. J.; Atwood, J. L. *Science* **1999**, *285*, 1049–1052.

[169] (a) Soldatov, D. V.; Moudrakovski, I. L.; Grachev, E. V.; Ripmeester, J. A. *J. Am. Chem. Soc.* **2006**, *128*, 6737–6744. (b) Soldatov, D. V.; Moudrakovski, I. L.; Ripmeester, J. A. *Angew. Chem. Int. Ed.* **2004**, *43*, 6308–6311.

[170] Chakrabarty, R.; Mukherjee, P. S.; Stang, P. J. *Chem. Rev.* **2011**, *111*, 6810–6918.

[171] Slater, A. G.; Cooper, A. I. *Science* **2015**, *348*, 988.

[172] (a) Atwood, J. L.; Barbour, L. J.; Jerga, A. *Science* **2002**, *296*, 2367–2369. (b) MacGillivray, L. R.; Atwood, J. L. *Nature* **1997**, *389*, 469–472. (c) Orr, G. W.; Barbour, L. J.; Atwood, J. L. *Science* **1999**, *285*, 1049–1052.

[173] Lim, S.; Kim, H.; Selvapalam, N.; Kim, K.-J.; Cho, S. J.; Seo, G.; Kim, K. *Angew. Chem. Int. Ed.* **2008**, *47*, 3352–3355.

[174] (a) Shimizu, L. S.; Hughes, A. D.; Smith, M. D.; Davis, M. J.; Zhang, B. P.; Loye, H.-C.; Shimizu, K. D. *J. Am. Chem. Soc.* **2003**, *125*, 14972–14973. (b) Dewal, M. B.;

Lufaso, M. W.; Hughes, A. D.; Samuel, S. A.; Pellechia, P.; Shimizu, L. S. Chem. Mater. 2006, 18, 4855–4864.

[175] (a) Plattner, D. A.; Beck, A. K.; Neuburger, M. *Helv. Chim. Acta* **2002**, *85*, 4000–4010. (b) Gleiter, R.; Werz, D. B.; Rausch, B. J. *Chem. Eur. J.* **2003**, *9*, 2676–2683. (c) Ghadiri, M. R.; Granja, J. R.; Buehler, L. K. *Nature* **1994**, *369*, 301–304. (d) Zhang, J.; Moore, J. S. *J. Am. Chem. Soc.* **1992**, *114*, 9701–9702. (e) Moore, J. S. *Acc. Chem. Res.* **1997**, *30*, 402–413. (f) Gauthier, D.; Baillargeon, P.; Drouin, J.; Dory, Y. L. *Angew. Chem., Int. Ed.* **2001**, *40*, 4635–4638.

[176] Silva, F. C. S.; Lima, S. M.; Demets, G. J.-F. *RSC Adv.* **2014**, *4*, 58796–58799.

[177] Mitra, T.; Jelfs, K. E.; Schmidtmann, M.; Ahmed, A.; Chong, S. Y.; Adams, D. J.; Cooper, A. I. *Nat. Chem.* **2013**, *5*, 276–281.

[178] Tian, J.; Thallapally, P.; Liu, J.; Exarhos, G. J.; Atwood, J. L. *Chem. Commun.* **2011**, *47*, 701–703.

[179] Dianin, J. *J. Russ. Phys. Chem. Soc.***1914**, *46*, 1310–1319.

[180] Baker, W.; Floyd, A. J.; McOmie, J. F. W.; Pope, G.; Weaving, A. S.; Wild, J. H. *J. Chem. Soc.***1956**, 2010–2017.

[181] Barrer, R. M.; Shanson,V. H. *J. Chem. Soc., Chem. Commun.***1976**, 333–334.

[182] Tian, J.; Thallapally, P. K.; McGrail B. P. *CrystEngComm.* **2012**, *14*, 1909–1919.

[183] (a) Sozzani, P.; Bracco, S.; Comotti, A.; Ferretti, L.; Simonutti, R. *Angew. Chem., Int. Ed.* **2005**, *44*, 1816–1820. (b) Comotti, A.; Bracco, S.; Ferretti, L.; Mauri, M.; Simonutti, M.; Sozzani, P. *Chem. Commun.* **2007**, 350–352.

[184] Mastalerz, M.; Oppel, I. M. *Angew. Chem., Int. Ed.* **2012**, *51*, 5252–5255.

[185] Chen, T.; Popov, I.; Kaveevivitchai, W.; Chuang, Y.; Chen, Y.; Daugulis, O.; Jacobson, A. J.; Miljanić, O. Š. *Nat. Comm.* **2014**, *5*, article number: 5131.

[186] Chen, T.-H.; Kaveevivitchai, W.; Jacobson, A. J.; Miljanić, O. Š. *Chem. Commun.* **2015**, *51*, 14096–14098.

[187] Do, H.; Daugulis, O. *J. Am. Chem. Soc.* **2011**, *133*, 13577–13586.

[188] Popovs, I. *A dissertation presented to University of Houston* **2014**.

[189] Brown, W. H.; Foote, C. S.; Iverson, B. L.; Anslyn, E. V. *Organic Chemistry* **2005**. Brooks/Cole Cengage Learning, CA, USA.

[190] Colombo, V.; Galli, S.; Choi, H. J.; Han, G. D.; Maspero, A.; Palmisano, G.; Masciocchi, N.; Long, J. R. *Chem. Sci.* **2011**, *2*, 1311–1319.

[191] Ramirez, M. A.; Cuadro, A. M.; Alvarez-Builla, J.; Castaño, O.; Andrés, J.; Mendicuti, F.; Clays, K.; Asselbergh, I.; Vaquero, J. *Org. Biomol. Chem.* **2012**, *10*, 1659–1669.

[192] Wang, Q.; Yu, C.; Long, H.; Du, Y.; Jin, Y.; Zhang, W. *Angew. Chem. Int. Ed.* **2015**, *54*, 7550–7554.

[193] Abe, H.; Aoyagi, Y.; Inouye, M. *Org. Lett.* **2005**, *7*, 59–61.